THERMAL RESPONSE OF INTEGRAL ABUTMENT BRIDGES WITH MSE WALLS: NUMERICAL ANALYSES AND A PRACTICAL ANALYSIS TOOL

Alfredo E. Arenas

Dissertation submitted to the faculty of the Virginia Polytechnic Institute and State University in partial fulfillment of the requirements for the degree of

Doctor of Philosophy
In
Civil and Environmental Engineering

George M. Filz
Thomas L. Brandon
James M. Duncan
Ronald D. Kriz

December 7th, 2010
Blacksburg, VA

Keywords:
Integral abutment bridges
Cyclic displacement
Skew angle
MSE wall embankment
Longitudinal and transverse loads

THERMAL RESPONSE OF INTEGRAL ABUTMENT BRIDGES WITH MSE WALLS: NUMERICAL ANALYSES AND A PRACTICAL ANALYSIS TOOL

By

Alfredo E. Arenas

George M. Filz, Chairman
Via Department of Civil and Environmental Engineering

ABSTRACT

The advantages of Integral Abutment Bridges (IABs) include reduced maintenance costs and increased useful life spans. However, comprehensive and practical analysis tools for design of IABs have not been developed to account for the impacts of thermal displacements on abutment and foundation components, including the components of mechanically stabilized earth (MSE) walls that are often used around the abutment piling.

During this research, over 65 three-dimensional numerical analyses were performed to investigate and quantify how different structural and geotechnical bridge components behave during thermal expansion and contraction of the bridge deck. In addition, separate three-dimensional numerical models were developed to evaluate the usefulness of corrugated steel pipes around the abutment piles.

The results of this research quantify the influence of design parameter variations on the effects of thermal displacement on system components, and thus provide guidelines for IAB design, where none had existed before. One of the findings is that corrugated steel pipes around abutment piles are not necessary.

One of the most important products of this research is an easy-to-use Excel spreadsheet, named IAB v2, that not only quantifies the impact of thermal displacement in the longitudinal direction, but also in the transverse direction when the abutment wall is at a skew angle to the bridge alignment. The spreadsheet accommodates seven different pile sizes, which can be oriented in weak or strong directions, with variable offset of the abutment from the MSE wall and for variable skew angles. The spreadsheet calculates the increment of displacements, forces, moments, and pressures on systems components due to thermal displacement of IABs.

ACKNOWLEDGEMENTS

I would like to express my gratitude to Professor George Filz for the opportunity of working with him on this research project. I have learned much from his approach in solving engineering problems and managing the research project. Through this experience my professional skills have grown and I have become a better researcher and engineer.

I would like thank to my committee members Professors Thomas Brandon, Michael Duncan and Ronald Kriz for their support during the development of this research and for providing the geotechnical tools acquired in their classes.

Special gratitude is to my wife Ivka, she has been the foundation of our family, encouraging and supporting me throughout all these years. Thanks to Florencia and Esperanza for their daily inspiration to finish this dissertation.

Thanks to my parents, brothers and “Abueli” for their unconditional support and love.

Thanks to my friend Lee Mills for hosting us and reviewing the full dissertation. His friendship and advice were key to walk the last mile of my dissertation.

Financial support for this research was provided by the Virginia Transportation Research Council.

TABLE OF CONTENT

LIST OF TABLES

LIST OF FIGURES

DEFINITIONS

VDOT:	Virginia Department of Transportation.
MSE wall	Mechanical Stabilized Earth Wall
Skew Angle:	Angle at which the front MSE wall is oriented with respect to a line perpendicular to the bridge centerline (Figure 7.29).
Skewed bridge:	Bridge built with a skew angle in the front MSE wall.
Non-skewed bridge:	Bridge with a skew angle equal to zero.
TIR:	Thermal induced response.
MSEW:	Interactive program for the design and analysis of MSE walls. MSEW was developed by ADAMA ENGINEERING.
Wing walls:	Extension of the front wall beyond the width of the bridge.
U-back walls:	MSE wall wrapping back around the approach embankment such that the MSE side walls are parallel to the road centerline.
Elephant ears:	Extension of the abutment beyond the bridge width.

CHAPTER 1

INTRODUCTION

1.1 Description of Integral Abutment Bridges

According to the Structure and Bridge Division of the Virginia Department of Transportation (VDOT), Integral Abutment Bridges (IABs) are becoming the first choice of engineers when designing or retrofitting bridges because of their superior performance and reduced maintenance needs.

Figure 1.1 shows a typical cross section of an IAB. This figure shows how the bridge deck, girders, abutment, and abutment piles form an integral structure, hence the name Integral Abutment Bridge. This figure also shows a mechanically stabilized earth (MSE) wall located under the bridge deck and in front of the embankment. The MSE wall facing is held in place by the MSE wall reinforcing strips, which extend from the MSE wall through the backfill. Figure 1.1 also shows the approach slab, which is structurally connected to the abutment in VDOT bridges, but not moment is transfer to it.

It is widely known that IABs offer several comparative advantages over bridges with expansion joints, including substantially reduced maintenance costs. Alampalli and Yannotti et al. (1998) found that the predominant cause of bridge deterioration is the flow of deck drainage waters contaminated with deicing chemicals through expansion joints.

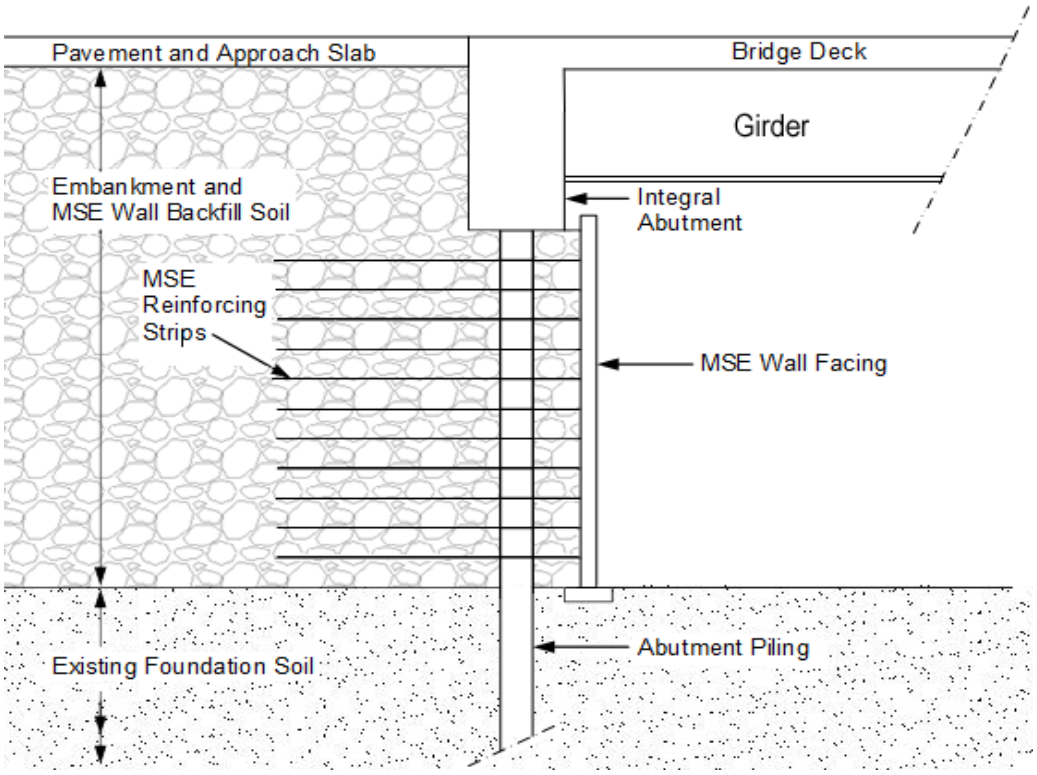

Figure 1.1 – Integral abutment bridge.

The most important advantages of Integral Abutment Bridges can be summarized as (Arsoy et al. 1999):

- Lower construction costs due to joint elimination.
- Lower maintenance costs. Conventional bridges have higher maintenance costs associated with deterioration of joints.
- Superior seismic performance.
- Fewer piles are needed per foundation, and no battered piles are needed.
- Simpler and faster construction.
- Improved riding quality because of the continuous bridge deck.

One drawback of integral abutment bridges is that they are subject to thermal displacements, which are the result of daily and seasonal temperature variations. Since these bridges are designed without joints, thermal displacements are directly transferred to the abutments and therefore to the embankments and the abutment foundation piles.

Currently, engineers face challenges when designing Integral Abutment Bridges because they do not know the magnitude and distribution of loads imposed due to thermal displacements. The nature of the problem is complex because of the vastly differing stiffnesses of the soil and structural components, the nonlinear response of the soil, and the complex three-dimensional geometries of IABs. Thus, it is the intent of this research to quantify the magnitude and distribution of loads in IAB components due to thermal expansion of bridge decks under different conditions of interest to VDOT. The focus of this research is on IABs with foundation piling in the backfill of MSE walls.

1.2 Need for Research on Integral Abutment Bridges

Many unknowns and points of controversy are related to Integral Abutment Bridges, and the significance of these uncertainties increases when long span bridges and skewed geometries are considered.

The following list shows several aspects of IABs where no design guidelines exist or no consensus has been reached:

- Distance between the back of the MSE wall face and the front of the abutment wall
- Orientation of piles
- Pile stresses and formation of plastic hinges
- Size and number of piles
- Influence of abutment design
- Rotation and lateral displacement of abutments for skewed bridges
- Strip tensile forces on both skewed and non-skewed bridges
- Lateral forces on piles for skewed bridges
- Implications of thermal displacement magnitude
- Distribution and magnitude of earth pressure behind the abutment
- Influence of Elasticized Polystyrene (EPS) behind the abutment and behind the MSE wall

- Soil/rock foundation type
- Reinforcing strips behind the abutment (in bridge direction)
- The use of sand in-filled steel cans around abutment piles

The intent of this research is to investigate these issues through the use of numerical models and to create easy-to-apply recommendations and analysis tools to help engineers with their designs.

1.3 Objectives and Scope of Dissertation

The primary objective of this research is to address the issues listed in the previous section through the use of numerical analyses. FLAC3D (Itasca 2006), which is a finite difference computer program, was the analysis tool selected for this research.

The scope of this research includes the following tasks:

a) Perform a literature review and nationwide survey

   A literature review was performed to compile information on limitation, advantages, construction procedures, and design alternatives of integral abutment bridges. A nationwide survey was conducted to complement the literature review information. Topics such as design, tolerances, and maximum dimensions, as well as challenges faced by engineers, were covered by the survey.

b) Analysis of corrugated steel pipe sleeves

   The usefulness of corrugated steel pipe sleeves infilled with loose sand was analyzed using FLAC3D. Different boundary conditions and sand densities were implemented in the model to represent potential field conditions.

c) Model generation and calibration

   A FLAC3D model of an IAB was created, and the numerical model was calibrated against field data obtained from an IAB located in New Jersey. Additional validation of FLAC3D was performed against MSEW software.

d) Parametric study

The principles learned during calibration were applied to generate a base case numerical model. This model was based on a bridge located in the vicinity of Alexandria, Virginia, because this bridge represents VDOT current design practices. Once the model was calibrated, 26 models were produced from the base case by changing one parameter at a time. After this phase was completed, it was noted that multiple parameter variation models were needed to answer questions about how to best combine the impacts of different parameters.

e) Key findings and recommendations

A detailed analysis was performed of the large amount of information from the numerical analyses, and key findings were identified. Based on the research results, recommendations were developed for design of IABs.

f) IAB v2 Spreadsheet

One of the most important products of this research is an easy-to-use Excel spreadsheet, named IAB v2, which not only quantifies the impact of thermal displacement in the longitudinal direction, but also in the transverse direction when the abutment wall is at a skew angle to the bridge alignment. The spreadsheet accommodates seven different pile sizes, which can be oriented in weak or strong directions, with variable offset of the abutment from the MSE wall and for variable skew angles. The spreadsheet calculates the increment of displacements, forces, moments, and pressures on system components due to thermal displacement of IABs.

Although there are many designs of integral abutment bridges, the scope of this research is limited to fully integral abutment bridges, with MSE walls retaining the embankments and with piling extending through the MSE backfill and into the foundation soil.

The loads considered during this research are gravitational forces and imposed thermal displacement. Recommendations are only given for the incremental loads due to thermal displacements. Recommendations are not provided for the effects of gravity loads, traffic, wind, seismic, or other loads, which we expect the designer to analyze separately using existing methods.

1.4 Organization and Content of Dissertation

This dissertation is divided into nine chapters and six appendices, with the first chapter being this introduction.

Chapter 2 presents a literature review, in which available information regarding IABs was collected and synthesized. In addition to the literature review, and as presented in Chapter 3, a nationwide survey was conducted. This survey addressed current IAB design details, maximum tolerances and dimensions, challenges when designing IABs and how they are overcome, instrumentation, and the main issues that should be addressed by a numerical study. The information generated by the survey complemented that found during the literature review.

Chapter 4 describes analyses of the usefulness of corrugated steel pipe sleeves. This matter was analyzed independently from other IAB design concerns. During this analysis, several 3D numerical models were implemented to investigate different boundary conditions, material properties, loading conditions.

Chapter 5 discusses numerical modeling procedures. This chapter starts by describing the principal components of the model, and how they are represented in FLAC3D. Then it describes how the soil-structure interaction is achieved in FLAC3D through the use of nonlinear springs. This chapter also includes a description of how the thermal displacement is applied to the bridge model, and it describes the numerical analysis methodology.

Chapter 6 describes the IAB in New Jersey that was field instrumented and monitored for over three years. This IAB was analyzed using the methods described in Chapter 5, and the results served as a calibration and validation point for the FLAC3D numerical modeling approach.

In Chapter 7, using the knowledge obtained from the numerical model of the IAB in New Jersey, a numerical model that suits Virginia design practices was crated. This model is the cornerstone of this research, because later model variations were compared to this one. This chapter addresses all of the design concerns listed in Section 1.2 (except for the use of corrugated steel pipe sleeves, which is addressed in Chapter 4), by applying a parametric variations technique to the base case, i.e., by changing a single input parameter at a time from the base case model. Also in this chapter, multiple input parameter variations are addressed by changing more than one input parameter at a time. These models helped to demonstrate the impacts of multiple parameters to provide information to predict their combined simultaneous effects.

Chapter 8 provides a discussion of the analysis results, in which the data is synthesized and organized in different categories. This exercise permitted identifying the key findings of the research. With the results properly arranged, multi-parameter polynomial equations were fitted to the data, thereby enabling prediction of the loads induced in bridge components due to thermal displacement. This chapter also presents one of the most important outputs of the research, a spreadsheet named "IAB v2", which the bridge loads caused by thermal displacements under a wide range of bridge configurations.

Chapter 9 presents a summary of the work accomplished in this research, including the key findings. Limitations of the analyses and recommendations for further research are also presented.

Appendix A provides a copy of the survey instrument. Also in this appendix, Table A.1 and Table A.2 respectively summarize the answers to questions concerning the criteria for using approach slabs and the support/connection systems for approach slabs.

Appendix B shows the full set of plots of the monitoring output parameters for the base case model. This set includes all the time-histories in the directions along and transverse to the bridge centerline.

Appendix C details where the single monitoring output points are located in the bridge.

Section 7.2 analyzes the impact of single parameter variation models on selected outputs of the base case model. Most of the information in Section 7.2 is presented as a percentage change from the base case model. Table D.1, in Appendix D, shows a summary of the information discussed in Section 7.2 . Through the use of general monitoring outputs, this table shows a summary for the following parameters: shear forces and moments in dowels (longitudinal and transverse directions), axial force in dowels, shear forces and moments in piles directly under the abutment and two feet under the abutment (longitudinal and transverse directions), axial force in piles and, normal and shear forces acting on interface 1 (between EPS and pile cap) and interface 2 (between EPS and abutment backwall).

Appendix E shows the tabulated results of the numerical models for each group of parameters, along with the fitted equations and coefficients, as well as the values of the coefficient of detemination, R^2.

Appendix F shows pile properties for several H piles (Skyline Steel et al. 2008).

CHAPTER 2

LITERATURE REVIEW

This chapter describes results of a literature review of the current state of practice of Integral Abutment Bridge design. The literature review was conducted using the following sources and searchable databases: the Virginia Tech Library, Ozawa Library in Patton Hall, ASCE Civil Engineering Database, Compendex, Inspec, NTIS, and Web of Science. The results of the literature search are organized and presented in terms of the following categories of information: Superstructure, Pile Foundations, Thermal Variation, Skew Angle, Abutment, Backfill, MSE Wall, Approach Slab, and Abutment Earth Pressure.

2.1 Superstructure

The deck and the girder comprise the superstructure. The literature review shows that all IAB designs use reinforced, cast-in-place concrete for the deck, while girder materials are steel or steel-reinforced concrete. For short bridge lengths, steel is preferred; for medium bridge lengths, cast-in-place concrete is used; and for long bridge lengths, prestressed concrete elements are desirable (Maruri and Petro 2005).

Alampalli and Yannotti (1998) compared integral bridges and conventional bridges, and they concluded that integral bridges have been functioning as designed with better performance than conventional bridges. Also, they found that steel superstructures performed better than concrete superstructures.

2.2 Pile Foundations

For relatively short IABs, almost any type of foundation is acceptable because the thermal displacements are small, but for longer bridges, the foundation type selection and design should consider the larger thermal displacements that can be occur (Dunker and Lui 2007).

The design of the foundation for Integral Abutment Bridges needs to accommodate expansion and contraction movements (Maruri and Petro 2005). Thermal expansion can produce soil pressures that control design of abutments and piles (Maruri and Petro 2005).

Specialized rules for designing the pile foundations of IABs have not been established, although a common practice is to use an equivalent cantilever beam column model, which allows for computing stresses along the pile (Hassiotis et al. 2005). In this method, the foundation pile is assumed to be fixed at a depth lc, where lateral piles movements are smaller than 4% of the pile top displacement. The fixity depth is computed based on pile properties and initial horizontal stiffness of the soil, as represented in a linear Winkler soil model (Fleming et al. 1985; Poulos and Davis 1980).

The most common foundation pile type is the steel H pile. The most common orientation is with the weak axis, i.e., the pile web direction, oriented perpendicular to the bridge centerline, but this practice is not universal (Maruri and Petro 2005). Mourad and Tabsh (1998) recommend orienting piles with the strong axis, i.e., the pile flange direction, oriented perpendicular to the bridge centerline to resist bending due to gravity load from the bridge deck. Mourad and Tabsh (1998) also recommend long and flexible piles because they distribute the load more uniformly. Other types of piles, as well as different pile materials, have been used. Concrete piles have not exhibited good performance under cyclic loads, generating cracks that may reduce the supporting capacity of the piles. Pipes piles have performed well under cyclic loads, but their high flexural stiffness imposes high stresses in the adjacent structure components (Arsoy et al. 2004).

Mourad and Tabsh (1998) found that the bending moments generated by gravity loads from the dead weight of the girders and bridge deck are significant and cannot be neglected in the design.

According to Maruri and Petro (2005) many designers offset the MSE wall face between 2 to 5 feet from the abutment and footing to provide enough space for MSE wall construction. In addition to the offset requirement, many states require the use of a steel sleeve filled with sand in an attempt to reduce pressure on the MSE wall from lateral pile movements and to reduce bending stresses in the piles (Hassiotis et al. 2006). The idea behind this last technique is that the

stiffness of the soil surrounding the steel sleeves is higher than the stiffness of the sand inside the sleeves.

Hoppes and Gomez (1996) found that integral abutments should not be used when piles cannot be driven at least 10 to 16 feet into the existing ground beneath the abutment fill.

Battering the front row of piles increases the resistance of abutments to expansion and contraction, but this practice can produce a fracture of the seat for the approach slab (Burke 1987). In addition, battered piles have reduced vertical load capacity compared to vertical piles. For these reasons, Burke (1987) does not recommend using battered piles.

The use of hinges connecting the pile cap to the abutment has been recognized (Edward Hoppe and Keith Weakley, personal communication, 2008) as an approach to reduce the moment imposed on piles by the thermal expansion and contraction of the bridge superstructure. Hinged pile caps are recommended for longer integral bridges to reduce piles stresses. As the need to build longer integral bridges grows, the role of integral bridges with hinges becomes more important (Arsoy et al. 2002).

2.3 Thermal Variation

The following formula was used to compute the total thermal displacement (AASHTO 1996):

$$d = \alpha * \Delta T * L \tag{2.1}$$

where d = the total displacement experienced by the bridge. The displacement experienced by each abutment is one-half of d.

α = the coefficient of linear thermal expansion. For both concrete and steel, α is approximately equal to 6.5×10^{-6} per ^{o}F.

ΔT = is the difference between the maximum and minimum temperatures that the bridge will experience.

L = the length of the bridge.

2.4 Skew Angle

Most states restrict the bridge skew angle to 30° or less (Hassiotis et al. 2006). This reduces rotational movement of the bridge in the horizontal plane. Also, it reduces stresses on the abutment, particularly on abutment piles, in the direction transverse to the bridge orientation (Hassiotis et al. 2006).

2.5 Abutment

Integral abutment bridges incorporate different designs for the abutment, but most of them fall in one of the following two categories: solid abutments or abutments with connections. Solid abutments are those that fully connect the upper part of the abutment, where the girders are embedded, with the pile cap. These types of abutments are capable of transferring large moments and displacements to the piles. Abutments with connections are those that incorporate a joint between the abutment and the pile cap so that no or reduced moment is transferred to the piles. Abutments with connections partially transmit horizontal displacements from the abutments to the pile caps (Arsoy et al. 2004).

VDOT mostly uses abutments with connections. The most common VDOT connection employs steel dowels, but VDOT has also used laminated pads to connect abutments to pile caps.

2.6 Backfill

According to Maruri and Petro (2005), the majority of states require compacted backfill behind IAB abutments, but a few states require an uncompacted backfill. In addition to the use of compacted backfills, several states that require the use of expanded polystyrene (EPS) or other compressible materials and/or light weight fills behind IAB abutments. The use of loose backfill and EPS are intended to reduce earth pressures behind abutments during bridge expansion (Maruri and Petro 2005).

A special case of EPS, known as elasticized EPS, has been studied for use behind bridge abutments. This material exhibits approximately linear elastic behavior up to about 10% strain and approximately linear but inelastic stress-strain behavior up to about 30% strain (Hoppe 2005). The advantage of using elasticized EPS is that it reduces passive earth pressures on the abutment, and it also absorbs cyclic abutment movements without disturbing the adjacent backfill, thereby reducing backfill settlement due to the cyclic movements.

A simple equation to compute elasticized EPS thickness has been used by VDOT, based on limiting EPS strain to a maximum of 10 % (Hoppe 2005). Reeves et al. (2001) found that a 150 mm thick layer of elasticized EPS reduced lateral earth pressures on rigid walls by approximately 50%, compared with lateral earth pressures on walls without the elasticized EPS.

According to Hoppe (2005), well-graded compacted granular backfill should be used to reduce differential settlements between the abutment and backfill. The main causes of differential settlement are: first, compression of the backfill material; second, settlement of the natural soil under the embankment; third, poor construction practices; fourth, high traffic loads; fifth, poor drainage; sixth, poor fill material; and seventh, loss of fill by erosion (Briaud et al. 1997).

2.7 MSE Wall

Virginia DOT states that all MSE wall designs are performed by private consultants (Keith Weakley, personal communication, 2008). Private engineering consultants typically follow FHWA recommendations for MSE wall designs, which are often checked by MSE wall suppliers.

MSE walls constructed for Virginia DOT use concrete panels that are six inches thick and range in width from 3 to 12 ft and in height from 3 to 6 ft. The MSE wall backfill is reinforced with galvanized steel strips, which are usually connected to the concrete panels at two elevations per panel.

Mourad and Tabsh (1998) state that MSE wing walls should be placed parallel to the bridge center line to maximize the use of the wing wall bending strength and reduce the passive earth pressure build up during the bridge expansion.

2.8 Approach Slab

Most states use an approach slab to mitigate the effects of backfill settlement, and thus provide a smoother transition from the road pavement to the approach slab pavement to the bridge deck pavement (Arsoy et al. 1999). According to the US Department of Transportation FHWA Technical Advisory (1980) "approach slabs are needed to span the area immediately behind integral abutments to prevent traffic compaction of material where the fill is partially disturbed by abutment movement. The approach slab should be anchored with reinforcing steel to the superstructure…"

Most states provide details of the connection between the approach slab and the abutment to create a monolithic structure. Thus, under thermal induced movements, the approach slab will move along with the superstructure. The connection has to transmit the abutment movement, but it also has to allow rotation to avoid transferring moment. This last requirement is achieved with particular design details of the reinforcement connection that transmit shear but not moment.

NJDOT places the approach slab over a bond-breaking material, such as polyethylene, to reduce friction between the slab and the supporting soil (Hassiotis et al. 2006).

The length of the approach slab is determined based on experience, finite element modeling, or approximate calculations (Hoppe 1999). Generally, the length of the approach slab is compatible with the expected settlement of the backfill. Researchers generally recommend that the approach slab length should be two to three times the height of the abutment (Hoppe 1999). This recommendation is based on the size of the wedge created by the passive failure developed when the bridge expands, and it is equals to the height of the abutment times the tangent of (45 degrees + $\phi/2$), where ϕ is the friction angle of the backfill. Hoppe (1999) conducted a survey and

obtained 39 state responses. The findings indicate that most states use a 20 ft long approach slab with a thickness of 9 inches.

Some DOTs prefer to not use approach slabs, because any remedial action necessary to rectify potential approach slab settlement would be significantly more expensive and inconvenient than re-grading settlement of the backfill located behind the abutment (Hoppe and Gomez 1996).

Alampalli and Yannotti (1998) noticed a close relationship between the condition of the approach slab and the length of the expandable portion of the bridge. The longer the bridge, the lower the condition rating of the approach slab.

2.9 Abutment Earth Pressures

The soil pressure used for the design of integral abutments and the abutment piles has been the subject of controversy and much research (Maruri and Petro 2005). There is no general agreement regarding the maximum pressures or the pressure distributions behind abutments (Mokwa and Duncan 2000).

Log-spiral earth pressure theory has been successfully used to compute passive pressure behind a reaction wall. This theory has been modified and combined with the p – y method to compute the passive resistance developed by pile groups and pile caps. This combined method also includes the "shadowing" effect of the piles within the group. Further analyses are needed to validate the method's applicability to compute passive resistance of abutment piles (Mokwa and Duncan 2000).

According to Hassiotis et al. (2006) and Hoppe and Gomez (1996), integral abutment bridges can conservatively be designed using fully developed passive pressure computed using Rankine theory). When Rankine passive theory is used for IAB design, soil friction angles associated with high soil densities must be applied (Hassiotis et al. 2006) because the soil right behind the abutment densifies under the thermal-cyclic action of the bridge.

Hoppe (2005) proposed a passive earth pressure coefficient $K_p = 4$ when EPS is used on the abutment backwall, although he states that further analysis must be done before this value is used in common design practice.

Xu et al. (2007) and Hassiotis et al. (2006) found that earth pressure systematically increases behind abutments with expansion-contraction cycles, eventually reaching states of stress close to full passive and active pressures.

The UK design standard BA42 for design of integral bridges (British Highway Agency 1996) suggests an earth pressure distribution for frame integral abutments. This earth pressure distribution uses a K* coefficient of pressure, which takes into account the bridge displacement induced by thermal differences. Since $K^* < K_p$, Xu et al. (2007) concluded that this distribution fails to include possible passive pressure developed over time.

Xu et al. (2007) recommended against using loose backfill behind integral abutment bridges because it will not reduce the tendency to develop high passive earth pressures under cycling loads, and it also produces larger settlements.

CHAPTER 3

NATIONWIDE SURVEY

3.1 Survey Description

A nation-wide survey was conducted to collect information about integral abutment bridges that have foundation piling for the abutments extending through the backfill of MSE walls.

The survey was mainly distributed to departments of transportation (DOTs) and companies working in this field. The survey included questions ranging from general aspects of Integral Abutments Bridges (IABs) to specific design details.

One of the goals of this survey was to determine current design practices in different agencies, to obtain information about the principal challenges that engineers face when designing integral abutment bridges, and to identify concerns that exist about current design practices.

Appendix A provides a copy of the survey instrument.

3.2 Detailed Survey Results

This section describes the detailed survey results, including the response rate and the responses organized according to various categories of information, such as overall bridge issues, piling, etc.

3.2.1 Response Rate

A total of 45 surveys were distributed, and 27 responses were received. Of the 27 responses, 21 completed the survey. The agencies that answered the survey are Alberta Transportation, Iowa DOT, Virginia DOT, Oklahoma DOT, Missouri DOT, Kansas DOT, Nebraska Department of Roads, Utah DOT, South Dakota DOT, West Virginia DOT, New Hampshire DOT, CalTrans, Pennsylvania DOT, New Jersey Turnpike Authority, Maryland State Highway, Tennessee DOT,

Illinois DOT, Wyoming DOT, Oregon DOT, Canada Ministry of Transportation, and South Carolina DOT.

The main reason that following six agencies did not complete the survey was that they do not use IABs or do not combine IABs with MSE walls in their designs:

- Arkansas DOT has not used a fully integral abutment bridges in an MSE embankment

- Texas DOT does not use fully integral abutment bridges. They explained that they do not have the soil conditions necessary for integral abutment bridges.

- New York DOT explained that they try to avoid the use of MSE walls when the abutments behind them require piles because of the difficulty of placing the MSE fill and strips around the piles. NYSDOT does not feel comfortable with an integral abutment that has a lot of movement behind an MSE wall. They have concerns with cyclic movements and the response of the face panels.

- The Arizona State Highway and Transportation Department does not use IABs with MSE walls in front of the abutments because they have had limited experience with integral bridges and tend to use them only for straight, short W-beam span bridges. They have not had a project where both methods (IABs and MSE walls) were considered appropriate.

- Arizona DOT is not using the details of integral abutment bridges as the survey described. ADOT is currently not considering the use of integral abutment bridges due to concerns about settlement in the approach slab.

- Integral abutment bridges are not used in Washington DOT bridges because WSDOT does not have any criteria for this type of bridge. WSDOT has concerns about the performance of integral abutments bridges in high seismic zones.

3.2.2 Overall Bridge Issues

The first question on the survey asked about the maximum span and length of IAB bridges. Many of the agencies only responded to the maximum length of the bridge, and they did not answer the maximum span question. Although relatively little information was collected related to the span length, a typical maximum span length of 150 ft applies for most of the agencies that answered. The longest reported span was 590 ft by Pennsylvania DOT. There was substantial variation in maximum overall bridge length, ranging from 300 ft in Alberta up to the longest bridge of 1175 ft in Tennessee. Common values of the maximum IAB length used by several agencies range from 500 ft to 600 ft.

Almost all the agencies use a skew angle limit of 30°. The biggest skew angle limit is 60° by Pennsylvania DOT.

None of the agencies have a limit for IAB bridge curvature.

Only 10% of the agencies reported having problem due to effects of skew angle in IABs. Specifically, Virginia DOT has experienced lateral movements towards the acute corner in bridges with skew angle as small as 5°.

3.2.3 Piles

As shown in Figure 3.1, 57% of the agencies use exclusively steel H-piles in their designs, 24% of the agencies use steel H-piles and pipe piles in their designs, and 19% of the agencies use H, pipe, and concrete piles in their designs.

It is important to highlight that all the agencies use steel H-piles in their IAB designs. Although the agencies that use more than one type of pile did not specify how much of each they use, there appears to be a tendency to mostly use steel H-piles.

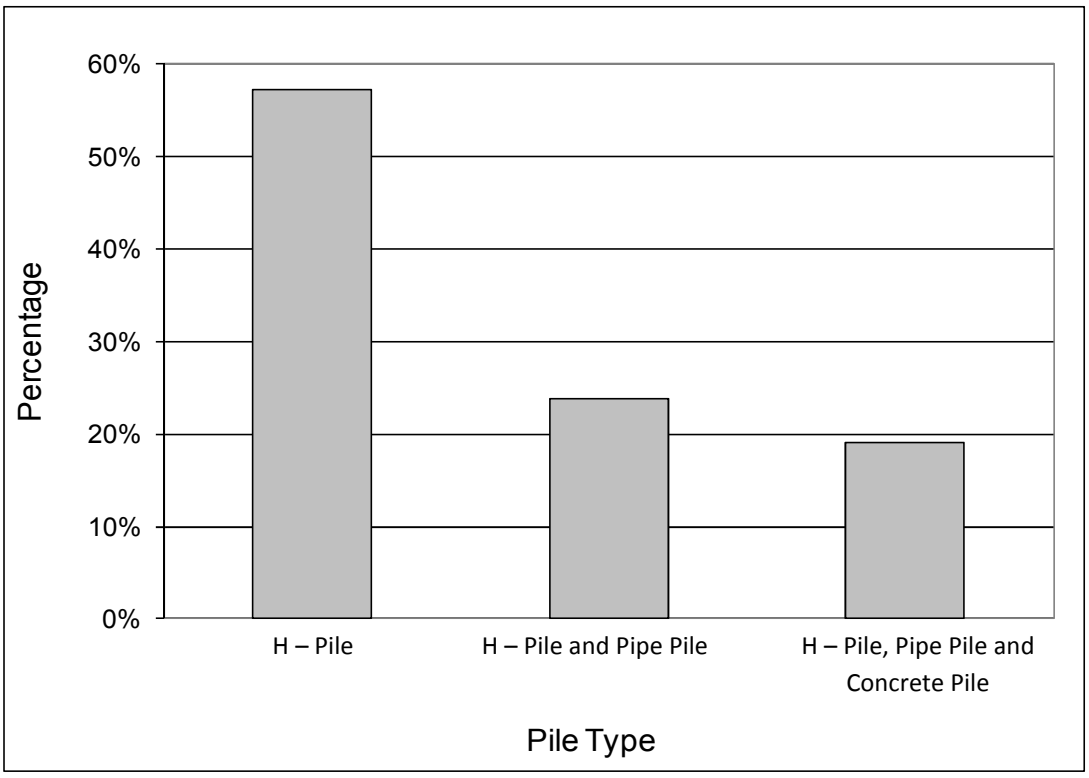

Figure 3.1 – Pile types used for IABs by agencies responding to the survey

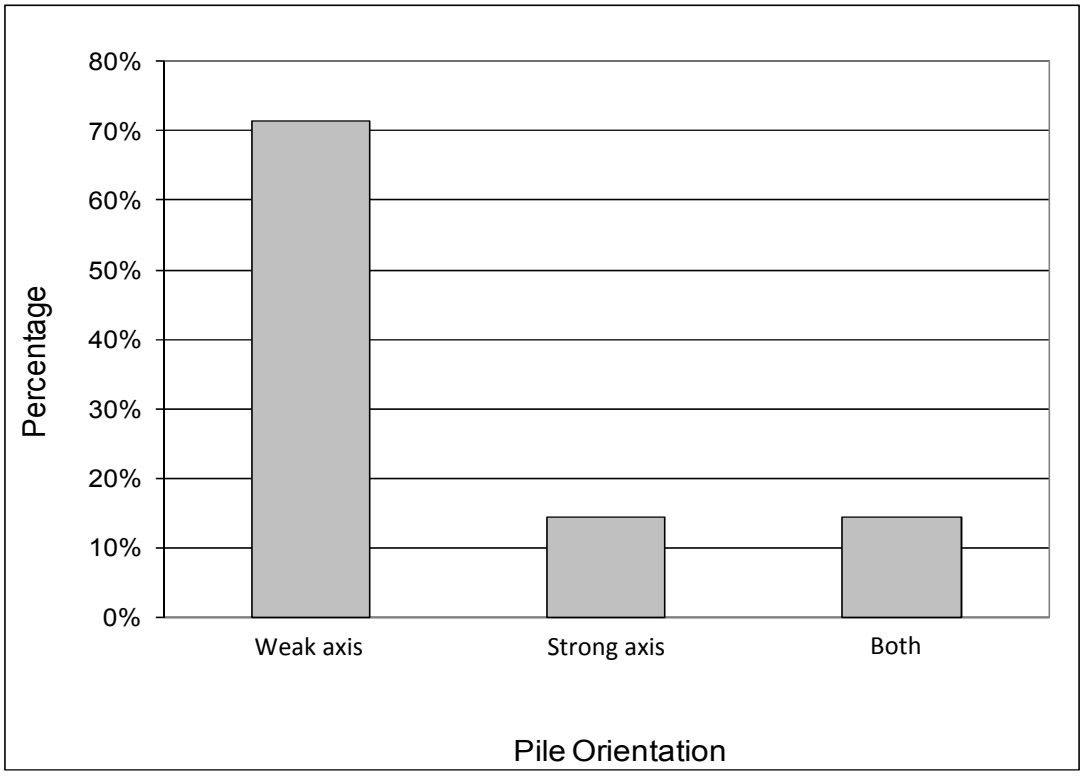

Figure 3.2 – Pile orientation distribution

Figure 3.2 shows that most of the agencies (71%) orient steel H-piles with their weak axes perpendicular to the bridge direction and only 14% orient steel H-piles with their strong axes perpendicular to the bridge direction. Fourteen percent of agencies orient steel H-piles in either direction.

The survey asked for descriptions of the IAB pile design methodology. Figure 3.3 shows the design criteria distribution among the surveyed agencies. Fifty three percent of the agencies use axial load as the only consideration for pile design. Axial, bending, and axial/bending criteria are used by 18% of the agencies. Axial and axial/bending criteria are used by 6% of the agencies. The "other" alternative was selected by 24% of agencies. This last selection does not mean that these agencies are using completely different criteria for pile design. Instead, an agency selecting "other" might be applying criteria that incorporate axial, bending and/or axial/bending criteria along with other requirements.

None of the agencies provided a design methodology that supports the use of a particular pile orientation.

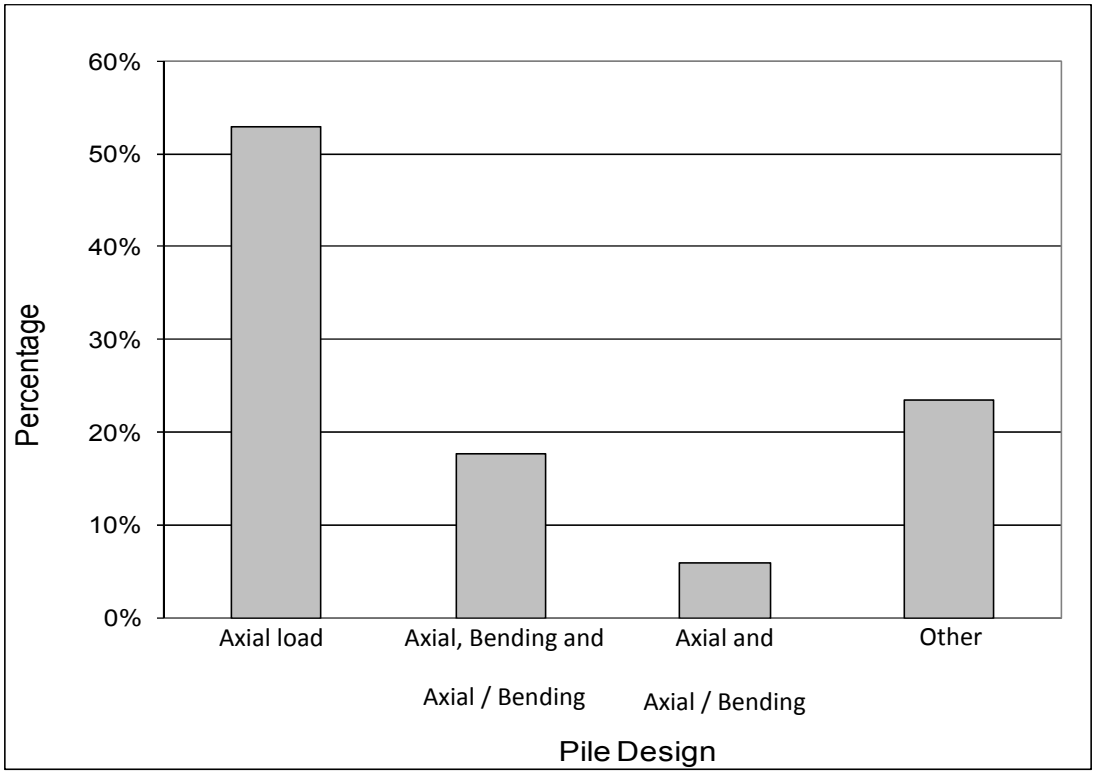

Figure 3.3 – Design criteria distribution

In addition to the design stress criteria shown in Figure 3.3, some of the agencies provided maximum lateral deflection for piles. The values range from 0.5 to 2.25 in., with the average being 1.5 in.

The survey also asked if designs include considerations for bending moment produced by skew angle and/or curvature. Twenty eight percent consider moments produced by the skew angle when larger than 20°. None of the surveyed agencies consider moments produced by curvature.

Corrugated steel sleeves filled with loose sand surrounding piles are used by 55% of the agencies. This topic is an investigation subject of the current research project because soil data in support of the practice is lacking.

3.2.4 MSE Wall

The offset between the MSE wall and the abutment piles used by the surveyed agencies ranges from 3 to 5 feet for those agencies using the corrugated steel sleeves filled with sand and from 3 to 5.6 feet for those that do not use the corrugated steel sleeves. The average distance used is 4.5 feet for both. This suggests that the corrugated steel sleeves do not influence the offset distance.

None of the agencies indicated that they account for higher tensile stresses on the MSE strips due to thermal contraction of the bridge. Only CalTrans says that they have special considerations accounting for higher stresses on the MSE strips. These considerations are defined by the seismic load, which governs the design and therefore, the MSE wall strips are designed for those loads. Because CalTrans uses IABs with a maximum length of 400 ft, loads imposed by thermal contraction probably do not exceed those imposed by seismic loads.

Most of the surveyed agencies (71% of the 14 agencies that responded to this question) use a well graded, free draining granular material for the MSE wall fill. Only one institution (7%) specified that they re-compact the natural soil. Other types of fill material were used for the MSE wall by 21% of the agencies, which generally required use of a select engineering fill with special requirements. For example, CalTrans specifies a select backfill with low corrosion

potential and high “compaction grading”. The results reflect that good quality material is generally used among the surveyed institutions.

The compaction requirement for the material in the MSE wall is practically the same for all these institutions, with 86% of the agencies requiring 95% of the standard proctor maximum density. Only 2 agencies have different requirements: South Dakota DOT specifies at least 4 passes with a heavy vibratory roller, and Canada Ministry of Transportation specifies 100% of the standard proctor maximum density.

3.2.5 Abutment

Similar results were obtained when the surveyed agencies were asked about the type of material and compaction requirement for the zone behind the abutment, but with a larger number of responses. A probable reason for more responses is that most of the agencies pay close attention to settlement and drainage problems right under the approach slab. In addition, good drainage control behind the abutment will help avoid drainage problem in the MSE wall fill.

Seventy-one percent of the 21 agencies that responded to this question use a well graded free-draining granular material behind the abutment. A re-compacted natural soil is used by 14% of the agencies. Fourteen percent of the agencies use other types of material behind the abutment. This last group still uses a granular material but with special requirements, which they did not provide in the survey.

Compaction specifications for this location were generally similar to those required for the MSE wall, i.e., most of the agencies (61%) require 95% of the standard proctor maximum density. The rest of the agencies (41%) employ a wide variety of specifications. Missouri DOT requires a density equal to the adjacent road fill, Nebraska Department of Roads has no density requirements, Idaho DOT requires an un-compacted material, and Wyoming DOT requires compacting the material as much as possible without damaging the reinforcement.

Answers to the survey question about the earth pressure used for design behind the abutment produced the most variability. Figure 3.4 shows the percentages of the agencies using an active earth pressure distribution (20%) and a passive earth pressure distribution (30%) behind the abutment. Only 5% of the agencies use an earth pressure distribution at rest. Forty-five percent of the agencies use a combination of earth pressure distributions. An example of this category is Utah DOT, which uses an active pressure distribution for wingwalls and a passive pressure distribution for the abutment.

Post-survey, some agencies were asked to specify the background supporting the use of active earth pressure distribution behind the abutment. New Jersey Turnpike Authority specifies that design is based upon AASHTO LRFD Bridge Design Specifications which generally stipulate that all "retaining structure" designs are to consider active earth pressure. Iowa DOT requires the MSE wall supplier to design a soil reinforcement anchorage system connected to the rear of the abutment to resist an active earth pressure of 40 pcf equivalent fluid pressure with a triangular distribution. Maryland State Highway uses a triangular active earth pressure distribution, based on AASHTO Standard Specifications and the assumption that the integral abutment deflects enough to produce active stress conditions.

Only 10% of the agencies use expanded polystyrene (EPS) behind the abutment or other method to reduce lateral earth pressure. Virginia DOT encourages this option, but it is not mandatory. Pennsylvania DOT specifies a 1" thick sheet of Styrofoam to be placed against the entire area of the back face of the abutment below the bottom of the approach slab. Although the technical literature shows that the use of EPS reduces the lateral earth pressure behind the abutment, only a few agencies recommend using it.

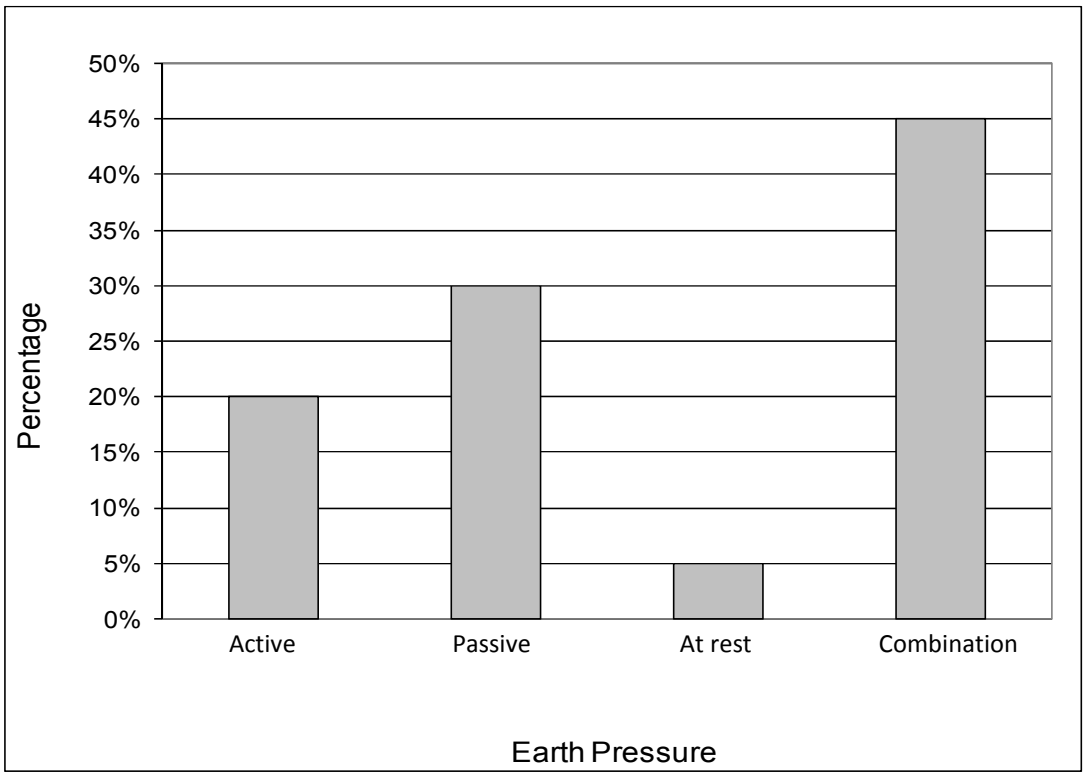

Figure 3.4 – Earth pressure distribution

3.2.6 Approach Slab

Questions concerning the criteria for the use of the approach slab and the support/connection system produced a wide variety of answers. Detailed information is provided in Appendix A, Table A.1 and Table A.2, respectively.

All the agencies that responded to the survey require an approach slab in their designs, but the design varies greatly among agencies. Most of the agencies use one of the three following types of connections between the approach slab and the bridge: a pinned connection with the abutment, a corbel with reinforcement, or a reinforced connection with the backwall. At the free end, away from the bridge, most of the agencies rest the approach slab on a sleeper slab, and some of them rest the approach slab directly on the grade.

3.2.7 Miscellaneous

The surveyed agencies were asked to provide the most important questions that need to be answered for IABs with MSE walls. The answers to this question were wide spread, but it is possible to classify them into the categories shown in Table 3.1.

Table 3.1 – Principal concerns related to IABs

Most Important Question	**Number of Agencies**
Joint details at end of approach slab for various bridge lengths.	1
Pile sleeve details and interaction	1
Moment produced by skew angles	1
EPS on backfills	1
Thermal movement interactions and design requirements	8
Seismic movement interactions and design requirements	2
Minimum distance between wall and abutment piles (including front and sides)	3
Distribution and magnitude of earth pressure	3
Creep behavior of geogrid and corrosion reducing life of IABs	1
Compaction of materials adjacent to structures such as piles, panels	1
Settlement when approach slab is not present	1
Piles stresses	2
Arrangement of piles and strips	2

These results indicate that most of the agencies are concerned about the effects of thermal movements on bridge structures. However, when agencies mention that thermal movement interactions and design guidelines to accommodate them are the most important issues, they also include several other topics like minimum distance between the MSE wall and abutment piles, forces on the strips/anchors/panels, moment and axial stresses on piles, stresses on the abutment, embankment settlement, earth pressure magnitude and distribution, etc.

Seismic concerns are important for CalTrans and Washington DOT.

An interesting result is that only one agency emphasized the importance of pile sleeve details and interactions, although 55 % of the surveyed agencies are using it.

Overall, general comments from the survey respondents about IABs are that they exhibit very good performance, and they are preferred due to elimination of expansion joints. Many agencies state that they will continue to use them and push their limits until problems arise. In addition, many agencies also recognize the need for guidelines for this type of bridge when designed with MSE walls.

Information regarding possible instrumentation of bridges was provided by Utah DOT, West Virginia DOT, New Jersey Turnpike Authority, and Canada Ministry of Transportation. Iowa DOT will be instrumenting and monitoring a bridge in Des Moines with MSE walls for the next two years.

3.3 Key Findings and Conclusions

The following list shows the key finding of the survey:

- 27 responses were collected, but only 78% of those answered the survey questions.
- The longest IAB is located in Tennessee with an overall length of 1175 ft. Typical maximum bridge lengths range from 500 to 600 ft.
- Most of the agencies use a skew limit of 30º and only 10% of the agencies have experienced problems with skewed bridges.
- Only 28% of the agencies have special design consideration for piles when skew angle is larger than 20º.
- 57% of the agencies use exclusively H piles for the abutment support, the rest use pipe and concrete piles in addition to H piles.
- 71% of the agencies orient the abutment piles for weak moment resistance (flanges parallel to bridge alignment).
- 53% of the agencies use axial load criteria when designing piles, the rest of the agencies use a combination of axial and bending criteria.
- 55% of the agencies use corrugated steel pipes around piles, but none of them provided data or analyses to justify their use.
- An average of 4.5 ft is used between the MSE wall and piles.

- None of the agencies have special considerations to address thermal forces when designing MSE walls.
- There is no consensus regarding what lateral earth pressure should be used for abutment design. Thirty-five percent of the agencies use active earth pressure distribution, 38% use passive earth pressure distribution, and the rest use a combination of the above.
- Only 10% of the agencies use EPS behind the abutment.
- All the agencies require approach slabs in their design, but the designs vary significantly among agencies.
- The most important concerns when designing IABs are: thermal displacement effects in bridge components, distance between MSE wall and piles, and lateral earth pressure behind the abutment.

The survey results confirmed that many unknowns exist in the present design practice of IABs. The survey results also show that there is special interest in the following topics: magnitude and distribution of earth pressure behind the abutment; magnitude and distribution of shear and bending moments in piles; settlements behind the abutment; and impacts of greater thermal displacements on system performance.

CHAPTER 4

CORRUGATED STEEL PIPE SLEEVES

Virginia DOT has been installing corrugated steel pipe sleeves around the piles of integral abutment bridges, with the objective of reducing stresses in the piles caused by cyclic thermal displacements. These corrugated pipes are infilled with loose sand after the MSE wall and backfill are completed. The numerical analyses described in this section were performed to address VDOT's interest in determining the usefulness of these steel corrugated pipes surrounding the piles.

4.1 Thermal Displacement

Arsoy et al. (2005) developed a double sine displacement function to represent both daily and seasonal thermal displacement (Eq. 4.1). Using this equation, simulated thermal displacements can be computed and applied to the centerline of a bridge in a numerical model. The maximum displacements imposed are half of the maximum displacements computed with Eq. (2.1).

$$\text{Displacement } f(t) = A \sin(2\pi t) + B \sin(2\pi t/365) \tag{4.1}$$

- A = Half of daily thermal displacement.
- B = Complement of half of the total displacement, thus the following is true $d = 2(A + B)$, with d from Eq. (2.1)
- t = Time measured in days.

Equation 4.1 has two parts: the first controls the daily displacement and the second controls the seasonal displacement. Equation 4.1 has a cyclic period of one year. A graphical representation of Eq. (4.1) is shown in Figure 4.1.

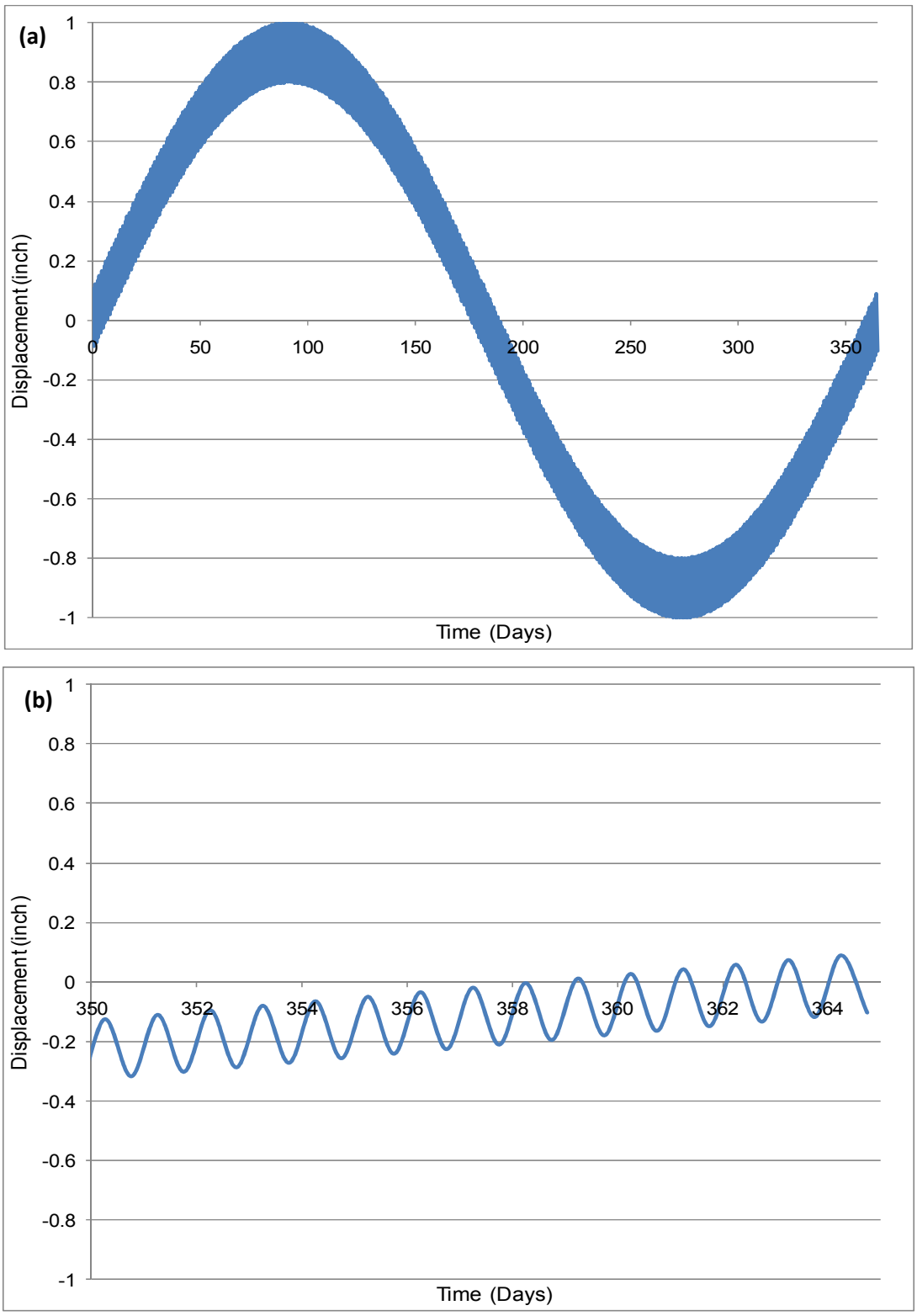

Figure 4.1 – Thermal displacement function (a) One year cycle (b) Expanded view of the last 15 days of the year

According to the FHWA, it is recommended to plan the bridge construction for completion in spring season. In this case, the thermal expansion and contraction displacements experienced by the bridge are close to being equal. The pattern displayed in Figure 4.1 represent a bridge completed in mid-spring season. At day zero, the bridge is completed. The bridge starts to expand when the temperature increases as the summer season approaches. The maximum bridge expansion is at midsummer, around day 95. From this point, the bridge contracts when the season changes into fall and later winter. The maximum bridge contraction is at midwinter, around day 270. Then the bridge start to expand again, and it moves back to the neural position at day 365.

4.2 Numerical Model

In the current research, special 3D numerical models were prepared to study the effect of the loose sand and steel pipe sleeves around the abutment piles (Figure 4.2(a)). These models consisted of a horizontal slice of the abutment system, with the pile represented as a solid component instead of as a uniaxial structural component. The pile was surrounded by sand, which was surrounded by shell elements representing the steel pipe sleeve, and backfill material was located beyond the steel pipe sleeve (Figure 4.2(b)).

The geotechnical program FLAC3D was used to analyze the model. FLAC3D uses the finite difference method to solve the model.

The Table 4.1 shows the material properties and the constitutive models for corrugated steel sleeves, sands, and backfill.

Table 4.1 – Material properties

Material	**Elastic Modulus E, psf**	**γ, pcf**	**ϕ, deg**	**Model**	**Poisson ratio ν**
Steel	4,177e6	485	-	Elastic	0.3
Loose Sand	280,000	115	30	Mohr	0.3
Medium Sand	540,000	123	34	Mohr	0.3
Dense Sand	800,000	130	38	Mohr	0.3
Backfill	1,300,000	120	38	Mohr	0.2

A cylinder was used to represent the pile in the numerical model. This was done because of mesh generation requirements in FLAC3D.

Even though the steel pipes are always infilled with loose sand, three sand densities were used during the numerical simulations: loose, medium, and dense. This was done to investigate the influence of density and because initially loose sand might be densified by cyclic pile movements.

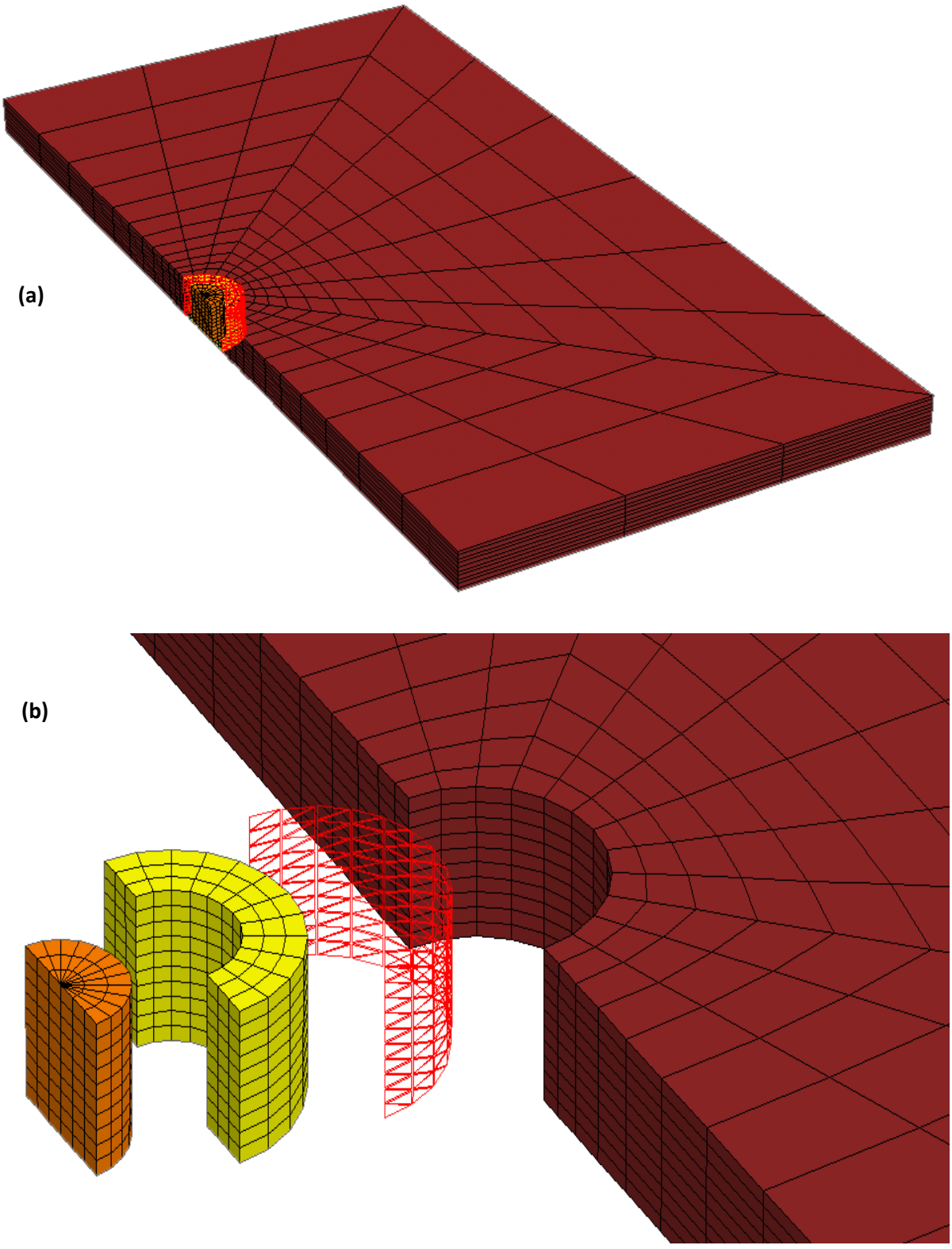

Figure 4.2 – Numerical model of pile-sand-sleeve system: (a) Full mesh of pile-sand-pipe system and (b) Zoomed-in and exploded view of pile-sand-pipe system, from left to right: pile, sand, steel pipe and backfill.

Two cases were analyzed, each one with two load sequences. In the first case, the model was initially subjected to gravitational forces, and then a vertical confining pressure of 1,300 psf was applied to the mesh surface (with no lateral displacement allowed at mesh boundaries). Once the model was in equilibrium, one of the load sequences was applied.

The second case is almost identical to the first case, but differs in the boundary condition imposed at the mesh surface. In this case, after the model was in equilibrium, the mesh boundary condition at the surface was changed to rollers, before one of the two load sequences was applied, thus no displacements are allow in the direction normal to the model surface.

The above cases represent two extreme boundary conditions to bracket the real soil boundary condition between these two cases.

For each of the above cases, two load sequences were applied:

- Loading Sequence 1: Pile is displaced monotonically until the soil fails.
- Loading Sequence 2: Pile is subjected to one year of cyclic thermal displacement (see section 4.1) and then it is displaced monotonically until the soil fails.

During the cyclic thermal displacement, the pile experiences a maximum total thermal displacement of 1" (Figure 4.1(a)), which corresponds to an integral abutment bridge of about 320 ft long and a temperature variation of 80 ºF, which represents typical conditions in Virginia according to the National Climatic Data Center (NCDC).

4.3 Results and Conclusions

Figure 4.3 and 4.4 graphically shows the result of the numerical model analysis. Figure 4.3 corresponds to the first case analysis, while Figure 4.4 corresponds to the second case. Figures 4.3(a) and 4.4(a) show results for non-cyclic loading, i.e. loading sequence 1. Results of the monotonic loading following the cyclic loading in loading sequence 2 are shown by Figures 4.3(b) and 4.4(b). Both figures display the force per unit length that is acting on the pile as it is displaced along the model symmetry line.

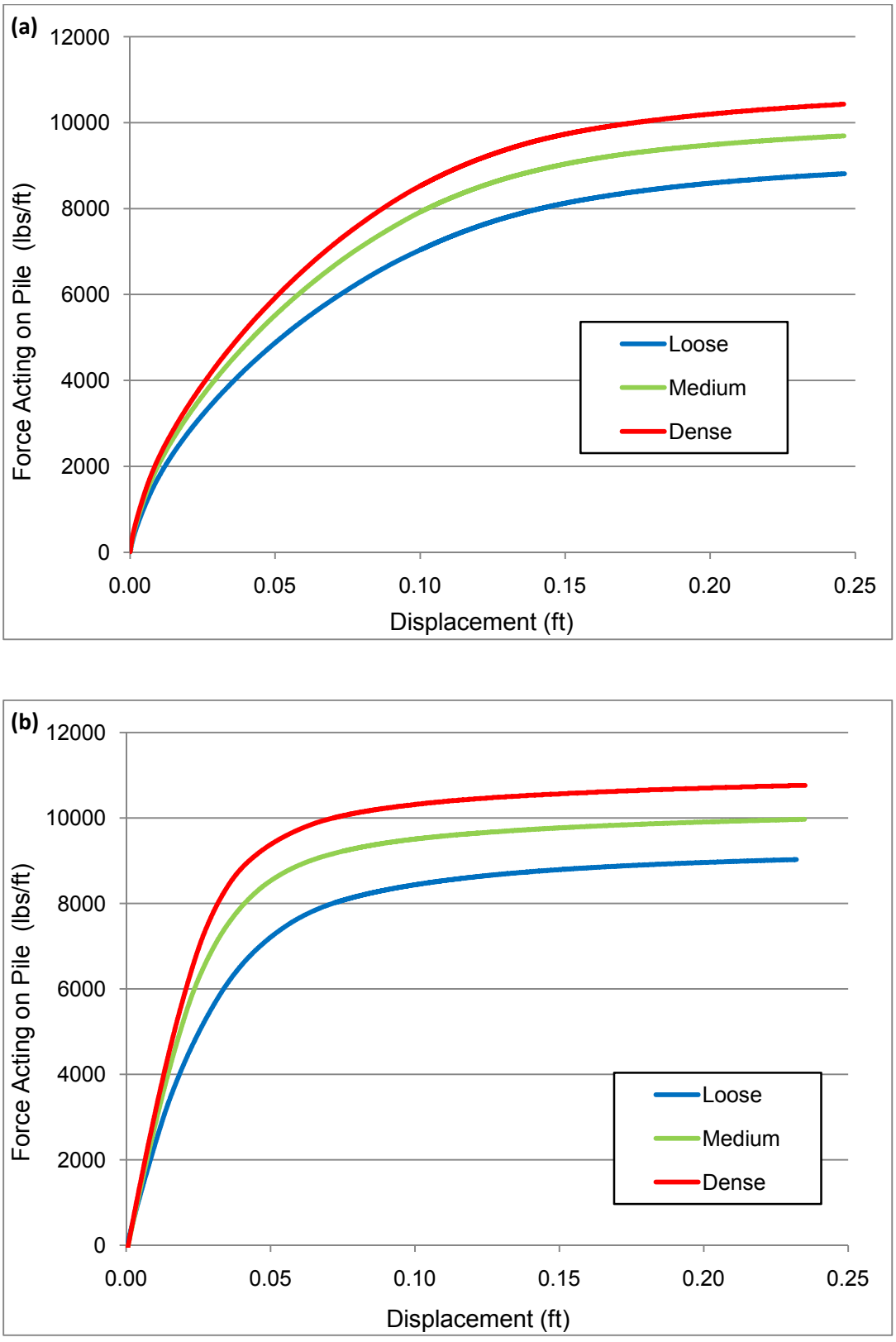

Figure 4.3 – First case analysis. (a) Load sequence 1 (b) Load sequence 2

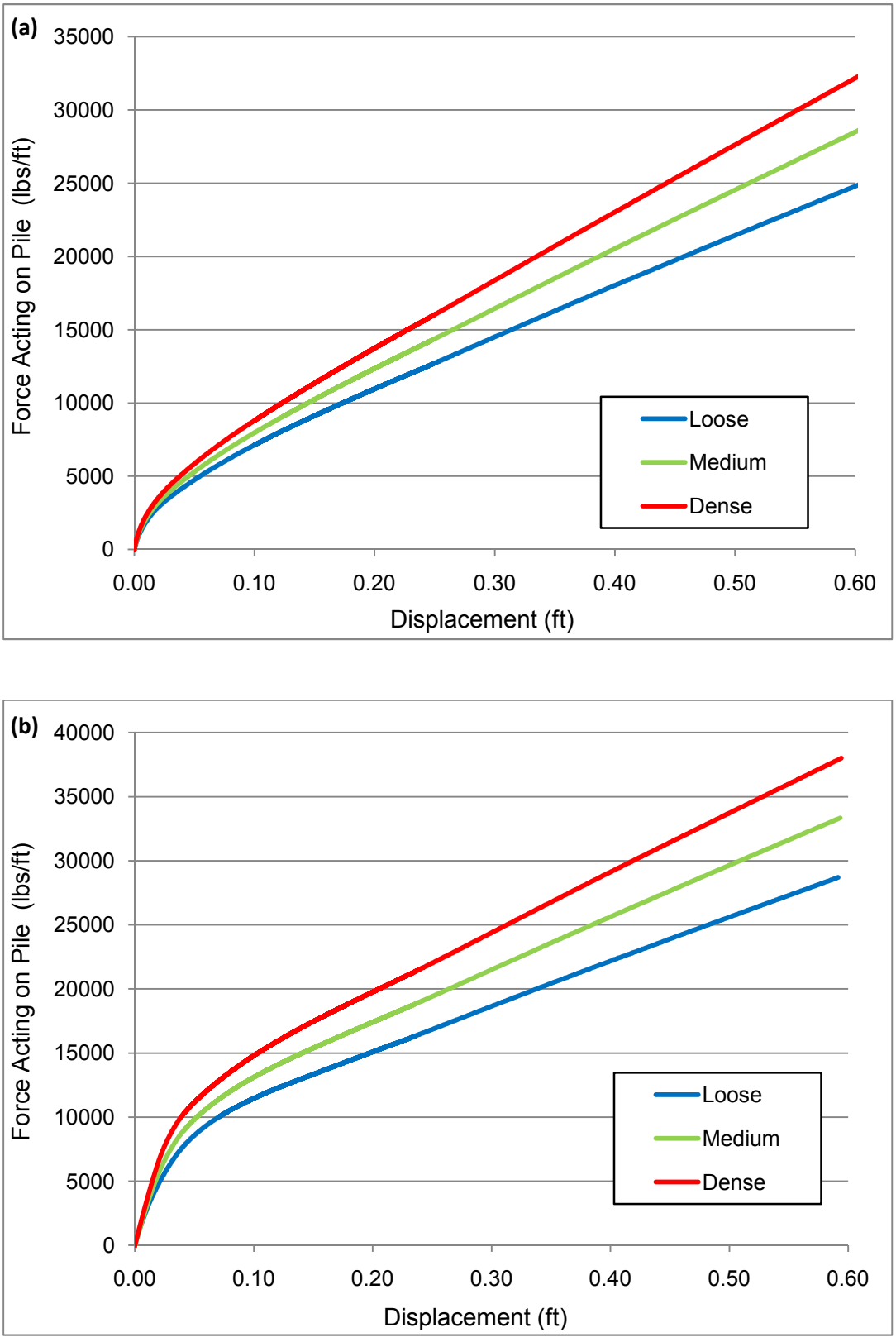

Figure 4.4 – Second case analysis. (a) Load sequence 1 (b) Load sequence 2

By comparing figures (a) and (b) in Figure 4.3 and in Figure 4.4, it can be seen that the soil has stiffened after one year of thermal displacement simulation. After this period of cyclic loading, the loose soil behaves even stiffer than the dense soil without the cyclic effect. The cyclically loaded soil is about twice as stiff as the soil without cyclic loading.

These results indicate that infilling steel pipes with loose sand will not reduce stresses on the pile, because the sand will densify due to the cyclic displacements. This indicates that the corrugated steel pipe sleeve will transfer as much displacement to the MSE wall as would be transferred without the sleeve.

This model was analyzed for a bridge 320 ft in length. The densification effect is expected to be greater for longer bridges, which it is the current trend, according to the national survey results described in Chapter 3.

CHAPTER 5

NUMERICAL MODELING PROCEDURES

A numerical model is a mathematical representation of a large scale structure. The goal of the model is to incorporate the important features of the large scale structure, while avoiding unnecessary complexity. The program FLAC3D was used to perform the calculations.

This chapter discusses the principal components of the model, the soil-structure interaction of strips and piles, the analysis methodology, and the research plan.

5.1 Model Principal Components

Figure 5.1 shows a cross section of an integral abutment bridge. The principal components considered in the numerical models are described below.

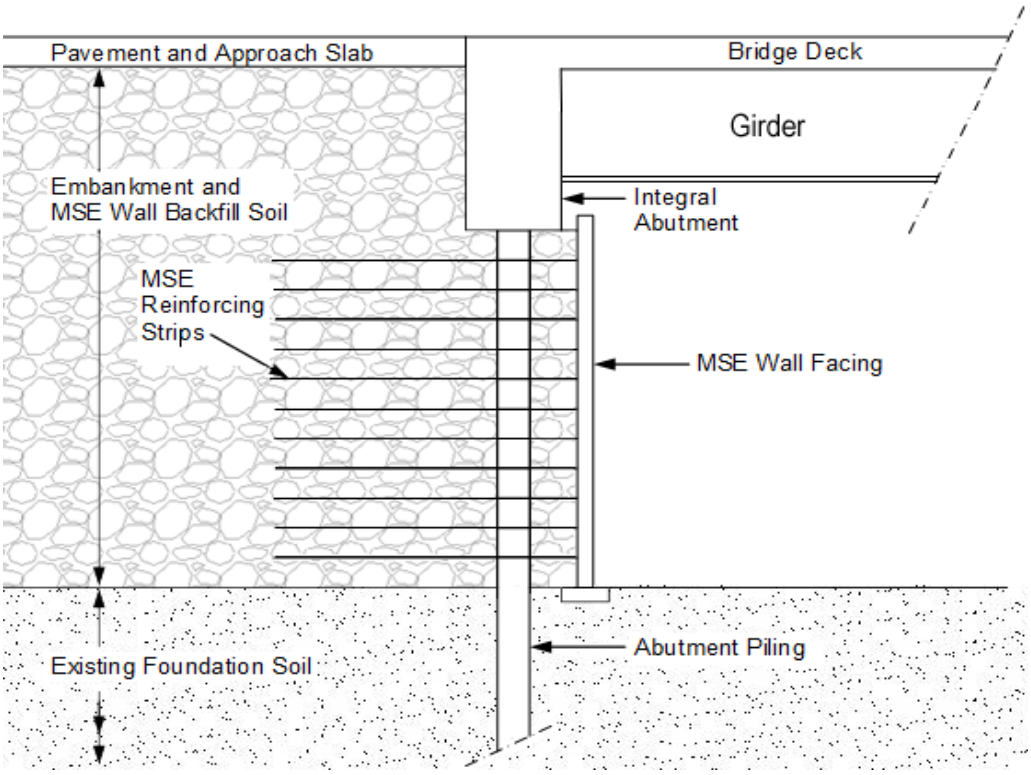

Figure 5.1 – Integral abutment bridge cross section

- **Foundation Soil/Rock**: The foundation geomaterial is the existing material in the field after surface clean up and excavation for the MSE wall foundation has been performed. This material was modeled with enough horizontal extent to avoid boundary effects on the model. VDOT personnel indicated that, in many circumstances, a competent bearing layer for foundation piling is encountered within 50 ft. Therefore all models included a foundation thickness of 50 ft.

- **Backfill**: VDOT and many states use a free draining aggregate for backfill, with less than 5% fines content (see Chapter 3). The aggregates considered in this study are either the ones used by VDOT or that used in the instrumented IAB in New Jersey and they are listed below.
    - #57 (VDOT et al. 2007)
    - 21B (VDOT et al. 2007)
    - I9 (Hassiotis et al. 2006).

  Although they have different designations and gradations, they all produce strong and stiff backfill when well compacted.

- **MSE Wall**: MSE wall systems typically include concrete panels, galvanized steel strips, and a pinned connection between the two. The concrete panels are 6 in. thick, they range from 3 to 12 ft wide, and they are 3 to 5 ft tall. The panels are placed in an alternate fashion, and they may have a rectangular, honeycomb, or cross shape. The steel strips can be prefabricated to any length, they are usually 2.5 to 3 in. wide, and they have small protuberances on the strip surfaces to improve friction with the backfill.

  In the numerical model, the concrete panels were simplified to shell elements with one strip connected to each element. The size of each shell element is such that the horizontal shell dimension corresponds to the horizontal strip spacing and the vertical shell dimension corresponds to the vertical strip spacing. The strips were represented by uniaxial elements in FLAC3D. This element is capable of being connected to the shell element and also being embedded in the backfill material. The interaction of the strip

element with the backfill material is achieved through a series of shear springs (See section 5.2).

- **Piles**: The most common abutment pile used by VDOT is the steel H pile, and therefore only H piles were considered in this research. The tips of the piles were pinned to represent contact with competent rock. The interaction with the foundation and backfill material was achieved through a series of normal and shear springs (See section 5.2)

- **Abutment**: VDOT only uses three types of abutment designs; steel dowel, laminated pad and solid abutment.

  Steel dowels are the most commonly used abutment design in Virginia. The abutment is divided into two structures: the upper portion where the girders are embedded and the pile cap. The joint between these two structures uses dowels. The dowels are steel bars, 7/8" diameter and 2 feet long, which are equally spaced along the bridge abutment.

  Laminated pads are the second most common abutment design used in Virginia. The upper portion of the abutment where the girders are embedded is connected to the pile cap with a laminated pad. The laminated pad is a special rubber block with mainly horizontal steel reinforcement. The laminated pads have high compression resistance and low shear resistance.

  Solid abutments are solid monolithic structures, with no joint between the abutment upper portion and the pile cap.

- **Girders**: In this research, the bridge girders are high performance steel (HPS) beams, which can be prefabricated to almost any length. The girders were represented by FLAC3D uniaxial elements called "beams". They are embedded in the abutment upper portion, and therefore they are able to transmit moment and displacement.

- **Bridge Deck and Approach Slab**: Neither the bridge deck nor the approach slab were separately represented in the numerical model, but the dead weight, stiffness, and in-plane constraints of the bridge deck were added to the girders.

- **EPS:** An elasticized polystyrene material was placed between the abutment backwall and the backfill soil for the base-case VDOT analysis and for most of the parametric analyses. This material is such that it responds as an approximately linear elastic material for strains up to 10%. In FLAC3D, this material was represented by a fine mesh of elastic tetrahedral elements.

- **Interfaces:** Three interfaces were defined in the models. The first interface is placed between the backfill soil and the EPS material. The second and third interfaces are both placed at the abutment, one over the pile cap portion of the abutment and the other in the upper portion of the abutment. Interfaces allow element surfaces to slide, separate, and come back into contact. Additionally, interfaces allow obtaining stress values right at the inter-element boundary, without having to perform interpolations or extrapolations.

5.2 Strips and Piles: Soil-Structure Interaction

The strip and pile properties are divided into two categories: mechanical and interaction properties. Mechanical properties are those inherent to the structural element, such as Young's modulus, moment of inertia, area, etc. Interaction properties are those that allow interaction between the structural component and the surrounding media. In this section, the focus is on the interaction properties.

Strips and piles are represented in FLAC3D using one dimensional finite elements, and they interact with the surrounding soil through spring connections. These springs have properties that allow FLAC3D to represent the interaction behavior of the structural component with the backfill material. The spring properties are computed for each specific combination of geometry, soil, structural component, and boundary condition.

The strip and pile interaction properties are:

- Strips
    - c_s, shear cohesive strength
    - ϕ_s, shear friction angle
    - k_s, shear stiffness
- Piles
    - c_s, shear cohesive strength
    - ϕ_s, shear friction angle
    - k_s, shear stiffness
    - c_n, normal cohesive strength
    - ϕ_n, normal friction angle
    - k_n, normal stiffness

In addition to the properties listed above, piles may include tip resistance properties (analogous to the normal properties). Tip resistance properties are used when piles are embedded in soil, without reaching competent rock, so that a limited tip capacity can be included in analyses. Tip resistances were not necessary in these analyses because the piles were assumed to bear on competent a rock foundation.

5.2.1 Spring Constitutive Model

Two types of spring are built in FLAC3d software, shear and normal springs. The constitutive model for shear springs in FLAC3D is shown in Figure 5.2. Figure 5.2(a) shows a plot of the bilinear spring response. As the spring deforms, the shear force per unit length in the spring increases. Deforming the spring means that the distance between the node of the structural component and the hosting media has changed. For a given deformation, the spring shear force increases with increasing spring stiffness, k_s, and it reaches a limiting value of Fs^{max} / L (Figure 5.2(b)), which is defined in Eq. 5.1.

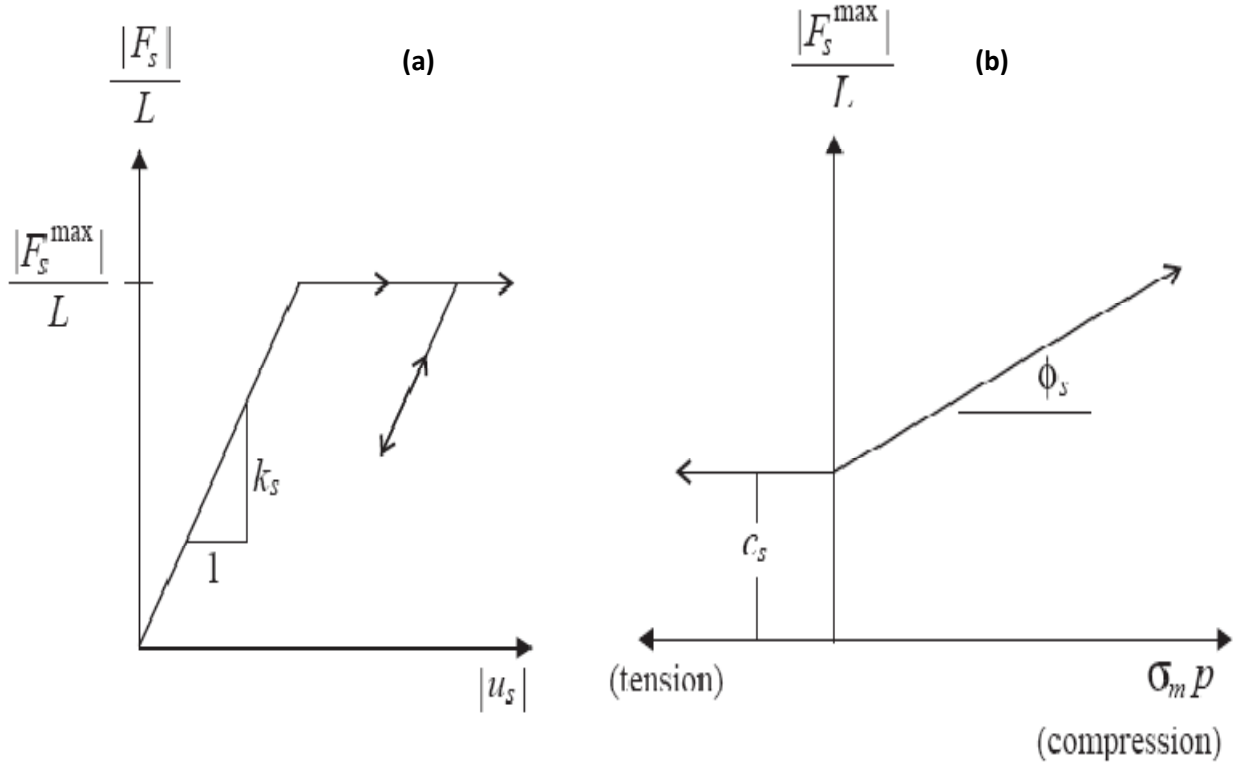

Figure 5.2 – Shear spring constitutive model (from FLAC3D manual): (a) Shear force/length vs. relative shear displacement, u_s, (b) Shear-strength/length vs. confining pressure times perimeter.

$$Fs^{max} / L = c_s + \sigma_m * p \tan(\phi_s) \quad (5.1)$$

where

c_s = shear interface cohesive strength per unit length

σ_m = average confining pressure

p = element exposed perimeter

ϕ_s = shear interface friction angle

Equation 5.1 defines the maximum interface shear force at which magnitude the structural element can slide through the hosting media.

Analogous to the shear spring interface, a normal spring interface is also connected at the structural element node. The constitutive model for normal springs is presented in Figure 5.3. The normal spring model is very similar to the shear spring model but with one exception, the

normal force minimum value can be zero or it can take negatives values depending how the FLAC3D option called "gap" is set, while the shear force minimum value is always zero. In this research, shear spring properties are used by MSE wall strips and piles, and normal spring properties are used by piles.

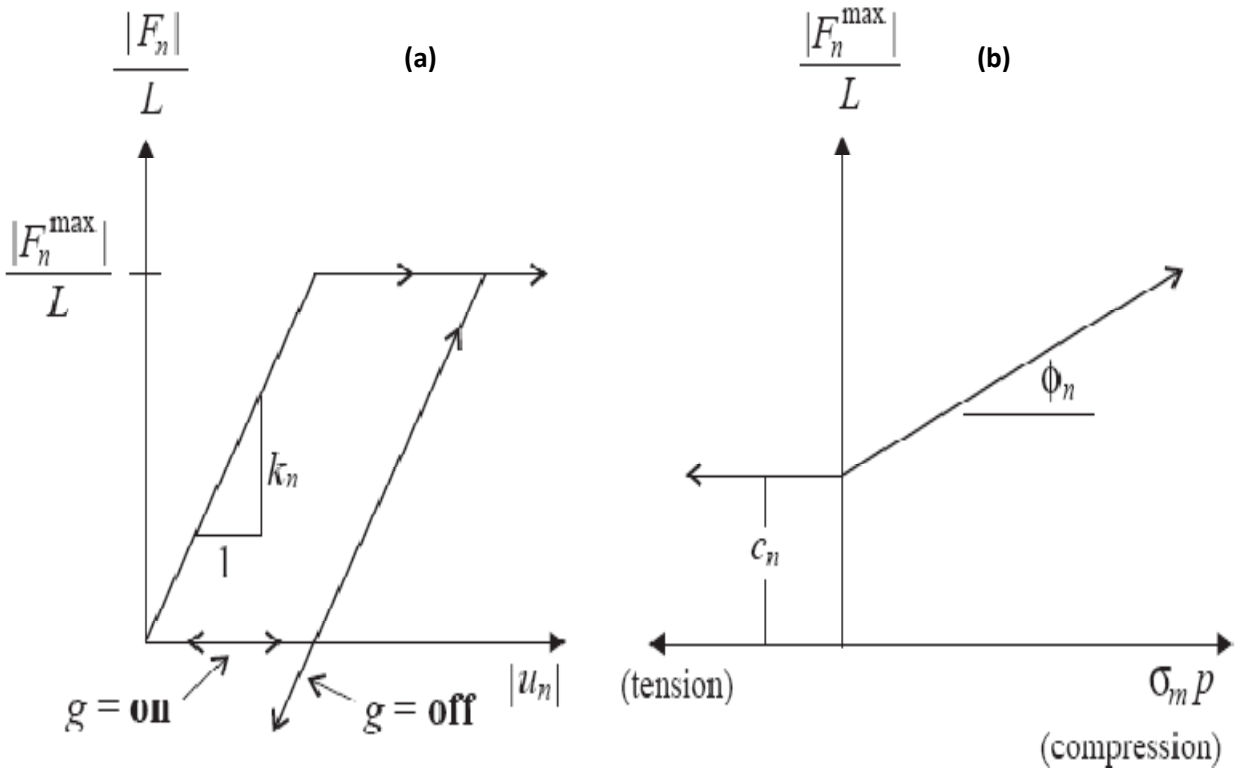

Figure 5.3 – Normal spring constitutive model (from FLAC3D manual): (a) Normal force/length vs. relative normal displacement, u_n, (b) Normal-strength/length vs. confining pressure times perimeter.

5.2.2 Spring Property Computation

This section describes the procedure to compute the spring properties. The procedure was repeated several times during this research to compute shear and normal spring properties.

To illustrate how to compute the spring properties, computation of pile normal spring properties are illustrated here, but this procedure can be applied to obtain normal or shear properties sets.

The following steps describe a procedure to compute interface parameters:

- Create a 3D model of the structural component and the surrounding hosting media. The model must include an interface between the structural component and the surrounding media, thus sliding or separation may occur.
- Select and apply a surface pressure to the model. This pressure represents the depth at which the structural component is located.
- Apply a constant displacement to the structural component. The displacement must be carry out beyond interface yield force. In this example the displacement must be normal to the pile axis.
- Record the applied force over the structural component, the average confining pressure and the displacement.
- Create a plot of Fs/ L vs. displacement.
- Repeat the above procedure for at least one more surface pressure. Although only two confining pressures are required, three confining pressures were used in this research for all models.

Figure 5.4 shows a symmetric model representing a single pile and the surrounding backfill material. In addition to the pile and soil elements, interface elements were placed around the pile elements (shown in blue). Note that the interface properties can be assumed based on published values because they represent a directly measurable shear stiffness and strength, which is in contrast to the calculated value of normal spring stiffness and strength for the pile, which are calculated to represent the three-dimensional problem of the pile moving into the soil.

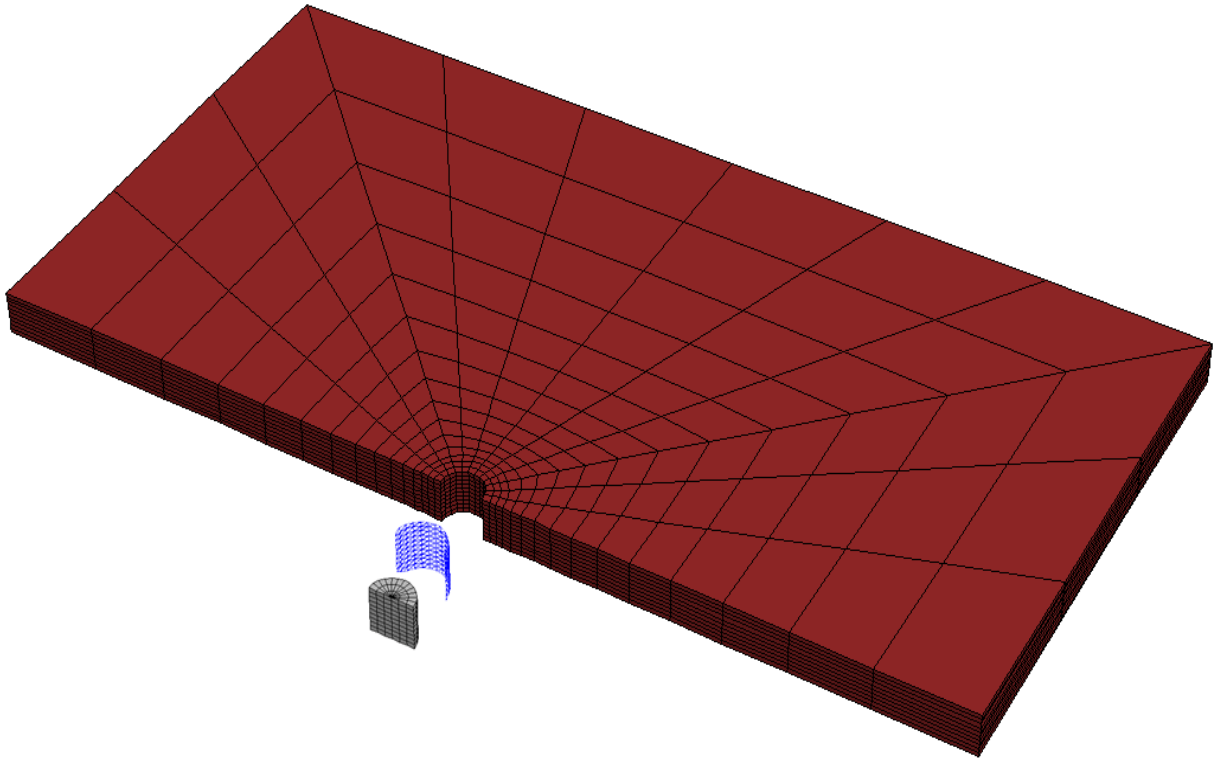

Figure 5.4 – Single pile 3D mesh

The blue line in Figure 5.5 shows the force exerted over the pile versus the pile lateral displacements. Toward the end of the analysis, it is possible to observe how the soil starts to fail under compression. As the test progresses, the soil can withstand no more load, and the force curve reaches a maximum value of 9,694 lbs/ft.

A red line has been added to Figure 5.5 to represent the average stiffness of the interface during loading prior to failure. The initial stiffness is computed as:

$$k_n = \frac{9{,}694}{0.11} = 88{,}127 \text{ lbs/ft/ft}$$

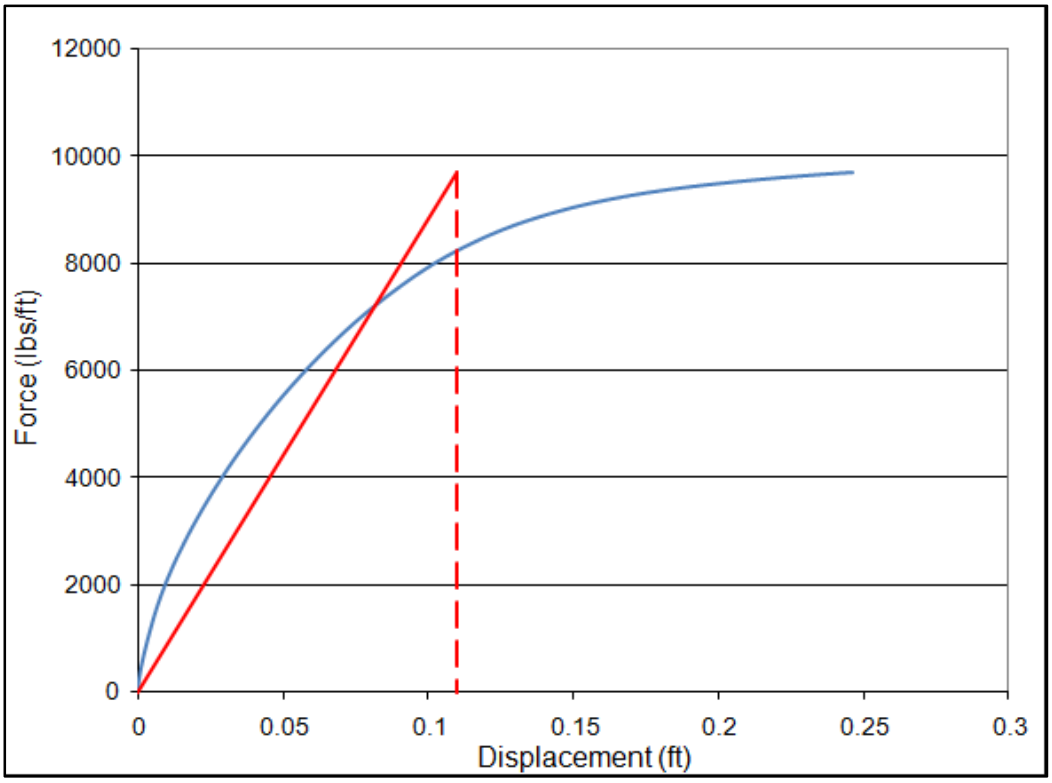

Figure 5.5 – Force exerted over pile vs. pile lateral displacement

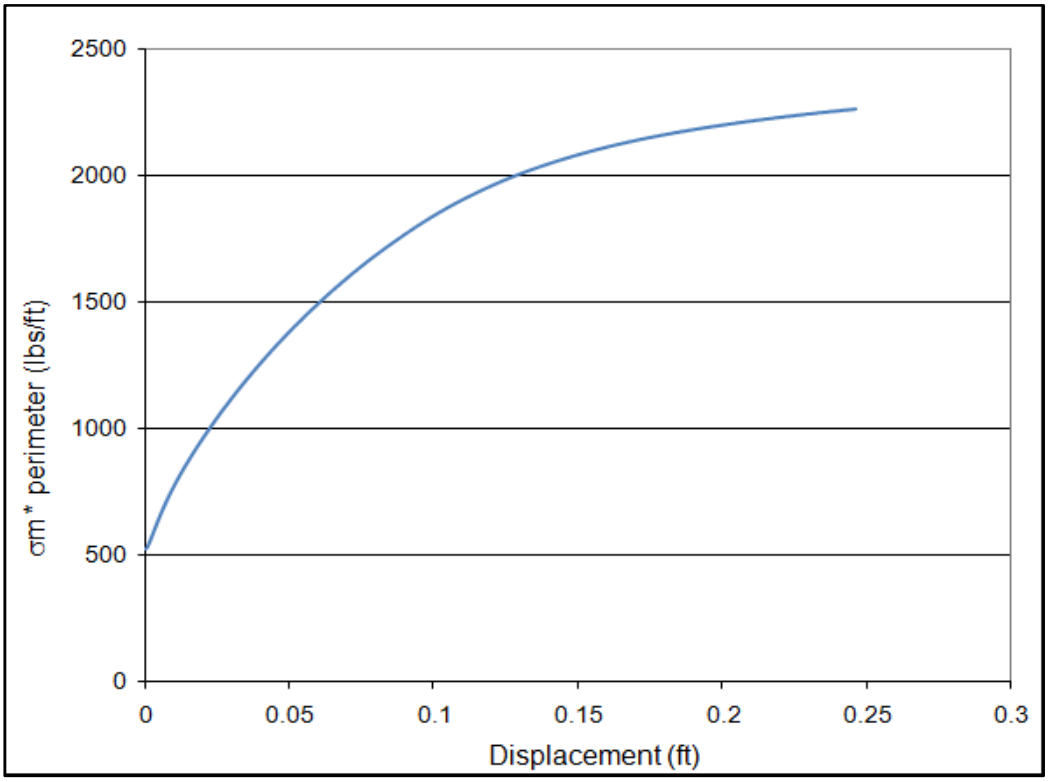

Figure 5.6 – Average confining pressure times pile perimeter vs. displacement

Figure 5.6 shows the pile displacement versus the average confining pressure times the pile perimeter. This parameter was monitored during the test previously described and it provides the average confining pressure around the pile when the soil fails.

Two additional analyses were completed at other confining pressures. Table 5.1 shows the results for all three analyses.

Table 5.1 – Pile lateral displacement test results

Force/L lbs/ft	**σm * p lbs/ft**	**Stiffness lbs/ft/ft**
9,694	2,263	88,127
16,730	3,868	97,267
31,686	7,326	95,569
	Average	93,655

Figure 5.7 shows the graphical representation of Table 5.1 following the scheme presented in Figure 5.2(b).

The first point on the line in Figure 5.7 is the test shown in Figures 5.5 and 5.6. That point has an x coordinate corresponding to the maximum confining pressure times the perimeter obtained from Figure 5.6 and y coordinate corresponding to the maximum force exerted over the pile obtained from Figure 5.5.

Once all three tests are plotted, a trend line was added and its equation is displayed at the upper left corner of Figure 5.7. From this equation, one can compute the normal spring "friction angle" and the spring "cohesive strength" per unit length.

The spring friction angle is computed as:

$$\phi = \tan^{-1}(4.3407) = 77^{o}$$

The spring cohesive strength is equal to 101 lbs/ft

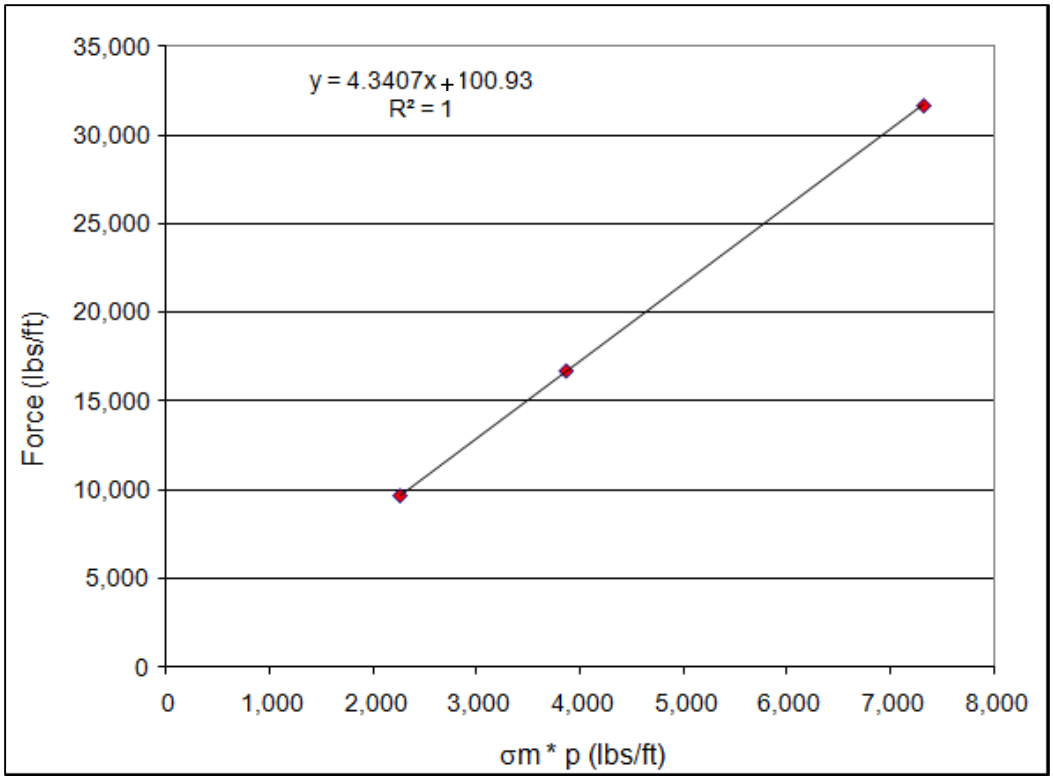

Figure 5.7 – Average confining pressure times pile perimeter vs. force exerted on pile (Table 5.1)

Summarizing, the pile normal spring properties are:

- c_n = 101 lbs/ft
- ϕ_n = 77 degrees
- k_n = 93,655 lbs/ft/ft

5.3 Analysis Methodology

5.3.1 FLAC3D

As previously mentioned, FLAC3D was the selected program to perform all the numerical analysis, because it is one of the few 3D geotechnical programs available that provide the user with absolute flexibility to control the analyses. Other existing 3D numerical programs are either not a complete package or they are limited to certain 3D geotechnical analyses. In addition, FLAC3D has been widely used by practitioners and the research community, and it has become

one of the standard programs for use in geotechnical numerical analysis. Also, FLAC3D is a dedicated geotechnical program, i.e., the geotechnical analysis capabilities are not just an expansion option of a base software package created for structural engineering applications. Instead, FLAC3D has been created as a powerful and comprehensive geotechnical tool for analysis. Finally, the FLAC3D solving engine is based on finite different analysis that has some advantages over finite element codes, including capability to handle large displacements and strains of unstable systems, including yield/failure over large areas or total collapse.

5.3.2 Constitutive Models

The constitutive models used for structural materials and soils in this research are elastic isotropic, elastic anisotropic, and Mohr Coulomb.

The elastic isotropic model was used for reinforced concrete and steel materials. Reinforced concrete was used in the abutment, pile cap, and MSE wall panels. Steel was used for the MSE wall strips, girders, and dowels.

The elastic anisotropic model was used for the laminated pad connection between the abutment and the pile cap. The elastic anisotropic model, which is also called the transversely isotropic model, gives the ability to simulate a layered elastic media, in which there are distinct elastic moduli in directions normal and parallel to the layers, as in a laminated pad.

The Mohr Coulomb model implemented in FLAC3D is conventional common model for representing shear failure in soils and rocks. This model uses a tension cut off and a non-associated flow rule. This model was used to simulate the behavior of shale foundation material, silty sand foundation soil, and backfill materials.

5.3.3 Construction Sequence

The construction sequence of each IAB model implemented in FLAC3D started with the foundation soil. The foundation soil mesh extended far enough from the central area of interest in the model that the foundation soil boundaries did not influence the results.

Once the foundation mesh was solved under gravitational forces to establish initial stresses, the MSE wall construction started. The MSE wall was constructed in 14 stages, ten of them corresponding to the MSE wall portion under the abutment, and the rest correspond to the MSE wall behind the abutment. Each stage consisted of backfill placement, concrete panel positioning in front of the backfill (forming the front MSE wall and the wingwalls), and placement of a layer of reinforcing strips. Before solving each stage for gravitational forces, all spring interfaces were attached to the backfill material, and the strip was connected to the concrete panel. Once the first stage of the MSE wall was under gravitational stresses, a new layer of backfill material was placed along with the corresponding concrete panels and MSE wall strips.

After the main portion of the MSE wall, i.e., the first 10 stages, was constructed and solved for gravitational forces, the piles were placed in the main body of the MSE wall fill and the foundation soil. As previously mentioned, the piles were fixed at the bottom of the model, representing contact with competent rock. Enough length was left above the main MSE wall portion to permit later embedment of the piles in the pile cap. It is worth noting that in the actual construction sequence, the piles are driven in the natural foundation soil before the MSE wall construction. The sequence used in the analyses facilitates connecting the pile springs to the backfill. As previously mentioned, this sequence should not significantly affect the results because of the following: First, the main objective of the research is to determine the incremental effect of thermal displacements. Gravitational effects are subtracted from final results. Second, the downdrag forces acting on the piles are smaller than the gravitational forces due to the superstructure self weight. Third, the axial loads on the piles are less affected by thermal displacements than any other output, as later demonstrated by this research.

After piles were in place, one of the abutment types was created around the length of the piles extending above the main body of the MSE wall fill.

Immediately after the abutment was ready, girders were placed in the model and embedded in the abutment upper portion. Although, the bridge deck was not separately modeled, its self weight, bending stiffness, and in-plane constraints exerted on the girders were included in the girder representation.

The model construction was completed by placing the remaining 4 stages of MSE wall and fill behind the abutment. Each stage was subdivided into 2 steps. In the first step, EPS material was placed behind the abutment and one of the interfaces was placed between the two materials. The EPS was supported by rollers to allow FLAC3D to solve the model for gravitational forces. In the second step, the rollers supporting the EPS material were removed, and the backfill material along with MSE panels and strips for the side walls were placed, and another interface was placed between the backfill and the EPS material.

Finally, a very important FLAC3D programming step was added to the model to obtain histories to track all the important outputs of the numerical model. The model was then ready to be subjected to thermal displacements.

5.3.4 Loading Considerations

During this research, only gravitational forces were imposed on the bridge model; no traffic loads were applied. This research focuses on the net impact of thermal displacements on the bridge response. The net impacts were computed by subtracting the gravitational effects from the final bridge response results.

5.3.5 Boundary Conditions

As previously stated, rollers were added to all faces around the foundation mesh and in the back of the bridge embankment fill.

During gravity analysis, the girder center line is allowed to freely move vertically, and the remaining degrees of freedom are constrained. During thermal displacement analysis, the only movement allowed in the girders was in the direction of their alignment, again with the rest of the degrees of freedom constrained.

Lateral movements of the MSE wall were constrained by the concrete panels comprising the MSE wall face.

5.3.6 Thermal Displacements

In this research, the thermal displacements calculated from the temperature change, the bridge length, and the coefficient of thermal expansion were imposed at the bridge centerline. The annual thermal cyclic displacements were simulated using equation 4.1.

Because the bridge girders are so stiff, the abutment displacements are almost exactly the same as the displacements imposed at the bridge centerline. Alternatively, coupled thermo-elastic analyses could be performed in which the bridge temperature changes would be imposed and the response calculated. Because the bridge girders are so stiff, large differences are not expected between coupled thermo-elastic analyses and the analyses described herein.

5.4 Research Plan

The research plan to investigate IAB performance includes two main parts, whose details and results are described in the following two chapters. Chapter 6 deals with the validation of the numerical model. In order to achieve this task, a model of an integral abutment bridge was created and calibrated using the program FLAC3D. The model was based on a New Jersey integral abutment bridge. This bridge was selected because it was instrumented and measurements had been taken for three years, which produced field data to use in calibrating and validating the numerical model.

Chapter 7 presents the analyses that comprise the main body of this research. First, a base case model was created and studied. Knowledge acquired from the calibration stage of the New Jersey bridge was applied when creating the base case model, which was modeled after a Virginia DOT bridge under construction in Alexandria, Virginia. This bridge was selected because it represents the current state of Virginia DOT practice, and it was being instrumented to obtain data that can be used for future validation of the model.

Chapter 7 also presents the results of different single parameter variation models that were created by changing one parameter at a time from the base case to determine their respective effects on the bridge performance. Later in Chapter 7, the research addresses multiple parameter variations that involved changing more than one parameter at a time from the base case model. This was done with the objective of obtaining useful correlations between the bridge input conditions and the response parameters. As described in Chapter 8, once these correlations were calibrated against the available data, they were implemented in a simple spreadsheet.

CHAPTER 6

MODEL CALIBRATION

To validate FLAC3D capabilities of modeling the interactions of an integral abutment bridge, as well to calibrate the numerical model, a comparison between numerical model output and field data was performed, as well as a comparison between FLAC3D and MSEW software. Details of the model, material properties and results, are discussed in this chapter.

6.1 Base Case – Integral Abutment Bridge over I-95, Trenton, NJ

6.1.1 Bridge Description

The integral abutment bridge described by Hassiotis et al (2006) was selected for the calibration and validation studies because it was instrumented and monitored for over three years. The bridge is located in the vicinity of Trenton, New Jersey. It was built over Interstate 95 (I-95) where Scotch Road crosses over the highway. Figure 6.1 shows an aerial view of the bridge.

The main bridge characteristics are:

- Six lanes with an overall width of 104.3 ft.
- Two continuous spans.
- Deck is supported by eleven HPS70W steel girders with a total length of 298 ft.
- The bridge has a skew angle of 15°.
- The abutments are 11 ft high with a cross section of 3 ft.
- Each abutment is supported on a single row of nineteen HP360x152 piles.
- Piles are oriented for weak axis bending.
- The piles are approximately 38.5 ft long and they rise about 15 ft above the foundation elevation.
- Each pile is surrounded by a corrugated steel sleeve backfilled with loose sand.
- The embankment is 24 ft high and the main MSE wall height is 14 ft.
- There are no wingwalls or U-back walls, only small and short “elephant ears”.

Figure 6.1 – Scotch Road integral abutment bridge

According to Hassiotis et al (2006), the bridge is still under observation to obtain measurements that will address long term interactions, including monitoring the observed build up of pressure behind the abutment. Hassiotis et al. (2005) and Hassiotis et al. (2006) describe in detail the project, the instrumentation, analyses, and conclusions reached.

The finite element model developed by Hassiotis's team only include a limited representation of the soil-structural interactions, i.e., their numerical analysis did not model the following system components: the foundation materials, the embankment soil, the MSE wall panels, or the MSE wall strips. The embankment soil was not explicitly modeled either behind the abutment or behind the MSE wall. Rather than model the embankment geometry and interactions, they used linear springs only behind the abutment and under the approach slab. Therefore, it is not very worthwhile to attempt comparing results from their numerical model with the results from this research. However, the field data from the report appendices by Hassiotis et al. (2005, 2006) is very useful for calibrating and validating the FLAC3D modeling approach used in this research.

6.1.2 Material Properties

Table 6.1 shows the material properties used in this research for FLAC3D numerical analyses of the Scotch Road IAB.

Table 6.1 – Material properties for Scotch Road numerical model

Material	Elastic Modulus E, psf	γ, pcf	ϕ, deg	Cohesion, psf	Model	Poisson ratio ν
Concrete	597e6	145	-	-	Elastic	0.14
Steel	4,177e6	485	-	-	Elastic	0.3
Shale	10,000,000	130	20	4000	Mohr	0.29
Backfill	1,300,000	120	38	-	Mohr	0.2

The properties shown in Table 6.1 are elastic modulus, unit weight, angle of internal friction, cohesion, and Poisson's ratio. The strength and deformability parameters were obtained by correlating typical soil values found in specialized geotechnical literature with the boring log information. The main references used in this research are "Soil Mechanics in Engineering Practice" by Terzaghi, et al. (1996), "Soil Strength and Slope Stability" by Duncan and Wright (2005), and FLAC3D recommendations (Itasca 2006).

Although FLAC3D requires shear modulus and bulk modulus as input for the Mohr Coulomb model, the information was presented in terms of elastic modulus and Poisson's ratio because those parameters allow for a better understanding of the physical properties.

Concrete material properties were assigned to the abutment and MSE wall concrete panels. Steel material properties were assigned to the MSE wall strips, girders, and abutment piles. Above the foundation elevation, piles went through the embankment, i.e., through the MSE wall fill material, and below this level, the piles were placed in the shale bedrock.

Table 6.2 shows the spring interface properties, which were computed following the procedure described in Section 5.2.

The structural elements have the following properties:

- Abutment H Piles
  - Area 30 in^2
  - Strong Moment of Inertia 1,050 in^4
  - Weak Moment of Inertia 380 in^4
  - Perimeter 57.6 in
- Girders
  - Area 147 in^2
  - Strong Moment of Inertia 113,036 in^4
  - Weak Moment of Inertia 4,323 in^4
- MSE wall strips
  - Area 3.5 in^2
  - Perimeter 9 in
- MSE wall panels
  - Thickness 6 in

Table 6.2 – Spring interface properties for Scotch Road numerical model.

Material Set #	Used for	Embedded in	Direction	Stiffness, k lbs/ft/ft	Cohesion, c lbs/ft	Friction Angle ϕ, degree
1	Strip	Backfill	Shear	1,843,111	0	37.7
2	Pile	Backfill	Shear	3,476,502	4	23.3
3	Pile	Backfill	Normal	283,254	112	76
4	Pile	Shale	Shear	14,128,684	0	12.9
5	Pile	Shale	Normal	1,369,500	10,076	71.6

6.1.3 Numerical Model Output Calibration

Field measurements used to calibrate the numerical model included the earth pressures behind the abutment and the moments in the foundation H piles immediately under the abutment. Earth pressures were monitored at two elevations. Figures 6.2 and 6.3 show the earth pressures measured behind the bridge abutment, at the location of pile number 9, near the centerline of the bridge. These figures illustrate the earth pressure at elevation 58 m and 56.5 m, respectively, which correspond to 2/3 and 1/5 of the abutment height. Figure 6.4 shows the foundation H pile

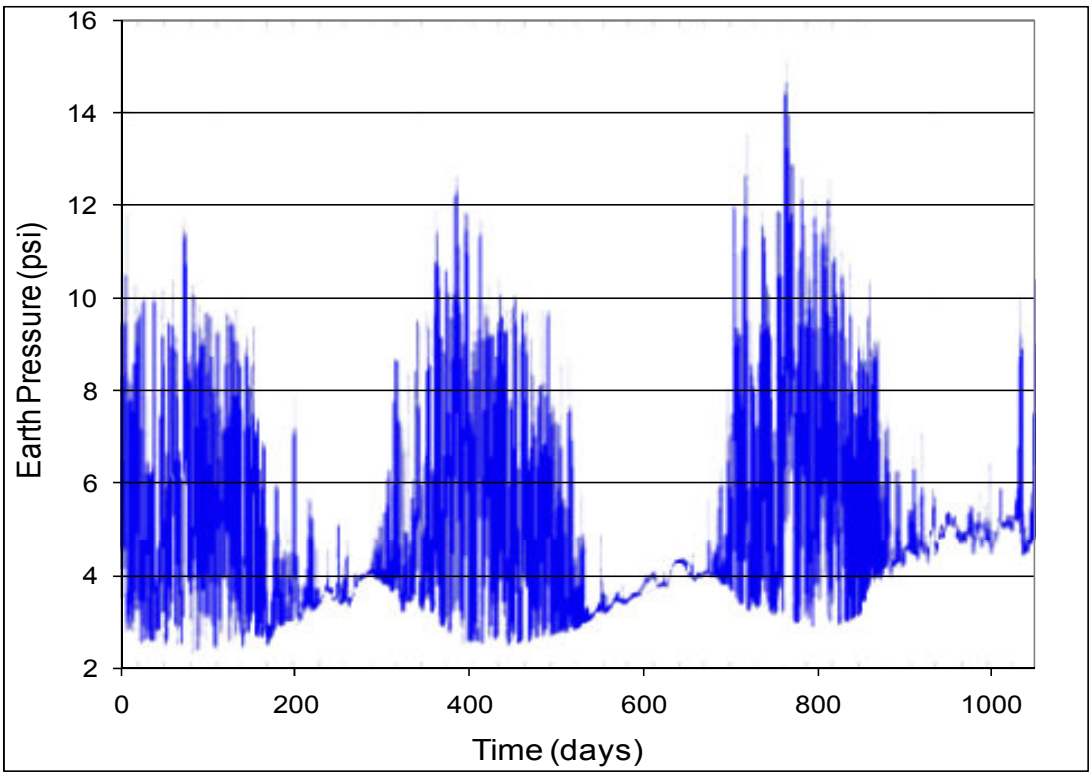

Figure 6.2 – Earth pressure behind the abutment, elevation 58 m

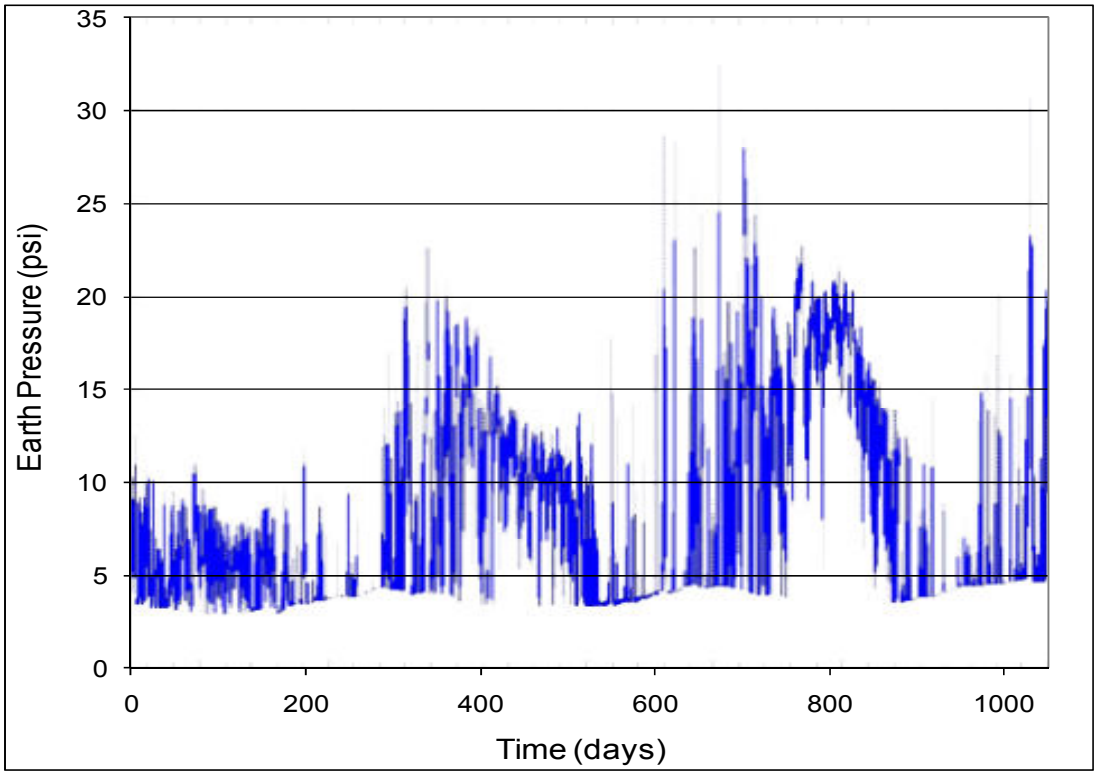

Figure 6.3 – Earth pressure behind the abutment, elevation 56.5 m

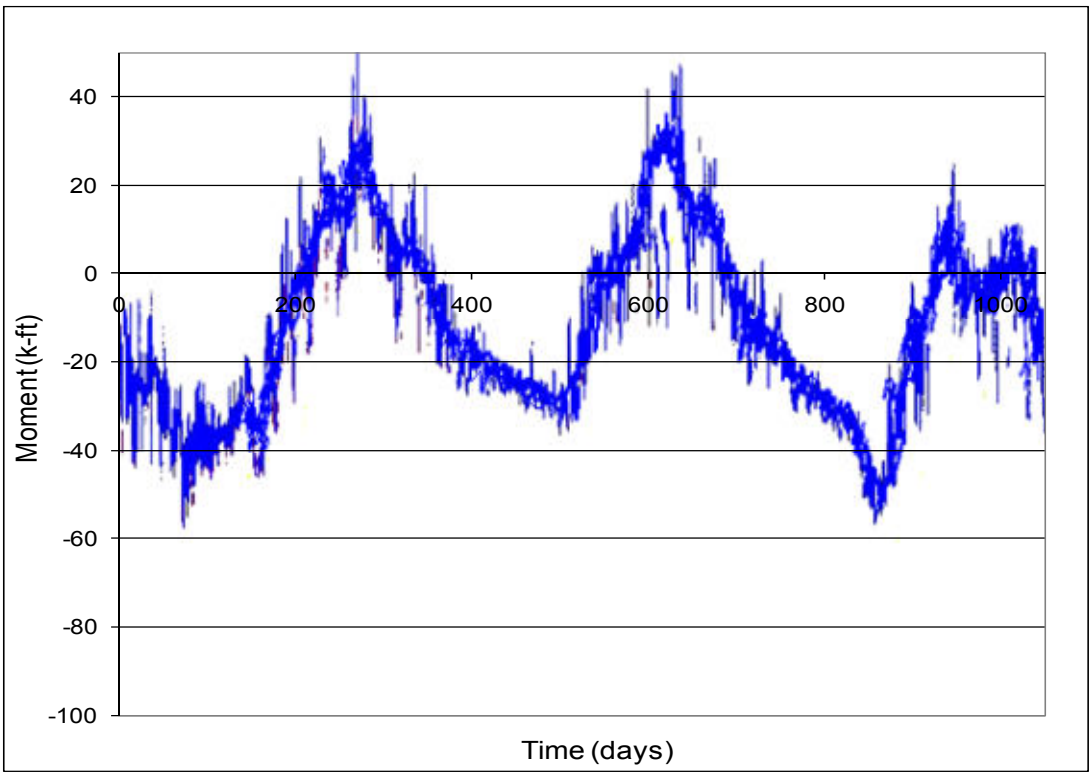

Figure 6.4 – Foundation H Pile moment, elevation 55.7 m

moment, measured at elevation 55.7 m, directly under the abutment. This measurement is located on pile number 9.

Ranges of reasonable strength and deformability parameters of the soil behind the abutment and beneath the abutment were obtained by correlation with index property values and SPT N-values, using the references mentioned above in Section 6.1.2. The specific values from within these ranges listed in Table 6.1 were selected to obtain a reasonable match between field measurements and numerical model outputs. Figures 6.5, 6.6, and 6.7 show the superposition of the numerical model outputs over the field measurements of Figure 6.2, 6.3, and 6.4.

Figures 6.5, 6.6, and 6.7 show that good agreement between field measurements and FLAC3D output was achieved, even though some of the field measurements exhibit erratic behavior. According to Hassiotis et al. (2006), the erratic values observed in the field measurements are due to freeze and thaw cycles and instrument reading failures.

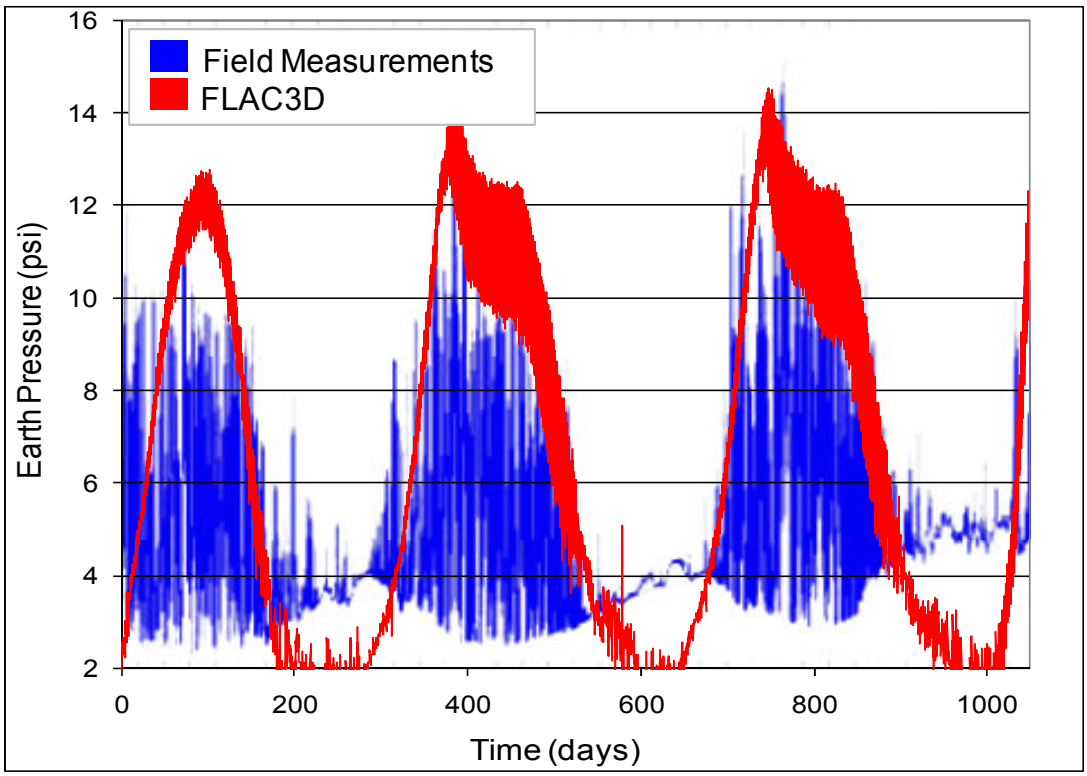

Figure 6.5 – Comparison between field measurement and FLAC3D. Earth pressure behind abutment at elevation 58 m

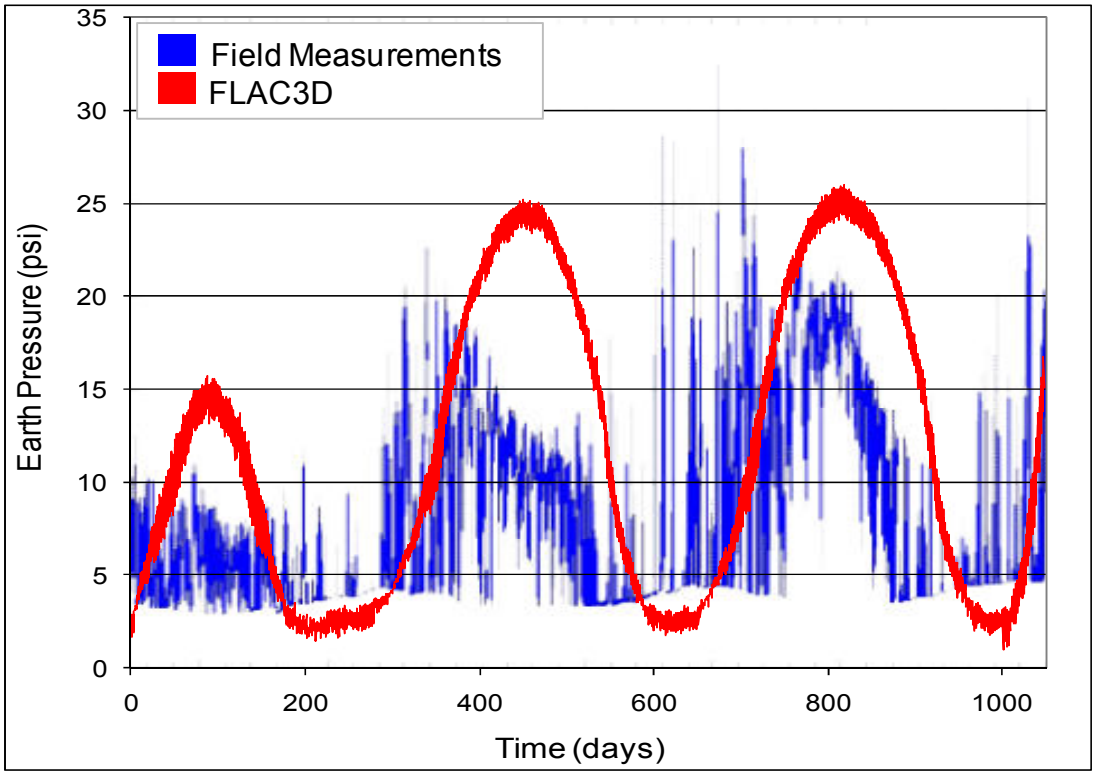

Figure 6.6 – Field measurement and FLAC3D. Earth pressure behind abutment at elev. 56.5 m

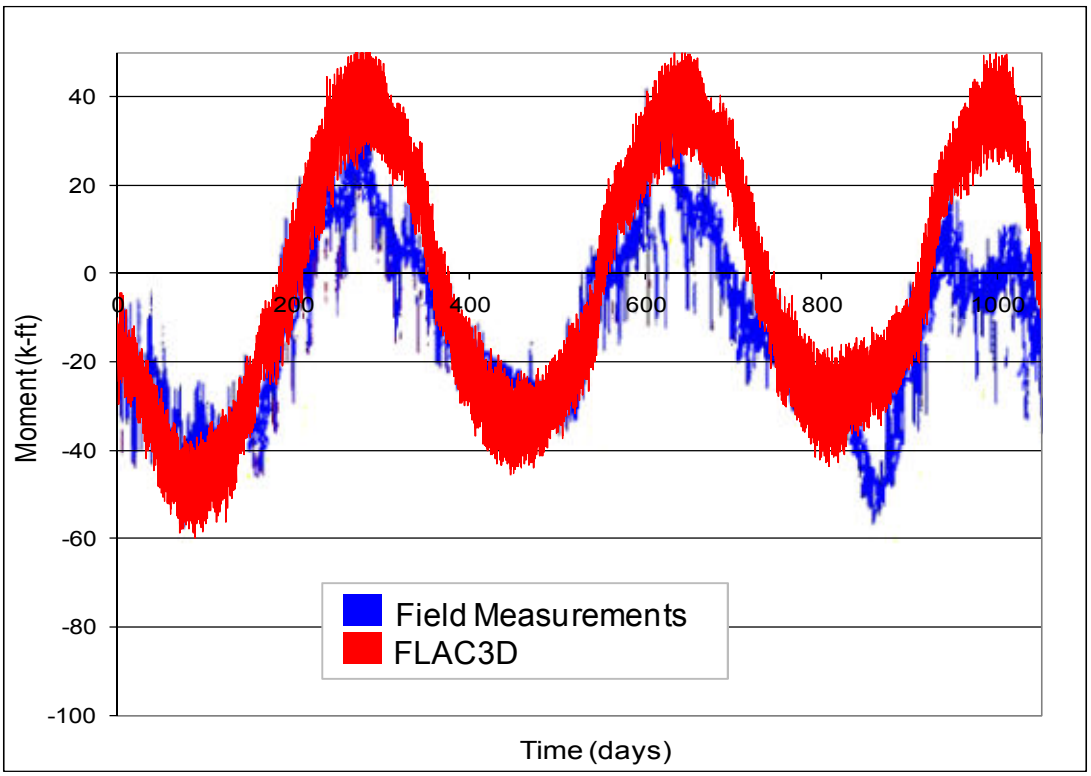

Figure 6.7 – Comparison between field measurement and FLAC3D. Moment on foundation H piles at elevation 55.7 m

The above results validate the results from FLAC3D, and they confirm that the numerical model is capable of representing important features of the soil-structure interaction, such as earth pressure build-up, bending moments, and cyclic characteristics of thermal displacements.

6.2 MSEW – Mechanical Stabilized Earth Wall

MSEW is an interactive program for the design and analysis of mechanically stabilized earth walls (ADAMA 2007). It follows the design guidelines of ***AASHTO98****/Demo 82,* ***AASHTO02****/FHWA-NHI-00-043,* ***AASHTO07****,* and ***NCMA97/98***. Among engineering practitioners, MSEW software is widely recognized as a standard tool for designing MSE walls.

A comparison between FLAC3D and MSEW software was performed. Figure 6.8 shows the model analyzed. The MSE wall in this figure is 22.7 feet tall and has 9 reinforced strips holding the front MSE wall. The space between the strip is 2.5 ft, except for the first strip, which is

positioned at 1.25 ft from the ground level. The backfill properties are those previously presented in Table 6.1 and 6.2

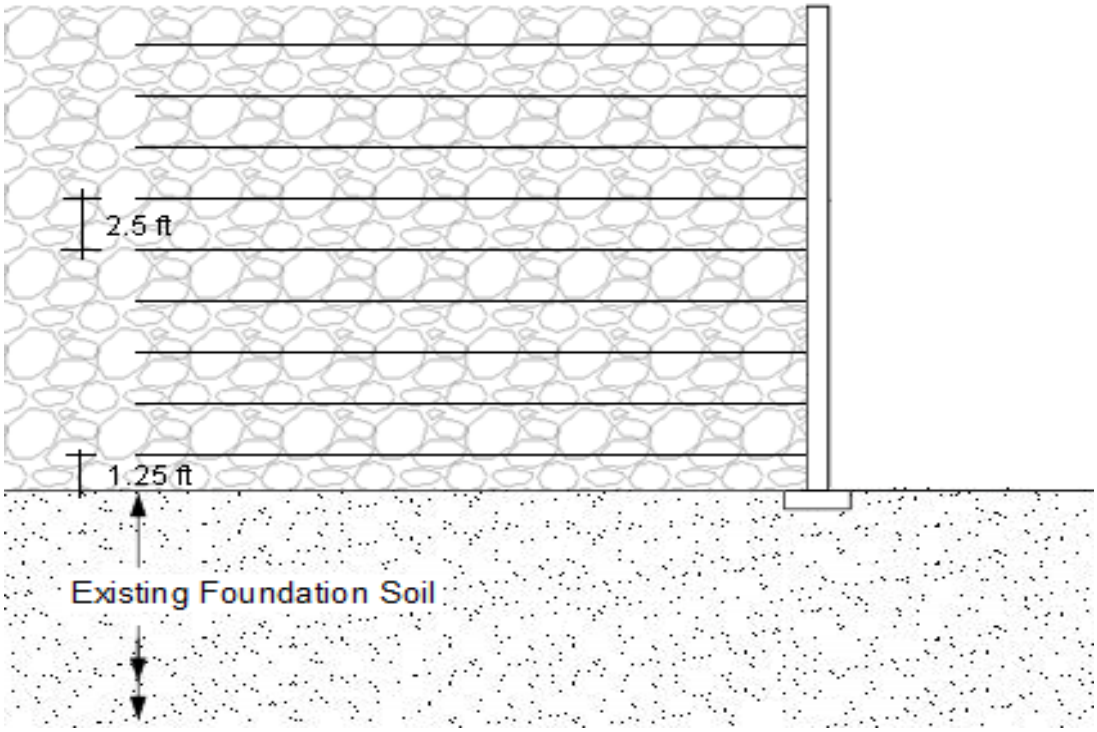

Figure 6.8 – MSE wall model used in comparison between FLAC3D and MSEW.

There are fundamental differences in the way the two programs analyze the model. In FLAC3D, the MSE wall is built in stages, as shown in Figure 6.9, such that the strips build tension as the MSE wall increases in height. As every new layer imposes a load on the previous layers, the underlying soil deforms and tensions the strips. Also, in FLAC3D, the foundation soil deforms by the construction sequence.

MSEW uses a pre-defined distribution of coefficients of lateral earth pressure established by FHWA (2001). The coefficient of lateral earth pressure K varies with depth, from 1.7 K_a, measured at the top of the MSE wall, to 1.2 K_a at 60% of the MSE wall height measured from the top. Beyond 60% of the MSE wall depth, K remains constant. Figure 6.10 shows the distribution of K behind the front MSE wall. Using this K distribution, the earth pressure on the

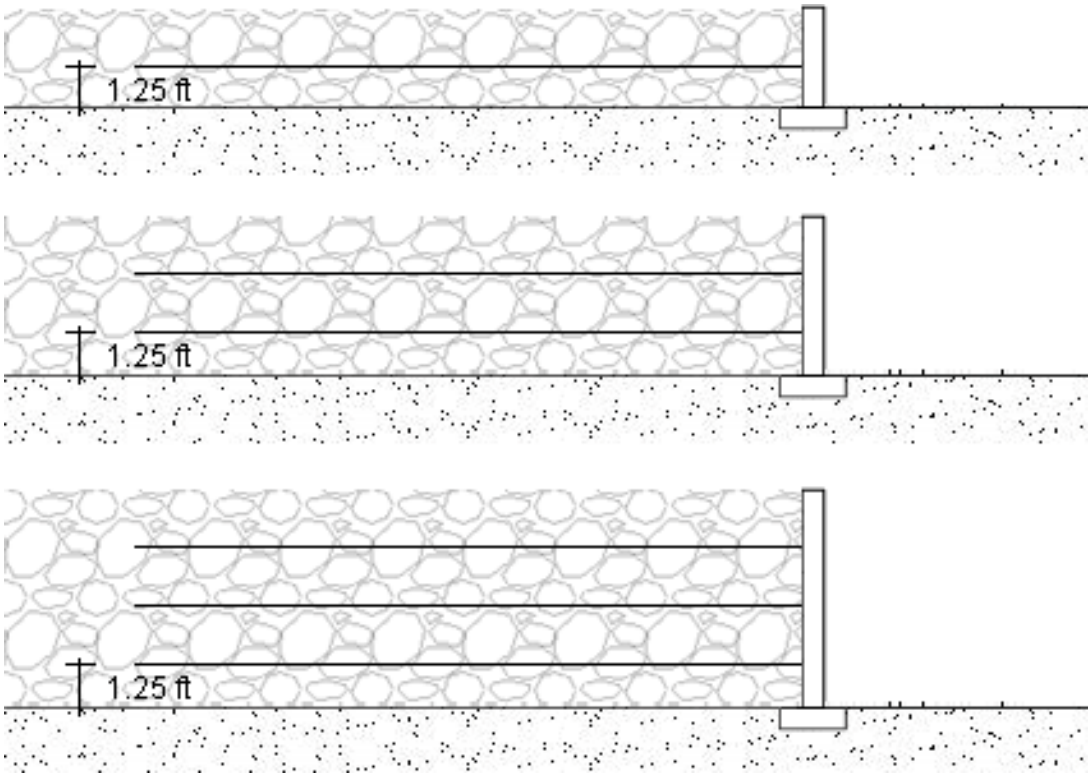

Figure 6.9 – FLAC3D MSE wall construction sequence

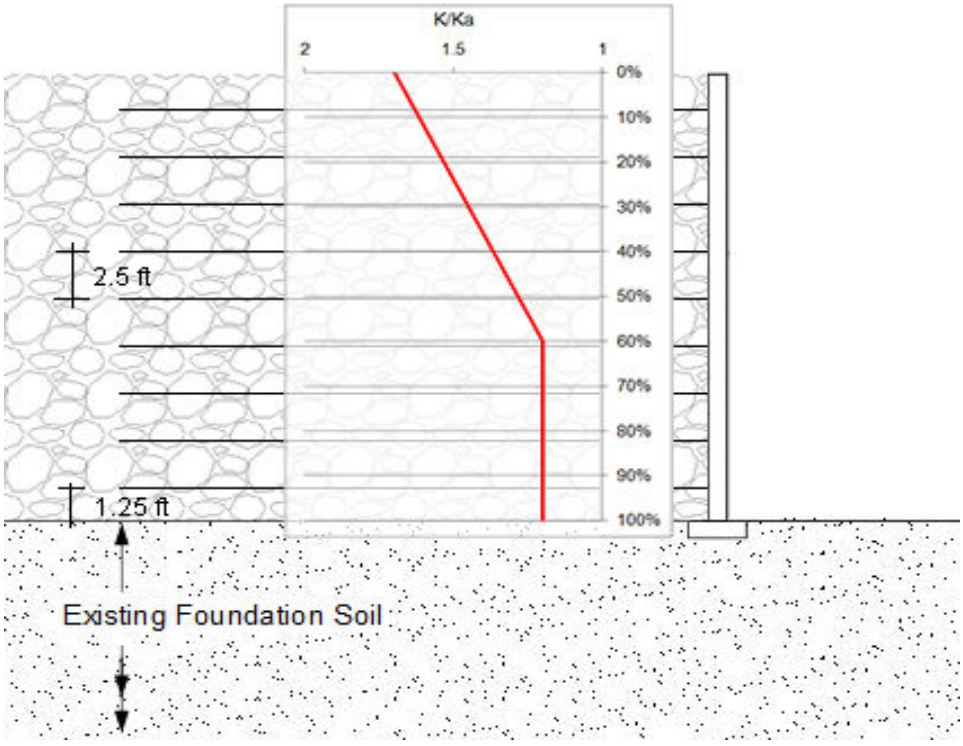

Figure 6.10 – Coefficient of lateral earth pressure distribution in MSEW

MSE wall can be computed. Then, the strip tensile forces can be computed using each strip tributary area and spacing.

Figure 6.11 shows the tensile forces in the strips of the MSE wall in Figure 6.8 computed by FLAC3D and MSEW. Both programs predict the same value of tensile force for the three top strips. Below this level, FLAC3D predicts less tensile force than MSEW. In FLAC3D, the soil located in the base of the MSE wall is limited in movement because it is constrained by the foundation soil so that less tensile force is necessary in the strips to resist the lateral pressure in the MSE wall fill. On the other hand MSEW mobilizes 1.2 Ka at the bottom of the MSE wall, regardless of foundation support, and consequently predicts higher tensile forces at the bottom of the MSE wall than FLAC3D for the conditions of this example.

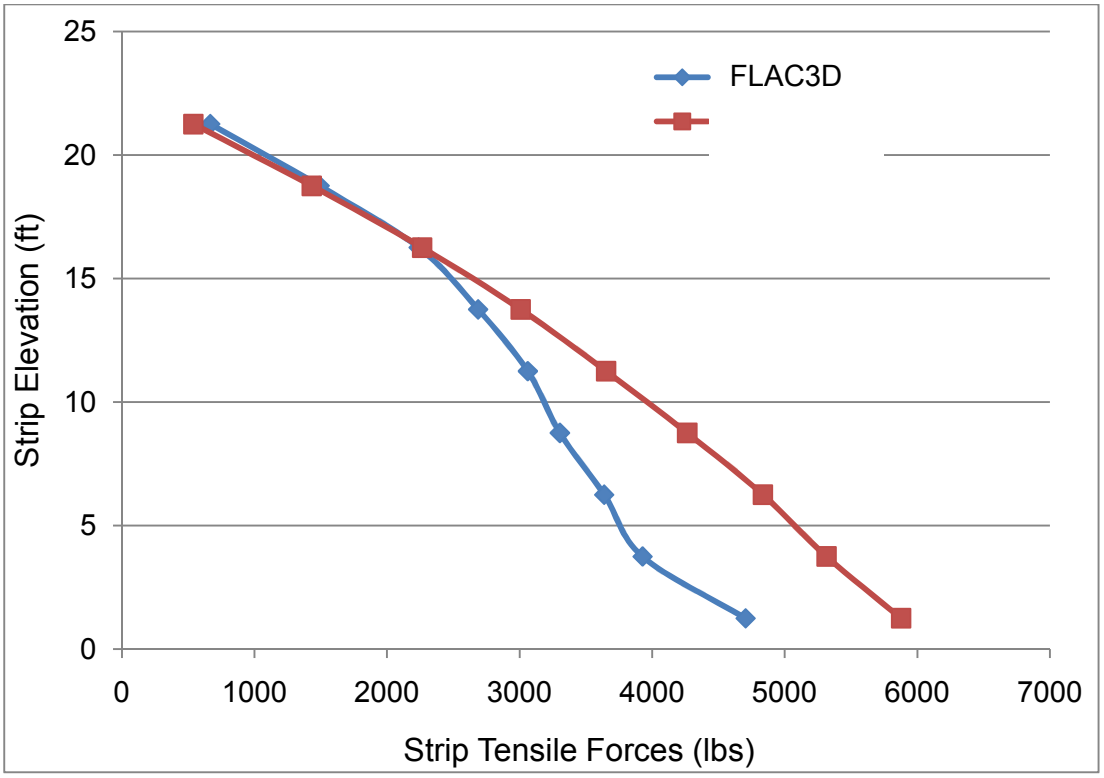

Figure 6.11 – Strips tensile forces comparison

The tensile force calculated by FLAC3D tends to go up in the strip located at the bottom of the MSE wall. This occurs due to lateral spreading of the foundation soil.

Although FLAC3D and MSEW exhibit some differences in the prediction of the strip tensile forces, particularly in the lower portion of the MSE wall, there is substantial agreement, and the differences can be understood based on the mechanics of the problem.

CHAPTER 7

RESEARCH BASE CASE AND PARAMETRIC STUDY

This chapter contains the main core of this research. It presents the base case model and how the parameter variations were created and analyzed. This chapter is divided into three main parts: the base case, the single parameter variations, and the multiple parameter variations. The analysis results are presented and discussed.

7.1 Base Case

This section provides a full description of the base case model, along with detailed information about the material properties used in the model, the monitoring output locations, sign conventions, and presentation and discussion of the results. Selected plots are provided to illustrate the most important findings for each output parameter of the base case model. Appendix B provides the full set of plots for all the output parameters for the base case model, including the time-histories in the directions along and transverse to the bridge centerline.

7.1.1 Source for Base Case Model: Integral Abutment Bridge over Telegraph Road, Alexandria, VA

The base case for this research study was taken from the fully integral abutment bridge located at the intersection of Interstate 95 (I-95) and Telegraph Road in Alexandria, Virginia. This bridge was selected because its west abutment (B672 – A) was instrumented, so it is logical to model this bridge for later comparison between numerical data and field measurements. In addition, this bridge represents the current state of practice of Virginia DOT designs of integral abutment bridges.

The main bridge characteristics are:

- Two lanes with an overall width of 35.8 ft.
- One continuous span.

- The deck is supported by five HPS70W steel girders with a total length of 166 ft. The girders supporting the bridge deck are 5.9 ft tall, and their flanges vary from 16 to 18 inches wide.
- The bridge has no skew angle.
- The abutments are 10.25 ft high, with a cross section of 3 ft.
- Each abutment is supported on a single row of seven HP12x53 piles.
- Piles are oriented for weak axis bending.
- The piles are approximately 70 ft long, and they rise about 25 ft above the foundation elevation.
- Each pile is surrounded by a corrugated steel sleeve backfilled with loose sand.
- The embankment is 33 ft high, and the main MSE wall height is 23 ft.
- The design incorporates a U-back MSE wall, which means that the MSE wall wraps back around the approach embankment such that MSE side walls are parallel to the road centerline

As directed by VDOT and VTRC personnel, three modifications were made so that the numerical models better fit the purposes of this research. First, the HP 12x53 piles in the bridge were replaced by HP 10x42 piles in the base case model. Second, reinforcing strips that were installed in the fill behind the abutment wall were removed from the base case model. Third, a larger thermal displacement than obtained from Eq. (2.1) was applied. Equation (2.1) gives a total thermal displacement of 1.5 in. for the telegraph road bridge, but a total thermal displacement of 6 in. was selected for the base case analysis to investigate the effects of the current trend to design longer integral abutment bridges. The total thermal displacement of 6 in. corresponds to applying a maximum displacement at the bridge centerline of 1.5 in. toward the abutment during bridge expansion and 1.5 in. away from the bridge abutment during bridge contraction. The sum of these displacements is 3 in., which is applied to one abutment and which corresponds to half of the total thermal displacement of 6 in. for the entire bridge.

In addition to the above modifications, the corrugated steel pipe sleeves were not modeled in any of the numerical analysis. This decision was made after the results from analyses of the steel pipe sleeves described in Chapter 4 were completed. Those results showed that the sand will densify under the cyclic thermal displacement action, so no benefit is obtained by placing them in the bridge.

The remaining characteristics of the design of the Telegraph Road Bridge are unchanged in the model. Figure 7.1 shows pictures of the bridge under construction. Table 7.1 provides the bridge dimensions, and Figure 7.2 shows a sketch of the bridge with letters designating the principal dimensions.

7.1.2 Numerical Model

The abutment B672 was modeled using FLAC3D. The construction sequence represented in the numerical model was described in Section 5.3.3. Figure 7.3 shows the base case model, except that some elements have been omitted for simplification. Figure 7.3 shows 7 piles, 32 dowels, and 5 girders, but the MSE wall structural components are displayed in a limited way, and only the front MSE wall concrete panels and a single line of vertically distributed strips are visible. As previously described, MSE walls are also modeled along the bridge side walls with strips oriented transversely to the bridge centerline.

Figure 7.1 – Telegraph Road Bridge in Alexandria, VA. Left: Abutment B672 under construction, showing concrete panels, foundation piles, and corrugated steel sleeves. Right: Abutment B672 almost completed, showing concrete panels, girders and abutment.

Table 7.1 – Abutment B672 dimensions and number of elements. Referred to Figure 7.2

Description	Letter in Figure 7.2	Number of elements across the bridge	Dimension
Embankment height	A	-	33.00 ft
Abutment height (above dowel)	B	-	7.25 ft
Abutment height (below dowel)	C	-	3.00 ft
Strip vertical spacing	D	10	2.50 ft
EPS thickness	E	-	2.67 ft
Abutment thickness	F	-	3.00 ft
Dowel	G	32	2.00 ft
Distance between abutment backwall and MSE wall	H	-	2.00 ft
Girder height	I	5	5.90 ft
MSE wall height	J	-	23.70 ft
Pile embedment (in foundation)	K	-	45.00 ft
Piles	L	7	70.00 ft
Strip length	M	10	23.00 ft
Abutment width		-	35.80 ft

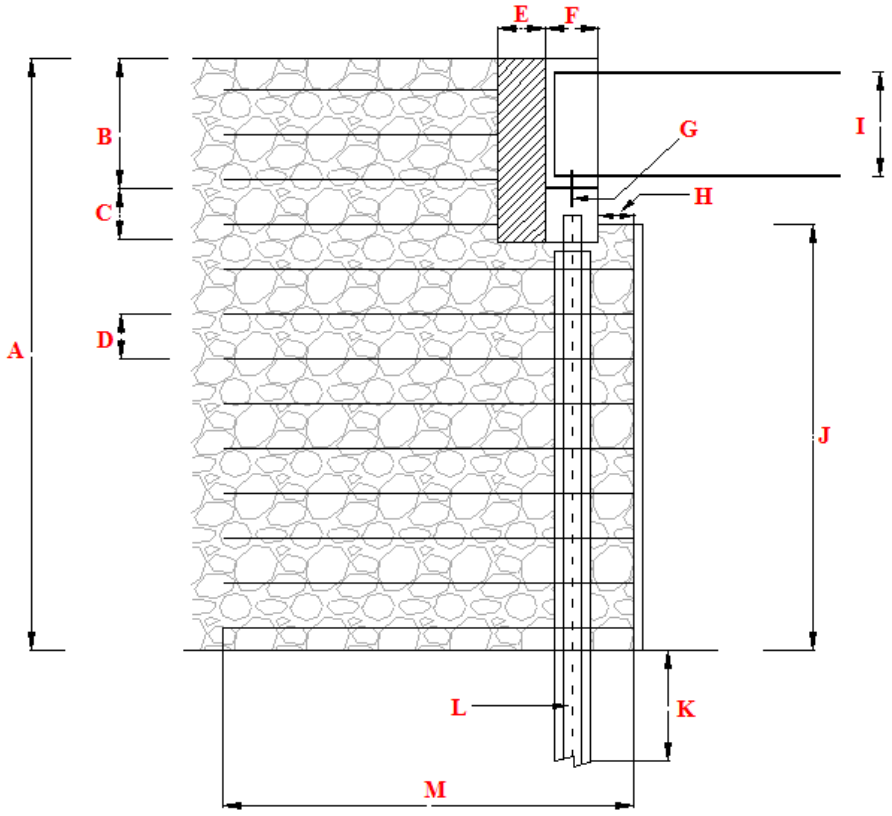

Figure 7.2 – Abutment B672 dimensions.

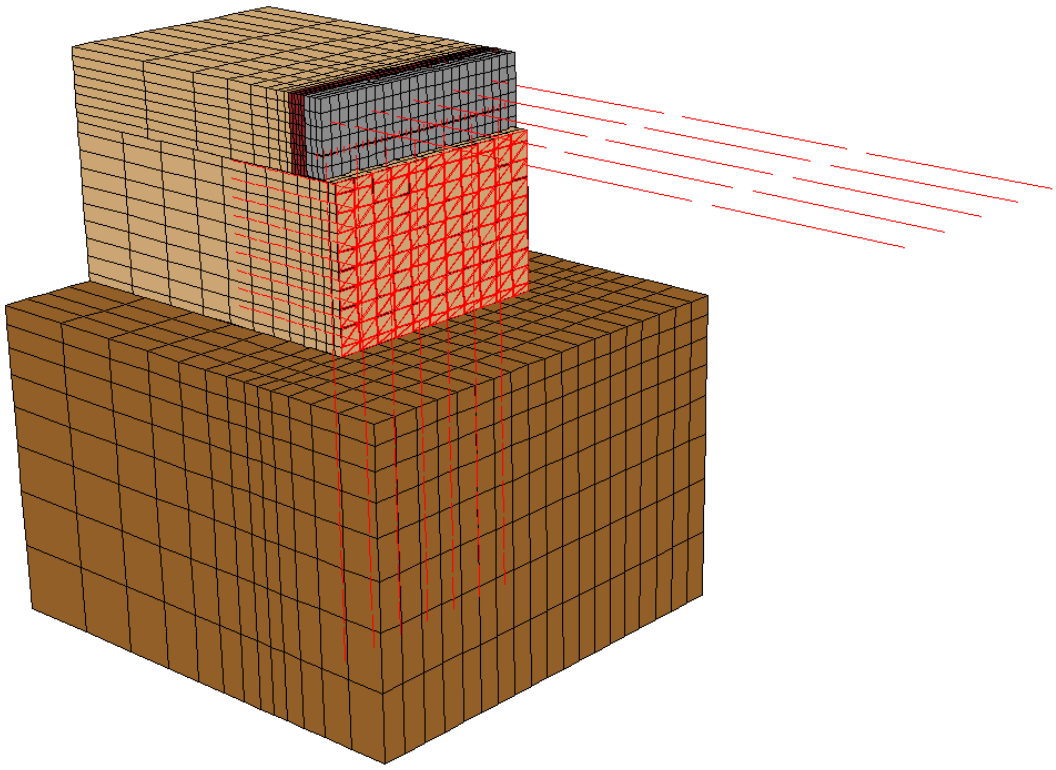

Figure 7.3 – Abutment B672 numerical model

The model is composed of more than 15,000 numerical entities, which are distributed as follow:

- Rectangular cuboid zones to represent the soil and abutment 4854
- Grid points of soil mesh 6480
- Structural nodes 2905
- Spring interfaces elements (links) 2885
- Beam elements (dowels and girders) 89
- Pile elements 140
- Shell elements (MSE concrete panels) 692
- Cable elements (strips) 2220
- Interface nodes 330
- Interface elements 552

7.1.3 Material Properties

Table 7.2 shows the material properties used in the Telegraph Road numerical model.

Table 7.2 – Material properties for Telegraph Road numerical model

Material	Elastic Modulus E, psf	γ, pcf	ϕ, deg	Model	Poisson's ratio ν
Concrete	597e6	145	-	Elastic	0.14
Steel	4,177e6	485	-	Elastic	0.3
Silty Sand	350,000	120	33	Mohr-Coulomb	0.3
Backfill	800,000	120	38	Mohr-Coulomb	0.2
EPS	5,500	0.87	-	Elastic	0.1

The properties shown in Table 7.2 are elastic modulus, unit weight, angle of internal friction, and Poisson's ratio. The strength and deformability parameters of the soil were obtained by correlating boring log information with soil property values found in geotechnical references, as discussed above in Section 6.1.2.

Concrete material properties were assigned to the abutment and MSE wall panels. Steel material property values were assigned to the MSE wall strips, girders, and abutment piles. Above the foundation elevation, the piles extend through the embankment, i.e., through the MSE wall fill, and below this level, the piles extend through the silty sand foundation soil.

Table 7.3 shows the spring interface properties. These properties were obtained following the procedure described in Section 5.2.2

Table 7.3 – Spring interface properties for Telegraph Road numerical model

Material Set #	Used by	Embedded in	Direction	Stiffness, k lbs/ft/ft	Cohesion, c lbs/ft	Friction Angle ϕ, degree
1	Strip	Backfill	Shear	1,460,746	0	36
2	Pile	Backfill	Shear	970,000	830	44.7
3	Pile	Backfill	Normal	262,000	0	77.7
4	Pile	Silty Sand	Shear	355,000	0	22.4
5	Pile	Silty Sand	Normal	80,000	4,200	63.6

The structural elements have the following properties:

- Abutment H Piles
  - Area 12.4 in^2
  - Strong Moment of Inertia 210 in^4

    - Weak Moment of Inertia 71.7 in^4
    - Perimeter 39.6 in
- Girders
    - Area 58.5 in^2
    - Strong Moment of Inertia 43,027 in^4
    - Weak Moment of Inertia 512 in^4
- Dowels
    - Section Circular
    - Area 0.6 in^2
    - Moment of Inertia 0.029 in^4
- MSE wall strips
    - Area 1 in^2
    - Perimeter 9 in
- MSE wall panels
    - Thickness 6 in

7.1.4 Monitoring Output

In order to capture the bridge response to thermal displacements, as well as to quantify the impact of geometry or property value changes, a series of monitoring output points were defined.

The monitoring point output tracks displacement, force, moment, or pressure changes at a specific position on the bridge, foundation, and MSE wall system. For example, shear forces were tracked during one year of thermal displacement simulation at the top of selected piles.

Table 7.4 summarizes the single monitoring output points used in this study. Appendix C details where the single monitoring output points are located.

In addition to the monitoring output points described in Table 7.4, global monitoring points were defined as well. The difference between the single monitoring points in Table 7.4 and the global monitoring points is that the single monitoring points track changes in one element or at one

location, so the collection of them describes how the monitored parameter is distributed across the bridge, whereas global monitoring points provide information about the average parameter value changes. For example, one of the global monitoring points is the total pile shear force in the longitudinal direction, which is the sum of the shear forces in all the abutment piles in that direction. Global monitoring points are useful for understanding what forces are acting in the abutment and the pile cap. The global monitoring points are listed in Table 7.5.

Table 7.4 – Summary of single monitoring output

Monitored Parameter	**Direction[1]**	**Where Monitored**	**Number of Monitored Points**
Displacement	Longitudinal and Transverse	Abutment	18
Shear Force	Longitudinal and Transverse	Dowels and Piles	20
Moment	Longitudinal and Transverse	Piles	24
Earth Pressure	Longitudinal	Behind EPS	10
Lateral Pressure	Longitudinal	Behind Abutment	10
Strip Tensile Force at Connection	Along Strip	Strips	21
Strip Max Tensile Force	Along Strip	Strips	21
Strip Max Tensile Force Position	Along Strip	Strips	21
Earth Pressure	Longitudinal and Transverse	MSE Wall	21
Axial Force	Axial Direction	Piles	9
Total			**175**

[1] "Longitudinal" direction is in the direction of the bridge alignment and "Transverse" direction is transverse to the bridge alignment.

Table 7.5 – Global monitoring output

Monitored Parameter	**Direction**	**Where Monitored**	**Number of Monitored Points**
Shear Force	Longitudinal and Transverse	Dowels and Piles	6
Moment	Longitudinal and Transverse	Dowels and Piles	6
Lateral Force	Longitudinal	Interface	2
Shear Force	Vertical	Interface	2
Axial Force	Axial Direction	Dowels and Piles	2
Total			**18**

7.1.5 Sign Convention

Figure 7.4 illustrates the sign convention for shear forces and moments in dowels and piles.

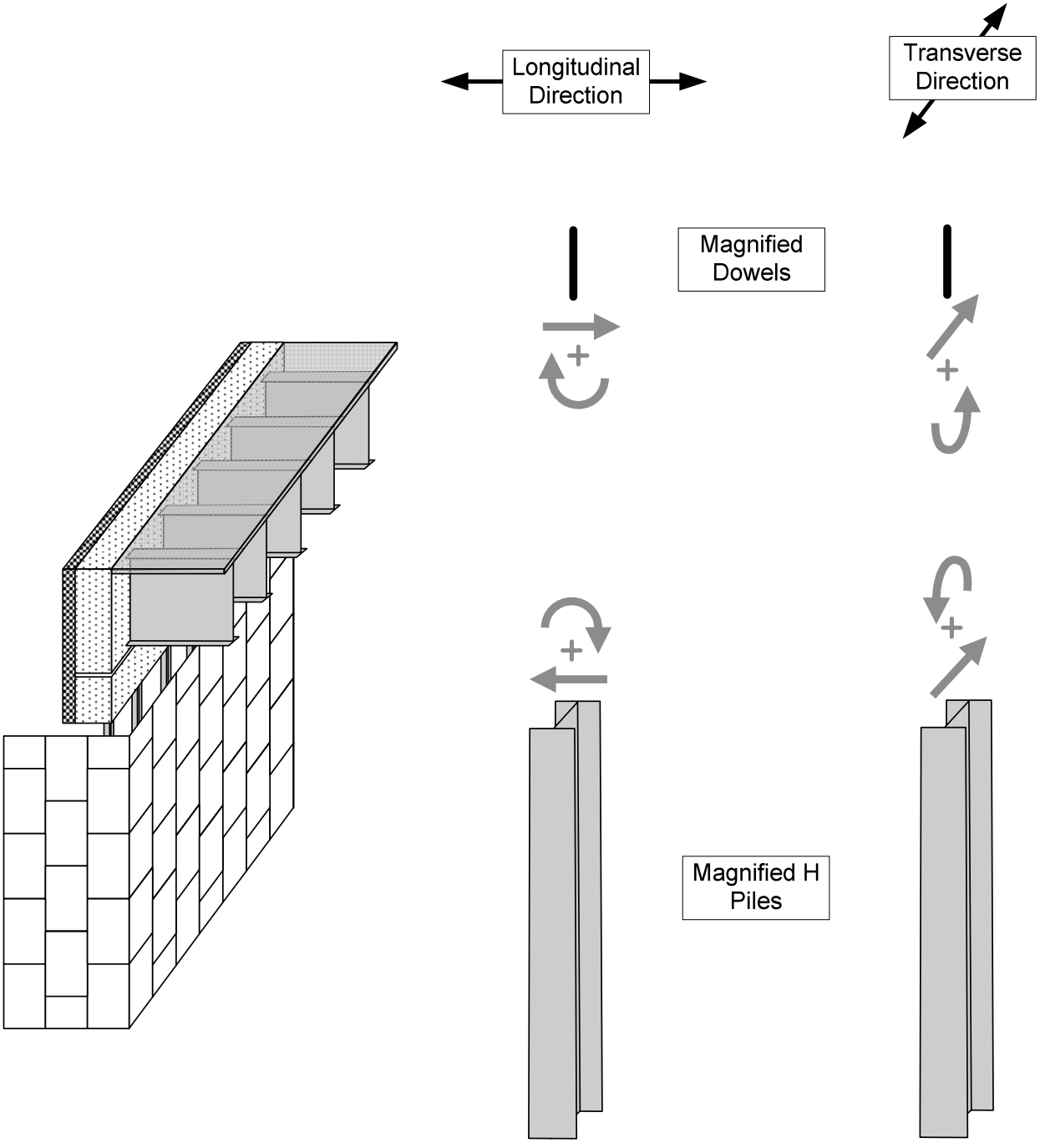

Figure 7.4 – Sign convention for shear forces and moments in dowels and piles.

7.1.6 Thermally-Induced Response (TIR)

During the analysis of thermal effects on the bridge response, the term "thermally-induced response" is used repeatedly. This term is used for referring to the largest impact of thermal displacement on a given output parameter.

In this research, thermally-induced response (TIR) is defined as whichever value of MAX and MIN has the largest absolute value, where MAX is the difference between the maximum value of the output parameter during the time-history and the value of the time history at the beginning of the year (i.e., due to gravitational forces) and MIN is the difference between the minimum value of the output parameter during the time-history and the value of the time history at the beginning of the year.

To illustrate these definitions, Figure 7.5 shows the time-history of four imaginary monitored output parameters. Applying the definitions of MAX, MIN, and TIR to the variations in Figure 7.5, the TIR values of the output parameters for each monitored point can be calculated, as follows:

- Figure 7.5a MAX= 6 - 0 = 6 MIN = -4 - 0 = -4 TIR = 6
- Figure 7.5b MAX= 8 - (-2) = 10 MIN = -8 - (-2) = -6 TIR = 10
- Figure 7.5c MAX= 10 - 6 = 4 MIN = -4 - 6 = -10 TIR = -10
- Figure 7.5d MAX= -8 - (-8) = 0 MIN = -14 - (-8) = -6 TIR = -6

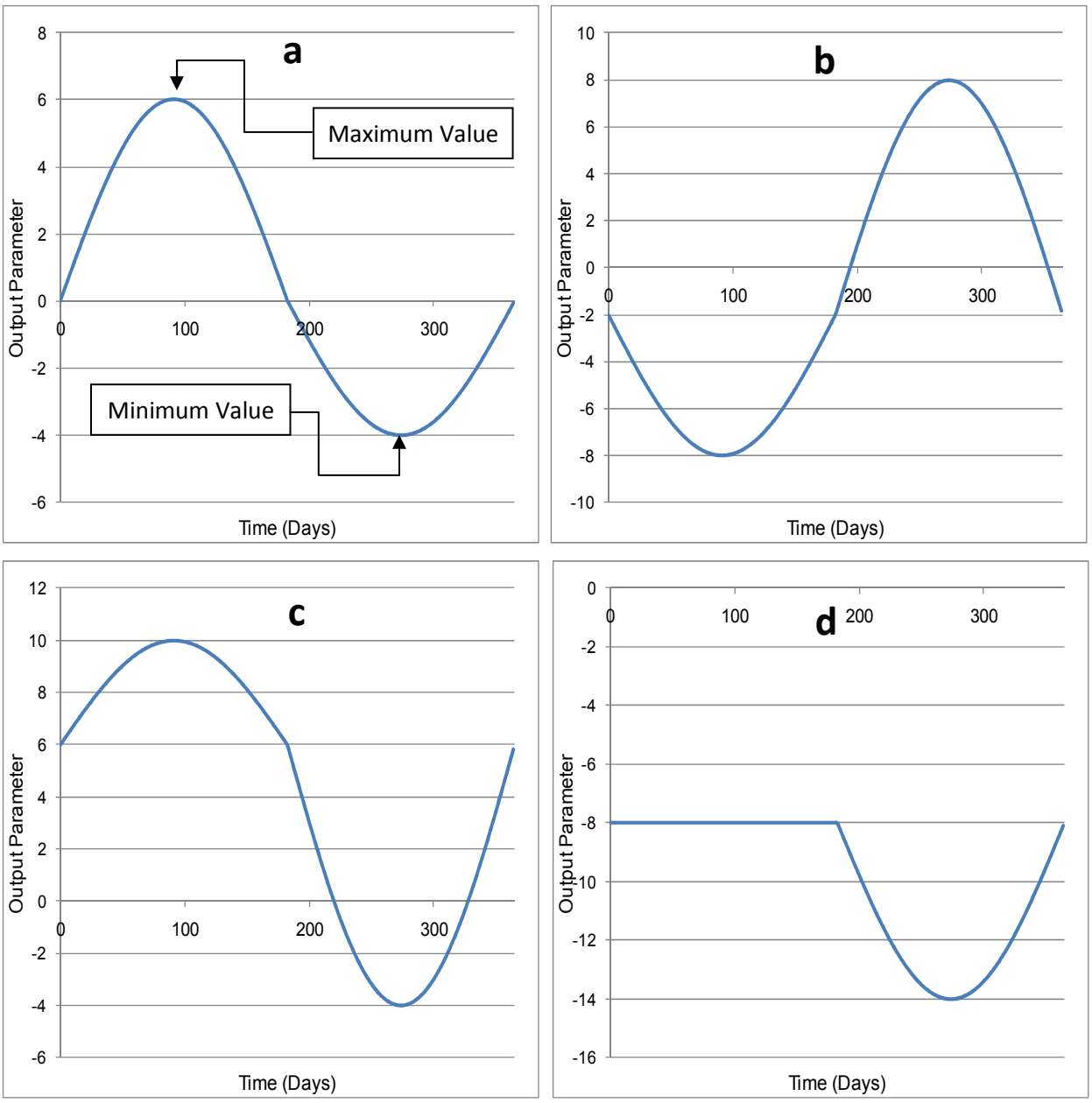

Figure 7.5 – Output parameter examples for computing the TIR.

7.1.7 Base Case Results

Since the input displacement at the girder centerline is of cyclic character, it is expected to produce similar responses for most of the monitoring points. Also, thermal displacements

produce bigger responses on those bridge components near the abutment, and the thermal response decreases as bridge components are positioned farther from the abutment.

The following describes in detail the analysis of the bridge response for the base case. Only the values in the longitudinal direction are discussed for the base case, since values in the transverse direction are not significant when skew angle is zero. The following discussion of the bridge response is based on the monitored points defined in Appendix C.

7.1.7.1 Displacements

Figure 7.6 presents the abutment displacements for the left and right side of the abutment, monitored for a year of cyclic displacement simulation. The cyclic character of the imposed displacement at the girder centerline is also displayed by all of the monitoring points. Since the base case model was built with skew angle equal to zero, the left and right displacements are equal. The orange line is the displacement at the top of the abutment, and this is equal to the imposed displacement of 3 inches, as described in section 7.1.1. The maximum values are at +0.125 ft and -0.125 ft, or +1.5 in. and -1.5 in., whose difference equals the total imposed displacement of 3 inches.

The first half of the year's cyclic simulation corresponds to movements into the bridge embankment, and the second half is for movement away from the embankment, toward the bridge deck centerline.

The displacements during the first half of the year at the top of the pile cap (brown line) are about half of those at the top of the abutment, and displacement at the pile cap bottom (green line) are about one third. The amplitude of the daily displacement is reduced as we move away from the bridge girder. The pile cap experiences a big rotation, as shown by the difference between the brown and green lines, and a big offset with respect to the upper abutment, as shown by the difference between the orange and brown lines.

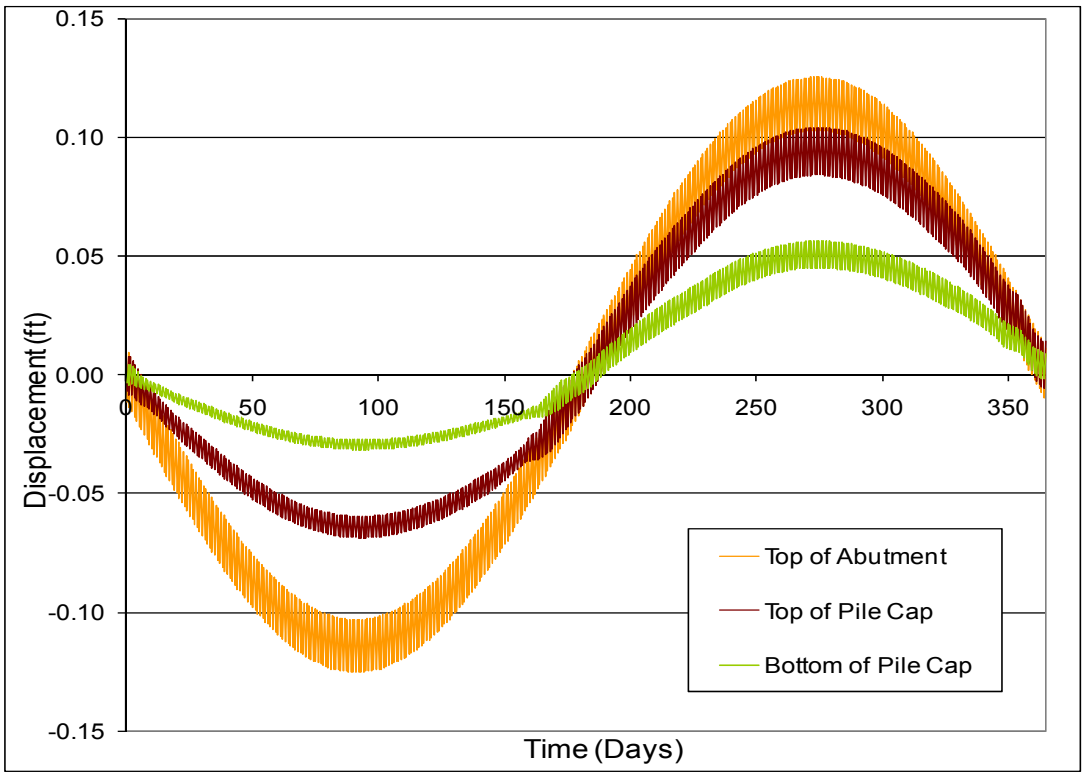

Figure 7.6 – Longitudinal displacement of bridge abutment for the base case

During the second half of the year, the pile cap experiences greater displacement, closely following the displacements at the top of the abutment. This happens because, during the first half of the year, the EPS and embankment fill soil offer resistance to pile cap motion, whereas during the second half of the year, the EPS and embankment fill soil tend to push the pile cap towards the bridge centerline. The amplitude of the daily displacement has increased in both the pile cap and the pile cap bottom because they are moving in more compliance with the abutment top.

These complex movements of the abutment system have implications on shear forces and moment results for the dowels and piles. Larger rotations are expected to produce larger moments, and larger offset displacements are expected to produce larger shear forces.

7.1.7.2 Shear Forces

Figure 7.7 shows shear forces for dowels, and Figure 7.8 shows shear forces for piles.

Dowel shear forces present a well defined and relatively simple cyclic response, while pile shear forces exhibit a more complex response. This occurs because dowels are isolated system components, and the shear forces produced in dowels only depend on relative displacements between the pile cap and the upper abutment. In contrast, the pile shear forces depend on the interaction of many bridge components, and the response is more complex. The bridge components that influence the pile shear forces include the MSE wall soil, the EPS and backfill soil behind the abutment, and proximity to structural components (concrete panels and/or MSE wall strips).

The location at which these forces were tracked are near the abutment. Thus, thermal displacements have a big influence. The maximum values of shear force are 10 to 15 times larger than the gravitational components, where the gravitational components are the values at the beginning of the thermal simulation year.

Dowel shear forces are all equal for non-skewed bridges, and they present their maximum value during the bridge expansion phase. Because all dowels exhibit the same response in non-skewed bridges, the response of only one dowel is presented in Figure 7.6.

Pile shear forces during the bridge expansion phase are complex, but their nature can be understand by considering the sets of normal and shear forces that act on the pile cap. Figure 7.9 shows the pile cap free body diagram, with forces for the following stages: the end of model construction (gravity loads only), maximum bridge expansion, and maximum bridge contraction. This figure shows that the shear force at the bottom of the pile cap always acts in the same direction, even during the bridge expansion. This occurs due to nonlinear and inelastic response of the soil behind the pile cap and around the piles. The reaction to the shear force acting at the bottom of the pile cap is the shear force acting on the piles, which is negative and remains negative during the cyclic simulation, according to the established sign convention.

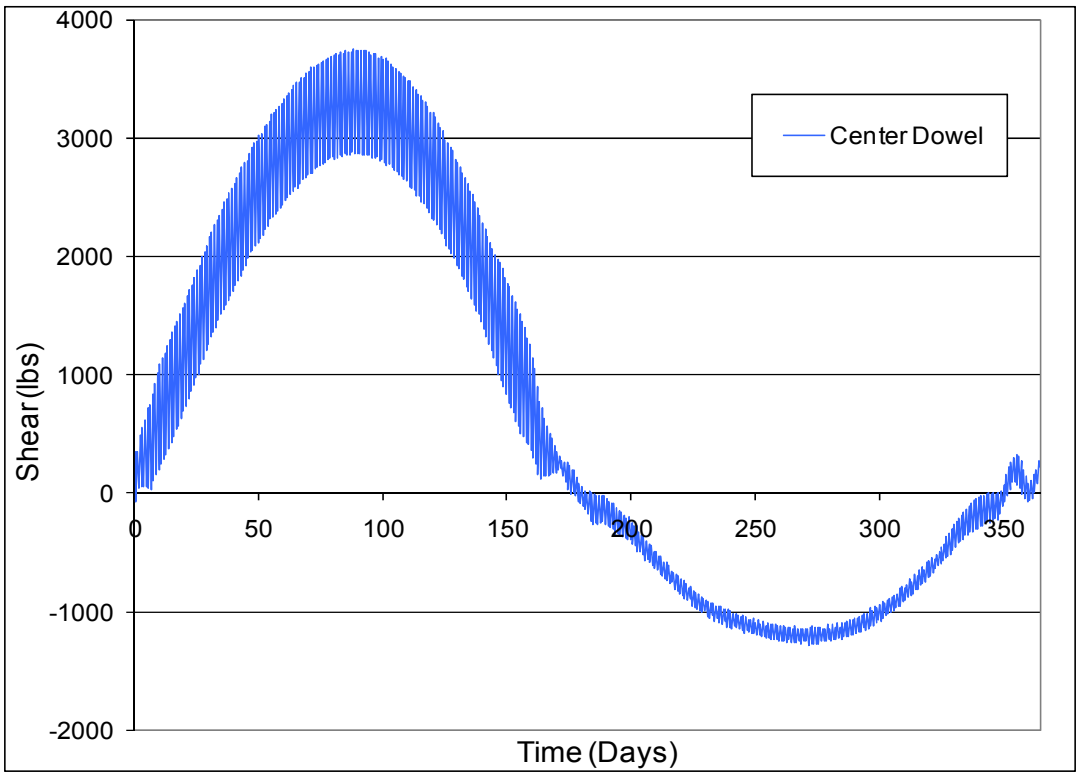

Figure 7.7 – Shear forces in dowels for the base case.

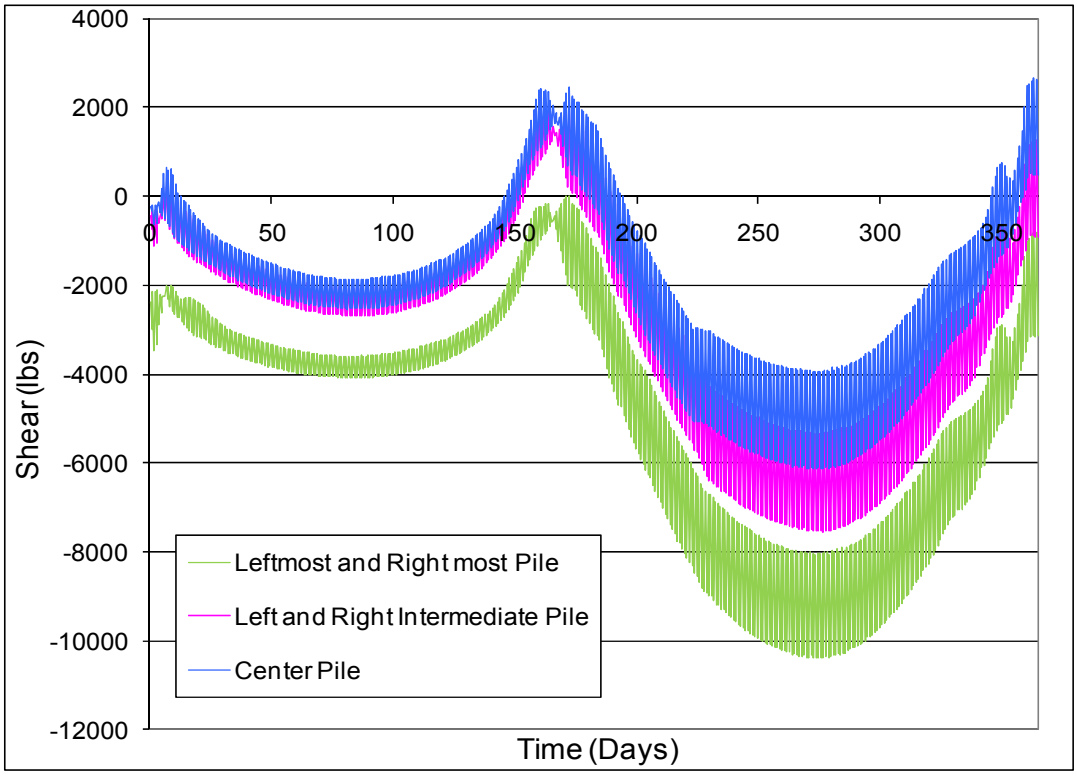

Figure 7.8 – Shear forces in piles for the base case.

Figure 7.8 shows that the magnitude of pile shear force is larger during the contraction phase, which occurs during the second half of the year, than during the expansion phase. Figure 7.6 shows that the displacement magnitudes at the bottom of the pile cap are also larger during the contraction phase than the expansion phase, although there is a sign reversal for the displacements but not for the shear forces, which occurs because of the inelastic soil response discussed above.

Figure 7.8 shows that the primary difference in response for the edge piles, intermediate piles, and center pile is an approximately constant shift in the shear force value at all times. This may be due to the proximity of the edge and intermediate piles concrete panel and strips of the MSE side walls.

Shear force values transverse to the bridge alignment are very small for non-skewed bridges.

For the base case analysis, the TIR of shear forces in dowels and piles is about 3.8 kips and 7.7 kips, respectively.

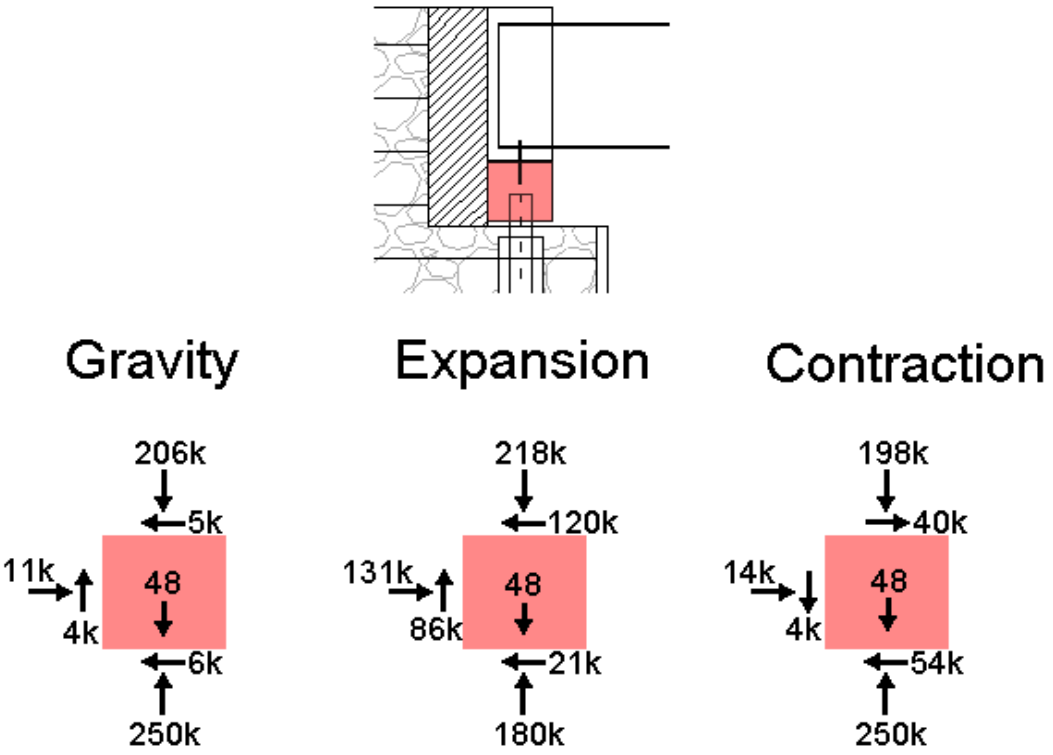

Figure 7.9 – Pile cap free body diagrams for the base case.

7.1.7.3 Moments

Figure 7.10 shows calculated moments immediately under the abutment pile cap, and Figure 7.11 shows moments for the same piles, but at locations 2 ft under the abutment pile cap.

Moments at locations immediately under the pile cap experience their maximum values during the bridge expansion phase. For the moments calculated at a location 2 ft under the abutment, the maximum values occur during the bridge contraction phase. However, Figures 7.10 and 7.11 show that the overall bending moment responses immediately below the abutment and 2 ft below the abutment are similar.

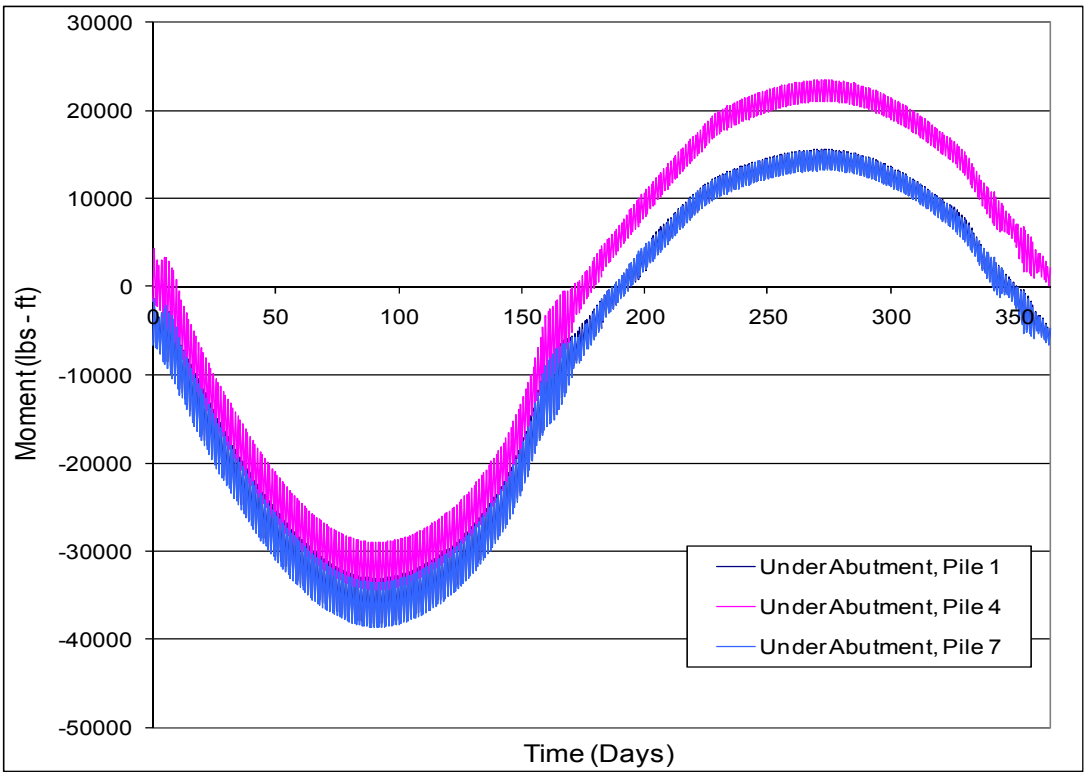

Figure 7.10 – Moment in abutment piles directly under the pile cap for the base case.

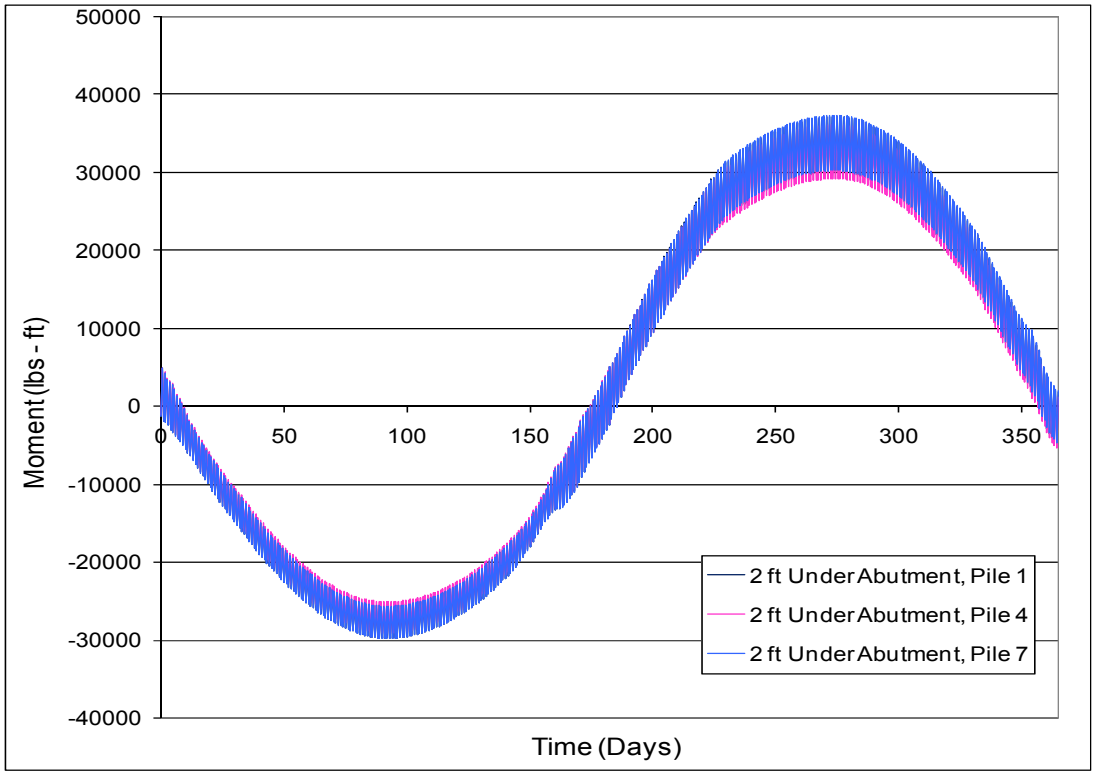

Figure 7.11 – Moment in abutment piles 2 feet under the pile cap for the base case.

The TIR of the moments is about 35 kip-ft for both positions presented in Figures 7.10 and 7.11 for the base case.

Moment values transverse to the bridge alignment are not significant for bridges with zero skew angle.

7.1.7.4 Earth Pressure behind Abutment

Figure 7.12 shows that the earth pressure behind the abutment has a cyclic character that is different from the displacement, shear, and moment responses. During the bridge expansion phase, the earth pressure behind the abutment builds and reaches a maximum value when the bridge is fully expanded.

When the bridge is returning to the initial position, the earth pressure decreases and finally reaches an approximate minimum or residual value. After that, the bridge moves to its fully contraction position. During this stage, the earth pressure remains approximately constant at its residual value, and the soil behind the abutment experiences settlement, as discussed below in Section 7.1.7.8.

After the bridge has reached its maximum contracted position, it starts to expand, and the earth pressure builds up again. Once the bridge has reached the initial position the earth pressure has increased to an earth pressure value that is 3 to 5 times as large as the initial value.

Figure 7.12 shows the calculated lateral earth pressure behind the abutment at two elevations along the bridge centerline. One of the elevations is at 2/3 of the abutment height, and the other is at 1/3 of the abutment height. The results indicate that the lateral earth pressure is almost the same at these two elevations. Each of the time histories in Figure 7.12 is representative of 5 monitoring points distributed horizontally across the abutment. Therefore, the earth pressure behind the abutment is approximately the same at all the monitored locations, regardless of their vertical and horizontal positions.

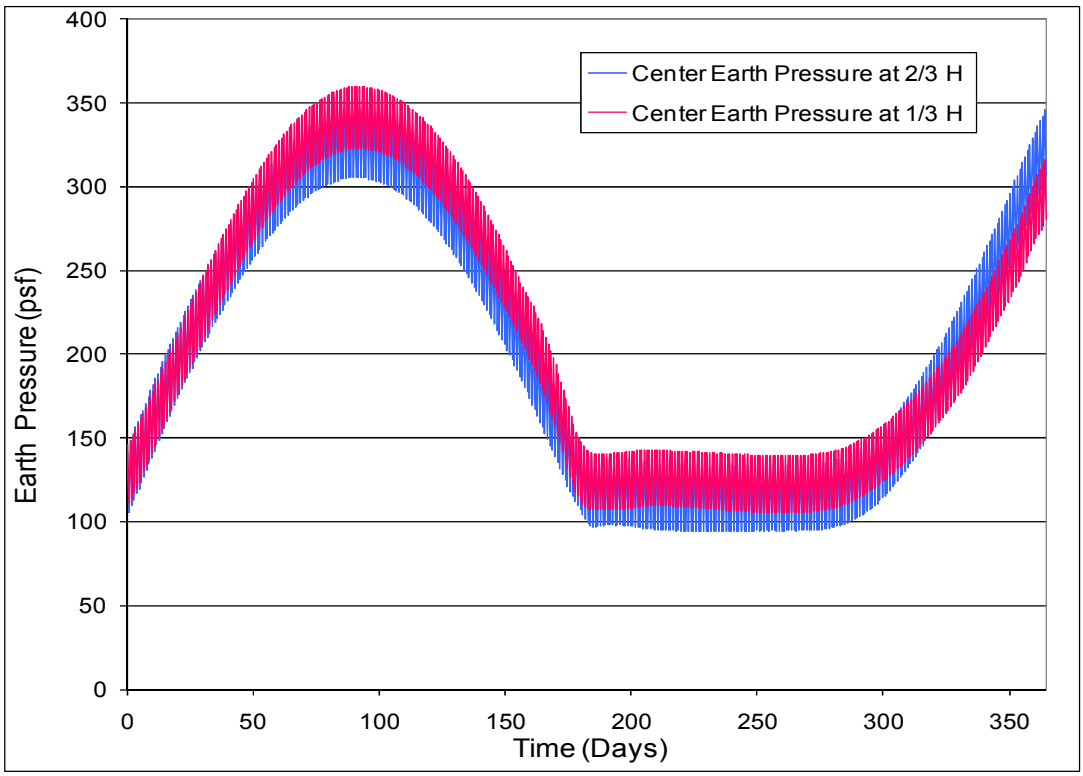

Figure 7.12 – Earth pressure behind the abutment for base case.

To investigate the long term effects of cyclic loading on lateral earth pressures, three years of thermal cyclic displacement were simulated for the base case, as shown in Figure 7.13. The earth pressure maximum value for the second year is 60% larger than the first year maximum value. The third year maximum value is only 6% larger than the second year maximum value. The soil behind the abutment adjusts significantly during the first year, and this produces the larger values of earth pressure in subsequent years.

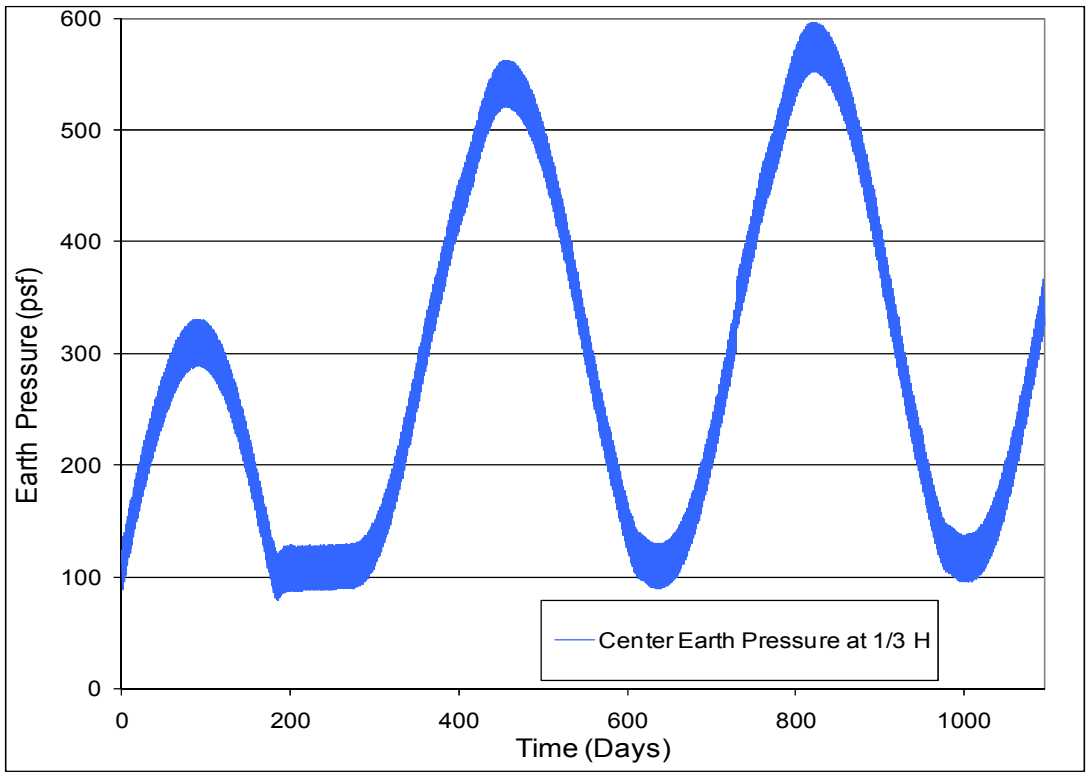

Figure 7.13 – Earth pressure behind the abutment for base case. Three years of numerical simulation.

7.1.7.5 Strip Tensile Forces

Figure 7.14 shows the strip tensile forces for one year of thermal displacement simulation. The results in Figure 7.14 are for strips located right under the abutment, thus the designation "top" in the figure. They are located at the top part of the main MSE wall in front of the abutment. Figure 7.14 shows six plot lines, three for the value of the strip tensile force at the MSE wall connection and three peak values that occur along the strip length. Figure 7.15 shows where the peak values are produced, with the distance measured from the strip connection with the front MSE wall, so that a distance equal to zero would imply that the peak and connection values are equal.

Figure 7.14 shows only the "top" strips because only the strips in the upper quarter of the MSE wall experience significant increases in tensile force due to thermal displacements, and the largest increase is observed by those strips directly under the abutment.

The tensile force for the strip in the middle position is shifted in relation to the edge positions. This is consistent with previous results for shear forces and moments.

During the bridge expansion stage, the connection values increase and the peak values decrease or stay approximately constant. When the bridge is in its maximum expanded position all the values match. After this point, the trends reverse and each set of strip tensile forces comes back to the initial values. During the bridge contraction stage, both the peak and the connection strip tensile forces increase. The maximum strip tensile forces occur during this stage.

For the "top" strips directly under the abutment, thermal displacements increase the strip tensile forces by about 75% at the MSE wall connections, and they increase the peak strip tensile forces by about 110%. When comparing the maximum strip tensile force at the MSE wall connection with the maximum strip tensile force of the peak, the peak tensile forces are about 50% to 75% larger than the strip tensile force at the MSE wall connection. This last point is displayed by Figure 7.14 at about day 270.

During the bridge expansion stage, the peak value location oscillates between the front and back of the abutment position, while during the contraction stage, the location is stationary at 8 ft from the front MSE wall face, as shown in Figure 7.15.

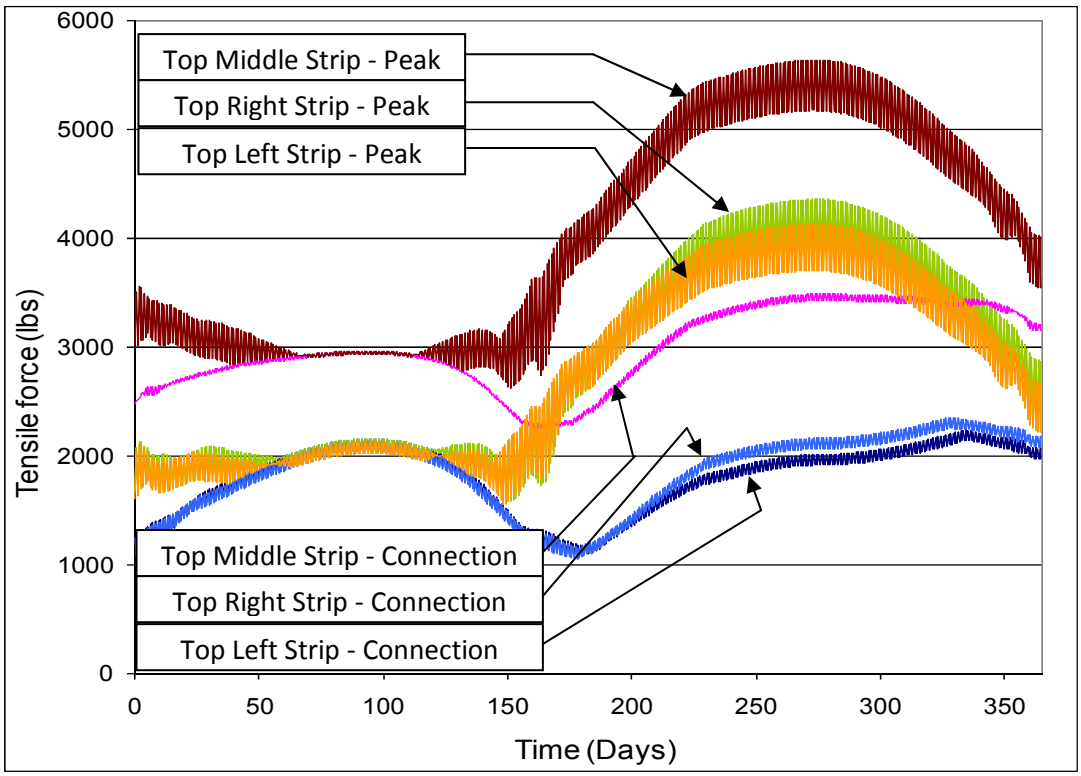

Figure 7.14 – Strip tensile forces at the connection and peak value for the base case

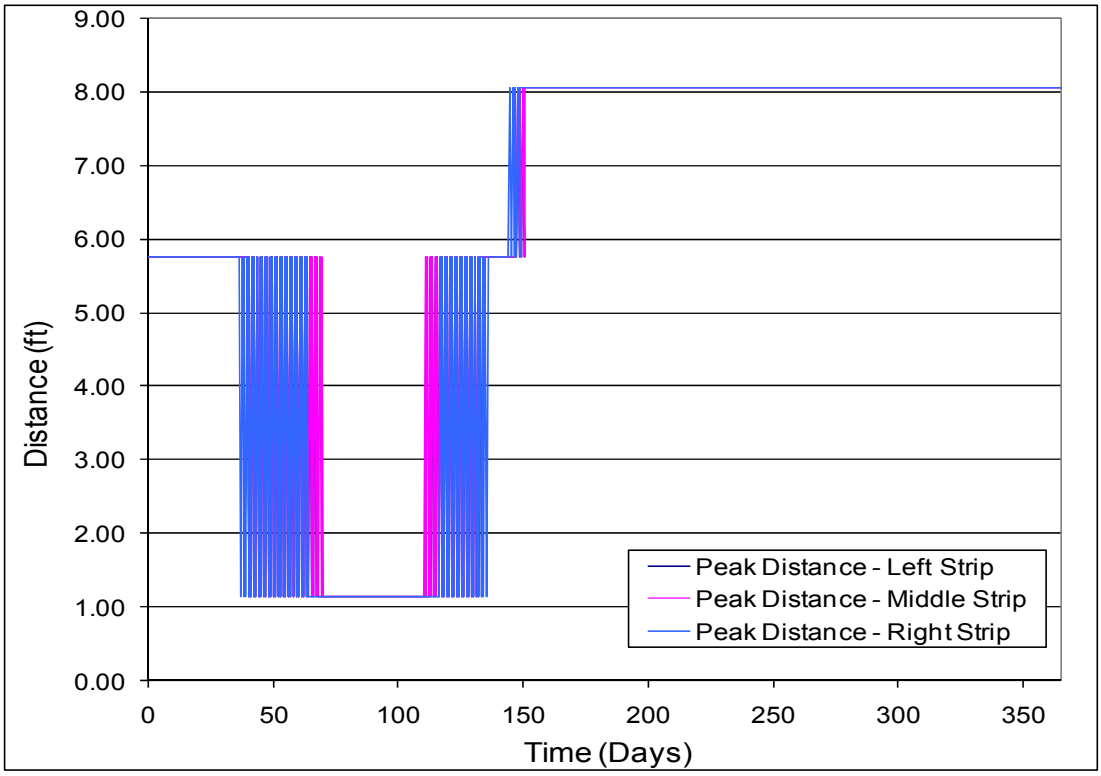

Figure 7.15 – Position of peak forces for the base case.

Since the base case does not include skew angle, the tensile force variation on the lateral walls due to thermal displacements is small. The monitored strips attached to the side walls near the abutment present a variation of 10% or less with respect to the gravity values. The peak tensile force and the tensile force at the connection for all strips monitored in both side walls matched, i.e. the maximum tensile force is at the MSE wall connection.

A strip tensile force build up is observed at the end of the first year. This effect is similar to the one produced for earth pressure behind the abutment, but at a smaller scale. No significant additional build up occurred for the following years.

7.1.7.6 MSE Wall Earth pressure

Figure 7.16 shows the earth pressure behind the front MSE wall. MSE wall earth pressures were tracked at positions corresponding to the monitoring locations for the strip tensile forces at the MSE wall connections.

Once again, the central earth pressure value is shifted compared with the left and right values, and the responses are only significant for those MSE wall panels near the abutment.

The maximum values occur during the bridge contraction stage, when the piles are pressing against the front MSE wall. This interaction is similar to the earth pressure behind the abutment, but is reversed in time, so that the flat response is produced during the first half of the year and the earth pressure build up is produced during the second half. During the contraction stage the responses are very flat, which is an effect produced by the countering influence of pile bending moments. During this stage, the piles are being moved toward the bridge deck, which by itself should increase the earth pressure on the front MSE wall. However, in addition to this movement, the curvature imposed by the pile cap rotation tends to push the piles away from the front MSE wall, which decreases the earth pressure against the front MSE wall. It is believed that these two movements counter act each other, producing the relatively flat response observed in the second half of the year.

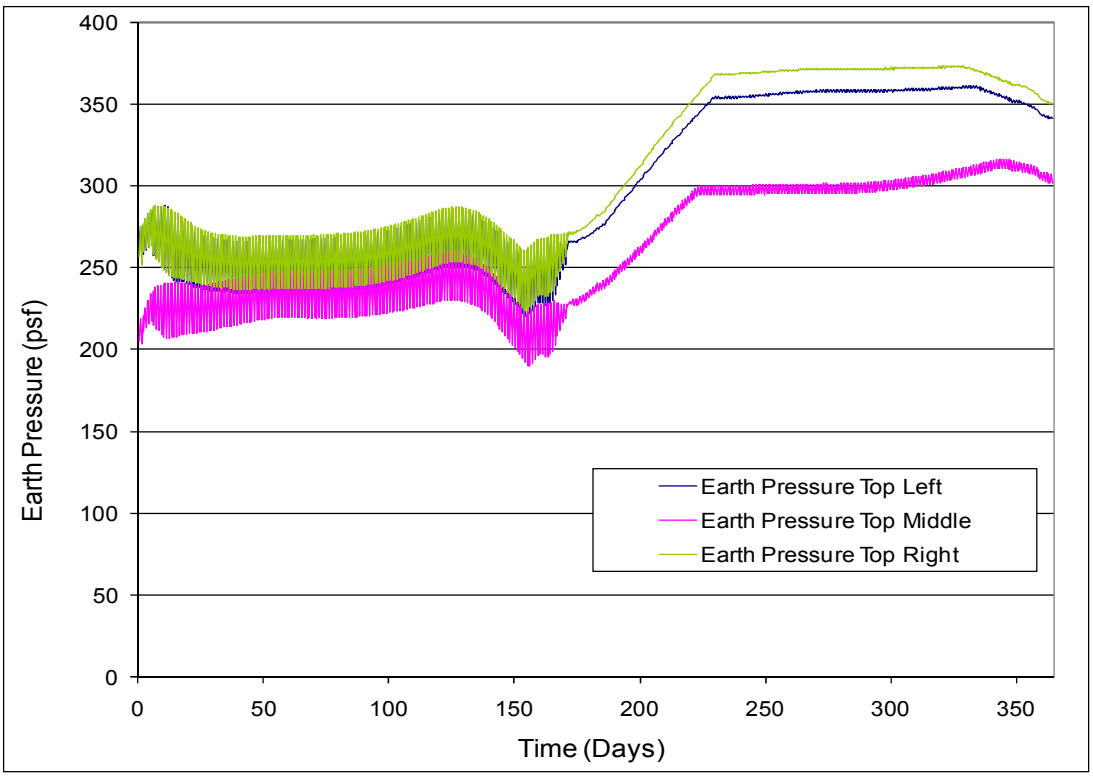

Figure 7.16 – MSE wall earth pressure at top position in the front MSE wall for the base case.

7.1.7.7 Axial Force

Figure 7.17 shows the pile axial forces tracked immediately under the abutment, at the position called "top of piles". Axial forces were monitored for the left (pile 1), center (pile 4), and right pile (pile 7).

The dowel axial loads remain mostly stationary, as indicated by the approximately constant force on the top of the pile cap in Figure 7.9. The dowel forces only change about ±5% with respect to the gravitational values.

The pile axial loads are the only bridge response that exhibits primarily a decrease in response to thermal displacements, as shown in Figure 7.9 (and subsequently, in Figure 7.17). The pile axial

loads decrease by about 25% from their gravitational values for locations directly under the abutment, and they decrease about by 10% at foundation level.

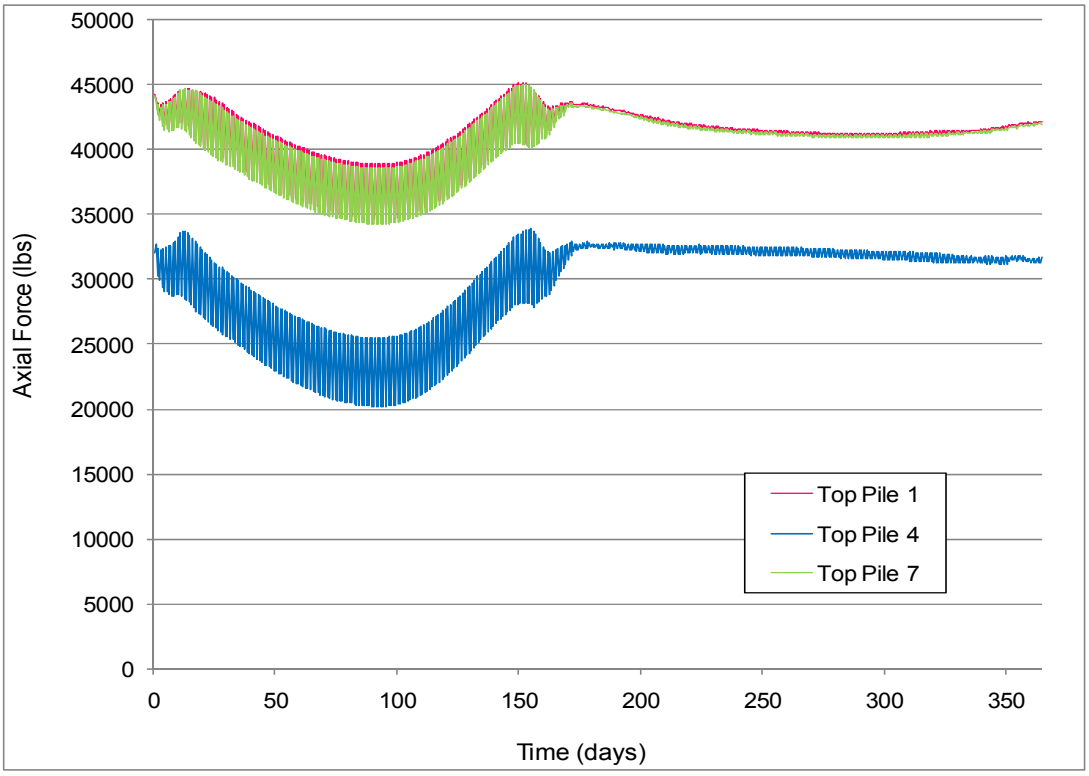

Figure 7.17 – Axial force in piles for the base case.

The pile axial load reduction is an indirect response to thermal displacements. Because the pile cap rotates towards the fill when the bridge is under expansion, upwards directed shear forces develop on the pile cap, producing a lifting effect. The opposite is not true when the bridge is under contraction because of the separation tendency between the EPS and the pile cap.

7.1.7.8 Backfill Settlement

Figure 7.18 shows the displacement time versus history of 8 nodes tracked behind the abutment for the base case. The eight nodes are located at the embankment surface along the bridge centerline, with Node 5570 closest to the abutment and Node 6439 farthest from the abutment.

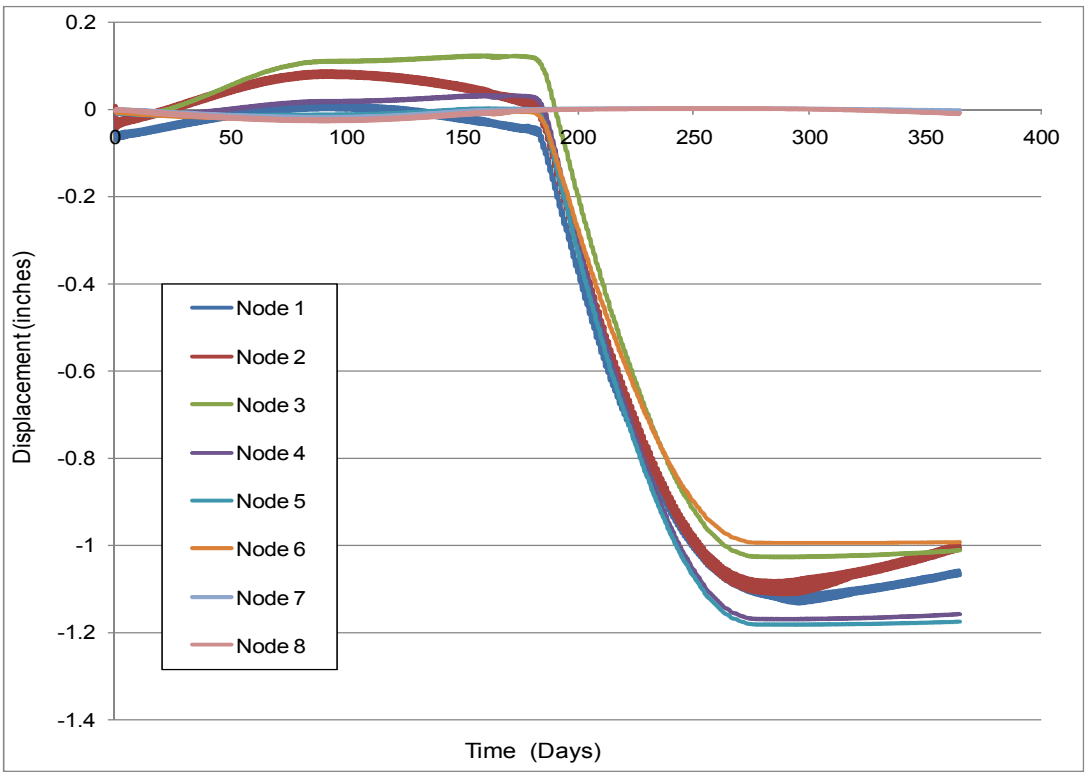

Figure 7.18 – Settlement behind abutment for the base case. Displacement history of 8 nodes.

Taking the information from Figure 7.18 and plotting the maximum, minimum, and final values of each-time history versus the distance from the abutment, the plot in Figure 7.19 was created. The maximum values come from the first half of the year, during the expansion stage, the minimum values come from the second half of the year, during the contraction stage, and the final values are the last values from the time-history plots. Figure 7.19 shows that, when the bridge is in its maximum expanded position, the soil and EPS material behind the abutment bulges, and when the bridge is in its minimum contracted position, the soil and EPS material settle. After the bridge has returned to the initial position, the three nodes closest to the abutment, corresponding to EPS material, experienced a rebound. The fourth node, corresponding to soil, experienced very little or no rebound. The accumulated settlement after one year of thermal cyclic simulation is 1.2 inches. This is for a total thermal displacement of 3 inches, as shown in Figure 7.6.

Chapter 2 discussed the length of approach slabs used in practice, and one of the options is to compute that length based on Rankine passive earth pressure theory, which produces a length of

the approach slab equal to tan (45 + ϕ/2) times the height of the abutment. In this particular case, ϕ = 38 degrees and the height of the abutment plus pile cap is 10.25 ft, so the resulting length of the approach slab would be 21 ft. Comparing the computed length with the results of Figure 7.18 indicates that this method might over-predict the area where settlement occurs in an IAB designed with EPS and dowels. According to Figure 7.18, the settlement occurs within 8 to 9 ft of the abutment, which is slightly less than the height of the abutment plus pile cap.

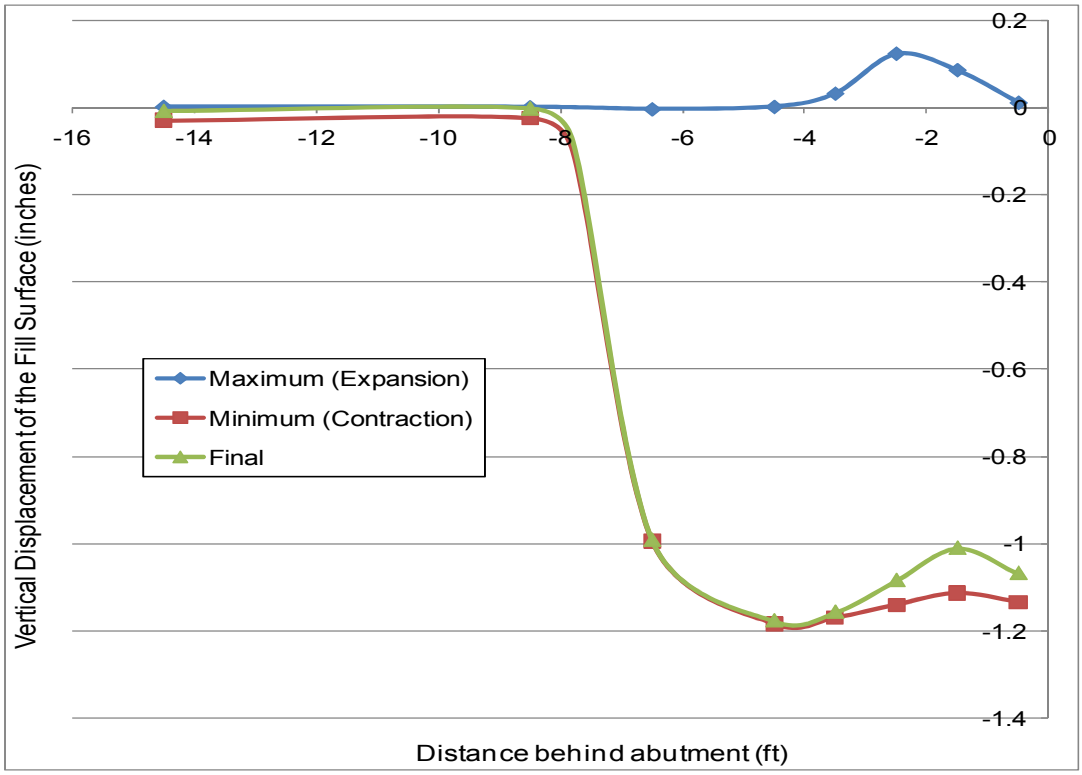

Figure 7.19 – Maximum, minimum, and final vertical displacements of the backfill surface behind the abutment for the base case.

7.1.8 Transverse Direction

So far, only the bridge response in the longitudinal direction (aligned with the bridge centerline) has been described. Although the transverse values were monitored during all of the analyses, they have not been discussed for the base case because they are very small when no skew angle is present.

For a bridge with zero skew angle, the transverse responses are a consequence of the Poisson effect. As an example of this, Figure 7.20 shows the piles shear forces right under the abutment. The magnitudes of these transverse shear forces are very much smaller than the longitudinal shear forces shown in Figure 7.8.

The Poisson effect produces the same amount of lateral expansion of the abutment in both directions. Thus, piles positioned at the same distance from the center pile experience an equal shear force acting in opposite directions. The pile located at the center of the abutment experiences little or no movement, so the pile shear force at this position is almost zero.

When the bridge expands, the transverse shear forces acting on the piles increase. Conversely, as the bridge contracts, the the transverse shear forces decrease.

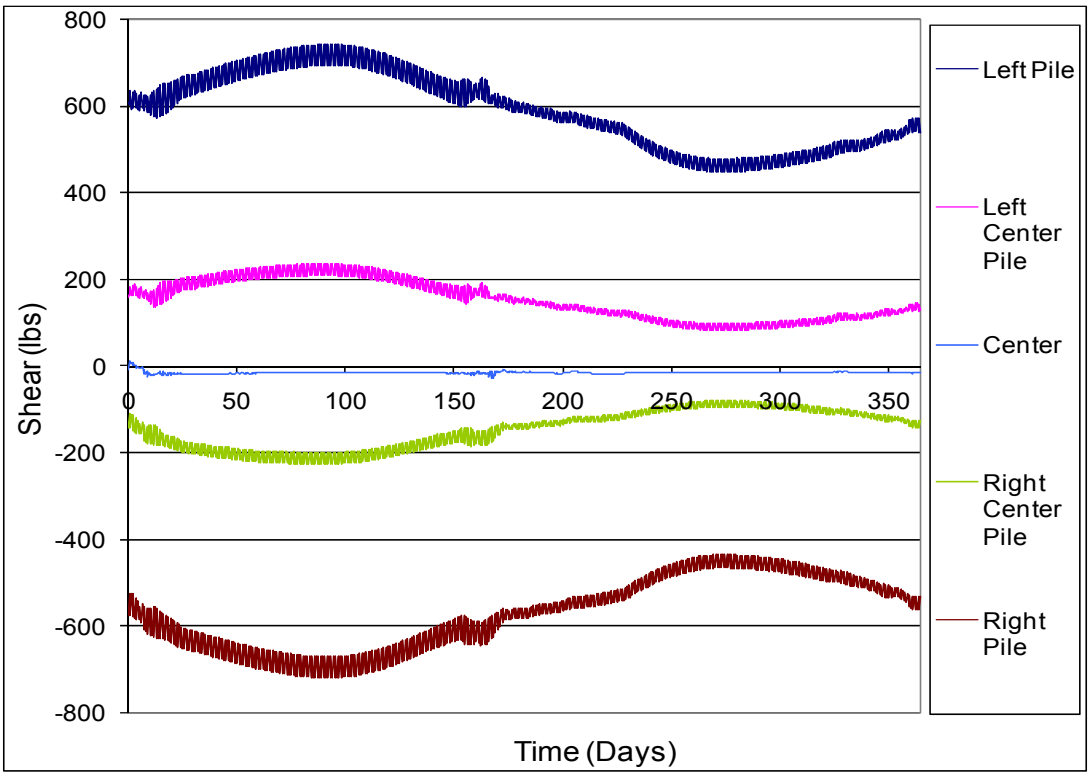

Figure 7.20 – Pile shear forces for the base case.

7.2 Parametric Variations

This section presents the single parameter variation cases studied in this research. These cases were created by changing only one parameter at a time in the base case model. Table D.1 in Appendix D provides the detailed analysis results that form the basis of the summary presented here. Table D.1 includes calculated values of shear forces and moments in dowels (longitudinal and transverse directions), axial force in dowels, shear forces and moments in piles directly under the abutment and two feet under the abutment (longitudinal and transverse directions), axial force in piles, and normal and shear forces acting over interface 1 (between EPS and pile cap) and interface 2 (between EPS and abutment backwall).

The key findings from the single parameter variation cases are discussed in this section.

7.2.1 Parametric Study Cases

In order to study the impact of different input parameters on the bridge response, a series of single parameter variation cases were created from a wide range of possible design choices. Using the recommendations of VDOT and VTRC engineers, the most important parameters in current designs were numerically implemented, such as abutment type, skew angle, offset between MSE wall and abutment piles, the use of EPS material, girders and MSE wall dimensions, foundation soil, pile size and orientation, and reinforcing strips behind the abutment. In addition to these parameters, different magnitudes of thermal displacement were analyzed to represent a wide range of bridge lengths.

Each case represents a change of only one parameter from the base case model. Table 7.6 lists the cases analyzed during this research. This table provides the case number, the value of the parameter in the base case model, the value of the parameter in the numbered case, and a brief description of what was changed.

Table 7.7 provides the geometries for Cases 12, 13, 14 and 15.

Table 7.6 – Parametric study cases

Case	Varied Parameter	Parameter Value		Description
		Base Case	Numbered Case	
1	Abutment type	Dowels	Laminated Pad	Laminated pad connecting the pile cap to the upper abutment.
2		Dowels	Solid	No joint at the pile cap, solid abutment.
3	Distance between abutment backwall and MSE wall	Distance 2’	Distance 0.5’	Distance changed to 0.5 ft.
4		Distance 2’	Distance 1’	Distance changed to 1 ft.
5		Distance 2’	Distance 3’	Distance changed to 3 ft.
6		Distance 2’	Distance 5’	Distance changed to 5 ft.
7	Thermal displacement	3”	0.75”	Thermal displacement reduced to 0.75”.
8		3”	1.5”	Thermal displacement reduced to 1.5”.
9		3”	4.5”	Thermal displacement increased to 4.5”.
10	EPS behind front MSE w.	No ESP	EPS	A 3” layer of EPS behind front MSE wall.
11	Foundation Material	Silty Sand	Shale Rock	Foundation geomaterial changed to shale rock.
12	Girder and MSE wall geometry	Geometry – Base Case	Geometry 1	Girder and abutment dimensions were reduced. See Table 3
13		Geometry – Base Case	Geometry 2	Girder and abutment dimensions were increased. See Table 3
14		Geometry – Base Case	Geometry 3	MSE wall height reduced to 17 ft. See Table 3
15		Geometry – Base Case	Geometry 4	MSE wall height increased to 30 ft. See Table 3
16	EPS behind abutment	EPS	No EPS	The layer of EPS material behind the abutment was removed.
17	Pile orientation	Weak	Strong	Piles orientation was changed from weak to strong bending moment
18	Pile Size	10x42	12x53	Pile size increased
19		10x42	14x73	Pile size increased
20	Strips behind the abutment	No Strip	Strips	Strip placed behind abutment
21	Bridge skew angle	No skew	10˚	Model modified to include skew of 10˚
22		No skew	20˚	Model modified to include skew of 20˚
23		No skew	35˚	Model modified to include skew of 35˚
24		No skew	40˚	Model modified to include skew of 40˚
25		No skew	45˚	Model modified to include skew of 45˚
26		No skew	50˚	Model modified to include skew of 50˚

Table 7.7 – Dimensions for Cases 12, 13, 14 and 15

Description	Dimensions				
	Base Case	Case 12	Case 13	Case 14	Case 15
Abutment thickness	3 ft	3 ft	3 ft	3 ft	3 ft
Total abutment height	10.25 ft	**9.5 ft**	**11 ft**	10.25 ft	10.25 ft
Girder flange width	16 in	16 in	16 in	16 in	16 in
Girder flange thickness	0.75 in	0.75 in	0.75 in	0.75 in	0.75 in
Girder web height[1]	69 in	**60 in**	**78 in**	69 in	69 in
MSE wall height	23.7 ft	23.7 ft	23.7 ft	**17 ft**	**30 ft**

[1]Does not includes flanges

7.2.2 Parametric Study Comparison with Base Case

In each of the following subsections, a single case or a group of cases is discussed in comparison with the base case model.

7.2.2.1 Abutment Design

Figure 7.21 shows the abutment designs used by Virginia DOT. From left to right, the abutment designs incorporate dowels (implemented in almost all of the numerical models), laminated pads, and solid abutments. Laminated pads and solid abutments correspond to case numbers 1 and 2, respectively.

Laminated pads and dowels have the objective of reducing the transferred movements from the upper part of the abutment to the pile cap.

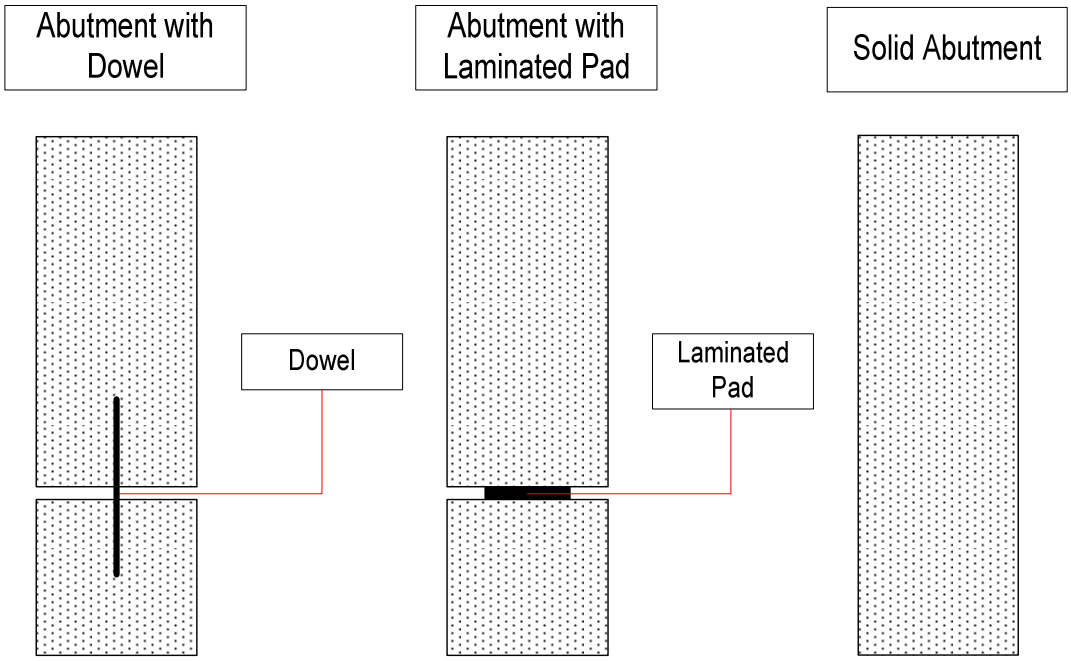

Figure 7.21 – Abutment designs.

The TIR changes with respect to the base case model due to the laminated pad design are:

- Displacement at top of pile cap: Decreased by 20% (-20%).
- Displacement at bottom of pile cap: Unchanged
- Upper abutment horizontal pressures: Unchanged
- Lower abutment horizontal pressures: Decreased by 12% (-12%)
- Pile moments: Decreased by 57% (-57%)
- Pile shear forces: Increased by 100% (+100%)
- MSE wall pressures: Increased by 40% (+40%)
- MSE wall strip tension at the connection: Increased by 53% (+53%)
- MSE wall peak strip tension: Increased by 26% (+26%)

The analyses show that laminated pads reduce the TIR movements of the top of the pile cap, while at the bottom of the pile cap, the horizontal displacement is about the same as in the base case. Therefore, the effect of the laminated pad in comparison with dowels is for the pile cap to rotate less than in the base case, although the tops of the piles displace about the same amount.

The reduction in TIR of moments in piles occurs due to smaller pile cap rotations. The TIR of shear forces in the piles are doubled in comparison with the base case. This occurs because the horizontal normal forces acting on the pile cap produced by the soil and EPS are very similar to the doweled case, but the laminated pad transfers less shear force than the dowels, so the piles must take more of the horizontal shear force applied by the soil and EPS.

The TIR changes in the MSE wall pressures and strip tensile forces are product of the increased shear forces acting on piles, which translates in larger pressures imposed by the piles over the front MSE wall.

The TIR changes with respect to the base case model due to the solid abutment design are:

- Displacement at top of pile cap: +24%.
- Displacement at bottom of pile cap: +100%
- Upper abutment horizontal pressures: -11%
- Lower abutment horizontal pressures: -2%
- Pile moments: +200%
- Pile shear forces: +500%
- MSE wall pressures: +163%
- MSE wall strip tension at the connection: +370%
- MSE wall peak strip tension: +163%

The analyses show that solid abutments experience more lateral displacement than abutments with dowels. The TIR of displacement at the top of the piles increased by 100% compared to abutments with dowels. The TIR of the earth pressure behind the abutment decreased at both upper and lower positions because, at the end of the gravitational-force stage, the solid abutment case has much larger horizontal earth pressure acting on the backwall, and since the maximum value remains almost the same, the TIR in earth pressure is reduced.

7.2.2.2 Abutment MSE Wall Distance

In Cases 3 through 6 the distance between the back of the front MSE wall and the abutment wall facing the bridge varies from 0.5 to 5 feet. Including the base case, the distances are 0.5, 1, 2, 3 and 5 feet.

The TIR changes with respect to the base case model due to variation of MSE wall distance are:

- Displacement at top of pile cap: Less than 3%
- Displacement at bottom of pile cap: Less than 3%
- Upper abutment horizontal pressures: Less than 3%
- Lower abutment horizontal pressures: Less than 10%
- Dowel moments: Less than 7%
- Pile moments: Less than 2%
- Dowel shear forces: Less than 7%
- Pile shear forces: Less than 4%
- MSE wall pressures: -12% to +63% (Figure 7.22)
- MSE wall strip tension at the connection: -7% to +88% (Figure 7.22)
- MSE wall peak strip tension: -25% to +10% (Figure 7.22)

The horizontal displacements of the top and bottom of the pile cap did not change more than 3%. This implies that shear forces and moments in dowels and piles do not significantly change, and the results show that the maximum change experienced by these output parameters is 10%, with the average being about 4%. The same applies to normal and shear forces acting on the pile cap.

The distance between the back of the front MSE wall and the abutment wall facing the bridge affects the strip tensile forces at both the connection and the peak, as well as the earth pressure on the front MSE wall. Figure 7.22 shows how these output parameters are affected by the aforementioned distance. The earth pressure on the front MSE wall and the strip tensile force at the connection are affected similarly, which is expected, given the proximity of these two output parameters. Also from Figure 7.22, abrupt changes are displayed in the TIR of those output parameters when the MSE wall is closer than 2 feet.

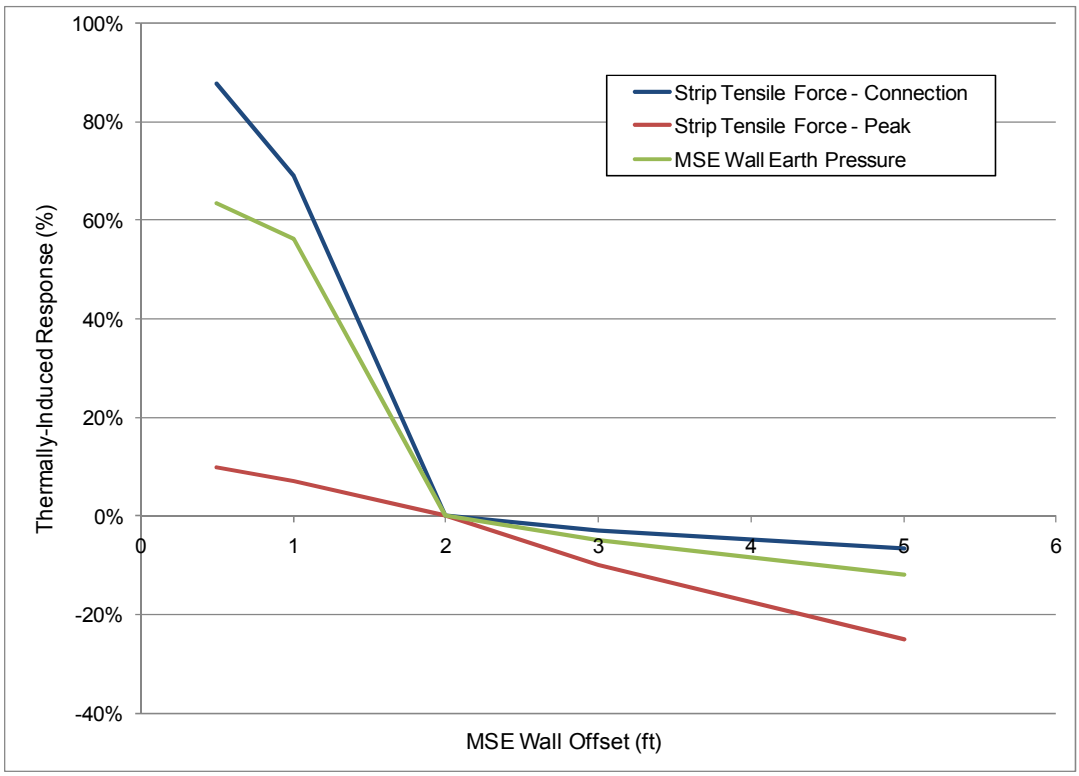

Figure 7.22 – Strip tensile forces and earth pressure at front MSE wall

The reduction in the TIR of the peak tensile force is more significant than for the two other mentioned output parameters, reaching a value of 25% for a distance of 5 ft from the front of the abutment to the back of the MSE wall. This occurs mainly because the peak value location has moved farther into the embankment, and thus the distance from the abutment has increased, making the thermal displacement effect less pronounced.

The TIR of earth pressure behind the abutment is barely affected by the distance between the abutment and the MSE wall, since the magnitude of the thermal displacements and the abutment design has not changed in Cases 3 through 6.

7.2.2.3 Thermal displacements

Cases 7, 8, and 9 correspond to different magnitudes of thermal displacement, i.e., 0.75”, 1.5”, and 4.5”, respectively. This range of displacements corresponds to bridges ranging from 166 ft to 996 ft, with total thermal increment of 115˚ F. Thermal displacement influences the response of

all bridge components, and all the output monitored points respond to changes in the magnitude of thermal displacements. The change in response is approximately proportional to the change in thermal displacement magnitude when other parameters are held constant.

The TIR changes with respect to the base case model due to variation of thermal displacement are:

- Displacement at top of pile cap: Proportional to thermal displacement
- Displacement at bottom of pile cap: Proportional to thermal displacement
- Upper abutment horizontal pressures: -54% to +17%
- Lower abutment horizontal pressures: -60% to +12%
- Dowel moments: -70% to +30% (Figure 7.23)
- Pile moments: -74% to +38% (Figure 7.23)
- Dowel shear forces: -70% to +30% (Figure 7.23)
- Pile shear forces: -63% to +35% (Figure 7.23)
- MSE wall pressures: -61% to +15% (Figure 7.22)
- MSE wall peak strip tension: -78% to +15% (Figure 7.22)

Figure 7.23 shows shear force and moment variations for piles and dowels versus thermal displacements. As shown in Figure 7.23(a), these four output parameters have very similar trends in response to changes in thermal displacements. It is interesting to see that, if the abutment thermal displacement is increased by 50%, the TIR increases between 30% to 40%, and when the thermal displacement is decreased by 50%, the TIR decreases between 30% to 55%. Although the percent changes shown in Figure 7.23(a) are very similar, Figure 7.23(b) shows that the magnitudes corresponding to the same parameters are not. This occurs because the values for the base case are different for the different output parameters.

Figure 7.24 shows the variation of normal force on the pile cap and the upper part of the abutment. These forces are very similar to the horizontal earth pressure responses previously described in section 7.1.6.4. These forces are computed by integrating the horizontal pressure of each interface over each corresponding area of the abutment. They are monitored in the interface elements, while those in section 7.1.6.4 are monitored in the soils right behind the abutment.

Figure 7.24 also shows the strip tensile forces monitored at the peak value and the change in earth pressures against the front MSE wall. The similarities of these four output parameters with those in Figure 7.23 confirm that thermal displacements produce a similar effect on all the output parameters.

Figure 7.24 illustrates that, the more the abutment is displaced, the greater are the responses. The maximum value for the normal forces on the abutment occur during the bridge expansion phase, and the maximum value for the strip tensile forces and the earth pressures on the front MSE wall occur during the bridge contraction phase. It is interesting that the four output parameters displayed in Figure 7.24 have similar responses, even though their maximum values are produced 180 days apart. An important consideration in assessing the results is that the EPS thickness behind the abutment changes according to the magnitude of the thermal displacement according to VDOT practice, with the EPS thickness determined according to Eq. 7.1. Thus, the larger the thermal displacement, the thicker the EPS material behind the abutment, and therefore, somewhat muted responses for the abutment and pile cap are expected when bigger thermal displacements are imposed, but the responses for these outputs still follow the same trend as displayed in Figure 7.24 for the strip tensile forces and the MSE wall pressures.

$$EPS_t = 10\,[0.01\,h + 0.67\,\Delta L] \tag{7.1}$$

where EPS_t = EPS thickness
h is the height of integral backwall in inches
ΔL is the total thermal displacement in inches

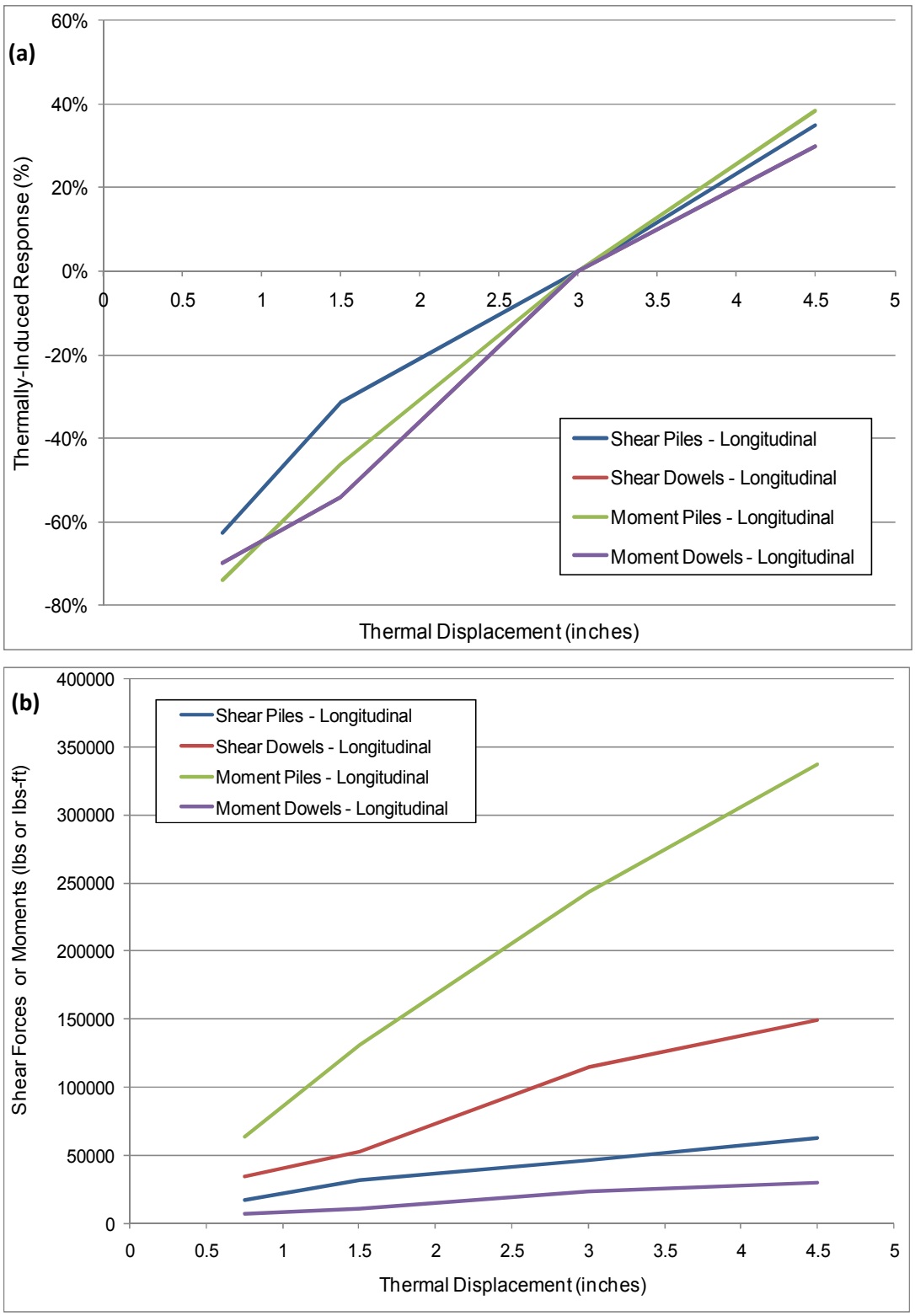

Figure 7.23 – Shear forces and moment variations vs. thermal displacements.

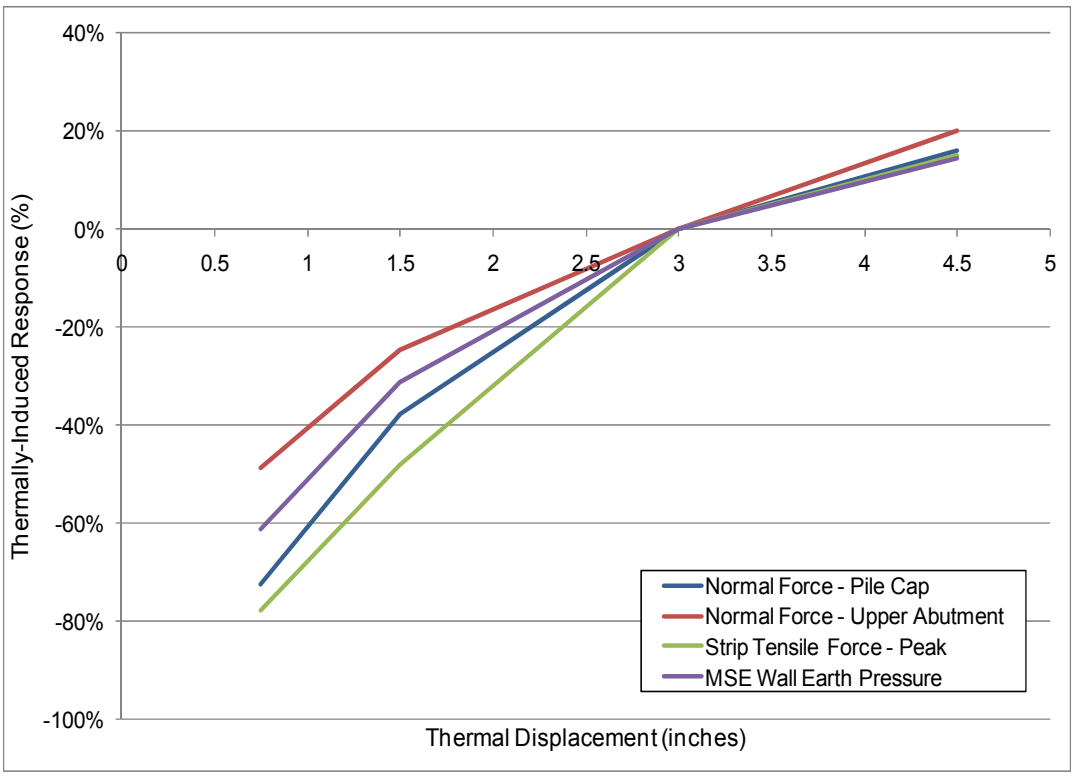

Figure 7.24 – Thermally-induced response of normal force on abutment, strip tensile force, and MSE wall earth pressure vs. thermal displacements.

7.2.2.4 EPS at Front MSE Wall and Shale Foundation

Case 10 was modified from the base case by placing a 4 inch thickness of EPS material behind the front MSE wall, and Case 11 was modified by changing the foundation material from silty sand to shale rock.

The TIR changes with respect to the base case model due to EPS and shale foundation are:

- Displacement at top of pile cap: Unchanged
- Displacement at bottom of pile cap: +1% for EPS case, -1% for shale case.
- Upper abutment horizontal pressures: Unchanged
- Lower abutment horizontal pressures: Unchanged
- Dowel moments: -1% for EPS case, +4% for shale case.
- Pile moments: -1% for EPS case, +8% for shale case.
- Dowel shear forces: -1% for EPS case, +4% for shale case.

- Pile shear forces: -9% for EPS case, +3% for shale case,
- MSE wall pressures: +15% for EPS case, +40% for shale case,
- MSE wall strip tension at the connection: -15% for EPS case, +25% for shale case.
- MSE wall peak strip tension: -15% for EPS case, +25% for shale case.

The parameter changes associated with these two cases do not significantly affect shear forces and moments in dowels and piles. The average percent change of TIR is 4%, with some output parameters being positively affected and some negatively affected.

In Case 10 the thermal movements imposed by the piles over the backfill soil are partially absorbed by the EPS behind the front MSE wall. This translates into a reduction in the TIR of shear forces and moments in piles and dowels. For the same reason, the TIR of strip tensile forces is reduced. The TIR of earth pressure acting on the front MSE wall is increased by 15%, but this result is not significant given that the maximum and the gravitational values are both smaller than those in the base case model.

In Case 11 the rock is much stiffer than the foundation soil, so that no lateral deflections are allowed at the pile foundation level. The displacement at the bottom of the pile cap is slightly less because of the laterally restricted piles at foundation level, but the top of the pile cap still moves the same amount, thus increasing the rotation of the pile cap and producing slightly larger shear forces and moments in piles and dowels. Although the TIR of reinforcing strip tensile forces and earth pressure behind the front MSE wall has increased, the increase is not significant because the maximum and gravitational values are smaller than those in the base case model. Those values are smaller because the stiffer foundation allows the piles to support more backfill soil weight through load transfer to the piles during backfill compression due to self weight.

The TIR of the earth pressure behind the abutment remains almost unaltered, because neither placing EPS material behind the front MSE wall, nor changing the foundation material, significantly affect the interaction of the abutment components.

7.2.2.5 Bridge Geometries

Cases 12 through 15 change the base case design geometries. Cases 12 and 13 change the size of the girders, and Cases 14 and 15 change the size of the main MSE wall height.

In Cases 12 and 13, the girder web height is decreased and increased by 9 inches, respectively. The strong moment of inertia is 43,027 in^4 in the base case, 31,139 in^4 (-28%) in Case 12, and 56,974 in^4 (+32%) in Case 13. The weak moment of inertia in the base case is 512 in^4, and this value remains the same for Cases 12 and 13 so that only one parameter was changed.

In Case 14, the height of the MSE wall main body, i.e. the portion below the abutment, was reduced to 17 ft, for an overall embankment height of 26.3 ft. In Case 15, the main MSE wall body was increased to 30ft, for an overall embankment height of 39.3 ft. The overall embankment height in the base case is 33 ft, and the changes in embankment heights represent a reduction of 20% and an increase of 19% in Cases 14 and 15, respectively.

The TIR changes with respect to the base case model due to variation in geometry (girders and MSE wall height) are:

- Displacement at top of pile cap: 0% for girder case, +1% for MSE wall case
- Displacement at bottom of pile cap: 0% for girder case, +5% for MSE wall case
- Upper abutment horizontal pressures: 0% for girder case, -3% for MSE wall case
- Lower abutment horizontal pressures: -1% for girder case, +4% for MSE wall case
- Dowel moments: 1% for girder case, +2% for MSE wall case
- Pile moments: -1% for girder case, +1% for MSE wall case
- Dowel shear forces: 0% for girder case, +2% for MSE wall case
- Pile shear forces: 0% for girder case, +6% for MSE wall case
- MSE wall pressures: +5% for girder case, +5% for MSE wall case
- MSE wall strip tension at the connection: +2% for girder case, +5% for MSE wall case
- MSE wall peak strip tension: 0% for girder case, +5% for MSE wall case

Although Cases 12 and 13 significantly changed the height of the girder web, these two cases produce less impact on the bridge response that any other cases. This is because all of the girders provide nearly complete restriction to rotation of the upper portion of the abutment, even the smallest of the three selected sizes. The change in the TIR of displacement at the abutment is exactly 0% for all locations on the abutment. Consequently, the shear forces and moments in dowels and piles do not change. The same is true for strip tensile forces, and for earth pressures on the front MSE wall and behind the abutment.

Cases 14 and 15 show very little influence on shear forces and moments in dowels and piles. This occurs because the response in the vicinity of the abutment is not significantly affected by conditions far from the abutment, such as those corresponding to changes in MSE wall height. The same conclusion applies to the earth pressure behind the abutment.

The MSE wall height does have a small effect on the TIR of strip tensile forces and the TIR of earth pressure acting on the front MSE wall. But it is important to note that those changes in the TIR are not significant because the maximum values remain about the same for the output parameters directly under the abutment. The changes in the TIR of these output parameters occur mostly with a short MSE wall. A short MSE wall behaves stiffer, and it limits the horizontal displacement transferred by the piles. Another reason that the TIR of these output parameters changes is that, in the short MSE wall, thermal movements are closer to the foundation level, and the monitored straps at the bottom of the MSE wall experience more thermal displacement.

7.2.2.6 No EPS behind the Abutment

Case 16 does not have EPS material behind the abutment, so that the soil and concrete abutment are in contact for this case.

The TIR changes with respect to the base case model due to removal of EPS material behind abutment are:

- Displacement at top of pile cap: +8%
- Displacement at bottom of pile cap: +10%

- Upper abutment horizontal pressures: 9 times bigger
- Lower abutment horizontal pressures: 20 times bigger
- Dowel moments: -16%
- Pile moments: -31%
- Dowel shear forces: -16%
- Pile shear forces: +44%
- MSE wall pressures: Unchanged
- MSE wall strip tension at the connection: Unchanged
- MSE wall peak strip tension: Unchanged

Since the abutment is in contact with the soil, which is a stiffer material than the EPS, the rotation of the pile cap is greatly reduced, as is the relative displacement between the upper abutment portion and the pile cap. In addition, the earth pressures against the abutment backwall are significantly increased. A result of these interactions is that the TIR of shear forces in the piles increases, but the TIR of moments in the piles and the TIR of shear forces and moments in the dowels decreases.

The maximum value of the strip tensile forces and earth pressure behind the front MSE wall increased by 8 to 15%, but the overall TIR values for these output parameters have not changed. This effect has the same origin as previously described for shear force TIR, which is the increase of earth pressure behind the abutment backwall.

The most important effect produced by this case is on the earth pressure behind the abutment. Figure 7.25 shows the lower monitoring point of the earth pressure behind the abutment. Two cases are displayed, the base case, which includes EPS behind the abutment, and Case 16, which does not include EPS behind the abutment.

The impact of removing the EPS from behind the abutment is large, and the TIR of earth pressure has increased for the upper monitoring location by a factor of 9, and it has increased for the lower measuring position by a factor of 20. The maximum earth pressure for the cyclic

simulated year has increased for the upper measuring position 6 times, and it has increased for the lower measuring position by 13.

Figure 7.26 shows four plots of earth pressure versus depth behind the abutment: (1) the earth pressure for the Rankine active condition, base case maximum values, the Rankine passive condition, and Case 16 maximum values. The maximum values of the earth pressure for the base case and Case 16 were calculated at the center of the abutment and at the two monitored elevations. Figure 7.26 shows that Rankine active conditions produce the smallest earth pressures distribution, and the base case maximum earth pressure is the next largest distribution. This last value, as previously described, produces close to a uniform distribution behind the abutment. The next larger distribution is the Rankine passive condition, and finally the largest distribution is the Case 16 maximum earth pressures. In this last case, the maximum earth pressures exceed the Rankine passive earth pressure values because friction is mobilized between the abutment and the backfill soil.

When comparing those four results, the effectiveness of the EPS material at reducing the earth pressure behind the abutment is evident.

Another way to present the information in Figure 7.26 is to plot the coefficient of lateral earth pressure versus the depth, as shown in Figure 7.27. The backfill soil has a friction angle of 38°, therefore the Rankine Ka and Kp values are 0.24 and 4.2, respectively. The Rankine active and passive coefficients plot as vertical lines in Figure 7.27, while the base case and Case 16 plot as inclined lines with a higher lateral earth pressure coefficient at shallower depths.

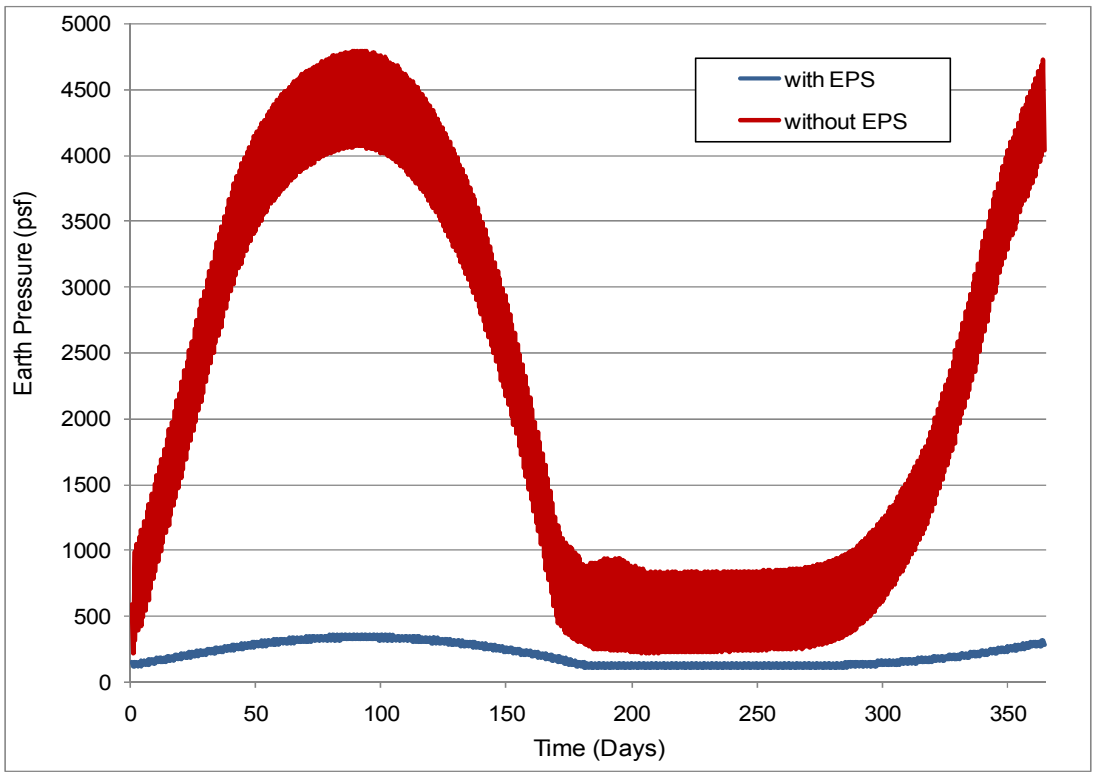

Figure 7.25 – Earth pressure behind the abutment. Comparison between base case with EPS and Case 16 without EPS. Lower monitoring point.

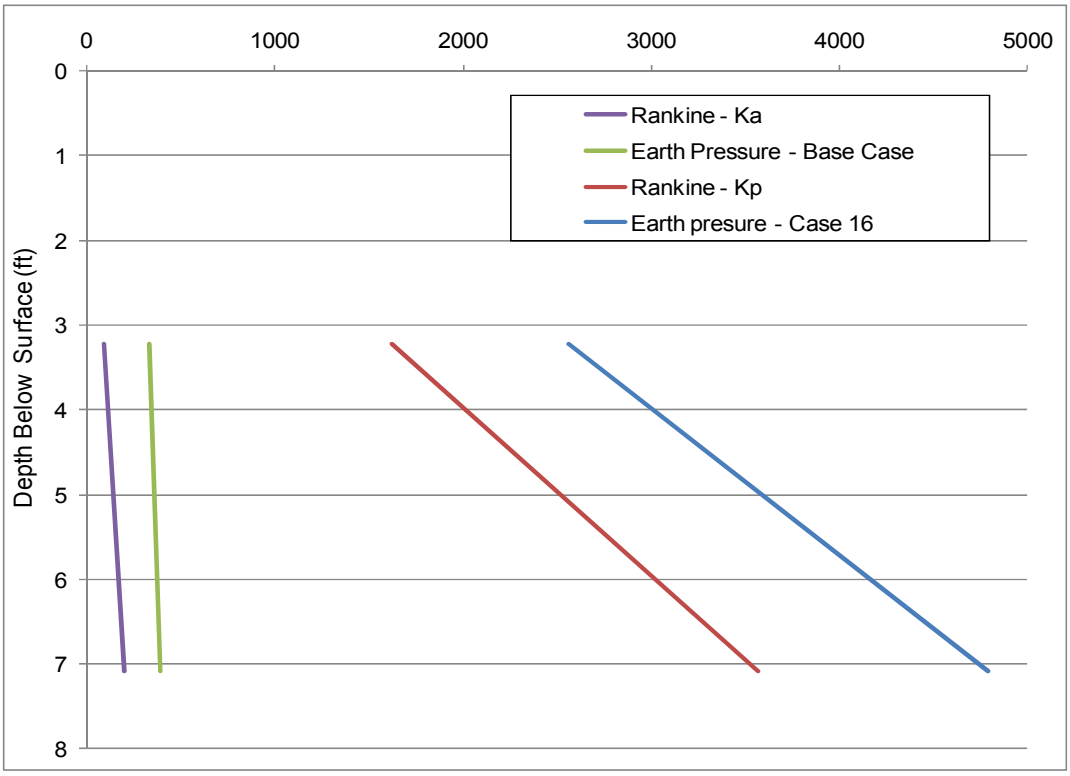

Figure 7.26 – Earth pressure behind the abutment vs. depth behind abutment.

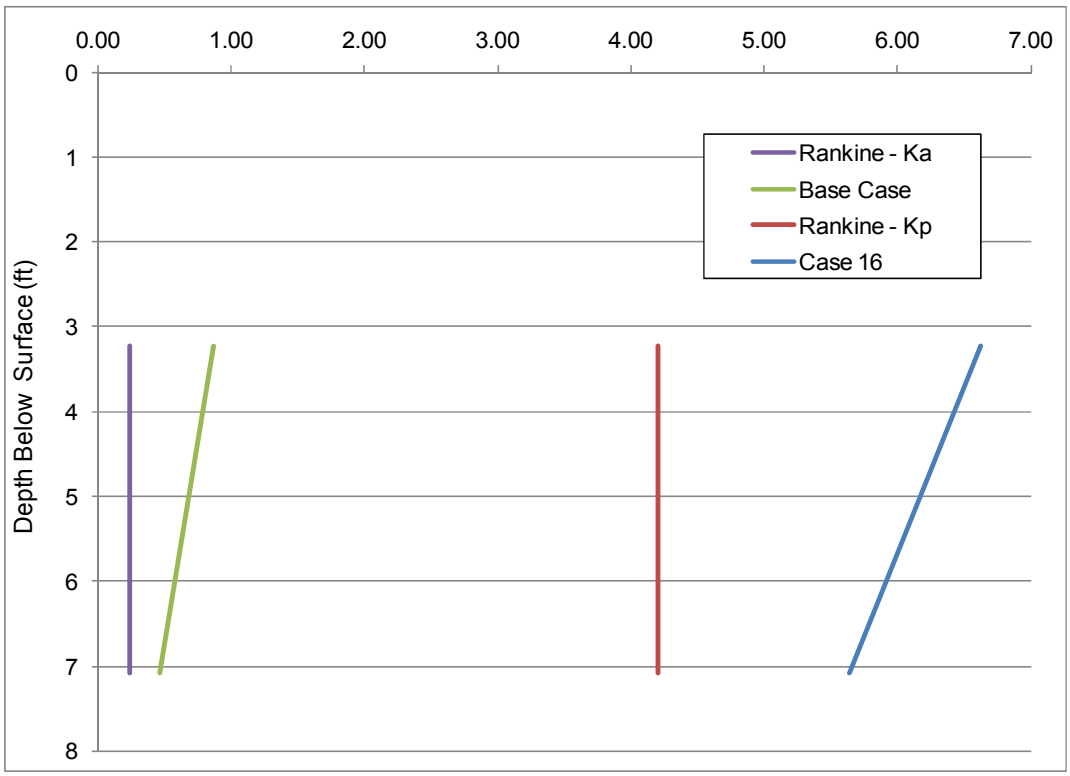

Figure 7.27 – Coefficient of lateral earth pressure vs. depth behind abutment

Figure 7.27 shows that the Rankine active conditions and the base case distribution are similar, and the Rankine passive condition and Case 16 distributions are similar, with the base case and Case 16 distributions shifted to the right of the corresponding active and passive pressure distributions. Interestingly in Figure 7.27, instead of the parallelism shown by Figure 7.26 between active and base case conditions and between passive and Case 16 conditions, a new parallelism develops between the active and passive conditions and between the base case and Case16.

Is important to notice that the absence of EPS material behind the abutment produces not only a big increase in the earth pressure behind the abutment, but it also changes the distribution of the earth pressure behind the abutment from being approximately uniform for the base case to increasing markedly with depth for Case 16.

7.2.2.7 Pile Strong Orientation and Pile Size

In Case 17, the abutment piles were rotated 90 degrees so that the piles are oriented for strong axis bending. Rotating the abutment piles from weak to strong axis is not one change at a time, as in the research plan for single parameter variations, rather, it is two changes at once. The first change reduces the moment of inertia in the direction traverse to the bridge centerline, and the second change increases the moment of inertia in the direction longitudinal to the bridge alignment. However, given that this case was built with no skew angle, the moments transverse to the bridge alignment are not important, thus these changes can be considered as one change at a time, i.e., only increasing the moment of inertia in the longitudinal direction. On the other hand, Chapter 8 shows that rotating piles 90 degrees is important for skewed bridges, because it sets a new category of analysis.

Cases 18 and 19 replace the abutment piles with bigger ones. The base case incorporates 10x42 H piles, Case 18 incorporates 12x53 H piles, and Case 19 incorporates 14x73 H piles.

The above information can be expressed in terms of moment of inertia in the direction of the bridge alignment, which increases in the order of 71.7 in^4, 127 in^4, 210 in^4, and 261 in^4 for the base case, Case 18, Case 17, and Case 19, respectively.

The TIR changes with respect to the base case model due to pile rotation and pile size changes are:

- Displacement at top of pile cap: -11% for strong, -7% for 12x53, -20% for 14x73
- Displacement at bottom of pile cap: -5% for strong, -2% for 12x53, -9% for 14x73
- Upper abutment horizontal pressures: -1% for strong, -1% for 12x53, -1% for 14x73
- Lower abutment horizontal pressures: -2% for strong, -2% for 12x53, -2% for 14x73
- Dowel moments: +23% for strong, +13% for 12x53, +27% for 14x73
- Pile moments: +30% for strong, +18% for 12x53, +38% for 14x73
- Dowel shear forces: +23% for strong, +13% for 12x53, +27% for 14x73
- Pile shear forces: +56% for strong, +37% for 12x53, +94% for 14x73
- MSE wall pressures: +41% for strong, +31% for 12x53, +80% for 14x73

- MSE wall strip tension at the connection: +28% for strong, +21% for 12x53, +52% for 14x73
- MSE wall peak strip tension: +55% for strong, +43% for 12x53, +112% for 14x73

All these cases restrict the pile cap rotation, but the upper abutment portion still displaces the same amount. As a result, the TIR of moments and shear forces in the dowels increased. Although the pile cap rotation has decreased, the TIR of moment and shear forces in piles increased because stiffer elements require smaller movements to produce larger forces.

These three cases produce very similar results for dowels and piles. The Case 17 results, which are for piles oriented for strong axis bending, are always between the results for Cases 18 and 19, and closer to Case 19. Orienting piles for strong bending moments attracts shear and moment to the dowels and piles.

The TIR of strip tensile forces and MSE wall earth pressure has increased, because stiffer and/or bigger piles displace more soil when oscillating due to thermal displacements.

The TIR of the earth pressure behind the abutment barely changes in these cases. These small changes are associated with the smaller pile cap rotation due to stiffer piles.

7.2.2.8 Strips behind the Abutment

Case 20 incorporates strips behind the abutment aligned with the bridge centerline. The strips holding the MSE wall concrete panels in the U-back wings of the MSE are still in place and without modifications.

This change from the base case design has little to no effect on the bridge response. Most of the parameters present no variation in the TIR of the bridge, and for those parameters presenting some variation, it is limited to 1% to 2%.

Because the strips positioned at the abutment backwall stiffen the soil behind the abutment, it was expected that the earth pressure at the abutment would increase, but the EPS material positioned behind the abutment is very effective, and it maintains relatively low values of earth pressure, and thus no TIR in earth pressure is observed with respect to the base case.

7.2.2.9 Skew Angle

Cases 21 through 26 change the base case design by incorporating skew angle. The skew angles considered are 10°, 20°, 35°, 40°, 45°, and 50° for Cases 21 through 26.

Only the longitudinal impact of parameter variations on the bridge response has been discussed for bridges with zero skew angle, but from now on the transverse response becomes important. For bridges with large skew angles, the transverse response magnitude can reach values that are comparable with the longitudinal direction. One of the key reasons for performing this research project is to provide design engineers with information about the response of skewed bridges, for which very little information was previously available.

Figure 7.28 shows how the skew angle was defined for this research. All models incorporate the definition of skew angle in Figure 7.28, and therefore, transverse result signs have to be changed if the skew is measured in the opposite direction. Further discussion regarding this sign convention appears in Chapter 8.

This research follows the definition of acute and obtuse corners provided by Virginia DOT, as shown in Figure 7.29.

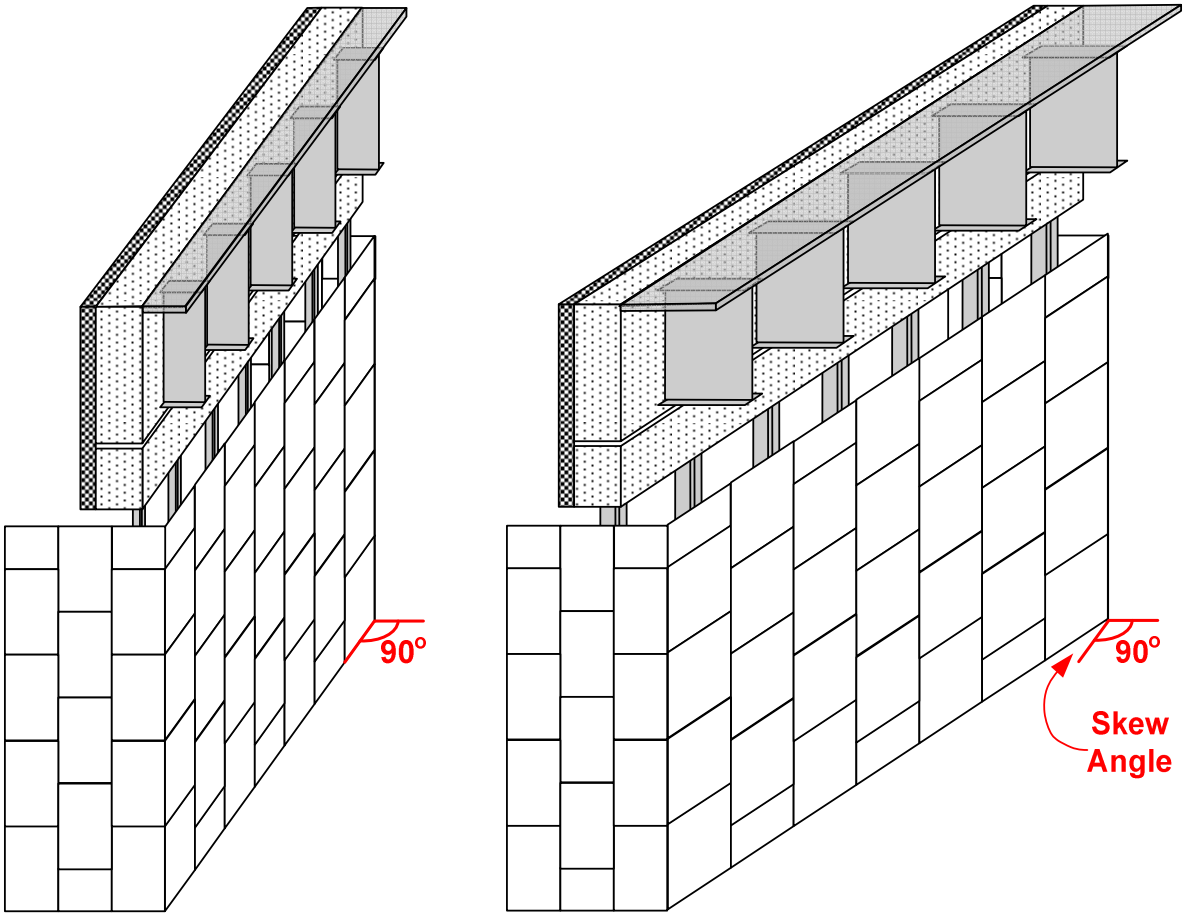

Figure 7.28 – Skew angle definition.

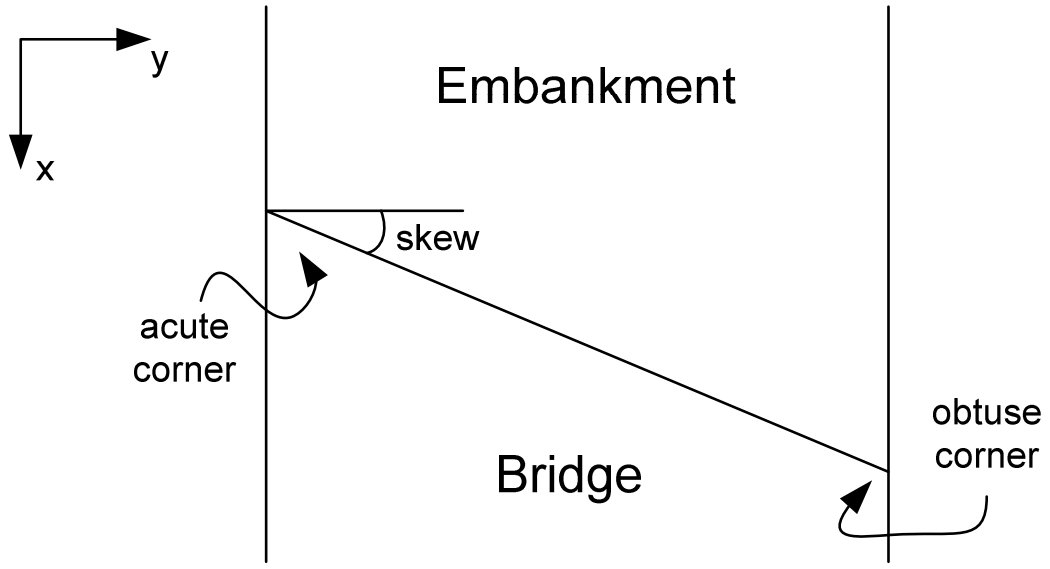

Figure 7.29 – Acute and obtuse corners definition.

The TIR changes with respect to the base case model due to skew angle (10˚ to 50˚) are:

- Longitudinal displ. at top of pile cap: -3% to -18% acute, +1% to -8% obtuse
- Longitudinal displ. at bottom of pile cap: 0% to +15% acute, +5% to +29% obtuse
- Transverse displacement at top of abutment: See Figure 7.30
- Upper abutment horizontal pressures: +7% to +47% acute, +3% to +17% obtuse
- Lower abutment horizontal pressures: -5% to -33% acute, -1% to -6% obtuse
- Dowel moments: +1% to +27%
- Pile moments: -14% to -169%
- Dowel shear forces: +1% to +27%
- Pile shear forces: +4% to +94%
- Transverse moments and shear forces: See Figure 7.32
- MSE wall pressures: +7% to +93%
- MSE wall strip tension at the connection: +6% to +115%
- MSE wall peak strip tension: +1% to +9%

Changes in the amplitude of the longitudinal displacement of the pile cap show that the pile cap rotation decreases with increasing skew angle. Displacement in the transverse direction increases as the skew angle increases. Figure 7.30 shows the longitudinal and transverse displacements versus the skew angle. The base case and all skewed models were subjected to a 3 inch maximum thermal displacement. Thus, the thermal displacement remained the same as the skew angle increased for the single parameter variation cases. Figure 7.30 shows the longitudinal maximum displacement at the top of the abutment as 1.5 inches, which occurs during the bridge expansion and contraction phases. The maximum transverse displacement occurs during the bridge expansion phase. As the skew angle increases, the transverse displacement at the top of the abutment increases, and it reaches a magnitude that is comparable with the magnitude of longitudinal displacements.

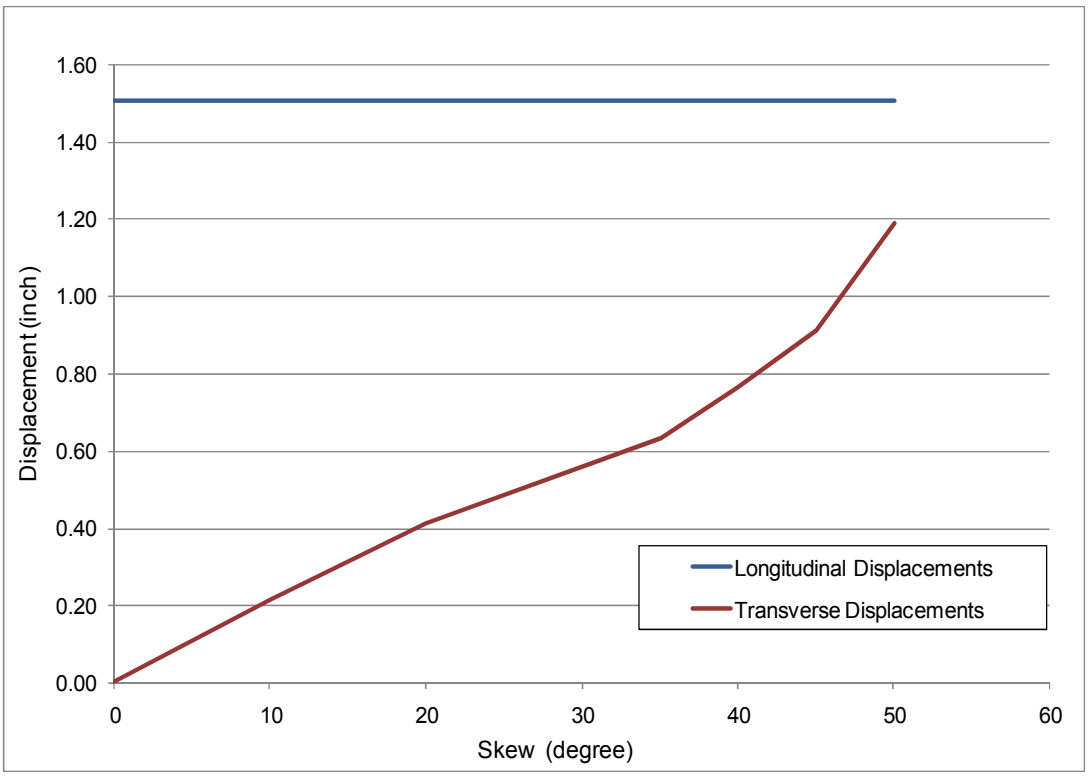

Figure 7.30 – Longitudinal and transverse displacement vs. skew angle.

Figure 7.31(a) shows the percentage variation in the TIR of shear forces and moments versus the skew angle for the longitudinal direction. In Figure 7.31(a), the TIR of shear forces in piles increases almost 100%. The TIR of shear forces and moments in dowels increases 27%. The TIR of moments in piles reduces up to 169%. All these effects are produced by the increase in fixity (reduction in rotation) of the pile cap.

The increase in the pile cap fixity is produced by a deviation from perpendicularity of the pile cap axis. When the skew angle is zero, the pile cap axis is perpendicular to the bridge centerline, and when the bridge displaces the abutment and pile cap, the pile cap can rotate because its axis is perpendicular to the thermal displacement movement. As the skew angle increases, the pile cap axis decreases its perpendicularity with respect to the bridge centerline. For each increase in skew angle, the pile cap reduces its rotation.

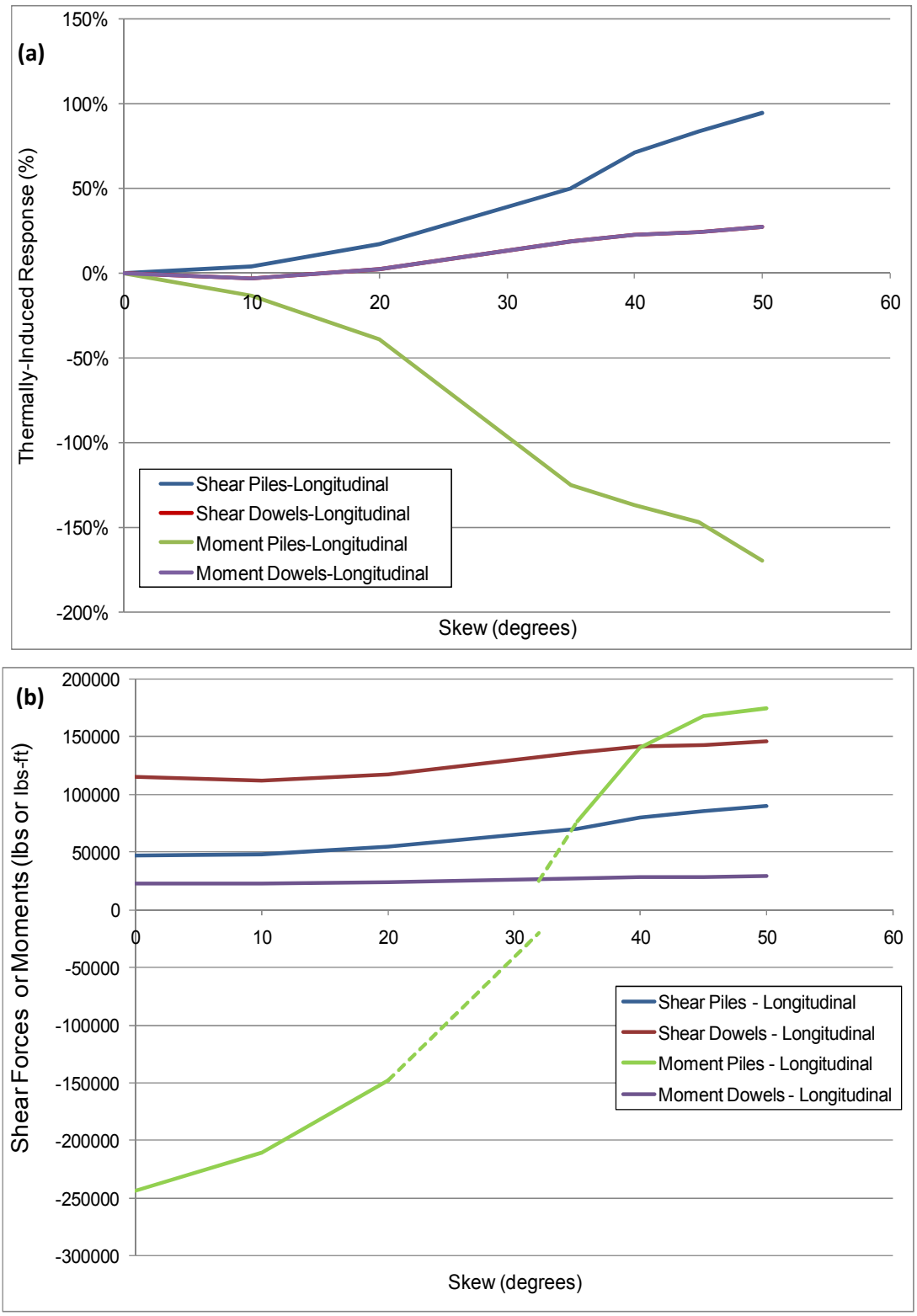

Figure 7.31 – Shear force and moment variations in the longitudinal direction vs. skew angle.

Figure 7.31(b) displays the same output parameters as Figure 7.31(a), but instead of showing the percentage change of the output parameter, this figure illustrates the corresponding magnitudes of the sum of the forces or moments of all the dowels or piles in the abutment. The magnitude of the moment in the piles changes sign as the skew angle increases. The moment reversal is produced by a reduction in rotation of the pile cap.

Analogous to Figure 7.31, Figure 7.32 shows the TIR variation of shear forces and moments versus skew angle for the transverse direction. Figure 7.32(a) shows that all four output parameters increase as the skew angle increases. It is evident that the TIR of moments in the piles increases significantly more than the other parameters. This occurs because the piles are oriented for strong-axis bending in the transverse direction so that small displacements produce big moments. Figure 7.32(b) shows the same information as 7.32(a), but with the moments in piles removed from the figure to permit expansion of the vertical axis. The moments in piles in Figure 7.32(a) have a similar shape to the shear forces in piles in Figure 7.32(b). This appears to indicate that shear forces and moments are more coupled in the transverse direction than the longitudinal direction, because the pile cap cannot rotate in this direction.

Figure 7.33 shows a comparison between shear forces and moments in piles in both directions, longitudinal and transverse. The output values at zero skew angle for the transverse direction always start from a magnitude near zero. This is in contrast to the longitudinal direction, which starts from the gravitational value. In the absence of skew angle, the model is symmetrical, and therefore no significant transverse forces act on the piles, and the only stresses acting on the piles are those related to the Poisson effect, which is very small compared to the transverse forces acting on the piles when skew angle is present

Figure 7.33(a) shows that shear forces in the transverse direction quickly increase as the skew angles increase. At a skew angle of about 20 degrees, the shear forces reach values comparable with those in the longitudinal direction.

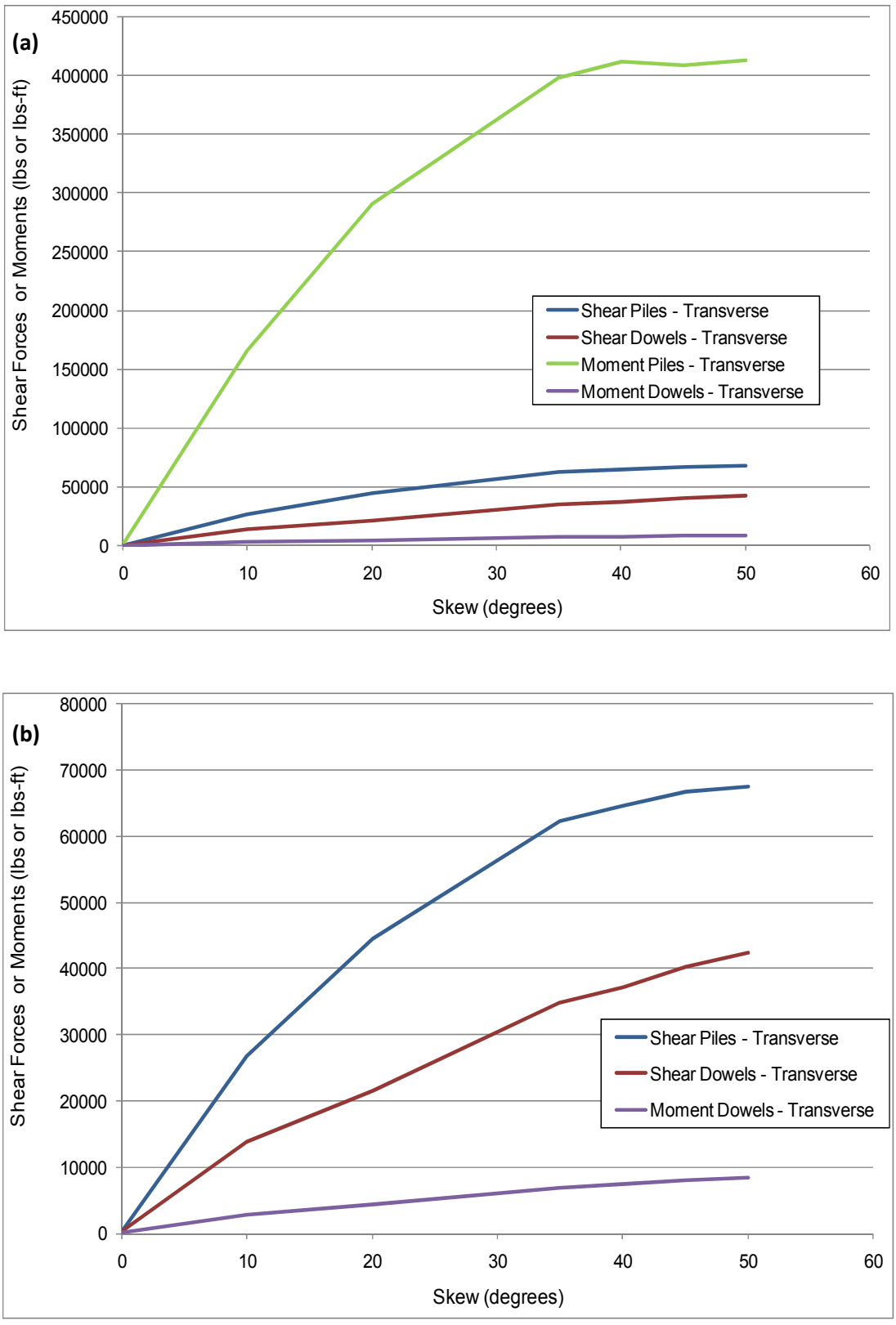

Figure 7.32 – Shear force and moment variations in the transverse direction vs. skew angle.

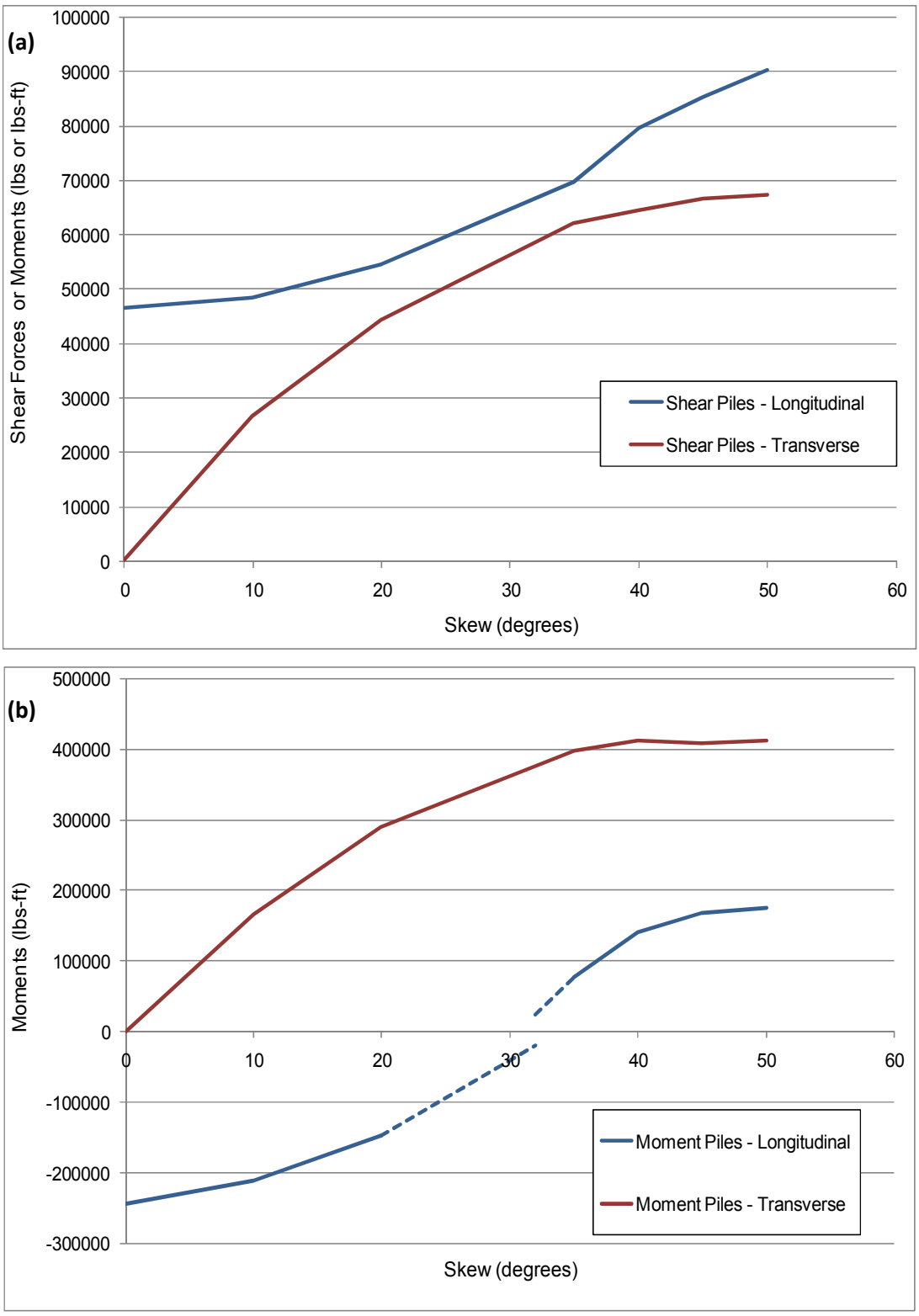

Figure 7.33 – Shear forces and moments in piles in longitudinal and transverse direction.

Figure 7.33(b) shows that longitudinal and transverse moments experience about the same change in magnitude, about 400 kip-ft, although the curves of the longitudinal and transverse moments have different shapes.

As shown in Chapter 8, these shapes will define the polynomial equation order that must be fitted to the data. For the transverse direction, a second order polynomial equation provides good results, but for the longitudinal direction, a third order polynomial equation is required.

The TIR of the strip tensile forces at the peak values only experience slight changes due to skew angle, but the TIR of the strip tensile forces at the connections with the MSE wall significantly change due to skew angle. Figure 7.34 displays the strip tensile forces at the acute corner for a bridge with a skew angle of 35 degrees. Comparing this figure with Figure 7.14, an increase of about 80% is observed in the maximum value of the strip tensile forces at the connection. On the other hand, the maximum value at the peak only changes about 7%. After reviewing all skewed bridge results, the trends show that, as the skew angle increases beyond 30 degrees, the strip tensile forces at the connection start to increase, and they match the peak maximum values for skew angles of about 45 to 50 degrees.

The TIR of the earth pressure on the front MSE wall experiences similar effects as the TIR of the strip tensile forces at the connection. Although the numerical analyses show that the TIR may increase up to 95%, this is not a significant result because the maximum value of the earth pressure actually drops an average of about 4%. The source of the TIR increase is the reduction of the initial gravitational earth pressure as the skew angle increase. The gravitational earth pressure decreased by a factor of 2 for the largest skew angles. This happens because the normal force exerted by the soil over the front MSE wall changes as the skew angle increases. It varied from pure normal force when the skew angle is zero to shear and normal force components, thus as the skew angle increases the shear component increases and the normal component reduces.

When skew angle is present, the earth pressure distribution behind the abutment is no longer close to homogeneous, as shown in Figure 7.35. As the skew angle increases, the earth pressures at the upper locations increase and the earth pressures at the lower locations decrease. The effect

is more accentuated at the acute corner and softer at the obtuse corner. The reduction in the TIR of the earth pressure at the lower position is due to the progressive reduction of the pile cap rotation as the skew angle increases. The increase in TIR of the earth pressure at the upper position is in response to the reduction in the lower position. The difference between the acute and obtuse corner is produced by the change in geometry and the action of transverse forces.

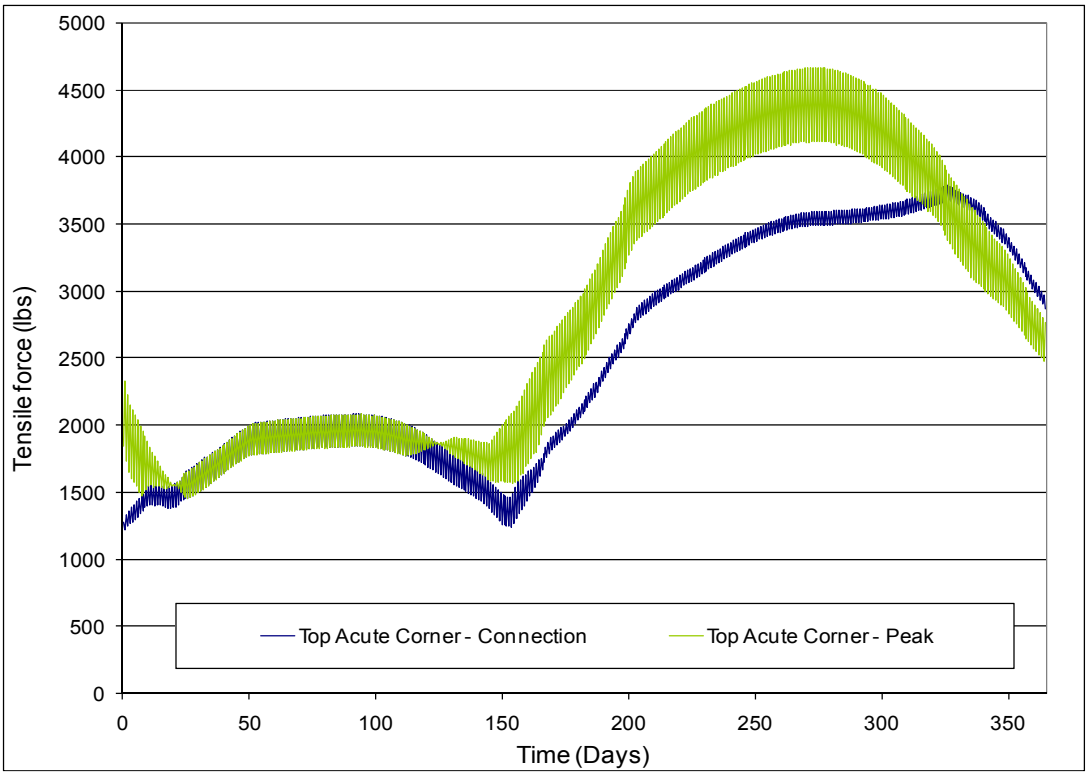

Figure 7.34 –Strip tensile force at the connection and peak for a 35° skewed bridge.

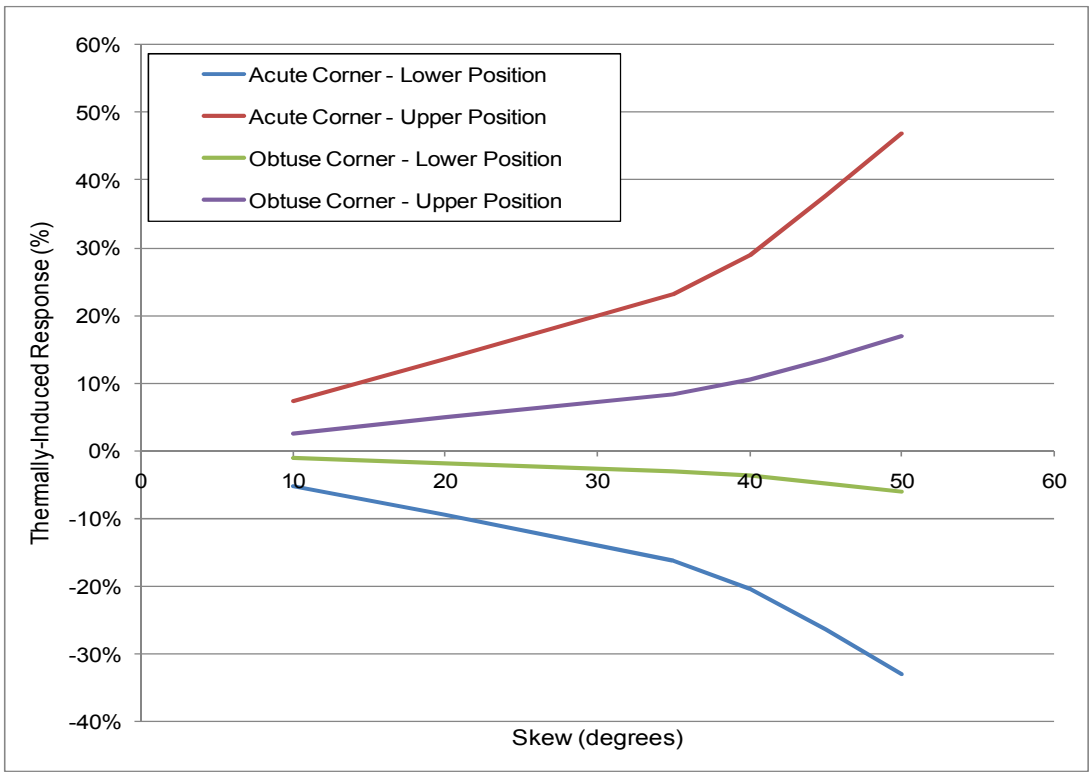

Figure 7.35 – TIR of earth pressure vs. skew angle.

7.2.3 Parametric Study Key Findings

The following list describes the key findings of single parameter variation cases and results described in Sections 7.1.7, 7.2.1 and 7.2.2:

- The distance between the pile centerline and the back of the MSE wall does not affect moments and shear forces in the dowels and piles, but it does affect the MSE wall reinforcing strip tensile forces and the MSE wall earth pressures.

- The earth pressure behind the abutment builds up during a one-year cycle of thermal displacements. The maximum earth pressure can increase up to 60% after the first year, but increases by less than 6 additional percentage points during the following years. The earth pressure build up is due mainly to nonlinear soil response to cyclic lateral displacements imposed by the abutment. The soil rearrangement produces a settlement of

about 1.2 inches for a thermal displacement of 3 inches, according to the numerical analyses.

- Shear forces and moments in the dowels and piles due to thermal displacement are, on average, 10 to 20 times larger than those imposed by self weight.

- Peak tensile forces in the reinforcing strips near the abutment can increase up to 110% due to thermal displacements. Depending on the reinforcement details, designs may need to take this into account.

- The use of 3" of EPS behind the MSE wall has marginal benefits on the effects of thermal displacements in the MSE wall, but it can reduce by 50% and 75% the strip tensile force and pressure on the MSE wall due to self weight.

- Thermal displacements only affect the pressures and strip tensions in the upper quarter of the MSE wall.

- Pile axial load is not significantly affected by thermal displacements, and it is the only output parameter that is reduced in magnitude by the thermal displacements.

- EPS behind the abutment reduces lateral earth pressures by a factor of 9 for the upper portion of the abutment and by a factor of 20 for the lower portion of the abutment, according to the numerical analyses.

- For skewed bridges, displacements in the transverse direction can reach about the same magnitudes as for the longitudinal displacement. This is also true for shear forces in piles.

- Skew angle progressively increases pile cap fixity, producing a reversal in the pile moments in the longitudinal direction.

- Skew angle affects the distribution and magnitude of the earth pressure behind the abutment.

- Skew angle progressively increases the maximum value of the strip tensile forces at the MSE wall connection. These tensile forces reach the same magnitude as the peak tensile forces for skew angles of 45 to 50 degrees.

7.3 Multiple Parameter Variations

This section considers the effects of changing more than one parameter at a time. In addition, per request of Virginia DOT engineers, results from two special cases are presented and analyzed in this section. Finally, the IAB v2 spreadsheet is introduced in this section.

7.3.1 Multiple Parameter Variation Cases

As described in section 7.2, the initial plan for this research only included varying one parameter at a time, but as the research progressed, it became apparent that varying multiple parameters simultaneously was necessary to fully understand and quantify thermal effects on the bridge abutment. In particular, combining parameter variations helped determine whether the influence of two or more parameters is multiplicative or additive, or whether their effects should be combined in some other way.

Table 7.8 shows a list of the cases of combined parameter variations analyzed during this research. The following acronyms are used in this table:

- T.D. = Thermal Displacement
- N.P.O. = New Pile Orientation (see Section 7.3.2)
- P.O. = Pile Orientation for weak or strong bending moments.
- D.M.A. = Distance between MSE wall and Abutment

Table 7.8 – Multiple parameter variation cases

Case	Parameter 1 Value	Parameter 2 Value	Parameter 3 Value	Parameter 4 Value	Parameter 5 Value
C1	T.D. 4.5 in	Skew 20º			
C2	T.D. 4.5 in	Skew 45º			
C3	N.P.O.	Skew 20º			
C4	N.P.O.	Skew 45º			
C5	T.D. 4.5 in	Tall MSE			
C6	Laminated Pad	Skew 20º			
C7	Laminated Pad	Skew 45º			
C8	Laminated Pad	T.D. 1.5 in			
C9	Laminated Pad	T.D. 4.5 in			
C10	Pile 14 x 73	T.D. 4.5 in			
C11	Pile 14 x 73	T.D. 4.5 in	Skew 20º		
C12	Pile 14 x 73	T.D. 4.5 in	Skew 45º		
C13	Pile 12 x 53	P.O. Strong			
C14	Pile 14 x 73	P.O. Strong			
C15	Pile 14 x 73	T.D. 4.5 in	Skew 20º	P.O. Strong	
C16	Pile 14 x 73	T.D. 4.5 in	Skew 45º	P.O. Strong	
C17	Laminated Pad	Skew 10º			
C18	Laminated Pad	Skew 35º			
C19	Laminated Pad	Skew 50º			
C20	Laminated Pad	Pile 10 x 42	P.O. Strong		
C21	Laminated Pad	Pile 12 x 53			
C22	Laminated Pad	Pile 12 x 53	P.O. Strong		
C23	Laminated Pad	Pile 14 x 73			
C24	Laminated Pad	Pile 14 x 73	P.O. Strong		
C25	Laminated Pad	Pile 14 x 73	Skew 20º		
C26	Laminated Pad	Pile 14 x 73	Skew 45º		
C27	Laminated Pad	Pile 14 x 73	Skew 20º	P.O. Strong	
C28	Laminated Pad	Pile 14 x 73	Skew 45º	P.O. Strong	
C29	Laminated Pad	Pile 14 x 73	Skew 20º	T.D. 4.5 in	
C30	Laminated Pad	Pile 14 x 73	Skew 45º	T.D. 4.5 in	
C31	Laminated Pad	Pile 14 x 73	Skew 20º	T.D. 4.5 in	P.O. Strong
C32	Laminated Pad	Pile 14 x 73	Skew 45º	T.D. 4.5 in	P.O. Strong

Table 7.8 – Multiple Parameter Variation Cases (cont.)

Case	Parameter 1 Value	Parameter 2 Value	Parameter 3 Value	Parameter 4 Value	Parameter 5 Value
C33	Laminated Pad	T.D. 0.75 in			
C34	Laminated Pad	D.M.A. 0.5 ft			
C35	Laminated Pad	D.M.A. 1 ft			
C36	Laminated Pad	D.M.A. 3 ft			
C37	Laminated Pad	D.M.A. 5 ft			

In light of the results from section 7.2, key input parameters having significant impact on the output parameters were selected. Accordingly, input parameters such as geometry, foundation material, and reinforcing strips behind the abutment were left out of this list because they do not produce a significant change in the bridge response. Other cases, such as the solid abutment, no EPS behind the abutment, and EPS behind the front MSE wall, were left out because they do not represent common design practices in Virginia, although they do produce big changes in the bridge response. The remaining parameters considered in the multiple parameter variation cases are:

- Abutment design
  - Dowels
  - Laminated pad
- Abutment – MSE wall distance
- Thermal displacement
- Pile type and orientation
- Skew angle

Cases C3 and C4 in Table 7.8 do not correspond to any of the above categories. They are special cases requested by VDOT engineers and discussed in the next section.

7.3.2 Special Cases

Although Cases C3 and C4 are multiple parameter variation cases (different pile orientation and variation in skew angle), they are special cases because the effects of pile orientation and skew angle are not combined quantitatively in the spreadsheet IAB. Instead, these cases address a specific question from VDOT engineers about whether the forces acting on piles in skewed bridges could be reduced by orienting the pile webs in alignment with the pile cap, regardless of skew angle.

Cases C3 and C4 were compared to Cases 21 and 24 respectively. The only difference between each pair of cases is the pile orientation. In Cases C3 and C4, the pile webs are parallel to the skewed abutment alignment, whereas in Cases 21 and 24, the pile webs are perpendicular to the skewed bridge alignment.

Orienting the pile webs parallel to the skewed abutment alignment reduces the TIR of moments and shear forces in the dowels by about 7% in the longitudinal direction, but this increases the same outputs by about 13% in the transverse direction.

Orienting the pile webs parallel to the skewed abutment alignment increases the TIR of moments in the piles in the longitudinal direction by about 52% and reduces the TIR of shear forces in the piles in the longitudinal direction by about 32%. In the transverse direction, the TIR of moments is reduced by 38%, and the TIR of shear force is increased by 23% as a result of orienting the pile webs parallel to the skewed abutment alignment.

At an elevation 2 feet under the bottom of the pile cap, these cases increase the TIR of pile moments and shear forces in the longitudinal direction by 74% and 22%, respectively. In the transverse direction, the TIR of moments and shear forces are reduced by 71% and 17%, respectively.

The TIR of strip tensile forces, as well as the TIR of the earth pressure behind the front MSE wall, is changed less than 6 percentage points by orienting the pile webs parallel to the abutment alignment.

On average the TIR of the earth pressure behind the abutment does not significantly change. The distribution follows the trends shown in Figure 7.35, but the responses are increased by an average of 15%, i.e., the upper part of the abutment produces an even greater TIR in the earth pressure, while the response is more diminished at the pile cap.

From the previous results, it is not clear whether it is beneficial to orient piles in the direction of the abutment alignment for skewed bridges, as done in Cases C3 and C4. Moments in the longitudinal direction increase significantly, while in the transverse direction they significantly decrease. Shear forces have an erratic behavior, showing no clear trends. Additional analyses should be performed to provide enough information to reach a conclusions about pile orientation.

7.3.3 Discussion of Results

This section discusses results from some of the multiple parameter variation cases in order to explain the effect of combining two or more parameters. There are so many combinations of multiple parameter cases that it is not practical to discuss all the results from all the combinations. Furthermore, many of these cases do not produce new effects on the bridge response, but instead they simply blend the effects from the initial set of cases described in section 7.2. However, several of the combinations do produce new effects, and by presenting some of these cases, it is possible understand the rest.

Table 7.9 shows the percentage change in dowel and pile moments with respect to the base case model. In this table, some of the cases are from the initial set of single parameter variations and others are from the list of multiple parameter variation cases. The selected cases illustrate important trends in the bridge response to thermal displacements.

Table 7.9 – Percentage change in moments in dowels and piles with respect to the base case. Single and multiple parameter variations.

Case	Input Parameters		Dowels	Piles
			lbs - ft	lbs - ft
9	T. D. 4.5in		30%	38%
19	Pile Type	14x73	27%	38%
22	Skew Angle	20	2%	-39%
25		45	24%	-147%
C1	T.D. 4.5in – skew 20deg		53%	-10%
C2	T.D. 4.5in – skew 45deg		83%	-170%
C10	Pile 14x73 - T.D. 4.5in		83%	107%
C11	Pile 14x73 - T.D. 4.5in – skew 20deg		90%	20%
C12	Pile 14x73 - T.D. 4.5in – skew 45deg		122%	-213%

Model C1 is a combination of Cases C9 and C22. Case 9 changes the thermal displacement from 3 in. to 4.5 in., and Case 22 incorporates a skew angle of 20 degrees. Case C1 includes a thermal displacement of 4.5 in. and a skew angle of 20 degrees. In Cases 9, 22, and C1, the TIR values of the moments in dowels increase by 30%, 2%, and 53%, respectively. An increase in the TIR of moments in dowels is expected, but the increase of 53% is much larger than the sum of the 30% increase from Case 9 and the 2% increase from Case 22. This finding indicates that there is an interaction of skew angle and thermal displacement magnitude.

In Case 9, the TIR of the moments in piles increases by 38%. In Cases 22 and C1, the TIR of the moment in piles reduces by 39% and 10% respectively. The result in Case C1 is hard to predict since the percentages produced by Case 9 and Case 22 are very similar but of opposite sign. Thus, a final result of -10% suggests a nonlinear combination of the effects of each parameter acting alone.

Case C2 combines Cases 9 and 25, incorporating a thermal displacement of 4.5 in. and a skew angle of 45 degrees. In Cases 9, 25, and C2, the TIR of the moments in dowel increase by 30%, 25%, and 83%, respectively. These results follow the same trend as the result in Case C1.

In Case 9, the TIR of the moments in piles increases by 38%. In Cases 25 and C2, the TIR of the moment in piles reduces by 147% and 170% respectively. A reduction of over 100% means the value in the multiple parameter variation case has experienced a reversal in sign. The increase in displacement intensifies the reversal effect of Case 25, thus producing the results of Case C2. The larger thermal displacements act as a booster response on other input parameters because it increases the effects of the other parameters.

Case C10 combines the largest size of piles analyzed during this research and a larger thermal displacement. Since Cases 9 and 19 produce increases in the TIR of moments, it is logical to expect that Case C2 will also produce an increased moment, which it does, but the magnitude of the increase is greater than the sum of the effects of each change acting alone.

Cases C11 and C12 combine all three input parameters at once: the largest pile, thermal displacement, and skew angle. Case C11 can be seen as a combination of those three parameters or as a combination of Cases C1 and 19. Similarly, Case C12 can be seen as a combination of Cases C2 and 19. When comparing Cases C1 – C11 and C2 – C12, it is evident that the introduction of a larger pile size in Cases C11 and C12 increases even more the TIR of moments in dowels. As an example, Case 19 increases the TIR of the moments in dowels by 27% over the base case, and adding this effect to Case C1 increases the C1 result from 53% to 90% for Case C11. Similarly, adding the effects of Case 19 to Case C2 increases the C2 result from 83% to 122% for Case C12.

In Case 19, the TIR of the moments in piles increases by 38%. In Case C1, it reduces by 10%, while in Case C11, it increases by 20%. This again illustrates the nonlinear interaction of skew angle and thermal displacement magnitude.

In Cases C2 and C12, the TIR of the moment in piles reduces by 170% and 213%, respectively, which can be compared to the 38% increase for Case 19. These results also confirm the nonlinear combination of the effects of each parameter.

After a thorough analysis of the five multiple variation cases described above, it is possible to understand the results of combining parameters. The general trends are predictable, i.e., it is possible to anticipate whether a specific combination of parameters will produce an increase or a decrease, but it is difficult to anticipate the magnitude of that change.

The initial idea of running multiple parameter variation models was to understand the effects of combining two or more parameters and develop an additive or multiplicative way to adjoin those effects. After running several models, it is clear that the effects of combining parameters cannot be predicted by simple addition or multiplication, and a more advanced technique must be used.

7.3.4 Spreadsheet Introduction

In the previous section, only moments in dowels and piles in the longitudinal direction were discussed. This information emanated from five multiple parameter variation models and their comparison with single parameter models. This information represents a very small portion of the information available, considering all the output parameters and over 65 numerical models. The previous section also showed that the nature of combining parameters is not trivial.

Therefore, in order to efficiently manage the large amount of information and make an easy implementation of complex equations, an Excel spreadsheet was selected to present the results of this research. The next chapter shows how the numerical information was transformed into an easy to use spreadsheet.

CHAPTER 8

IAB v2 SPREADSHEET

This chapter presents analysis and arrangement of the information from the numerical models into different groups. Multiparameter polynomial equations are fitted to the results of the numerical analyses. IAB v2 is the implementation of these equations in an easy to use Excel spreadsheet for designing integral abutment bridges. At the end of this chapter, two examples illustrate how to use this spreadsheet.

8.1 Arrangement of Data

8.1.1 Dowels and Laminated Pads

Table 8.1 shows moments and shear forces of the base case and skewed models for cases designed with dowels. These outputs were monitored in the piles in the longitudinal direction at two positions, right under the abutment and 2 ft under the abutment.

Analogous to Table 8.1, Table 8.2 shows moments and shear forces of the base case and skewed models (cases C6, C7, C17, C18, and C19) for cases designed with laminated pads. Again, these outputs were monitored in the piles in the longitudinal direction at two positions, right under the abutment and 2 ft under the abutment.

Previously in Section 7.2, a comparison between the base case and case number 1, which has a laminated pad abutment design, was performed, and conclusions were described, such as reduction in moments and an increase in shear forces in the longitudinal direction resulting from use of laminated pads. Those findings can be confirmed by comparing the first line of each table.

The addition of multiple parameter variation cases to the research data provided new information about the behavior of laminated pad design. When comparing column A of Table 8.1 with that in Table 8.2, it can be seen that moments in the first table change sign, i.e., piles experience a moment reversal as the skew angle increases for abutments with dowels; whereas, in the second

table they do not reverse, but increase in negative magnitude as the skew angle increases for abutments with laminated pads.

Table 8.1 – Global moments and shear forces in abutments with dowels. Output monitored at two positions in the piles for moments and shears in the longitudinal direction.

Case		Under the Abutment		2 ft Under the Abutment	
		Moment	**Shear**	**Moment**	**Shear**
		lbs – ft	**lbs**	**lbs – ft**	**lbs**
Base Case		-243,593	-46,503	245,777	-38,751
Skew Angle	10	-210,430	-48,395	238,343	-32,892
	20	-147,714	-54,632	196,714	-22,616
	35	61,129	-69,759	135,095	-21,315
	40	89,944	-79,513	123,983	-19,336
	45	114,448	-85,301	99,818	27,567
	50	168,735	-90,275	78,043	39,016
		A	**B**	**C**	**D**

Table 8.2 – Global moments and shear forces in abutments with laminated pads. Output monitored at two positions in piles for moments and shears in the longitudinal direction.

Case		Under the Abutment		2 ft Under the Abutment	
		Moment	**Shear**	**Moment**	**Shear**
		lbs – ft	**lbs**	**lbs – ft**	**lbs**
Base Case		-105,662	-93,345	-115,597	-36,930
Skew Angle	10	-111,329	-94,994	-109,490	-36,179
	20	-143,833	-99,000	-95,222	-46,996
	35	-193,095	-105,194	-51,370	-51,053
	45	-222,612	-109,000	25,365	-46,758
	50	-238,000	-111,000	26,368	-43,996
		A	**B**	**C**	**D**

In the above tables, column B shows the shear forces in piles. Both designs, dowels and laminated pads, show that shear forces increase with skew angle increments, but when dowels are used, the shear forces almost doubled (+100%) the value of the base case for a skew angle of 50 degrees. When laminated pads are used, the shear force value increases less than 20% for a skew angle of 50 degrees.

Each table presents in column C the moment in piles at 2 ft under the abutment. Although moments in both tables change as the skew angle increases, the changes are very different. The moments in Table 8.1 start from a positive value and then decrease, while those in Table 8.2 start from a negative value and then increase to a positive value.

Shear forces in piles calculated at 2 ft under the abutment, as listed in column D of both tables, start from values very similar when skew angle is not present. Once the skew angle increases, shear forces displayed in Table 8.1 experience a reversal in sign, while those in Table 8.2 exhibit a peak negative value at about 35 degrees.

Tables 8.1 and 8.2 clearly show that the two designs present very different responses to skew angle. Their response is mainly controlled by the different constraints imposed on the piles by each design. Therefore, the first division of the numerical data corresponds to the abutment design, and this division has two groups, which are abutments designed using dowels and abutments designed using laminated pads.

Virginia DOT does not use solid abutment designs, so they are not analyzed in this research in as much detail as are the designs incorporating dowels and laminated pads, and solid abutment designs are not included in IAB v2.

8.1.2 Weak Axis and Strong Axis Pile Orientation

Table 8.3 shows moments and shear forces monitored in piles at two elevations, right under the abutment and 2 ft below the abutment. These outputs were monitored in both directions, longitudinal and transverse. Table 8.3 compares cases C11 and C12 with cases C15 and C16, respectively. Case C11 was designed with an H pile 14x73, 4.5 in. of thermal displacement and a skew angle of 20 degrees. Case C12 was designed with the same pile and thermal displacement as case C11, but with a skew angle of 45 degrees. Cases C15 and C16 are the same as cases C11 and C12, but they differ in that the H pile 14x73 was oriented for strong axis bending in the direction of the bridge alignment.

When comparing the outputs in columns A, C, D, E, G, and H, between weak and strong cases, it is evident that the pile orientation has an important influence on the magnitude and direction of moments and shear forces.

Table 8.3 – Moments and shear forces in abutments with dowels. Output monitored at two positions in piles for moments and shears in the longitudinal and transverse directions.

Case		Under the Abutment				2 ft Under the Abutment			
		Longitudinal		Transverse		Longitudinal		Transverse	
		Moment	Shear	Moment	Shear	Moment	Shear	Moment	Shear
		lbs - ft	lbs	lbs - ft	lbs	lbs - ft	lbs	lbs - ft	lbs
C11	Weak	-292,443	-128,407	637,355	-61,304	472,166	-45,191	-542,898	-66,632
C12	Weak	274,483	-174,238	860,013	-94,415	169,833	74,121	-684,425	-94,100
C15	Strong	497,630	-158,177	274,226	44,444	-760,665	-69,823	181,831	39,501
C16	Strong	-185,525	-175,313	564,421	89,305	-541,565	73,328	378,613	79,624
		A	B	C	D	E	F	G	H

In the presence of skew angle, rotating the pile axis can drastically change the constraint conditions of the elements interacting with the pile. For example, when the piles are oriented for weak axis bending and a skew angle of 20 degrees is present, the pile cap can still rotate and produces the negative moment displayed by case C11 in column A. If the pile is rotated for strong bending moment, case C15, the pile cap won't be able to rotate as much as before because the strong axis will increase the rotation constraints, and thus, the sign reversal displayed in column A for case C15.

Table 8.4 displays information that is analogous to that in Table 8.3, but with laminated pads. Cases C29 and C30 are like cases C11 and C12, but the dowels in the abutment were replaced by laminated pads. Cases C31 and C32 are the strong-orientation versions of cases C29 and C30. Cases C25 through C28 are equivalent to cases C29 through C32, but the thermal displacement has been reduced from 4.5 in to 3 in.

Table 8.4 – Moments and shear forces in abutments with laminated pads. Output monitored at two positions in piles for moments and shear in the longitudinal and transverse directions. L.P. = Laminated Pad.

Case	Parameters					Under the Abutment				2 ft Under the Abutment			
						Longitudinal		Transverse		Longitudinal		Transverse	
	Abutment Design	Pile type	Skew Angle	Thermal Displace.	Pile Orienta.	Moment	Shear	Moment	Shear	Moment	Shear	Moment	Shear
						lbs - ft	Lbs	lbs - ft	lbs	lbs - ft	lbs	lbs - ft	lbs
C25	L.P.	HP 14x73	20º	3.0 in	Weak	-229,440	-123,378	342,550	-34,902	-203,788	-57,580	269,945	-36,660
C26	L.P.	HP 14x73	45º	3.0 in	Weak	-229,440	-137,686	508,585	-59,580	45,921	-65,806	384,575	-58,192
C29	L.P.	HP 14x73	20º	3.0 in	Strong	-312,739	-170,498	520,585	-52,301	-301,875	-83,125	411,723	-55,632
C30	L.P.	HP 14x73	45º	3.0 in	Strong	-536,128	-204,423	763,351	-88,548	68,993	-95,284	578,963	-85,728
C27	L.P.	HP 14x73	20º	4.5 in	Weak	193,608	-136,937	158,858	26,813	371,655	-69,879	103,062	22,697
C28	L.P.	HP 14x73	45º	4.5 in	Weak	-158,538	-140,702	330,133	56,008	-171,755	-70,907	213,543	49,516
C31	L.P.	HP 14x73	20º	4.5 in	Strong	278,498	-189,694	245,124	40,367	552,350	-99,695	161,098	35,466
C32	L.P.	HP 14x73	45º	4.5 in	Strong	-243,158	-207,670	503,018	82,533	-257,860	-100,727	331,210	72,039
						A	B	C	D	E	F	G	H

Again, columns A, C, D, E, G, and H of Table 8.4 show the impact of the pile orientation on moment and shear forces. This table provides even more evidence of the impact of the pile orientation, particularly when the effects of pile orientation are combined with those of thermal displacements. Table 8.4 shows 4 cases with 3 in. of thermal displacement (C25 through C28) and 4 cases with 4.5 in. of thermal displacement (C29 through C32). When comparing any of the following pairs, C25 – C29, C26 – C30, C27 – C31, or C28 – C32, it is evident that the effect of going from 3 in. to 4.5 in. of thermal displacements is to magnify the response, but it does not affect the sign. On the other hand, rotating the piles from weak to strong bending axis may affect not only the magnitude of the moment and shear, but also the sign.

Tables 8.3 and 8.4 indicate that rotating piles from their weak axis orientation to their strong axis orientation produces results that do not belong to the same group. As mentioned in chapter 7, rotating piles 90 degrees from their weak orientation changes the moment of inertia in two directions at once. Therefore, if both directions are included in the same group, consistent results would not be expected for skewed bridges.

Only 12 of the 65 models are oriented for strong bending moment. Analysis efforts were concentrated on the weak bending moment orientation because Virginia DOT mainly orients abutment piles for weak axis bending.

8.1.3 Numerical Data Groups

In the previous two sections, the numerical data was divided into 4 groups. The first and greatest division separates the numerical data into two groups. One group corresponds to those models designed with doweled abutments (dowel group), and the other group corresponds to those models designed with laminated pad abutments (laminated pad group).

The second division separates the dowel and laminated pad groups each into two subgroups, weak and strong pile orientation. This subdivision only applies to moments, shear forces, and axial loads in dowels and piles in the longitudinal and transverse directions.

The second division does not apply to the rest of the output parameters, such as the earth pressure at the front MSE wall because they do not show a behavior dependent on the pile orientation. Although some of these output parameters are a function of the pile stiffness (which is dependent of the pile size and orientation), their behavior is independent of the pile orientation.

Tables 8.5 and 8.6 show how the numerical data were arranged in sub-groups with similar characteristics. The information in Table 8.5 is for the dowel group, and the information displayed in Table 8.6 is for the laminated pad group.

Two considerations were applied when dividing the numerical data into the sub-groups listed in Tables 8.5 and 8.6. First, the data belong either to the dowel or laminated pad groups and either to weak or strong groups. Second, the magnitude of the output is determined by the same input parameters.

Tables 8.5 and 8.6 display in the first column the name assigned to the group. The second column indicates whether the abutment design incorporates dowels or laminated pads. The third column shows the pile orientation. The fourth column presents the input parameters that control the magnitude and direction of the output parameters. Column five displays the output parameters. The sixth column shows the type of elements or where the output parameters were monitored. The seventh column presents the direction for which the output parameters are valid. Finally, the last column shows the number of models in the sub-group. Note that group names provide an indication of the group characteristics. For example, group names starting with "D" apply to abutments designed with dowels, and group names starting with "LP" apply to abutments designed with laminated pads.

Table 8.5 – Numerical data sub-groups (dowel group).

Group	Abutment Design	Pile Orientation	Input Parameters	Output Parameters	Applies to	Longitudinal / Transverse	Number of Cases
DW1	Dowel	Weak	• Thermal Displacement • Pile Stiffness • Skew Angle	• Moments • Shear Forces • Axial Forces	• Dowels • Piles	Both	17
DS2	Dowel	Strong	• Thermal Displacement • Pile Stiffness • Skew Angle	• Moments • Shear Forces • Axial Forces	• Dowels • Piles	Both	5
DEA3	Dowel	-	• Thermal Displacement • Skew Angle	• Earth Pressure	• Behind Abutment	Longitudinal	16
DETM4	Dowel	Both	• Distance Abutment - MSE • Thermal Displacement • Pile Stiffness	• Earth Pressure • Tensile Forces	• Behind Front MSE wall • Peak Tensile Force Along Strip	Longitudinal	13
DTD5	Dowel	Both	• Thermal Displacement • Skew Angle • Pile Stiffness	• Displacement	• Bridge	Transverse	10

Table 8.6 – Numerical data sub-groups (laminated pad group).

Group	Abutment Design	Pile Orientation	Input Parameters	Output Parameters	Applies to	Longitudinal / Transverse	Number of Cases
LPW1	Laminated Pad	Weak	• Thermal Displacement • Pile Stiffness • Skew Angle	• Moments • Shear Forces • Axial Forces	• Dowels • Piles	Both	15
LPS2	Laminated Pad	Strong	• Thermal Displacement • Pile Stiffness • Skew Angle	• Moments • Shear Forces • Axial Forces	• Dowels • Piles	Both	7
LPEA3	Laminated Pad	-	• Thermal Displacement • Skew Angle	• Earth Pressure	• Behind Abutment	Longitudinal	13
LPETM4	Laminated Pad	Both	• Distance Abutment - MSE • Thermal Displacement • Pile Stiffness	• Earth Pressure • Tensile Forces	• Behind Front MSE wall • Peak Tensile Force Along Strip	Longitudinal	13
LPTD5	Laminated Pad	Both	• Thermal Displacement • Skew Angle • Pile Stiffness	• Displacement	• Bridge	Transverse	9

8.2 Fitting Multiparameter Polynomial Equations to Data

8.2.1 General description

The input parameters of the numerical data have discrete values, and they were selected in collaboration with VDOT/VTRC engineers to best represent the range of current and projected design practice in Virginia.

In order to transform the discrete numerical data into continuous information and make it accessible in an easy to use spreadsheet, one alternative might be implementing linear interpolation of the tabulated numerical data. However, linear interpolation in many cases is not the best representation of the trend of the output parameters. A better alternative is to use polynomial equations to represent the output trends.

As shown by Tables 8.5 and 8.6, each output parameter depends on at least two input parameters and in most cases three. Thus, the polynomial equations must have multiple input parameters.

Equations (8.1) and (8.2) are the multiparameter polynomial equations for two and three input parameters, respectively. Equation (8.1) was fitted to the DEA3 and LPEA3 group models in Tables 8.5 and 8.6, while Eq. (8.2) was fitted to most of the remaining groups in the tables.

$$OP = a_0 + a_1 x + a_2 y + a_3 x^2 + a_4 y^2 + a_5 xy \tag{8.1}$$

$$OP = a_0 + a_1 x + a_2 y + a_3 z + a_4 x^2 + a_5 y^2 + a_6 z^2 + a_7 xy + a_8 xz + a_9 yz \tag{8.2}$$

where OP = Output parameter (Listed in Tables 8.5 and 8.6).

a_n = Polynomial constants.

x, y, z = Input parameters (Listed in Tables 8.5 and 8.6).

As previously discussed, there are cases in which a higher order polynomial equation is needed. Section 7.2.2.8 showed that the longitudinal moments acting on piles are reversed as the skew

angle is increased. A review of Figures 7.31 and 7.33 makes evident that a second order polynomial equation will not appropriately fit the data, rather a third order polynomial equation would be appropriate. Therefore, in those cases where the numerical data experiences a reversal, it is better to use Eq. (8.3).

$$OP = a_0 + a_1x + a_2y + a_3z + a_4x^2 + a_5y^2 + a_6z^2 + a_7xy + a_8xz + a_9yz + a_{10}x^3 + a_{11}x^2y + a_{12}x^2z + a_{13}xyz \quad (8.3)$$

where OP = Output parameter (Listed in Table 8.5 and 8.6).

a_n = Polynomial constants.

x, y, z = Input parameters (Listed in Table 8.5 and 8.6).

The second line in Eq. (8.3) shows the terms that extend Eq. (8.2) into a third order multiparameter polynomial equation. The second line also shows that only the "x" input parameter is raised to the third power and the rest of the terms are just the permutations with the other input parameters. This was done for two reasons. First, the numerical data from Figures 7.31 and 7.33 show that moments are only reversed by the skew angle input parameter, and this effect is not reproduced by any other input parameter. Second, raising only one input parameter to the third power limits the number of numerical models necessary to calibrate the polynomial constants.

The second order polynomial equation with three input parameters shown in Eq. (8.2) needs at least 10 points (10 numerical model cases) to calibrate the polynomial constants. Tables 8.5 and 8.6 show that sub-groups DS2 and LPS2, respectively, have 5 and 7 numerical model cases in their sub-groups. Thus, for these sub-groups only linear equations were fitted to the data, i.e. only the first four terms of Eq. (8.2) were used to fit the numerical data, as shown by Eq. (8.4). Although the relatively small number of analyses for these cases limits the predictive capability of the fitted equations, they have reduced importance for Virginia DOT because VDOT avoids the use of piles oriented for strong axis bending in their designs. Consequently, highly accurate predictions are not as necessary for designs with strong-axis bending as for weak-axis bending.

$$OP = a_0 + a_1 x + a_2 y + a_3 z \quad (8.4)$$

where OP = Output parameter (Listed in Table 8.5 and 8.6).

a_n = Polynomial constants.

x, y, z = Input parameters (Listed in Table 8.5 and 8.6).

8.2.2 Polynomial Calibration

This section shows the details of calibrating the polynomial constants against the numerical data. For this purpose, only the calibration of the constants in sub-group DW1 will be shown since the rest of the constants in the remaining groups were calibrated using an analogous process. Appendix E shows the tabulated results of the numerical models for each group along with the calibrated constant and the coefficient of determination, R^2.

Table 8.7 shows the results of numerical modeling for group DW1. This table presents moments and shear forces for dowels and piles in both directions, longitudinal and transverse. The transverse information is only displayed when skew angle is present. Under the piles section, "Pos 1" refers to the position directly under the abutment and "Pos 2" refers to the position 2 ft under the abutment. Also in this table, axial forces for dowels and piles are displayed. Near the bottom of this table is the equation used to fit the numerical data.

The values in Table 8.7 are the global monitored output points. These were used because they exhibit a smoother response to thermal displacements and the difference in the output in skewed bridges of elements in the acute corner with respect to those in the obtuse corner is not significant for the output parameters shown in Table 8.7. On the other hand, the earth pressure behind the abutment has a significantly different response between the acute an obtuse corners. For this case, single monitoring points were used to establish the polynomial constants.

Table 8.7 – Group DW1 numerical results.

Cases		Dowels					Piles								
		Longitudinal		Transverse		Axial	Longitudinal Pos 1		Transverse Pos 1		Longitudinal Pos 2		Transverse Pos 2		Axial
		Moment	Shear	Moment	Shear		Moment	Shear	Moment	Shear	Moment	Shear	Moment	Shear	
		lbs - ft	lbs	lbs - ft	lbs	lbs	lbs - ft	lbs	lbs - ft	lbs	lbs - ft	lbs	lbs - ft	lbs	lbs
Base Case		22,998	114,963			10,975	-243,593	-46,503			245,777	-38,751			73,075
Thermal Displ.	0.75"	6,923	34,628			19,075	-63,521	-17,436			68,666	-9,983			16,475
	1.5"	10,570	52,848			18,450	-131,084	-31,853			129,584	-20,761			34,625
	4.5"	29,829	149,139			13,275	-337,335	-62,710			342,443	-52,890			75,375
Pile Types	12x53	26,015	130,025			13,250	-287,135	-63,714			336,912	-39,010			72,725
	14x73	29,123	145,635			12,575	-335,705	-90,070			472,856	-39,914			70,000
Skew Angle	10	23,228	116,113	-2,772	13,860	12,075	-210,430	-48,395	165,424	-26,632	238,343	-32,892	-110,866	-23,109	65,850
	20	23,445	117,179	-4,311	21,553	16,625	-147,714	-54,632	283,330	-44,508	196,714	-22,616	-189,886	-39,581	61,200
	35	27,224	136,129	-6,966	34,830	13,625	61,129	-69,759	409,717	-62,241	135,095	-21,315	-274,589	-57,237	49,925
	40	28,245	141,187	-7,461	37,303	11,950	89,944	-79,513	431,855	-64,525	123,983	-19,336	-289,426	-60,329	38,700
	45	28,587	142,941	-8,070	40,351	13,950	114,448	-85,301	446,814	-66,760	99,818	27,567	-299,451	-62,419	27,075
	50	29,228	146,135	-8,498	42,490	14,550	168,735	-90,275	451,632	-67,480	78,043	39,016	-302,680	-63,092	18,500
C1 4.5in - 20deg		35,280	176,398	-5,445	27,225	16,350	-220,227	-70,203	426,078	-63,452	265,065	-30,678	-294,035	-59,262	74,150
C2 4.5in - 45deg		42,030	210,151	-11,396	56,980	15,800	171,198	-123,891	601,283	-95,598	152,370	39,628	-440,030	-86,717	28,150
C10 14x73 - 4.5in		42,165	210,822			17,175	-503,273	-125,261			683,160	-44,270			100,025
C11 14x73 - 4.5in - 20deg		43,655	218,273	-4,808	24,039	16,200	-292,443	-128,407	637,355	-61,304	472,166	-45,191	-542,898	-66,632	70,425
C12 14x73 - 4.5in - 45deg		51,107	255,543	-9,908	49,542	17,375	274,483	-174,238	860,013	-94,415	169,833	74,121	-684,425	-94,100	29,950
Polynomial Equation		**8.2**	**8.2**	**8.2**	**8.2**	**8.2**	**8.3**	**8.2**	**8.2**	**8.2**	**8.2**	**8.3**	**8.2**	**8.2**	**8.2**
R^2		**0.9977**	**0.9977**	**0.9862**	**0.9862**	**0.8191**	**0.9883**	**0.9913**	**0.9909**	**0.9847**	**0.9811**	**0.8621**	**0.9875**	**0.9934**	**0.9804**
		A	**B**	**C**	**D**	**E**	**F**	**G**	**H**	**I**	**J**	**K**	**L**	**M**	**N**

The procedure for calibrating the constants was performed using Microsoft Excel and is described below:

- For each case in Table 8.7, compile the values of the input parameters. According to Table 8.5, the group DW1 depends on the thermal displacement, the pile stiffness (weak orientation only), and the skew angle. Thus, the values for the base case are 3 in., 71.7 in.^{4}, and 0˚ skew angle. For case C11, the values are 4.5 in., 261 in.^{4}, and 20˚ of skew angle, etc.

  Appendix F shows pile properties for several H piles (Skyline Steel 2008). These values were used for the moments of inertia.

  Table 8.8 shows the entire list of values of the input parameters for group DW1 from Table 8.7.

Table 8.8 – Input parameter values for the DW1 cases listed in Table 8.7

Cases		**Input Parameters[1]**		
		Thermal Displacement (in)	**Pile Stiffness (in^4)**	**Skew Angle (degrees)**
Base Case		3	71.7	0
Thermal Displacement	0.75"	0.75	71.7	0
	1.5"	1.5	71.7	0
	4.5"	4.5	71.7	0
Pile Types	12x53	3	127	0
	14x73	3	261	0
Skew Angle	10	3	71.7	10
	20	3	71.7	20
	35	3	71.7	35
	40	3	71.7	40
	45	3	71.7	45
	50	3	71.7	50
C1	4.5in - 20deg	4.5	71.7	20
C2	4.5in - 45deg	4.5	71.7	45
C10	14x73 - 4.5in	4.5	261	0
C11	14x73 - 4.5in - 20deg	4.5	261	20
C12	14x73 - 4.5in - 45deg	4.5	261	45

Note 1: These values correspond to x, y and z in Eqs. (8.2), (8.3), and (8.4).

- Initialize the constant values for each output parameter to any value, for example 1.

- Using the values listed in Table 8.8, the appropriate equation listed in Table 8.7, and the initial constant values, compute the output parameter values as follow:

  Base case, moments in dowels:

$$OP = a_0 + a_1x + a_2y + a_3z + a_4x^2 + a_5y^2 + a_6z^2 + a_7xy + a_8xz + a_9yz$$

$$OP = 1 + 1 * 3 + 1 * 71.7 + 1 * 0 + 1 * 3^2 + 1 * 71.7^2 + 1 * 0^2 + 1 * 3 * 71.7 + 1 * 3 * 0 + 1 * 71.7 * 0 = 5{,}441\ lbs * ft$$

- For each case listed in Table 8.7, compute the square of the difference, and then add them up in a cell labeled the Total Square Difference (TSD). The square of the difference is computed as:

$$Square\ of\ the\ Difference = (TOP - COP)^2$$

  where TOP = Target output parameter value
  COP = Computed output parameter value

- Utilizing the Microsoft Excel solver feature, minimize the TSD cell by changing the polynomial constant cells.

After Microsoft Excel solver has reached an optimal solution, the value for the moment in dowels for the base case has changed from 5,441 lbs*ft to 21,614 lbs*ft, which is only 6% smaller than the target value in Table 8.7. After applying the previously described process to all the output parameters in Table 8.7, the polynomial constants are obtained for each column in Table 8.7. The calibrated polynomial constant values are displayed in Table 8.9.

As previously mentioned, Table 8.7 shows the R^2 values for all the output parameters. R-squared, R^2, provides information about the quality of the fit, i.e., how well the calibrated polynomial equation predicts the numerical data values.

Table 8.9 – Calibrated polynomial constants for the DW1 sub-group

Constants	Dowels					Piles								
	Longitudinal		Transverse		Axial	Longitudinal Pos 1		Transverse Pos 1		Longitudinal Pos 2		Transverse Pos 2		Axial
	Moment	Shear	Moment	Shear		Moment	Shear	Moment	Shear	Moment	Shear	Moment	Shear	
a0	-1463	-7141	-1115	5582	10947	3622	-15405	-88954	-19544	-53321	4394	148141	1725	-18898
a1	5944	29697	-1475	7372	3338	-71607	-11388	13992	-8055	100243	-12829	27602	-6650	37687
a2	61	301	36	-181	-32	174	53	60	478	384	-248	-1568	180	88
a3	-42	-211	-68	338	-336	-9782	1115	9522	-1315	1545	4852	-7572	-1263	777
a4	-59	-294	221	-1107	-400	592	1286	-1573	744	-5101	1192	-6130	572	-3569
a5	-0.16	-0.81	-0.11	0.55	0.04	-0.03	-0.22	-1.23	-1.36	0.66	0.74	5.26	-0.48	-0.28
a6	1.17	5.89	0.72	-3.61	3.18	558.18	-21.90	-180.44	19.97	13.53	-212.35	143.90	20.60	-15.53
a7	10.51	52.61	0.24	-1.18	1.97	-222.12	-61.90	271.66	-7.87	157.88	-3.45	-217.58	-12.50	6.48
a8	53.09	265.44	-37.40	186.98	39.88	1263.14	-302.33	2569.38	-254.51	-1469.48	-933.17	-1994.29	-292.98	-295.28
a9	-0.04	-0.18	0.07	-0.35	0.22	-12.33	-0.76	13.08	-0.34	-18.47	-8.26	-10.26	-0.49	-0.02
a10						-7.36					2.40			
a11						21.21					28.74			
a12						0.19					0.20			
a13						7.56					-0.10			

Most of the R^2 values in Table 8.7, as well as those in the tables of Appendix E, range from 0.97 to 1, which means that most of the calibrated polynomial equations are predicting the numerical values very accurately. Two exceptions to the agreement between predicted and numerical values are the axial force acting in dowels shown in column E, and the shear force acting in piles shown in column K.

The R^2 value in column E is 0.82, which is the lowest among 62 calibrated polynomial equations (including those in Appendix E). The reason for this lower R^2 value is the highly variable numerical data in the thermal displacement and skew angle cases. Dowel axial forces are sensitive parameters, and small changes in input parameters produce big changes in the output parameter time history. For this reason, the time history is more variable and more difficult to evaluate than for other outputs. For the axial load in the dowels, this should not be a point of great concern because the thermal induced axial force is, on average. less than 6% of the gravitational force.

Eq. (8.3) was fitted to the shear forces in piles, and the R^2 value in column K for this fit is 0.86. The relatively low R^2 value is produced by the hard-to-predict behavior of the output reversal when skew angle is present. This is not a very important issue because the shear forces in piles in column G are always larger in magnitude than those in column K. Thus, the shear forces from column K will not be reported, because the spreadsheet always provides the most critical values, which are those in column G for this situation.

8.3 IAB v2 Spreadsheet

This section presents one of the most important outcomes of this research, the IAB v2 Spreadsheet. This spreadsheet was developed to aid designer engineers when designing IABs.

It is important to remember that the values presented in the IAB v2 are thermally-induced increments and they need to be added to the geostatic values.

The spreadsheet features are:

- Variable MSE wall – abutment distance (0.5 ft to 5 ft)
- Variable skew angle (0˚ to 50˚)
- 7 sizes of abutment H piles (HP 10x42, HP 10x57, HP 12x53, HP 12x63, HP 12x74, HP 12x84, HP 14x73)
- Piles orientation in the strong and weak axis directions
- Variable bridge length
- Dowel and laminated pad abutment designs
- Outputs due to thermal displacement effects:
    - Thermal displacement curve
    - Moments in dowels and piles
    - Shear forces in dowels and piles
    - Axial forces in dowels and piles
    - Earth pressure magnitude and distribution behind the abutment
    - MSE wall tensile strip forces (at the connection with MSE wall and peak value)
    - Earth pressure behind MSE wall
    - Transverse displacement (when skew angle is present)
- Output in longitudinal and transverse direction

The spreadsheet is composed of three work sheets; Input, Output, and Comp. The first is the input sheet, where the user is required to provide the geometry and design of the bridge. The second is the output sheet, where the computed results are displayed, and lastly, the third sheet is where the polynomial constants are stored. The third sheet is not an active part of IAB v2; its purpose is to store the polynomial constants and compute the output parameter values according to the user input values, and thus, users have no need to visit the Comp sheet.

8.3.1 Input page

Figure 8.1 shows the IAB v2 input page. The input page was arranged so it is easy and logical to use. The user must fill or select the information in 13 yellow highlighted boxes.

Below the input cells, the input page displays the definition of the skew angle used in this research. Question number 3 asks about which sign convention is used to define the skew angle, as shown in the accompanying picture. The answer to this question is very important, because it defines the direction of the traverse output parameters consistently with the skew angle.

Following Figure 8.1, a detailed description of each cell of the input page is provided.

Integral Abutment Bridge v.2

Geometry			
Bridge Length	1	L (ft)	200
Skew Angle	2	α (°)	30
Is skew defined as Figure A or B?	3	◉ Fig. A ○ Fig. B	

Piles		
Type	6	HP 14 x 73
Number of Piles	7	7
Orientation	8	◉ Weak ○ Strong

MSE wall			
Distance between MSE wall and Abutment	4	D (ft)	2

Abutment			
ESP at abutment backwall?	9	◉ Yes ○ No	
Abutment height?	10	H (ft)	10
Abutment design	11	◉ Dowels ○ Laminated Pad	
Number of Dowel	12	32	

Thermal Displacement			
Annual Temperature Variation	5	ΔT (°F)	90

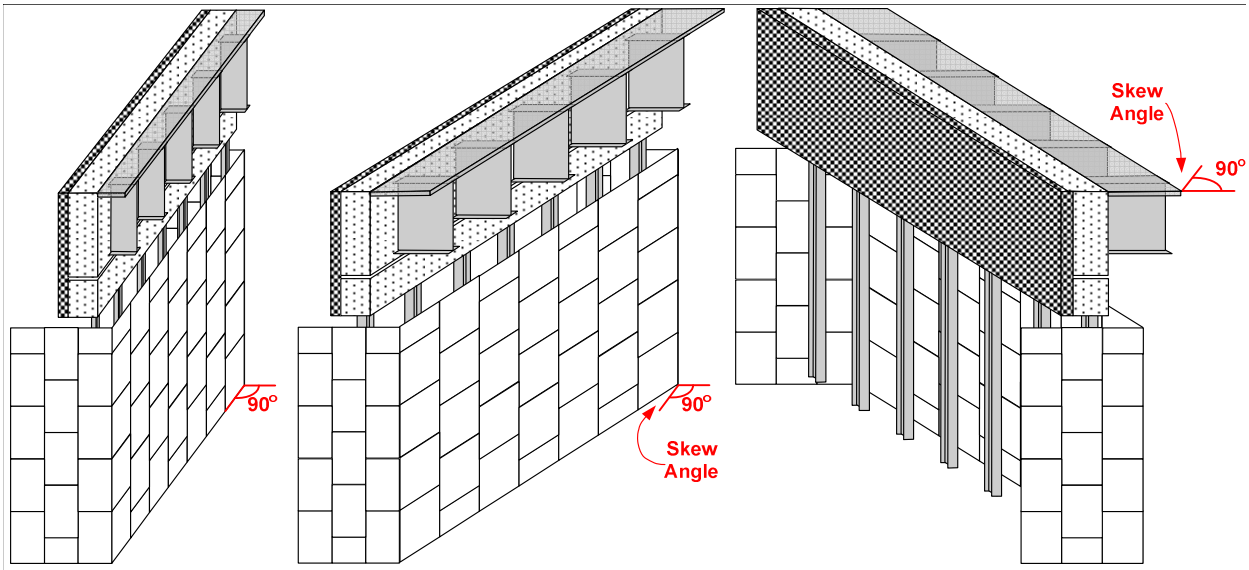

Figure A

Figure B

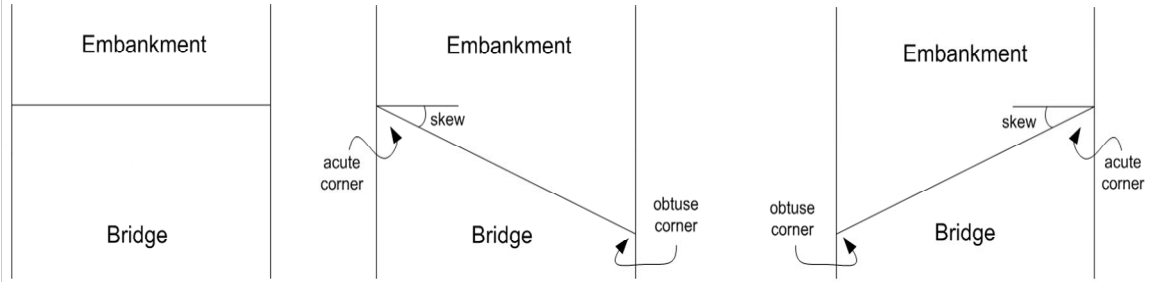

Figure 8.1 – IAB v2 spreadsheet input page.

1. Total bridge length, from one abutment to the other.

2. Skew angle. Use only positive values ranging from 0 to 50 degrees.

3. Defines the orientation of the skew angle.

4. Distance between the back face of the front MSE wall and the front face of the abutment front wall (the face towards the bridge). This distance is used to compute the distance between the pile centerline and the back face of the front MSE wall. A standard abutment thickness of 3 ft is used in this computation. Thus, the distance between the pile centerline and the back face of the front MSE wall equals 1.5 + D and D is limited to 0.5 $\leq$ D $\leq$ 5 ft.

5. Annual temperature variation. If the lowest temperature in winter is 20 °F and highest temperature in summer is 100 °F, then input #4 is 80 °F. The national climatic data center has statistical information for USA.

6. Pile drop down menu (7 pile types are listed).

7. Number of piles embedded in the pile cap across the bridge width.

8. Pile orientation with respect to the bridge alignment. Select between weak or strong axis orientation. Weak axis means that the web of the H pile is perpendicular to the bridge longitudinal direction.

9. This selection indicates whether EPS material is placed behind the abutment backwall. The EPS thickness is determined in accordance with VDOT guidelines (Virginia DOT guidelines “Integral/Jointless Bridges”, Chapter 20).

10. Height of the abutment, measured from the bottom of the pile cap to the top of the abutment.

11 Abutment design. Select between doweled or laminated pad.

12 If dowels are selected for the abutment design, the number of dowels must be entered in this cell.

8.3.1 Output page

The output page represented in Figure 8.2 is composed of 9 blocks of outputs, one plot of the thermal displacements, and one diagram (not shown in Figure 8.2) defining the sign convention of the output. The diagram defining the sign convention of the output is the same as Figure 7.4.

The plot presented in the upper right corner is the graphical expression of Eq. (4.1). In this example, the third row in the first block of outputs shows a value for the "Annual Displacement at one Abutment" of 0.70 in. which is exactly the maximum amplitude from peak to peak of the thermal displacement plot.

The output page provides the "global" and "per element" values for moments, shear forces, and axial forces. The global values are the sum of each element output of the same type in the bridge. For example, global shear force in piles is the sum of all pile shear forces in the bridge for a given direction. Per element values are the global values divided by the number of elements across the bridge.

Finally, block 10 in the output page shown in Figure 8.2 displays the transverse displacement of the bridge when skew angle is present. This output parameter does not reverse its sign when answering "NO" to question number 3 in the input page. The transverse displacement is always toward the acute corner of the bridge as defined in Figure 7.29.

Following Figure 8.21, a detailed description of each portion of the output page is provided.

Thermal Displacement (1)		
Total Annual Thermal Disp.	1.40	in
Total Daily Thermal Disp.	0.16	in
Annual Disp. at one Abutment	0.70	in
Daily Disp. at one Abutment	0.08	in
Parameter A in eq. 4 1	0.04	in
Parameter B in eq. 4 1	0.31	in

EPS (3)		
Recommended EPS thickness	17	in

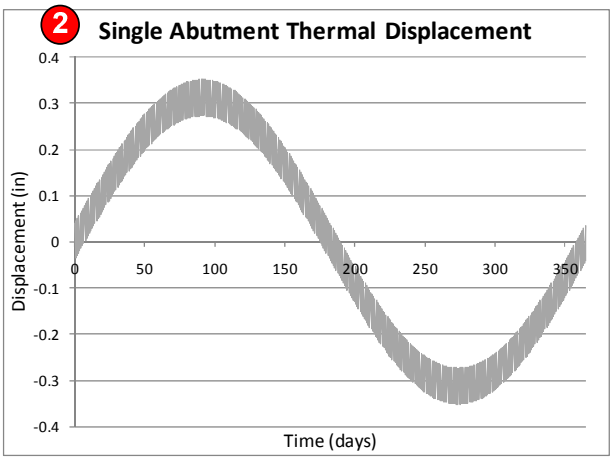

MOMENTS (4)		Global		Per element	
Moment in Dowels - Longitudinal		9.3	kips-ft	0.3	kips-ft
Moment in Dowels - Transverse		-	kips-ft	-	kips-ft
Moment in Piles - Longitudinal	2 ft under Abutment	188.8	kips-ft	27.0	kips-ft
Moment in Piles - Transverse	Under Abutment	-	kips-ft	-	kips-ft

SHEAR FORCES (5)		Global		Per element	
Shear force in Dowels - Longitudinal		46.7	kips	1.5	kips
Shear force in Dowels - Transverse		-	kips	-	kips
Shear in Piles - Longitudinal	Under Abutment	-34.9	kips	-5.0	kips
Shear in Piles - Transverse	2 ft under Abutment	-	kips	-	kips

AXIAL FORCES (6)	Global		Per element	
Axial force in Dowels	8.1	kips	0.3	kips
Axial force in Piles	-11.0	kips	-1.6	kips

EARTH PRESSURE BEHIND ABUTMENT (7)			
Acute Corner	Elev. 1/3 H	63	psf
	Elev. 2/3 H	130	psf
Obtuse Corner	Elev. 1/3 H	59	psf
	Elev. 2/3 H	128	psf

MSE WALL EARTH PRESSURE (8)		
MSE wall earth pressure	63	psf

STRIP TENSILE FORCE (9)		
At connection with MSE Wall	91	psf
Maximum Value	111	psf

TRANSVERSE DISPLACEMENT (10)		
Transverse Displacement	-	inch

Figure 8.2 – IAB v2 spreadsheet output page

1. Thermal Displacement: This section presents six results:
    a) Total annual thermal displacement experienced by the bridge.
    b) Total daily thermal displacement experienced by the bridge.
    c) Annual thermal displacement experienced by one abutment. Half of result (a).
    d) Daily thermal displacement experienced by one abutment. Half of result (b).
    e) The next two results are parameters A and B, defined in Eq. (4.1).

2. Graphical representation of Eq. 4.1, using parameters A and B from output 1.

3. Recommended EPS thickness. Chapter 20 in the Virginia DOT guidelines titled "Integral/Jointless Bridges", provide the following equation:

$$EPS_t = 10\,[0.01\,h + 0.67\,\Delta L]$$

where EPS_t is the EPS thickness in inches
h is the height of the integral backwall in inches, including both the pile cap and the upper part of the abutment
ΔL is the total thermal displacement in inches

Not including the recommended EPS thickness will dramatically increase the earth pressure behind the abutment and will change its distribution.

4. Moments: This section includes 4 sets of results, each one with a "global" and "per element" result. The "global" result is the overall bridge response, and the "per element" result is simply the global result divided by the number of elements across the bridge.

The first two sets of results correspond to dowel moments, one in the longitudinal direction and one in the transverse direction. The next two sets of results are analogous results for piles.

Moments in piles have one extra cell of information. Next to the cell describing the direction, there is another cell indicating whether the maximum moment occurs right under the abutment or 2 ft below the abutment. The location for the maximum moment depends on the pile cap fixity condition, which is influenced by abutment type and skew angle.

5. Shear Forces: The same comments that apply to item 4, moments, also apply to shear forces.

6. Axial forces: This section is composed of two sets of results. The first is the increment in axial load experienced by dowels, and the second is the reduction of axial force experienced by piles. For design purposes, it is conservative to ignore the reduction in axial forces in the piles.

7. Earth Pressure behind Abutment: This section includes two sets of results, each set providing results for two elevations. One elevation is at 1/3 of the abutment height, and the other is at 2/3 of the abutment height. The results are provided at the acute and obtuse corners, which were defined in Figure 7.29.

8. MSE Wall Earth Pressures: This section provides the increment in earth pressure behind the upper quarter of the front wall. This value can also be applied to the side walls for the MSE facing panels closest to the abutment when the skew angle is 10 degrees or larger. At other locations and for smaller skew angles, the FLAC3D results indicate that it is not necessary to apply an increment of pressure to the MSE side walls due to thermal displacements.

9. Strip Tensile Force: Two results are provided in this section: first, the strip tensile force at the MSE connection, and second, the maximum tensile force along the strip. These values only apply to the upper quarter of the front MSE wall face.

The results for the strip tensile force have units of pressure, which were obtained by dividing the increment of strip tensile force by the strip tributary area (horizontal spacing times vertical spacing). The reverse procedure should be used to obtain the increment of strip tensile forced to be used for design.

10 Transverse Displacement: This result provides the maximum displacement in the transverse bridge direction, when skew angle is present.

8.4 Examples

The following paragraphs present two examples that use the IAB v2 spreadsheet. In the first example, the skew angle will be varied from 0 to 50 degrees in 10 degree increments. This is done for three pile sizes. In the second example, the distance between the front MSE wall and the abutment will be decreased from 4.5 ft to 0.5 ft in increments of 1 ft. This analysis will be repeated for three pile sizes.

8.4.1 Example 1

Figure 8.3 shows the input page for Example 1. The bridge under analysis is 600 feet long, consisting of two, 300 ft continuous spans. The distance between the front of the abutment and the back of the front MSE wall is 2 ft. The annual temperature variation is 100 ˚F. Seven piles oriented for weak axis bending moment support each abutment the superstructure. Thirty two dowels connect the upper abutment with the pile cap. The abutment height including the pile cap and the upper portion of the abutment is 10 ft. The vertical and horizontal spacing of the MSE wall reinforcing strips is 2.5 ft.

The red and blue arrows show where the parametric changes are made in this example. First, the skew angle will be varied from 0 to 50 degrees in 10 degree increments, i.e., the value indicated by the red arrow progressively changes. In addition, the process will be repeated for two more pile sizes beside the one indicated by the blue arrow. A total of three pile sizes are analyzed: H 10x42, H 12x63 and H 14x73.

Table 8.10 shows the global results for Example 1 for the smallest pile. The results in this table are the maximum magnitude of the values at the position directly under the abutment and 2 feet under the abutment. For example, the moment for the longitudinal direction for a skew angle of 10 degrees is the maximum magnitude between -195 kip-ft (directly under the abutment) and 180 kip-ft (2 ft under the abutment), which is -195 kip-ft.

The absolute magnitude of the moments and shear forces increase with the skew angle, except for the longitudinal moments in piles, which decrease as the skew angle increases. The longitudinal moments in piles in Table 8.10 exhibit a trend similar to that displayed in column C of Table 8.1, where the moment decreases as the skew angle increases.

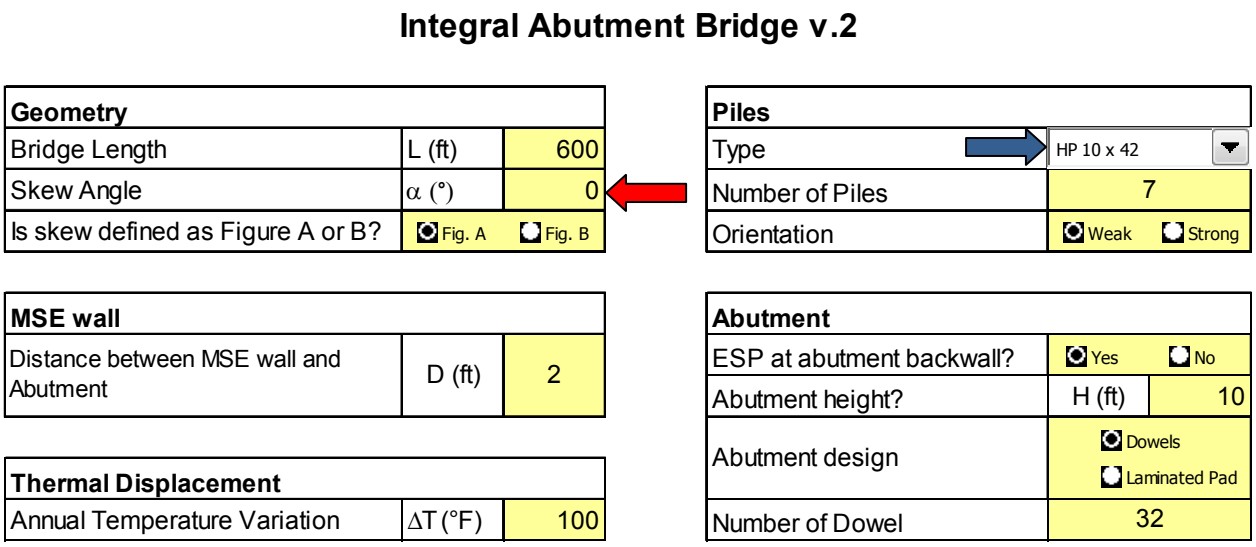

Figure 8.3 – Example 1 input page

Table 8.10 – Global output results of Example 1, pile H 10x42

Output Parameter		Unit	Skew Angle (degrees)					
			0	10	20	30	40	50
Moment in Dowels - Longitudinal		kip - ft	17	18	19	21	22	24
Moment in Dowels - Transverse		kip - ft	-	-3	-4	-5	-6	-7
Moment in Piles - Longitudinal		kip - ft	211	-195	152	126	104	125
Moment in Piles - Longitudinal (0 ft)		kip - ft	-196	-195	-125	-18	80	125
Moment in Piles - Longitudinal (2 ft)		kip - ft	211	180	152	126	104	84
Moment in Piles - Transverse		kip - ft	-	125	236	310	349	351
Shear force in Dowels -		kips	87	92	97	104	112	122
Shear force in Dowels - Transverse		kips	-	14	20	26	31	35
Shear in Piles - Longitudinal		kips	-43	-41	-44	-52	-64	-80
Shear in Piles - Transverse		kips	-	-26	-39	-48	-54	-55
Axial force in Dowels		kips	15	13	12	11	11	11
Axial force in Piles		kips	-56	-55	-51	-44	-34	-21
Earth Pressure Abutment	Acute Elev. 1/3 H	psf	200	189	178	166	154	140
	Acute Elev. 2/3 H	psf	221	227	239	256	279	308
Earth Pressure Abutment	Obtuse Elev. 1/3 H	psf	209	201	195	191	188	186
	Obtuse Elev. 2/3 H	psf	220	219	222	228	236	248
MSE wall earth pressure		psf	104	104	104	104	104	104
Strip Tensile Force at MSE Wall		psf	89	89	89	270	270	270
Strip Tensile Force Maximum Value		psf	270	270	270	270	270	270
Transverse Displacement		in	-	0.12	0.27	0.43	0.60	0.80

It is important to notice that the largest magnitude of bending moment in Table 8.10 corresponds to moments in piles in the transverse direction at large skew angles.

As previously mentioned, axial forces in dowels are almost stationary and axial forces in piles decrease because of shear forces between the abutment and EPS acting on the pile cap. Pile axial forces significantly decrease when skew angle is zero due the pile cap rotation, but this effect is drastically diminished as the skew angle increases.

The earth pressure behind the abutment follows the trend showed in Figure 7.35. The values at the acute and obtuse corners should be equal when skew angle is zero, but they are not exactly

the same due to slight inaccuracies in the polynomial fits to the data. In this case, the difference between values at opposite sides of the abutment is less than 5%, which is acceptable.

The MSE wall earth pressure and the strip tensile forces do not change across the table, because the magnitudes of these values do not depend on skew angle. Instead, they depend most strongly on the distance between the front MSE wall and the abutment.

Using the strip spacing, a designer can compute the extra loads that an MSE wall is expected to experience due to thermal effects. For the conditions represented in Figure 8.3 and Table 8.10, the strip loads due to thermal effects are 89 lbs per square foot of wall at the connection and 250 lbs per square foot of wall at the peak value. These amounts are added to the initial gravity values in the upper quarter of the front MSE wall. For example, if the strips are installed at a 2.5 ft by 2.5 ft spacing, a tensile force of 556 lbs should be added to the initial value at the connection with the MSE wall, and a tensile force of 1,563 lbs should be added to the initial peak value. In both cases, these additional forces apply to those strips in the upper quarter of the front MSE wall.

Table 8.10 also shows that the displacement toward the acute corner increases with the skew angle, reaching a maximum value of 0.8 in. at a skew angle of 50 degrees.

Tables 8.11 and 8.12 show Example 1 global results for H 12x63 piles and H 14x73 piles, respectively. Most of the output parameters exhibit increased magnitude in Table 8.11 and again in Table 8.12 compared to Table 8.10, except the earth pressure behind the abutment, which depends on the thermal displacement magnitude and the skew angle.

The maximum transverse displacement consistently decreases each tine the pile size is increased because a bigger pile imposes more restriction on the pile cap, allowing for less transverse displacement.

Table 8.11 – Global output results of Example 1, pile H 12x63

Output Parameter		Unit	Skew Angle (degrees)					
			0	10	20	30	40	50
Moment in Dowels - Longitudinal		kip - ft	21	22	23	25	26	28
Moment in Dowels - Transverse		kip - ft	-	-2	-3	-4	-5	-6
Moment in Piles - Longitudinal		kip - ft	284	238	195	155	117	157
Moment in Piles - Transverse		kip - ft	-	170	291	376	425	438
Shear force in Dowels -		kips	107	111	117	123	131	141
Shear force in Dowels - Transverse		kips	-	8	15	20	25	29
Shear in Piles - Longitudinal		kips	-54	-53	-57	-65	-77	-94
Shear in Piles - Transverse		kips	-	-17	-31	-41	-47	-49
Axial force in Dowels		kips	13	12	10	10	10	11
Axial force in Piles		kips	-59	-58	-54	-48	-37	-24
Earth Pressure Abutment	Acute Elev. 1/3 H	psf	200	189	178	166	154	140
	Acute Elev. 2/3 H	psf	221	227	239	256	279	308
Earth Pressure Abutment	Obtuse Elev. 1/3 H	psf	209	201	195	191	188	186
	Obtuse Elev. 2/3 H	psf	220	219	222	228	236	248
MSE wall earth pressure		psf	115	115	115	115	115	115
Strip Tensile Force at MSE Wall		psf	125	125	125	294	294	294
Strip Tensile Force Maximum Value		psf	294	294	294	294	294	294
Transverse Displacement		in	-	0.11	0.24	0.39	0.56	0.74

Table 8.12 – Global output results of Example 1, pile H 14x73

Output Parameter		Unit	Skew Angle (degrees)					
			0	10	20	30	40	50
Moment in Dowels - Longitudinal		kip - ft	23	24	25	27	28	30
Moment in Dowels - Transverse		kip - ft	-	-3	-4	-5	-6	-6
Moment in Piles - Longitudinal		kip - ft	395	329	266	206	148	199
Moment in Piles - Transverse		kip - ft	-	204	340	439	502	529
Shear force in Dowels -		kips	116	121	126	133	140	149
Shear force in Dowels - Transverse		kips	-	13	19	24	28	32
Shear in Piles - Longitudinal		kips	-74	-74	-78	-87	-100	-118
Shear in Piles - Transverse		kips	-	-25	-39	-49	-55	-57
Axial force in Dowels		kips	12	11	10	10	10	11
Axial force in Piles		kips	-58	-57	-53	-46	-36	-23
Earth Pressure Abutment	Acute Elev. 1/3 H	psf	200	189	178	166	154	140
	Acute Elev. 2/3 H	psf	221	227	239	256	279	308
Earth Pressure Abutment	Obtuse Elev. 1/3 H	psf	209	201	195	191	188	186
	Obtuse Elev. 2/3 H	psf	220	219	222	228	236	248
MSE wall earth pressure		psf	127	127	127	127	127	127
Strip Tensile Force at MSE Wall		psf	167	167	167	345	345	345
Strip Tensile Force Maximum Value		psf	345	345	345	345	345	345
Transverse Displacement		in	-	0.10	0.22	0.35	0.50	0.67

8.4.2 Example 2

In Example 2 the distance between the front face of the abutment and the back face of the MSE wall changes from 4.5 ft to 0.5 ft.

Since the only output parameters affected by the distance between the abutment and the front MSE wall are the earth pressure at the front MSE wall and the strip tensile forces, no other output parameters are discussed here for this example. Table 8.13 shows the global results for Example 2 with piles H 10x42, H 12x63, and H 14x73.

Table 8.13 – Global output results of Example 2 for piles H 10x42, H 12x63, and H 14x73.

Output Parameter	Pile	Unit	Distance Between Front MSE Wall and Abutment (ft)				
			4.5	3.5	2.5	1.5	0.5
MSE wall earth pressure	H 10x42	psf	89	88	96	115	143
Strip Tensile Force at MSE Wall		psf	28	38	67	116	185
Strip Tensile Force Peak Value		psf	202	218	238	262	289
MSE wall earth pressure	H 12x63	psf	98	97	107	126	155
Strip Tensile Force at MSE Wall		psf	55	68	101	154	226
Strip Tensile Force Peak Value		psf	241	260	282	308	337
MSE wall earth pressure	H 14x73	psf	108	108	118	138	168
Strip Tensile Force at MSE Wall		psf	85	103	140	198	276
Strip Tensile Force Peak Value		psf	283	305	330	359	392

Table 8.13 shows how the earth pressure at the front MSE wall and the strip tensile forces increase as the distance between the abutment and the front MSE wall is reduced.

The polynomial equation fitted to the MSE wall pressures is capable of approximating the shape of the curve presented in Figure 7.22 In this figure, big increments in MSE wall pressure are observed when the abutment is close to the front MSE wall. As the abutment is positioned at a greater distance from the front MSE wall, the earth pressures and the strip tensile forces are reduced, but at a slower rate as the distance increases.

The largest values in Table 8.13 for these three output parameters occur for the H 14x73 pile with a distance of 0.5 ft between the front of the abutment and the back of the MSE wall face. The values are 168 psf for the earth pressure, 276 psf for reinforcing strip tension at the connection to the MSE wall, and 392 psf for the peak reinforcing strip tension. If the strip spacing is 2.5 ft by 2.5 ft for this case, a designer should include the following thermal effects in the upper quarter of the front MSE wall: add a pressure of 168 psf to the MSE wall face, add 1,725 lbs to the tensile force in the reinforcing strips at the MSE wall connections, and add 2,450 lbs to the peak tensile force in the reinforcing strips.

CHAPTER 9

SUMMARY AND CONCLUSION

This chapter begins with a summary of the work accomplished during this research. Next, the findings and conclusions are described. Then, a cost and benefit discussion is presented, including an estimate of the savings from eliminating the corrugated steel pipe sleeves around abutment piles. This is followed by a description of the limitations of the analyses. Finally, recommendations are made for further research.

9.1 Summary of Work Accomplished

The following tasks were completed:

a) An extensive literature review was performed to compile information about integral abutment bridges, including design practices, advantages, construction procedures, and design alternatives.

b) A nationwide survey was conducted to complement the literature review information. Topics such as design practices, tolerances, and maximum dimensions, as well as challenges faced by design engineers, were covered in the survey.

c) The effectiveness of corrugated steel pipe sleeves was analyzed using FLAC3D software. Three-dimensional models of the corrugated steel pile sleeve system were analyzed under different boundary conditions. The analyses were completed for three sand densities and two load sequences to study the effectiveness of the sleeves and the impacts of cyclic loading.

d) Numerical modeling procedures were assessed and selected to create a reliable and consistent numerical model for analyses of the effects of cyclic thermal displacements on IABs with foundation piling in MSE wall backfill. Appropriate modeling equivalents and procedures were developed and assessed for use in FLAC3D to represent IAB

components, interactions of strips and piles with adjacent soil, IAB construction sequence, loads, and boundary conditions.

e) The FLAC3D modeling procedures were validated and calibrated against field data obtained from an IAB located in New Jersey. Additional validation was performed by comparing FLAC3D results with output of MSEW software (ADAMA 2007).

f) A three-dimensional base-case numerical model was generated using FLAC3D to represent features of an IAB bridge at Telegraph Road in Alexandria, Virginia. This bridge was selected because it incorporates current VDOT design practices. Some differences between the base model and the Telegraph Road bridge were implemented as requested by VDOT/VTRC engineers so that the base case model would be centered on issues of interest to VDOT, such as incorporating relatively large thermal displacements associated with the trend towards larger IABs. The numerical model was de-bugged and the results checked for consistency.

g) The base-case model was used in a parametric study to investigate the impacts of changing one parameter at a time. In total, 26 three-dimensional analyses were performed with individual parameter variations. The variations included changes in geometry such as wall heights and skew angles that required generating new meshes. Important results were extracted, compiled, and assessed for consistency.

h) After analyses of the individual parameter variations were completed, it was noted that multiple parameter variation models were needed to answer questions about how individual parameter variations interact and how best to quantitatively combine the effects of multiple parameter variations. Thirty-seven numerical models of multi-parameter variations were needed to create a robust set of numerical data to quantify the interactions of important design input parameters that influence IAB performance. Altogether, 63 numerical models were analyses, including the base case, the individual parameter variations, and the multiple parameter variations.

i) A vast quantity of numerical data was generated because 193 separate output parameters were monitored over a year of cyclic thermal displacements for 63 three-dimensional

numerical analyses. The results were analyzed to extract the maximum components of thermally-induced response for each parameter. Extracting the maximums produced 12,159 data values. To make this information accessible to design engineers and to permit interpolating between discrete input values used in the parametric analyses, multi-variable polynomial equations were fit to the data values.

j) An easy-to-use Excel spreadsheet, named IAB v2, was developed to permit design engineers to enter the important input parameter values and apply the multi-variable polynomial equations to calculate the output parameter values. The spreadsheet accommodates seven different pile sizes, which can be oriented in weak or strong axis bending directions, with variable offset of the abutment from the MSE wall and for variable skew angles. The spreadsheet calculates the increment of longitudinal and transverse displacements, forces, moments, and pressures on system components due to thermal displacement of IABs.

9.2 Findings and Conclusions

Conclusions drawn from the national survey presented in Chapter 3 include the following:

a) The survey shows that a national tendency of building longer IABs is taking place in the US. The typical maximum bridge lengths reported by state DOTs range from 500 – 600 ft. Currently the longest IAB is located in Tennessee with an overall length of 1175 ft.

b) Most of the agencies use a skew limit of 30º, and less than a third of them have special considerations for piles when the skew angle is larger than 20º.

c) Fifty-five percent of the responding agencies use corrugated steel pipes around piles, but none of them provided data or analyses to justify their use.

d) None of the agencies have special considerations to address the effects of thermally-induced displacements when designing MSE walls

e) There is no consensus regarding what lateral earth pressure should be used for abutment design. Thirty-five percent of the agencies use an active earth pressure distribution, 38% use a passive earth pressure distribution, and the rest use a combination of the above.

f) Only 10% of the agencies use EPS behind the abutment.

g) The responding agencies indicated that the most important concerns when designing IABs are: thermal displacement effects in bridge components, distance between MSE wall and piles, and lateral earth pressure behind the abutment.

Conclusions drawn from the numerical analyses include the following:

a) The results presented in Chapter 4 suggest that the use of steel pipe sleeves should be discontinued because this approach does not accomplish its intended purpose of reducing pile shear forces and moments. Furthermore, this is a difficult construction procedure that unnecessarily complicates construction and increases costs.

b) The numerical analyses show that driving abutment piles to a hard bearing stratum reduces the tension in the MSE wall straps in the lower portion of the wall.

c) The use of EPS at the abutment backwall is highly recommended because it significantly reduces the earth pressure behind the abutment. On the other hand, the use of EPS behind the MSE wall is not recommended, because it has only marginal beneficial effects, and it is expected to significantly complicate construction procedures.

d) According to this research, in bridges with less than 20° skew angle, the abutment piles should be oriented for weak axis bending because this orientation produces smaller loads and moments in dowels and abutment piles. For higher skew angles, pile orientation should be analyzed on a case-by-case basis using the IAB v2 spreadsheet because transverse bending moments may reach considerable values when abutment piles are oriented for weak bending moments.

e) The IAB v2 spreadsheet is recommended for computing the response of different bridge components to thermal displacements. As with any analysis tool, the designer should give careful consideration to the quality of input information, the impacts of the output on bridge design, and the basis for and limitations of the output. The limitations of the numerical analyses that form the basis of IAB v2 are discussed below.

9.3 Costs and Benefits Assessment

The primary benefit of this research is increased reliability and ease of designing IABs with abutment piling in MSE wall backfill. IABs are an important bridge technology for VDOT, and prior to this research, there were no reliable methods to design these systems for thermal displacements. As a result, designs were based on assumptions that may have been unnecessarily conservative in some cases and unconservative in others. Now, a rational methodology exists for designing IABs to accommodate thermal displacements, so that these bridges can be designed more safely and economically.

An additional benefit of this research is that corrugated steel sleeves infilled with loose sand can be eliminated from IAB designs. According to Barry Bryant from Bryant Contracting, the following are costs associated with typical installation of corrugated steel pipes on VDOT IABs:

- A 24 in. diameter, 16 gauge corrugated steel pipe is about US$ 16.50 per linear ft.
- Sand infilling the steel pipe is about US$ 1.50 per linear ft
- Labor, overhead and equipment is about US$ 4.50 per linear ft.
- The total cost is US$ 22.50 per linear ft. More generally, the cost is between US $20 – US $30 per linear ft.

The analyzed base case needs 23 ft of corrugated steel pipe per pile. Therefore the cost per pile is between US$ 460 to US$ 690, and using 7 piles per abutment, the total cost of installing corrugated steel pipes in the base case bridge is US$ 6,440 to US$ 9,660. This cost can be saved

as a result of this research. For wider bridges with more abutment piles the saving of not using corrugated steel piles filled with sand increases.

9.4 Model Limitations

The work described here only considers IABs with abutment piling in MSE wall backfill, with U-back designs for the MSE wing walls, i.e., the MSE wall wraps the abutment with MSE side walls parallel to the bridge alignment. Other MSE wall arrangements may respond differently.

The time for bridge completion is spring, so another limitation is that the thermal displacements imposed in the analyses are neutral position centered, as shown in Figure 4.1(a). This models a bridge that is constructed during spring, around April to May, producing close to symmetrical expansion and contraction displacements. If a bridge is set during the summer, most of its thermal displacement will be of contraction character, and the assumption of symmetrical expansion and contraction will no longer apply. One way to address this situation is by doubling the annual temperature range. Although the resulting doubled displacements would not represent the thermal displacements that would actually occur, this approach will provide safe output because the correct maximum bridge contraction values will be applied (see Figures 7.11 and 7.8). However, the shear forces and moments will be over-predicted in this approach because the peak values of these outputs occur during expansion, as shown in Figures 7.7 and 7.10.

Since Virginia DOT mainly designs IABs with weak pile axis orientation, only a few analyses were run with strong pile axis orientation. Given the relatively low number of strong pile axis orientation models, linear equations were used to fit the data, and somewhat lower confidence is associated with predicting forces and moments when strong pile orientation is selected than when weak axis pile orientation is selected in IAV v2.

9.5 Recommendation for Further Research

The following have been identified as topics for which additional research may improve the state of knowledge:

a) This research only studied IABs with steel girders in the bridge deck. Virginia DOT desires to extend the present study to consider concrete girders. A preliminarily analysis of concrete and steel girder sections indicates that the moments of inertia of concrete girders are about 2.1 to 2.8 times larger than the moments of inertia of steel girders. In Chapter 7, section 7.2.2.5, the girder height was changed by ± 9 in., which translates to a girder moment-of-inertia change of approximately ± 30%, respectively. A bigger moment of inertia produced by concrete girders may or may not change the abutment rotation above the hinge. The abutment rotation above the hinge depends on the degree of pile cap fixity. The pile cap can be restrained from rotation either by piles with a strong bending moment orientation or by increasing skew angle. For a pile cap free to rotate, it is likely that the increment in moment of inertia of the girders will not change the abutment rotation above the hinge, and thus, current result will apply. But for a restrained pile cap, a big increment in moment of inertia might change the abutment rotation above the hinge, imposing different loads on dowels and piles. Because current results might not apply to bridges with large moments of intertia, particularly when combined with large skew angles, additional analyses of bridges with concrete girders are recommended.

b) Strong axis orientation of piles might be advantageous for cases where skew angle is large. Table 9.1 shows maximum moment and shear forces for 4 cases designed with piles H 14x73. Cases C11 and C12 have the abutment piles oriented for weak axis bending moment, and cases C15 and C16 for strong axis bending moment. It is evident from Table 9.1 that, for small skew angles, the weak orientation is preferred (cases C11 and C15), but for larger skew angles, it might be better to orient the pile for strong bending moment (cases C12 and C16). If future research proves that piles oriented for strong bending moments are beneficial when the skew angle is large, several numerical models will be needed to enlarge the data base for strong pile orientation.

Table 9.1 – Moments and shear forces in piles. Piles in strong and weak axis orientation for skew angles of 20˚ and 45˚.

Model Name	Skew Angle	Longitudinal		Transverse	
		Moments	Shear	Moments	Shear
C11	20 deg	-292,443	-128,407	637,355	-61,304
C15	20 deg	497,630	-158,177	274,226	44,444
C12	45 deg	274,483	-174,238	860,013	-94,415
C16	45 deg	-185,525	-175,313	564,421	89,305

c) As discussed above in the limitations section, the analyses in this research represent bridges completed during the spring, for which expansion and contraction cycles are neutral centered. Additional analyses should be performed to investigate the influence of bridge completion during other times of the year.

d) Settlements behind the abutment computed in Section 7.1.7.8 showed that the settlements extend a distance equal to the abutment height into the backfill. The use of the Rankine passive wedge by some agencies to compute the area of influence where the settlements occur seems overly conservative. However, since the settlements were computed only for the Base Case, more research on this topic is warranted to see if the same conclusion found for the Base Case also holds for other input parameters combinations. Ideally, such research would include field data of surface settlement profiles behind integral abutment walls. Such research may show that approach slabs can be safely shortened.

e) The Telegraph Road bridge in Alexandria, Virginia, has been instrumented. It is recommended that the instrumentation data be reduced and assessed, and that the results compared with IAB v2. If the instrumentation data are consistent with IAB v2, then this would support the research results, and no further investigation would be needed. If the data are not consistent with IAB v2, then it may be necessary to numerically analyze the Telegraph Road bridge to recalibrate the numerical modeling procedures to the new data,

repeat the analyses of the parameter variations with the revised modeling procedures, and revise the IAB v2 spreadsheet.

In the author's opinion, the two most important additional research topics in the above list are items (e) validation against the Telegraph Road bridge data and (c) investigation of bridge completion at other times of the year than spring. VDOT may also be interested in items (a) concrete bridge girders, (b) additional analyses of strong axis pile orientations, and (d) extent of settlements behind abutments for use in determining the required length of approach slabs.

REFERENCES

AASHTO (1996), Standard Specifications for Highway Bridges, 16th ed.,Washington, D.C., 1996.

Abendroth, R., Greimann, L., Ebner, P. (1989) "Abutment pile design for jointless bridges" Journal of structural engineering New York, N.Y., v 115, n 11, p 2914-2929, Nov 1989

Alampalli, S., and Yannotti, A. P. (1998). "In-Service Performance of Integral Bridges and Jointless Decks," Transportation Research Record, n 1624, Sep, 1998, p 1-7.

Arsoy, S., Barker, R.M., and Duncan, J.M. (1999). "The Behavior of Integral Abutment Bridges," VTRC 00-CR3. Vigirnia Transportation Research Council, Charlottesville. 33 p.

Arsoy, S., Barker, R.M., and Duncan, J.M. (2002). "Experimental and Analytical Investigations of the Piles and Abutments of Integral Bridges," VTRC 02-CR6. Vigirnia Transportation Research Council, Charlottesville. 55 p.

Arsoy, S., Duncan, J.M., and Barker, R.M. (2004). "Performance of piles supporting integral bridges," Transportation Research Record, n 1808, 2002, p 162-167

Arsoy, S., Duncan, J.M., and Barker, R.M. (2004). "Behavior of a semiintegral bridge abutment under static and temperature-induced cyclic loading'" Journal of Bridge Engineering, v 9, n 2, March/April, 2004, p 193-199

Arsoy, S., Duncan, J.M., and Barker, R.M. (2005). "Approach to evaluating damage from thermal bridge displacements," Transportation Research Record, n 1936, 2005, p 124-129.

Briaud, J.L., James, R.W., and Hoffman, S.B. (1997). "Settlement of bridge approaches : (the bump at the end of the bridge)," Transportation Research Borad, Washington D.C.

British Highway Agency. 1996. The design of integral bridges. British Code BA42/96. Design Manual for Roads and Bridges, The Design Manual for Roads and Bridges (DMRB) is a series of 15 volumes that provide official standards, advice notes and other documents relating to the design, assessment and operation of trunk roads, including motorways in the UnitPart 12. British Highway Agency, London, UK.

Burke, M.P. (1987). "Bridge Approach Pavements, Integral Bridges and Cycle control Joints," Transportation Research Record, n 1113, 1987, p 54-65

Duncan, J. M., and Mokwa, R. L. (2001). "Passive earth pressures: Theories and tests," Journal of Geotechnical and Geoenvironmental Engineering, v 127, n 3, March, 2001, p 248-257

Dunker, K.F., and Lui, D. (2007). “Foundations for Integral Abutments,” Practice Periodical on Structural Design and Construction, ASCE, v 12, 2007, 22-30.

Filz, G.M., and Duncan, J.M. (1993). "Drift of Flush-Mounted Pressure Cell Readings," Geotechnical Testing Journal, ASTM, 16(4), 432-441.

Filz, G.M., and Brandon, T.L. (1994). “Static and Dynamic Measurements Using Embedded Earth Pressure Cells," Transportation Research Record, No. 1432, 86-95.

Fleming, W. G., Weltman, A. J., Randolph M. E., Elsonet W. K. (1985). “Piling Engineering”. Halsted Press, New York, N.Y

Girton, D.D., Hawinson, T.R., Greimann, L.F. (1991) “Validation of Design Recommendations for Integral-Abutment Piles,” Journal of Structural Engineering, Vol. 117, No 7

Hassiotis, S., Lopez, J., and Bermudez, R. (2005). “Full-Scale Testing of an Integral Abutment Bridge,” Proceedings of the Integral Abutment and Jointless Bridges Conference, FHWA, Baltimore, 199-210.

Hassiotis, S., Khodair, Y., Roman, E., and Dehne, Y. (2006) “Evaluation of Integral abutments,” Department of Transportation of New Jersey State, New Jersey

Hoppe, E., and Gomez, J. P. (1996). “Field Study of Integral Backwall Bridge,” VTRC 97 – R7. Virginia Transportation Research Council, Charlottesville. 47 p.

Hoppe, E. (1999). “Guidelines for the Use, Design, and Construction of Bridge Approach Slabs,” VTRC 00-R4. Vigirnia Transportation Research Council, Charlottesville. 39 p.

Hoppe, E. (2005). “Field Study of Integral Backwall with Elastic Inclusion,” Proceedings of the Integral Abutment and Jointless Bridges Conference, FHWA, Baltimore, 257-269.

Hoppe, E. (2005). “Field Study of Integral Backwall with Elastic Inclusion,” VTRC 05-R28. Vigirnia Transportation Research Council, Charlottesville. 33 p.

Horvath, J.S., (2000). “Integral-Abutment Bridges: Problems and Innovative Solutions Using EPS Geofoam and Other Geosynthetics,” Manhattan College Research Report No. CE/GE-00-2, Bronx, New York.

Itasca Consulting Group Inc. (2006). FLAC3D, Fast Lagrangian Analysis of Continua in 3 Dimensions, version 3.1, Minneapolis

Maruri, R., and Petro, S. (2005). “Integral Abutments and Jointless Bridges (IAJB) 2004 Survey Summary,” Proceedings of the Integral Abutment and Jointless Bridges Conference, FHWA, Baltimore, 12-29.

Mistry, V. (2005) “Integral Abutments and Joinless Bridges,” Proceedings of the Integral Abutment and Jointless Bridges Conference, FHWA, Baltimore, 3-11

Mokwa, R.L., and Duncan, J.M. (2000). “Investigation of The Resistance if Pile Caps and Integral Abutments to Lateral Loading,” VTRC 00 – CR4. Virginia Transportation Research Council, Charlottesville. 66 p.

Mourad, S., and Tabsh, S.W. (1998). “Pile Forces in Integral Abutment Bridges Subjected to Truck Loads,” Transportation Research Record, n 1633, 1998, p 77-83.

NCHRP (2004). “Guideline and Recommended Standart for Geofoam Applications in Highway Embankments,” National Cooperative Highway Research Program, report 529, Washington D.C.

Poulos, H. G., and Davis, E. H. (1980). “Pile foundation analysis and design”. John Wiley & Sons, New York, N.Y

Reeves, J.N., Filz, G.M., and Van Wagoner, D.D. (2001). “Elasticized Geofoam for Reduction of Compaction-Induced Lateral Earth Pressures,” Proc. Geosynthetics Conference 2001, Industrial Fabrics Association International, 755-766.

Sandford, T.C., Elgaaly, M. (1993). “Skew effects on backfill pressures at frame bridge abutments,” Transportation Research Record, n 1415, 1993, p 1-11

Spyrakos, C., and Loannidis , G. (2003). “Seismic behavior of a post-tensioned integral bridge including soil–structure interaction (SSI),” Soil Dynamics and Earthquake Engineering, v 23, n 1, January, 2003, p 53-63

Terzaghi, K., Peck, R., and Mesri, G. (1996) “Soil Mechanics in Engineering Practice” Third Edition, John Wiley and Sons.

Virginia Department of Transportation (2007). “Design Aids – Typcal details, Chapter 20,” Volume 5, part 2, http://www.virginiadot.org/business/bridge-v5p2.asp.

Virginia Department of Transportation (2007). “Proposed bridge on ramp H-2 over ramp H-4 Fairfax Co. - .07 Mi. W. of int. Telgraph Rd. Proj. 0095-96A-105. B673”.

Xu, M., Clayton, C.RI., and Bloodworth A.G. (2007). “The Earth Pressure Behind Full-height Frame Integral Abutments Supporting Granular Fill,” Canadian geotechnical journal, v 44, No 3, 284.

APPENDIX A

INTEGRAL ABUTMENT BRIDGE (IAB) SURVEY

The purpose of this survey is to collect information about integral abutment bridges that have foundation piling for the abutments extending through the backfill of mechanically stabilized earth (MSE) walls, as shown schematically in Figure 1 below. The survey results will be used to help guide a research project sponsored by the Virginia Transportation Research Council and conducted by Virginia Tech.

One of the issues inspiring the research is that, as the bridge contracts and expands due to daily and seasonal temperature fluctuations, the abutment piles are moved towards and away from the MSE wall facing. Such movements could impose large loads on the wall facing and the reinforcing strips, which could damage the wall facing and/or the connections between the reinforcing strips and the wall facing.

The survey on the following pages is designed to obtain information about this issue and other aspects of integral abutment bridges (IABs) to help guide the research project in practically useful directions. The survey contains questions that range from general aspects of IABs to specific design details.

If you are not the right person in your organization to complete this survey, please forward it to someone who is. The survey should be completed and returned to Mr. Alfredo Arenas, c/o Professor George Filz, Civil and Environmental Engineering Department, Virginia Tech, Blacksburg, VA 24061 by [date]. Thank you in advance for your contribution.

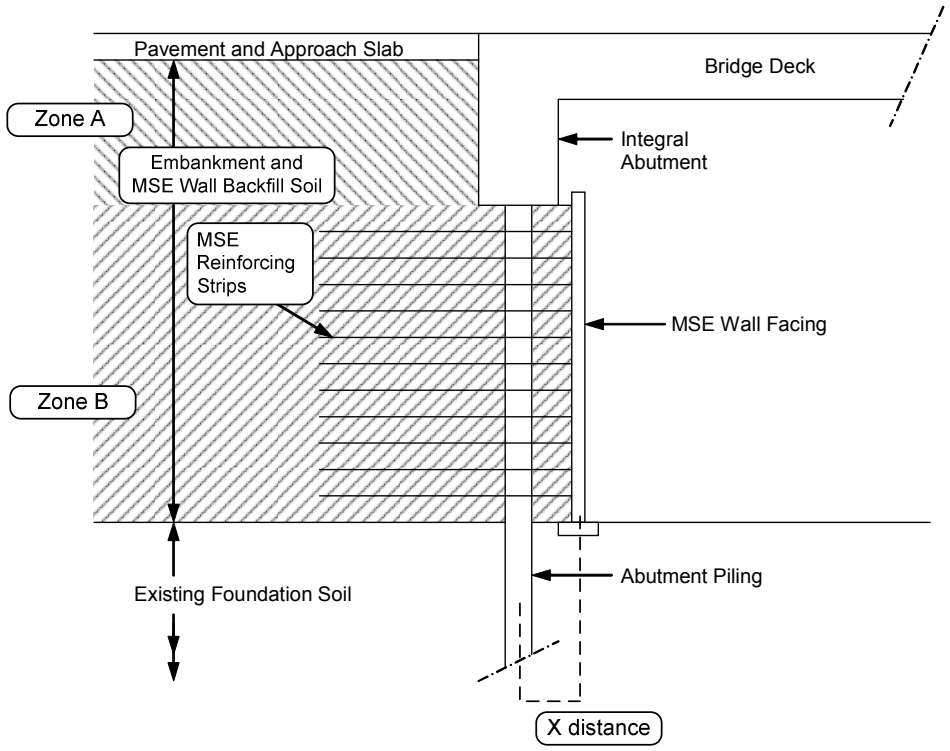

Figure 1. Profile View of Integral Abutment Bridge and MSE wall

INTEGRAL ABUTMENT BRIDGES (IAB) SURVEY

Bridge

1.- What are the maximum span and the maximum length of current IAB designs?

_____

2.- Does the current IAB design criteria specify limits for skew angle and curvature?

☐ Yes, skew limit _____ ☐ No
curvature limit _____

3.- Have any constructed bridges experienced problems due to skew or curvature?

☐ Yes ☐ No

If yes, please provide bridge information:

bridge length _____ ☐ concrete girders ☐ steel girders
☐ integral ☐ semi-integral ☐ other _____
skew _____
curvature _____

If yes, please explain the problem:

_____
_____
_____

Piles

4.- What pile types and orientations are used for IABs?

☐ H – pile ☐ weak axis ☐ strong axis ☐ other _____
☐ pipe pile
☐ concrete pile
☐ other _____

5.- Does current IAB design include corrugated steel sleeves filled with loose sand fill (or any other method) to reduce piles stresses due to bridge movements?

_____
_____
_____

6.- Please describe your IAB pile design methodology for axial loads and for lateral loads.

_____
_____

7.- In addition to bending moments produced by thermal expansion and contraction, does the current IAB design criteria account for bending moments produced by skew angles and/or curvature?

_____
_____
_____

8.- What are the pile deflection tolerance and capacity criteria for IABs?

deflection _____

☐ axial, load criteria _____
☐ bending, moment criteria _____
☐ axial / bending, criteria _____
☐ other _____

MSE Wall

9.- What is the offset between the MSE wall and the abutment foundation piles, distance X (center to center) shown in Figure 1?.

_____

10.- Do you or the MSE constructor/designer apply special considerations to account for higher tensile stresses on the MSE straps due to bridge contraction? If so, please explain.

_____
_____
_____

11.- What type of backfill material is specified in the current design? (Figure 1, Zone B)

☐ well graded free drainage granular material ☐ crushed sandstone type
☐ re – compacted natural soil ☐ other _____

12.- What are the compaction specifications for the backfill? (Figure 1, Zone B)

_____
_____
_____

Abutment

13.- What type of backfill material is specified in the current design? (Figure 1, Zone A)

☐ well graded free drainage granular material ☐ crushed sandstone type
☐ re – compacted natural soil ☐ other _____

14.- What are the compactions specifications for the backfill? (Figure 1, Zone A)

_____
_____
_____

15.- What type of earth pressure is accounted in designs? (Figure 1, Zone A)

☐ active ☐ passive
☐ active / passive ☐ other _____

16.- Does the current design procedure include specifications for expanded polystyrene (EPS) against the abutment wall to reduce lateral earth pressure?

_____
_____
_____

Approach Slab

17.- Do you use approach slabs? If so, what support / connection system are provide at the ends of the approach slabs?

_____
_____
_____

18.- Do you provide a special treatment beneath the approach slab to reduce friction between the slab and the underlying soil? If so, please describe the treatment.

_____
_____
_____

Miscellaneous

19.- What do you see as the most important questions that need to be answered for IABs with MSE walls?

_____

_____
_____

20.- So far, we have collected the references listed on pages 6 and 7. Are there any other references we should obtain?

_____
_____
_____

21.- It will be very helpful to improve the state of practice to instrument an IAB with an MSE wall. Do you know about any projects that can be instrumented?

_____
_____
_____

Criteria / Design	Number of agencies using it
Always require / Use design manual for different length	1
Always require for bridges of 100 ft or longer.	1
Is required or detailed in every IAB	8
Always require / Extend approach slab to end of wing walls and provide sleeper slab under end of approach slab	2
Always require with concrete pavement	1
Always require with a minimum of 20 ft	1
Always require with a minimum of 25 ft	1
Always require with a minimum of 30 ft	1
Use it when ADT 500 or greater, or ADTT 100 or greater, or Total movement 0.5” or greater	1
Always require / Provide an expansion joint between the end panel and the approach pavement where the range of abutment movement is one (1) inch or less	1

Table A.1 – Criteria / Design for the use of Approach Slab

Support / connection system	Number of agencies using it
Dowelled to end of superstructure.	2
Placed on a corbel where it is permitted to move	1
Typically a sleeper slab at the free end, and a notched seat in the backwall at the bridge	1
Approach slabs sit on backwall and are connected to deck w/ reinforcing. Other end sit on grade	1
6" wide concrete corbel and #5@12" epoxy rebar	2
Keyed grade beam where expansion joint is and a pinned connection to the abutment	1
Sleeper slab with expansion joint at pavement interface. Pinned with dowels at abutment	2
For movements greater than 2" use strip seals	1
On the abutment end, approach slab on a ledger that is cast into the back face of the abutment with rebar, bent in the shape of a right angle, from the front face of the abutment into the approach slab. On the side away from the bridge, the approach slab rest on a sleeper slab	1
Direct connection to abutment	1
Approach slabs shall be doweled to the end bent or pavement rest with #6 bars at 12 in on center. The anchors shall be detailed to act as a hinge so that the approach slab can rotate downward without stress as the embankment settles	1
Reinforcement bars "connect" the integral abutment and approach slab. A sleeper slab is provided at the "pavement"/other end of the approach slab	1
Supported on the integral abutment at one end and a "sleeper slab" at the other end. A positive connection with reinforcement steel (that is assumed to be pinned) is provided at the integral abutment.	1
Approach slab rests on a corbel at the abutment and is connected with # 5 bars at 12" centers. Additionally, the approach pavement is connected to the bridge deck at the abutment with 10' long # 5 bar splicers at 12" centers (4'into bridge deck and 6' into approach pavement). The approach pavement rests on a common sleeper slab at the roadway pavement transition and the structure movements are taken with a PJS joint at this location	1
Approach slabs are typically placed on a corbel at the abutments, and are not connected to the abutments. The remainder of the approach slab is placed directly on the reinforced backfill	2

Table A.2 – Criteria / Design for the support/connection system of Approach Slab

APPENDIX B

BASE CASE MONITORING OUTPUT PLOTS

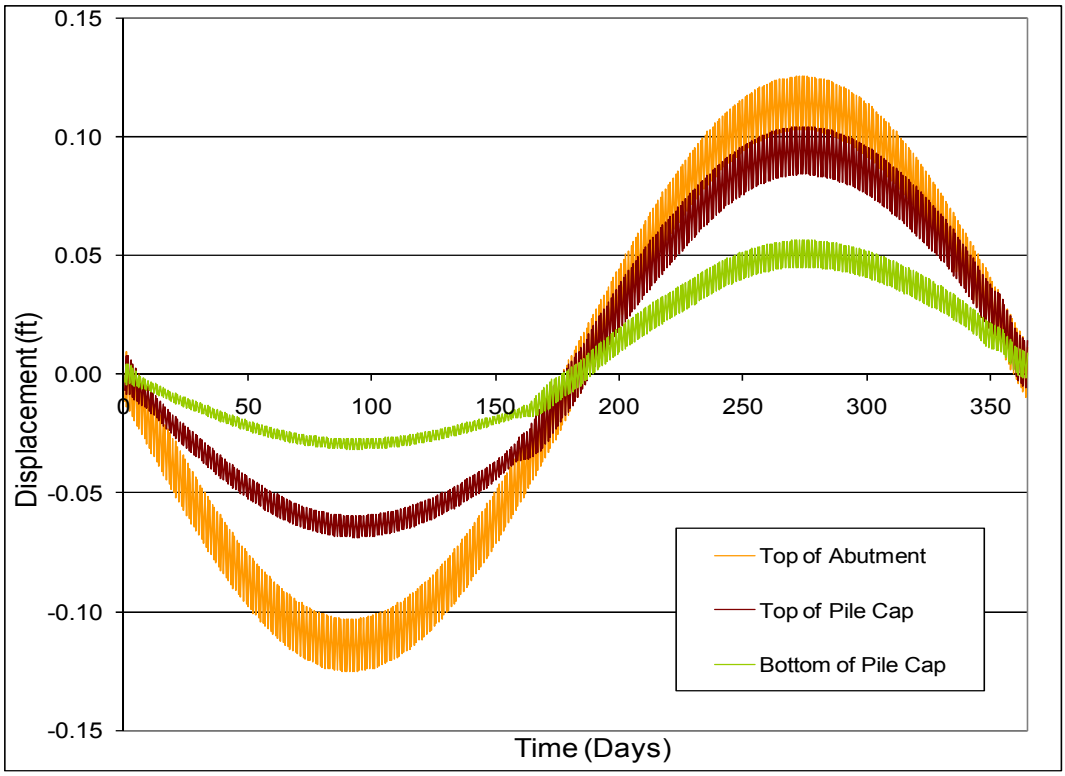

Figure B.1 – Abutment longitudinal displacement.

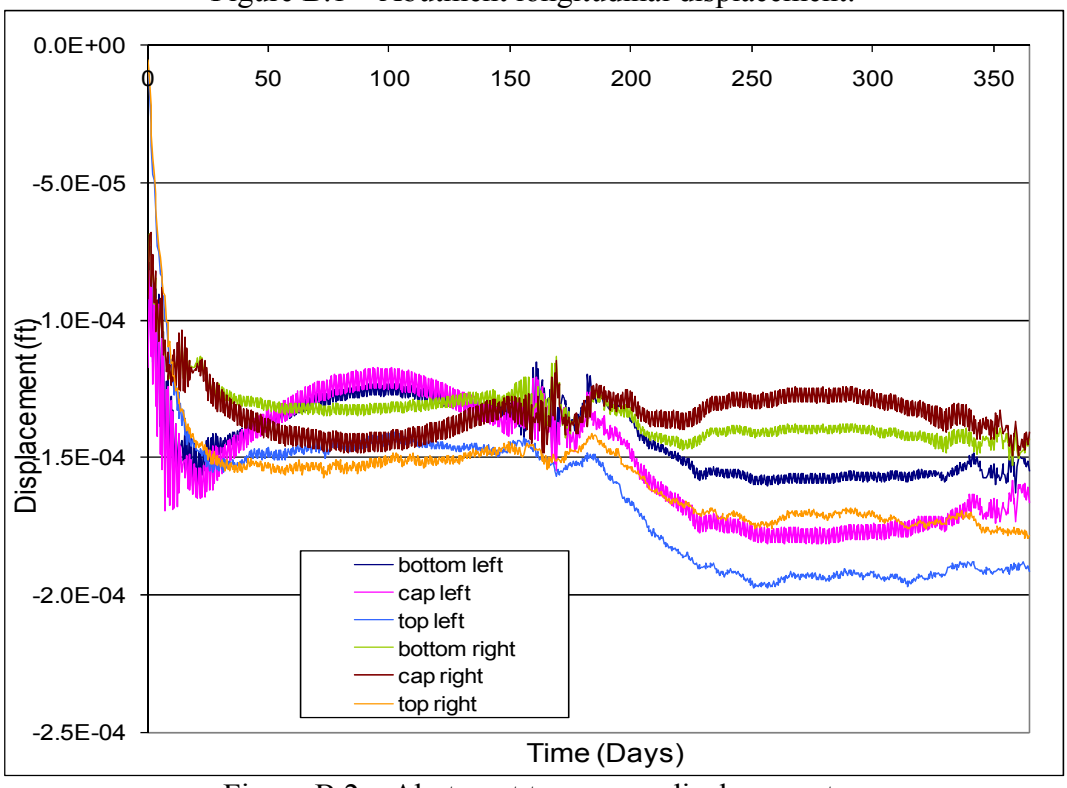

Figure B.2 – Abutment transverse displacement.

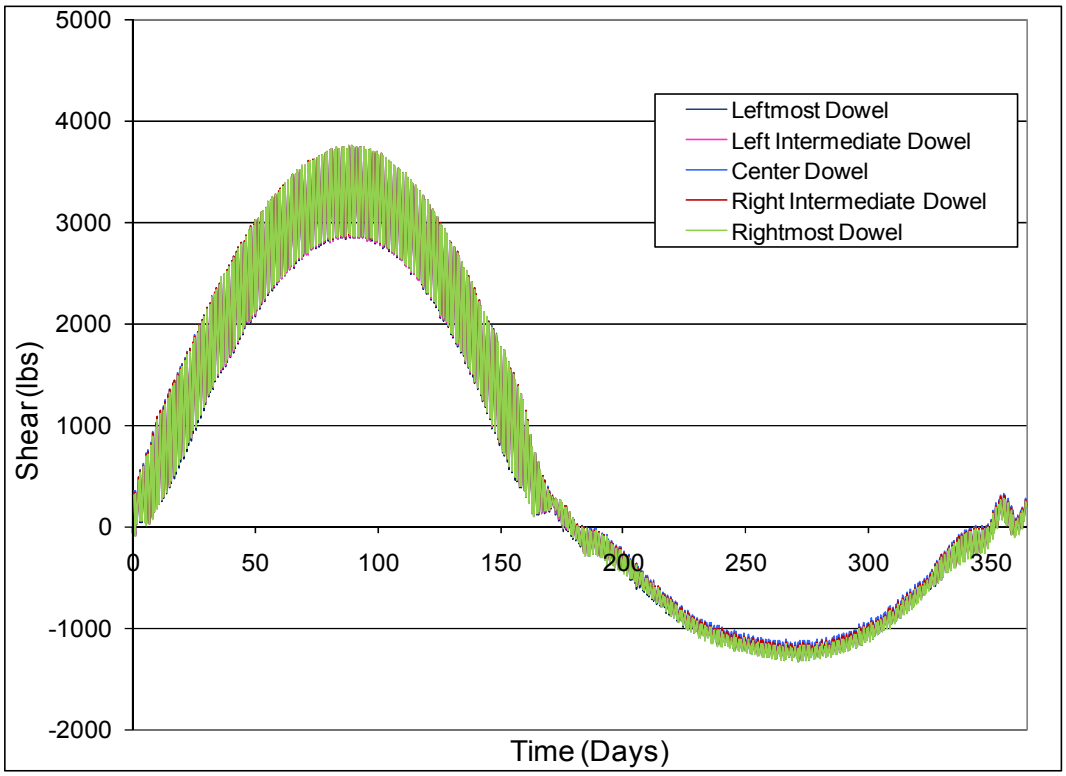

Figure B.3 – Longitudinal shear forces in dowels.

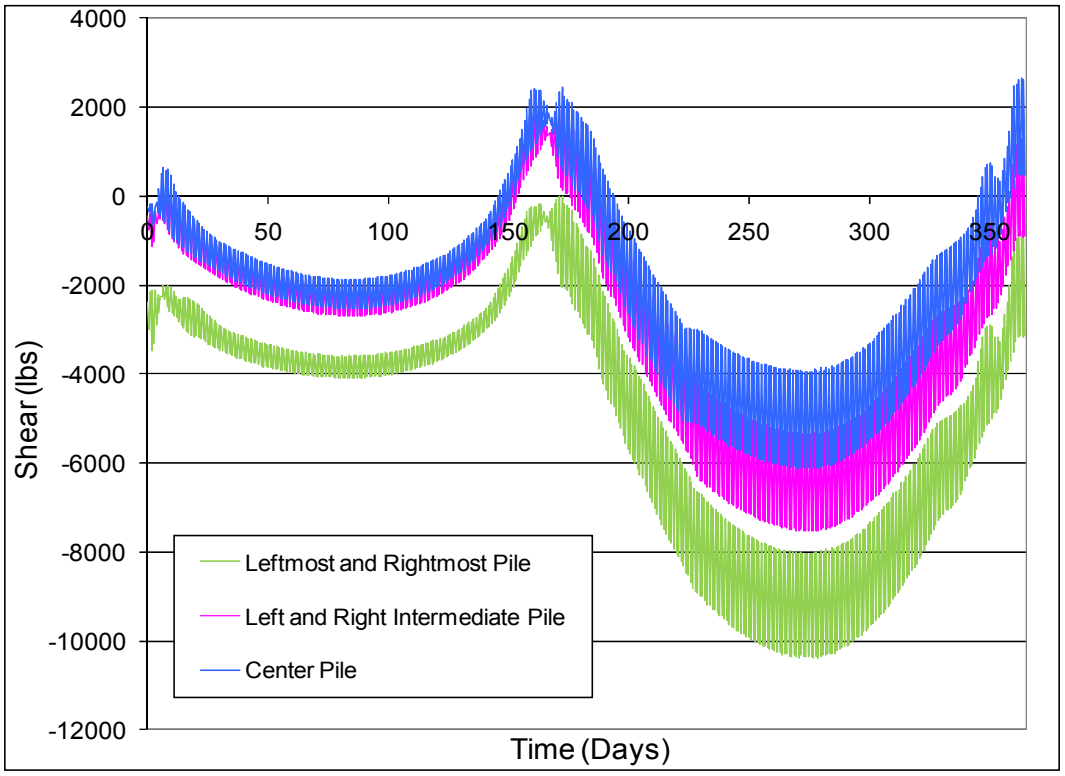

Figure B.4 – Longitudinal shear forces in piles under abutment.

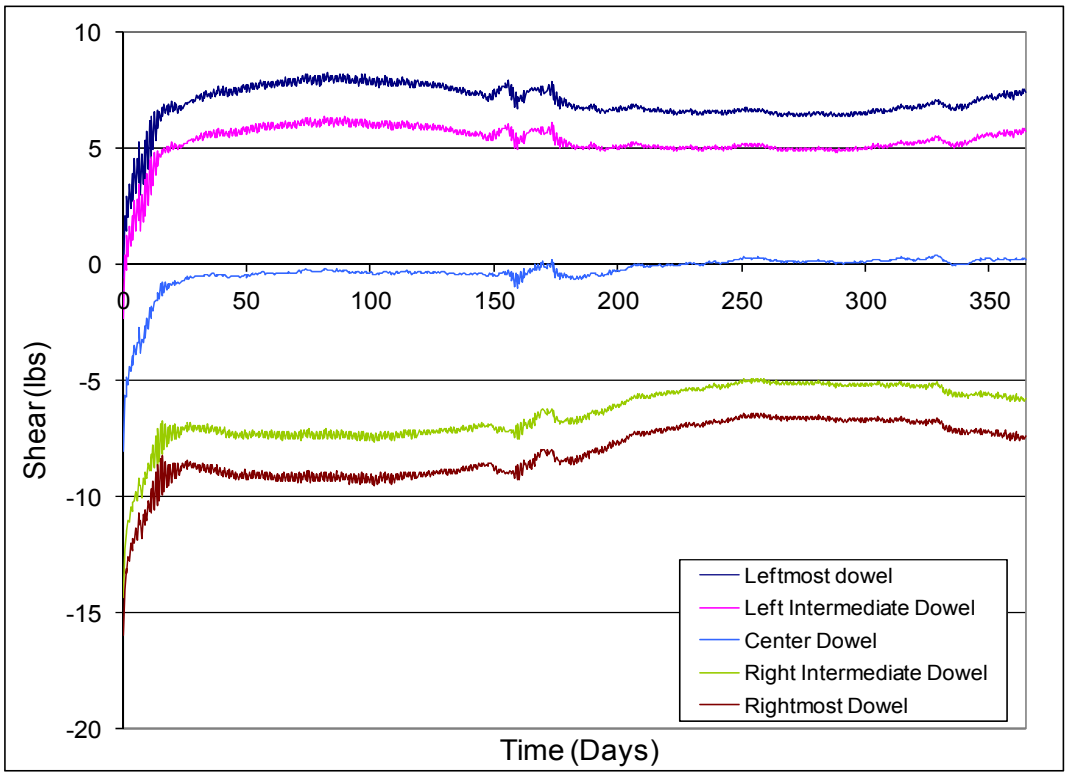

Figure B.5 – Transverse shear forces in dowels.

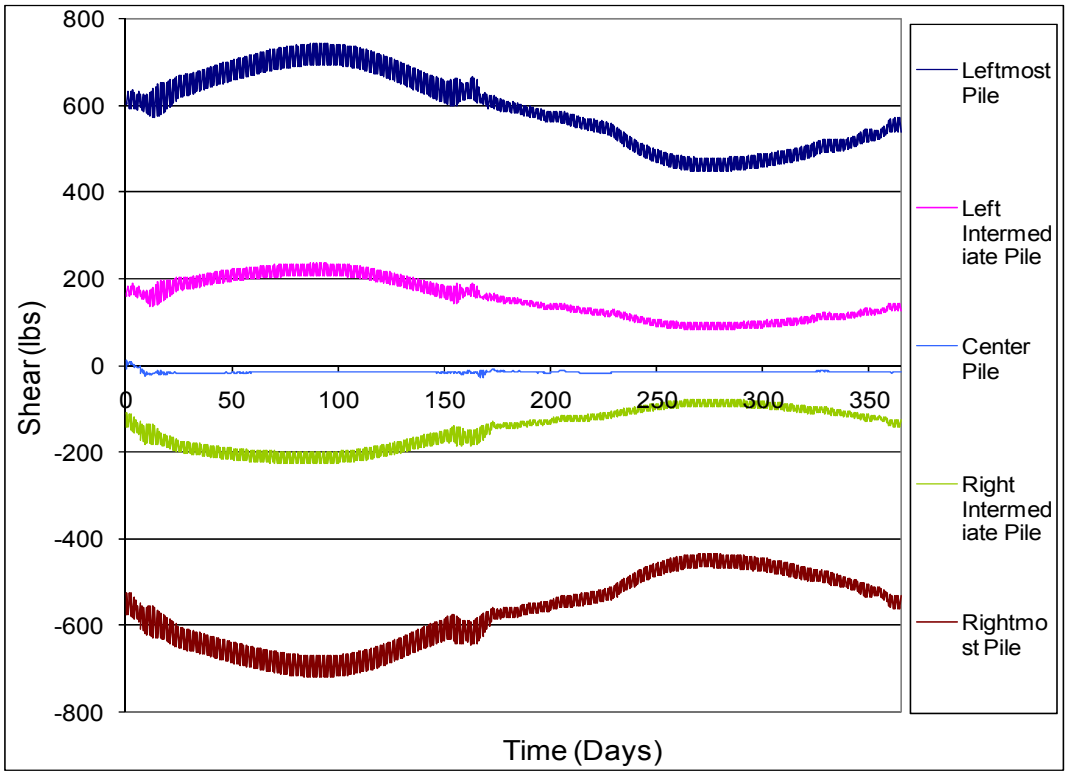

Figure B.6 – Transverse shear forces in piles under abutment.

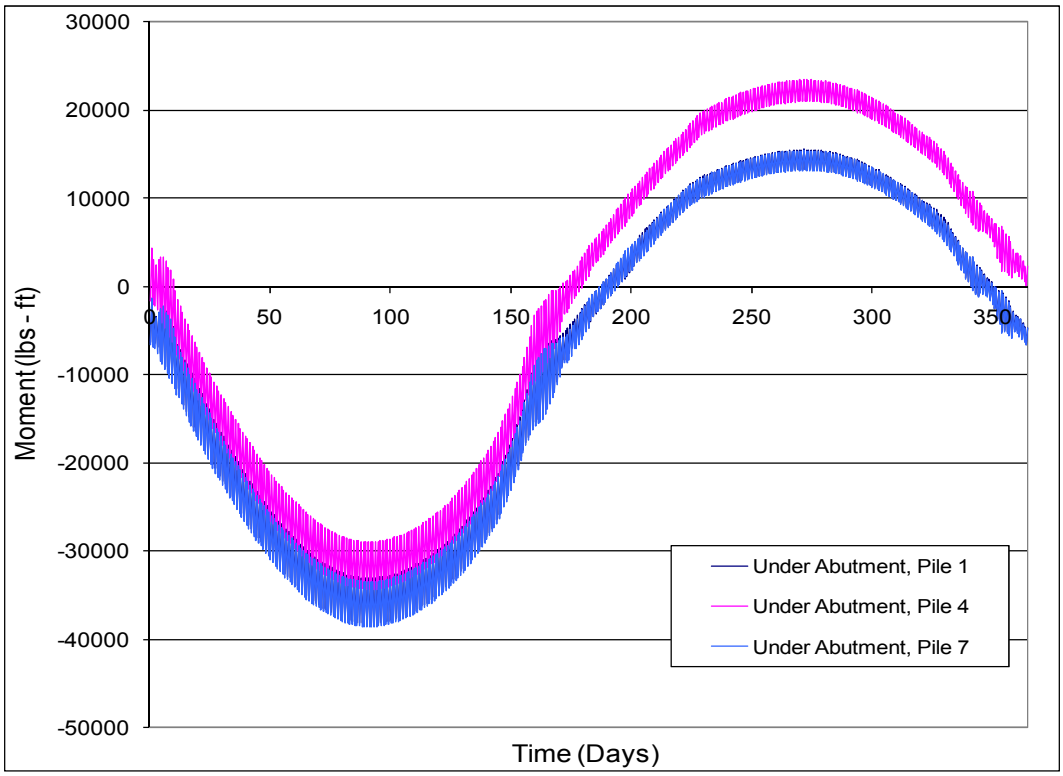

Figure B.7 – Longitudinal moments in piles under abutment.

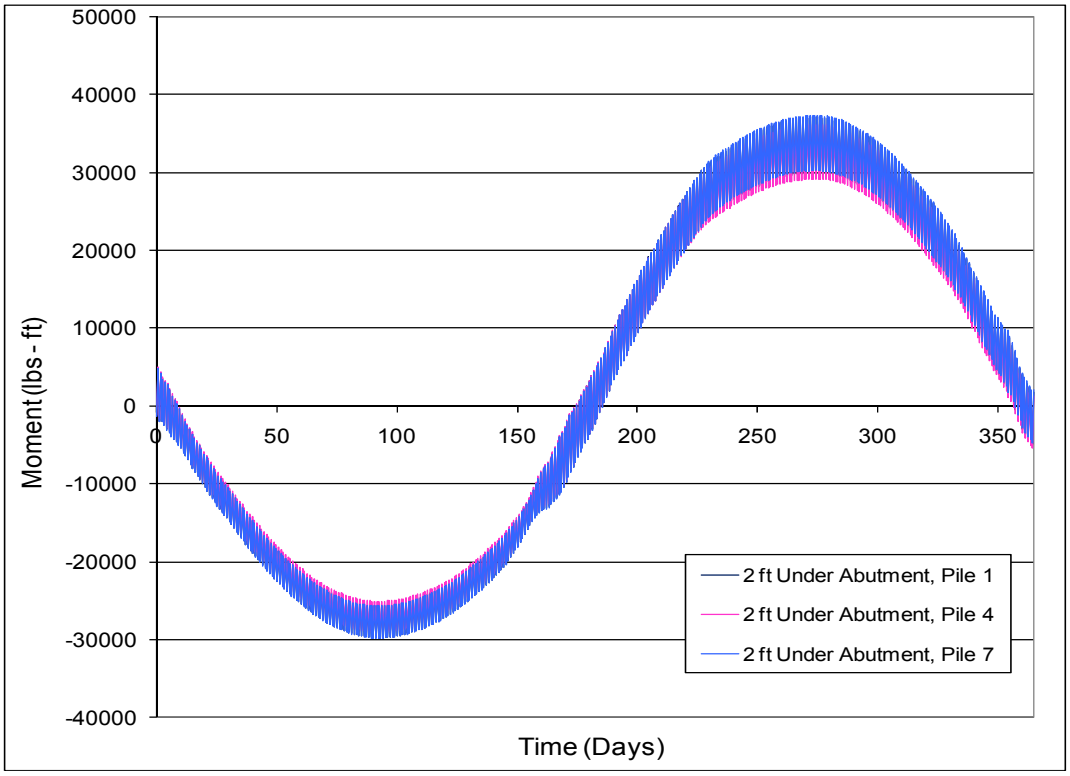

Figure B.8 – Longitudinal moments in piles 2ft under abutment.

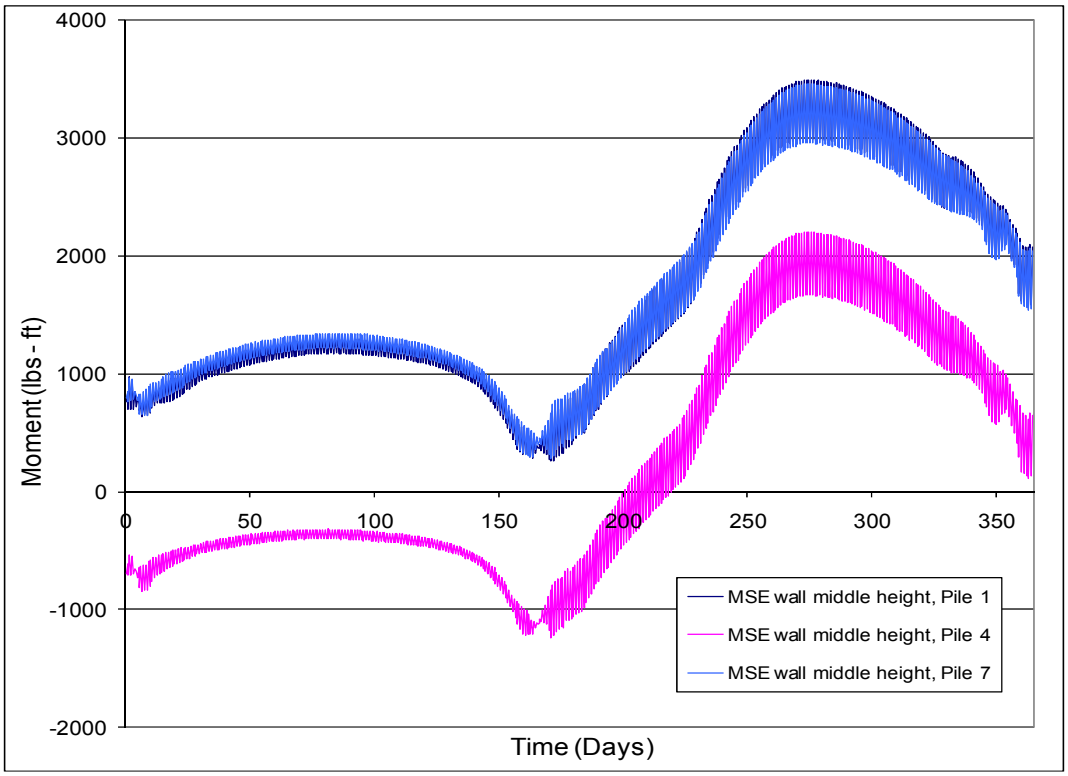

Figure B.9 – Longitudinal moments in piles at MSE wall middle height.

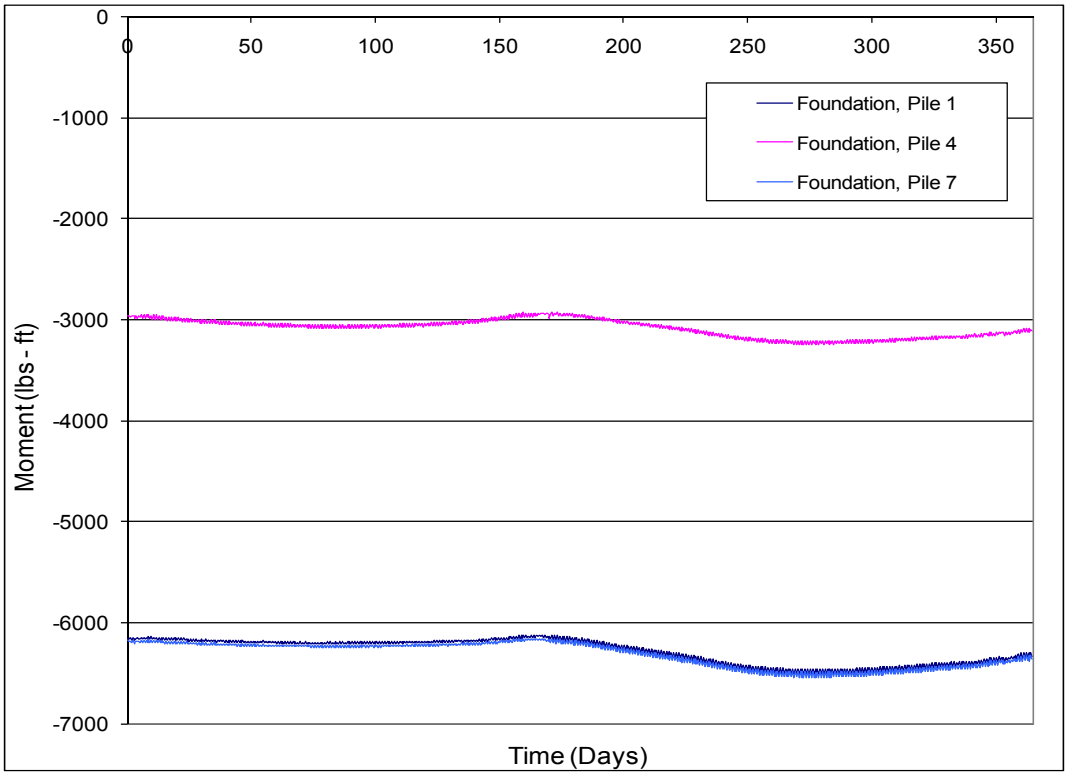

Figure B.10 – Longitudinal moments in piles at foundation elevation.

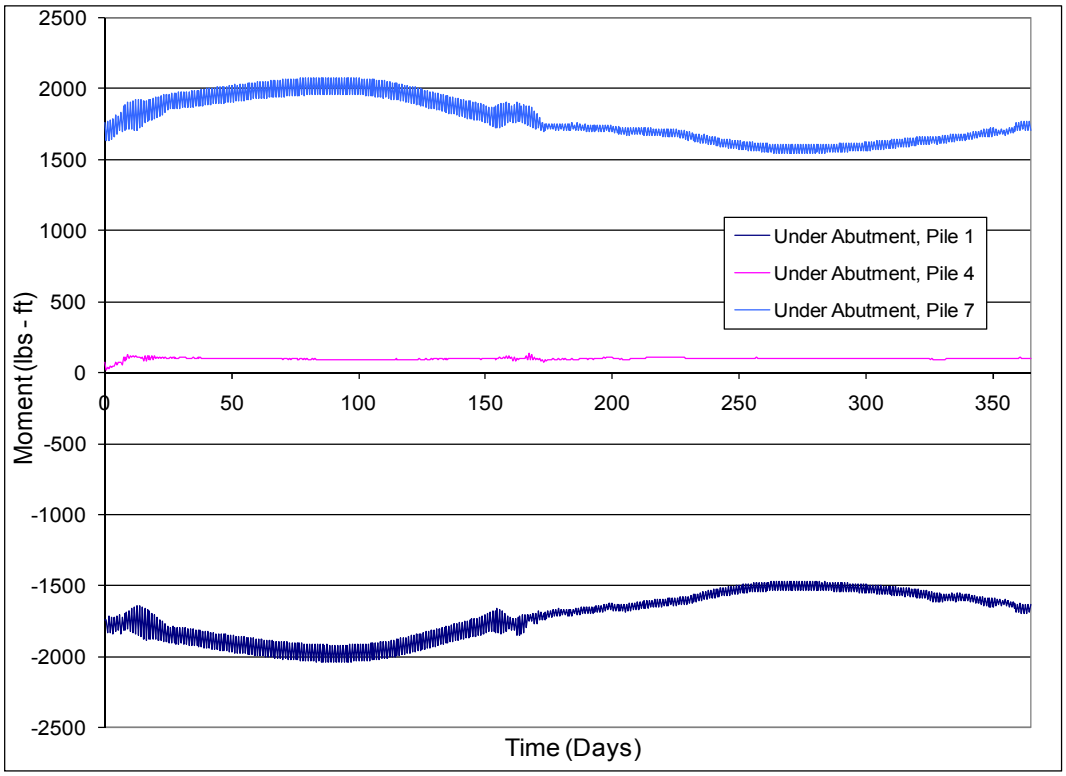

Figure B.11 – Transverse moments in piles under abutment.

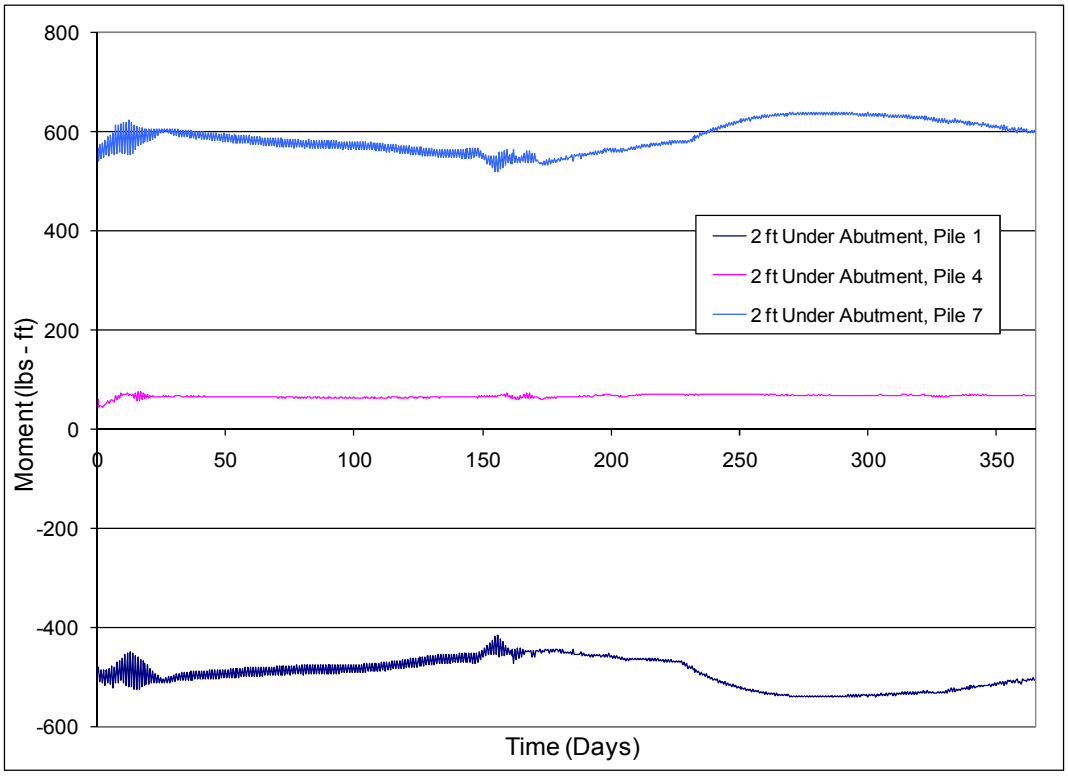

Figure B.12 – Transverse moments in piles 2 ft under abutment.

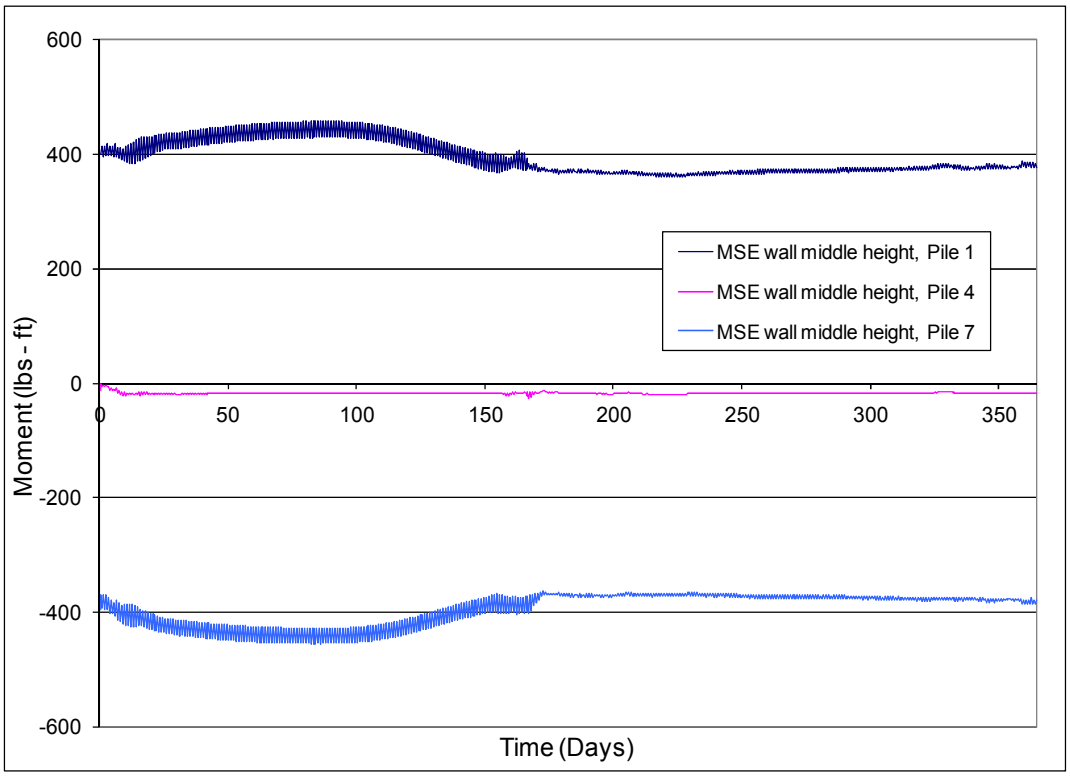

Figure B.13 – Transverse moments in piles at MSE wall middle height.

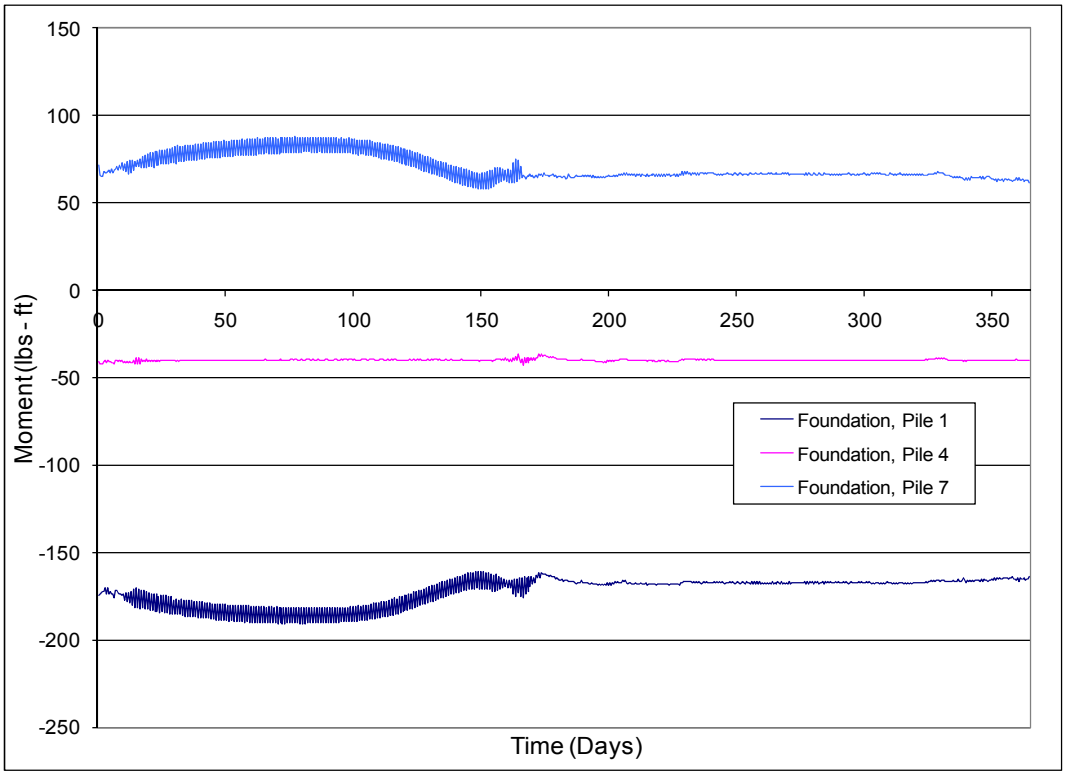

Figure B.14 – Transverse moments in piles at foundation elevation.

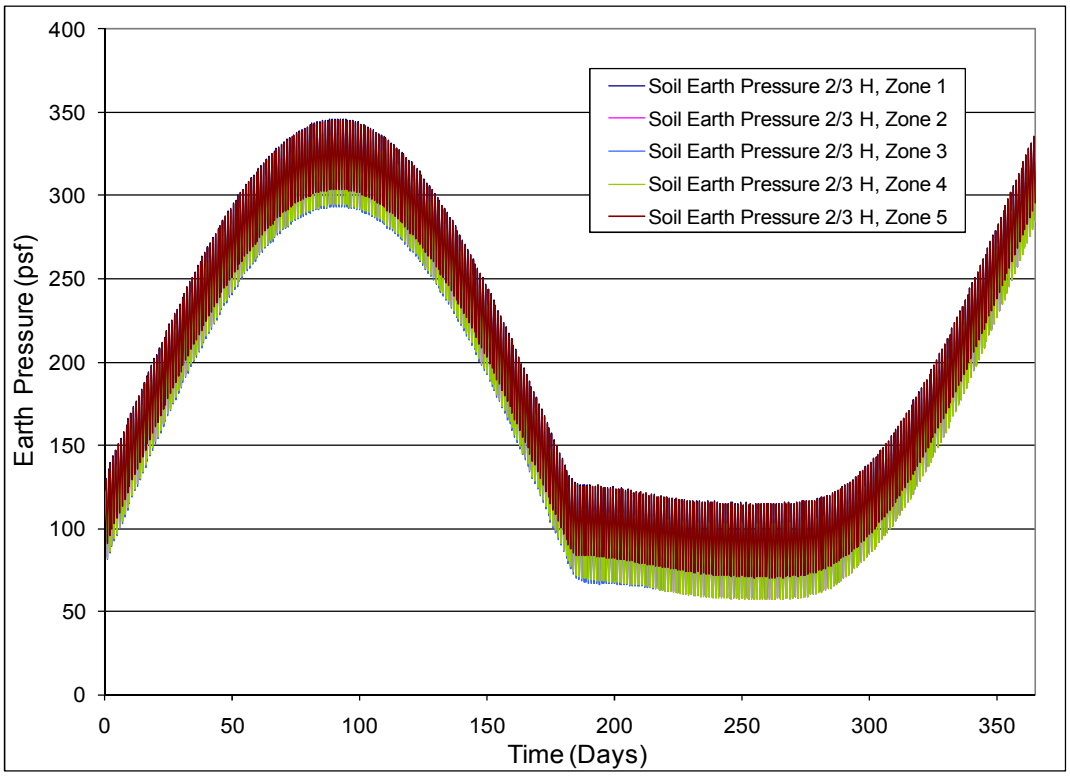

Figure B.15 – Soil earth pressure measured at 2/3 of abutment height.

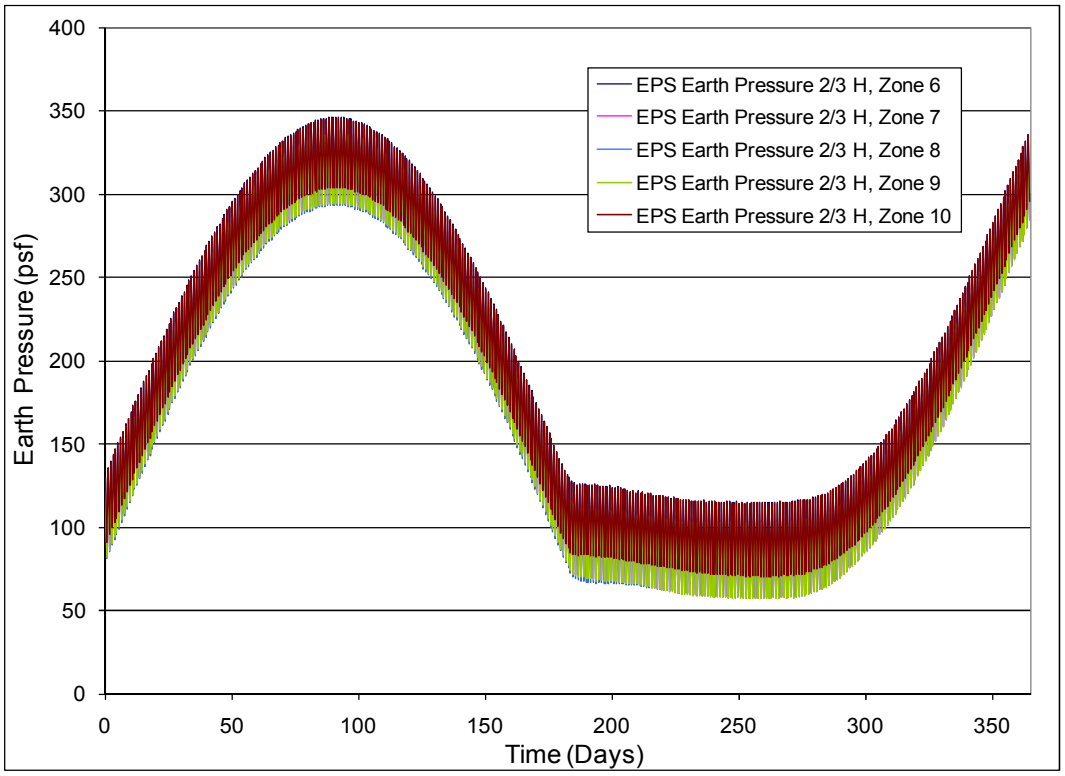

Figure B.16 – EPS earth pressure measured at 2/3 of abutment height.

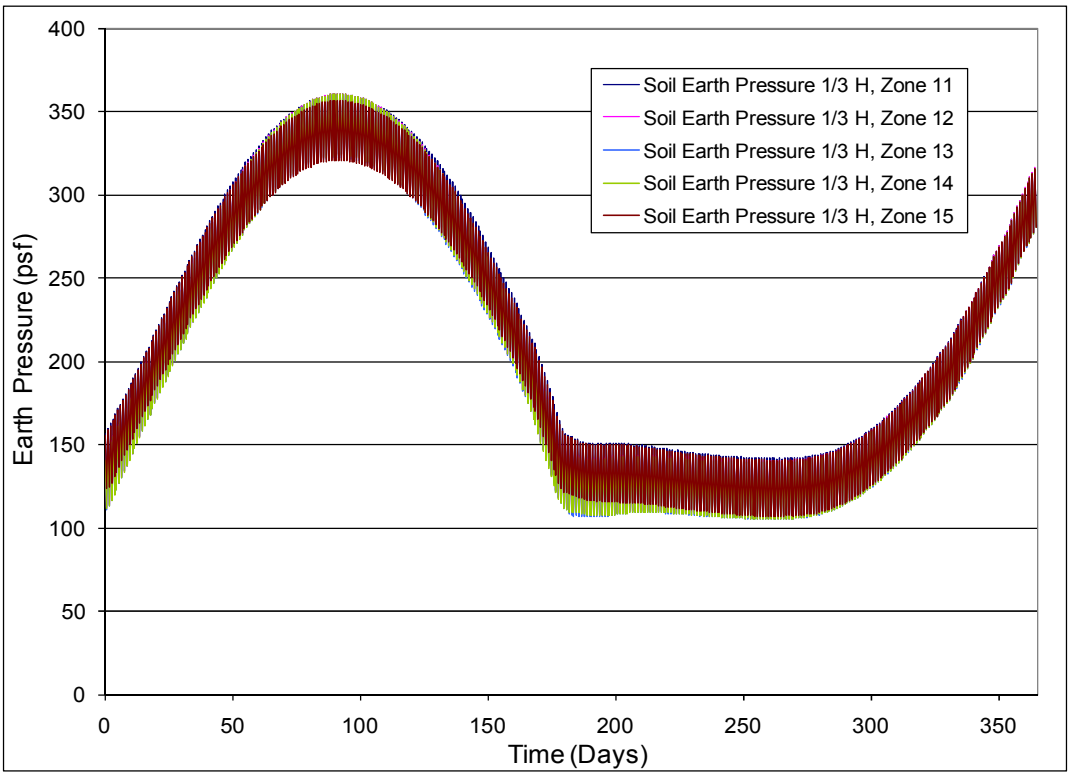

Figure B.17 – Soil earth pressure measured at 1/3 of abutment height.

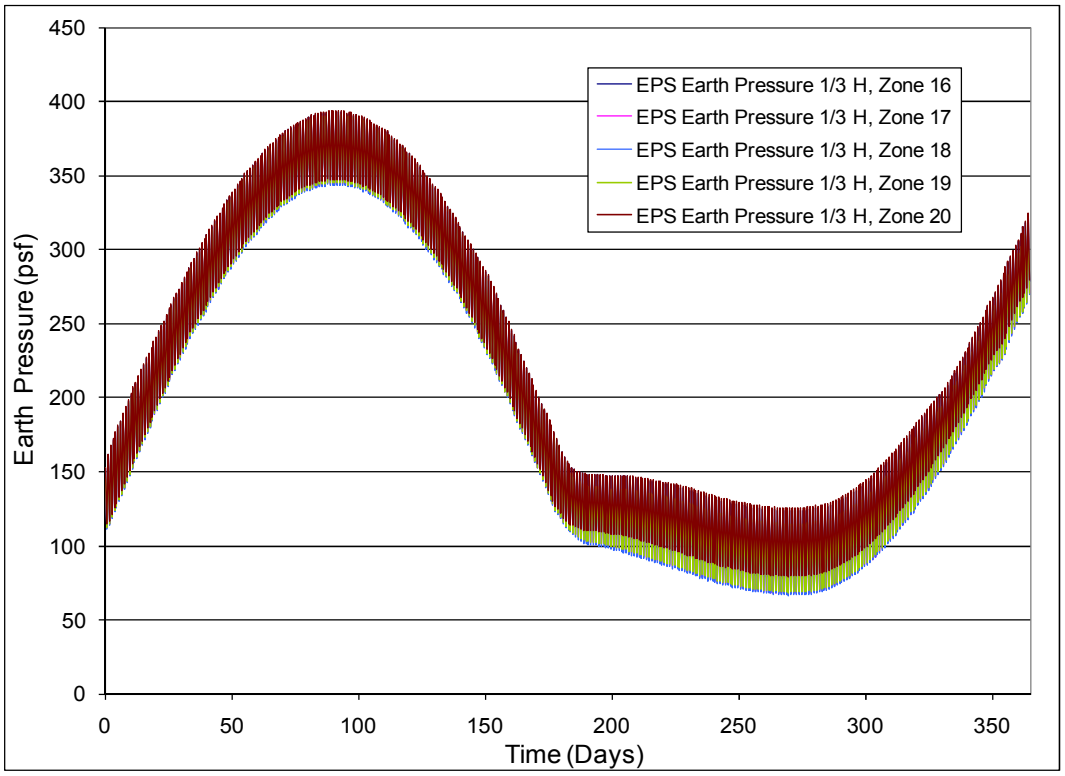

Figure B.18 – EPS earth pressure measured at 1/3 of abutment height.

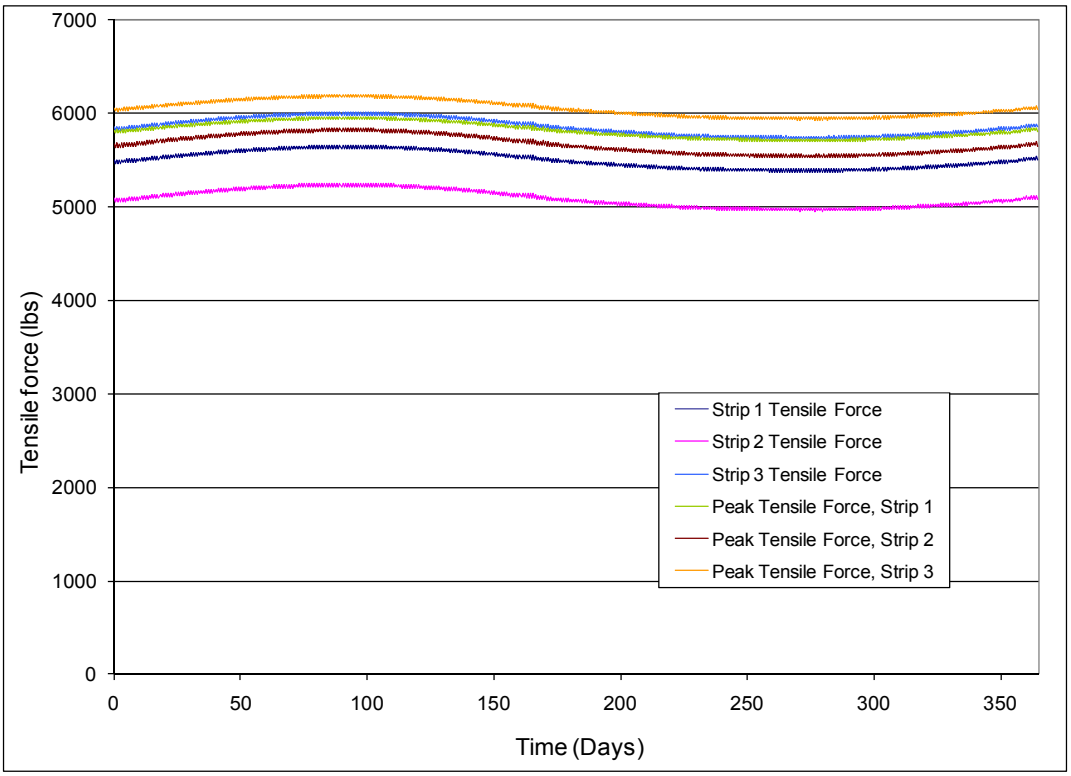

Figure B.19 – Strip tensile force at MSE wall connection and peak value.

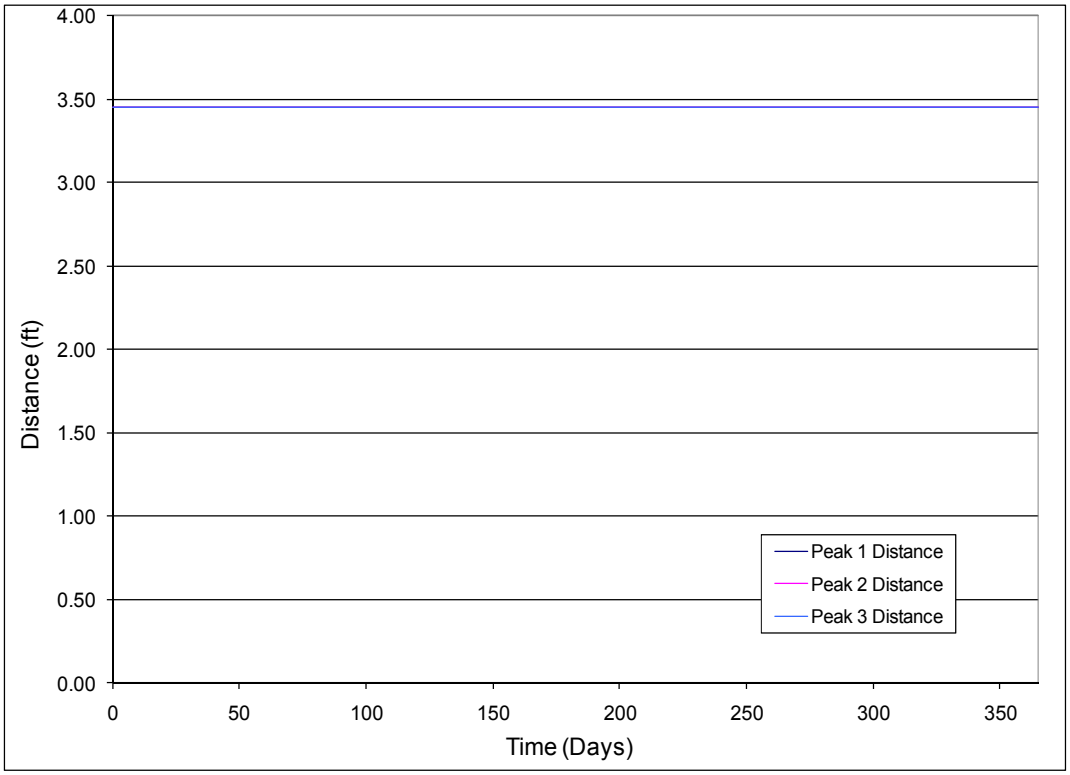

Figure B.20 – Distance measured from MSE wall at which peak values are produced.

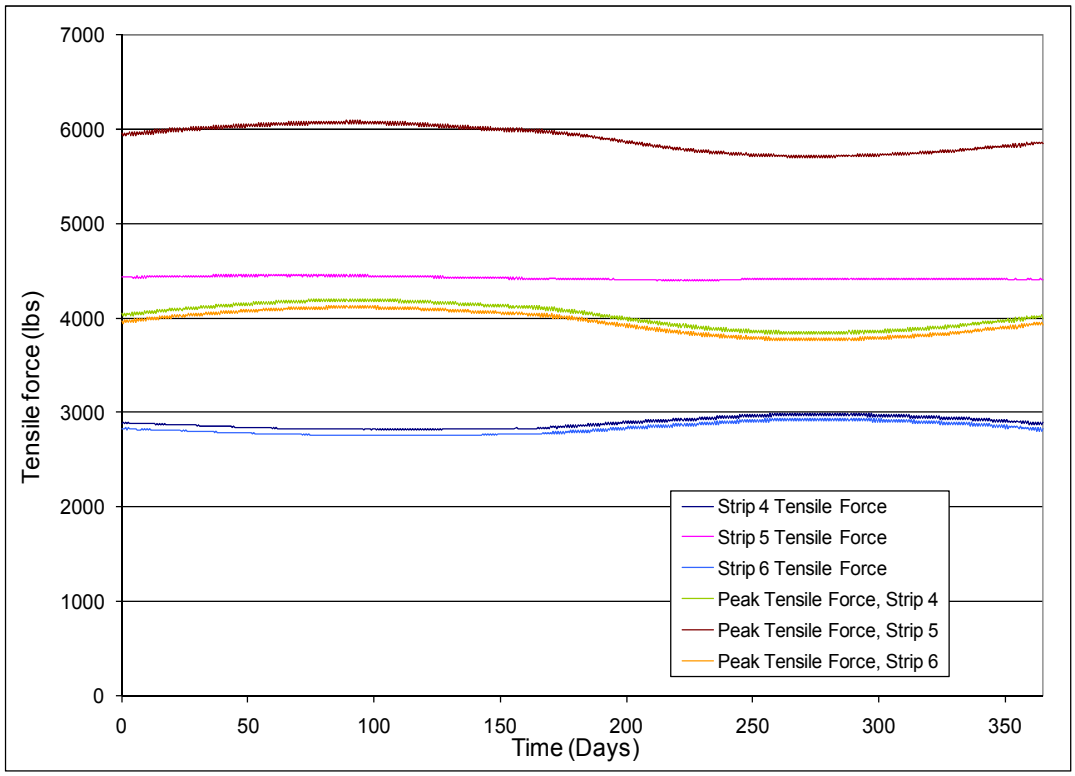

Figure B.21 – Strip tensile force at MSE wall connection and peak value.

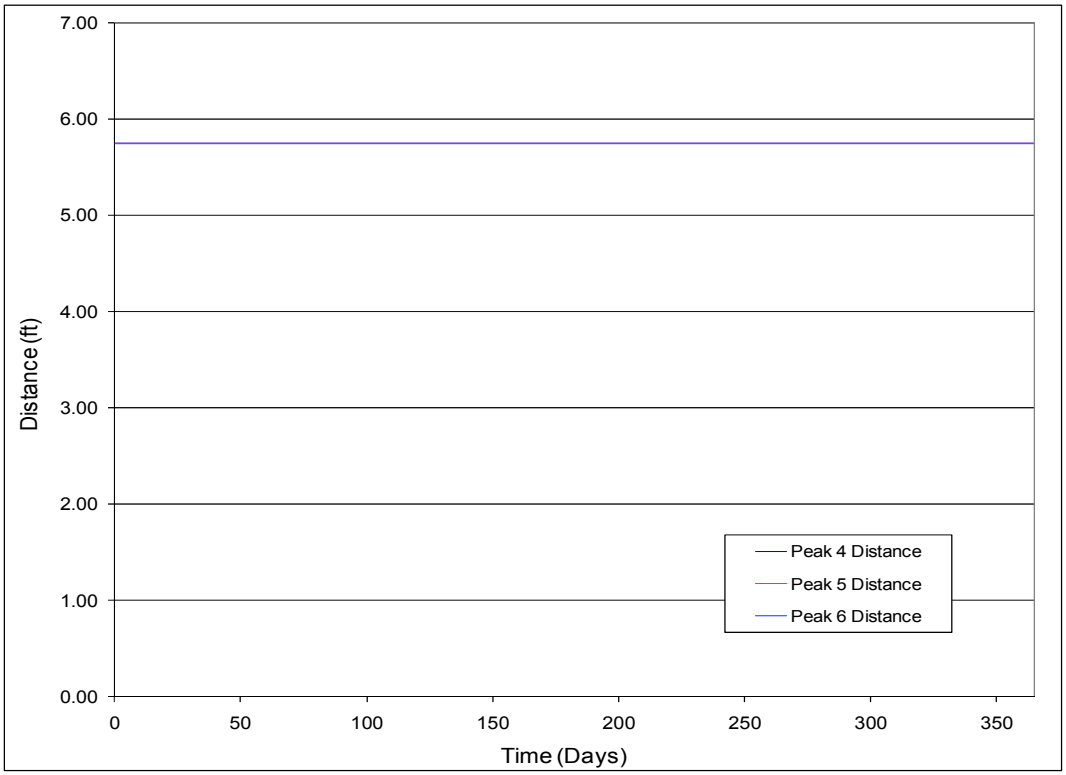

Figure B.22 – Distance measured from MSE wall at which peak values are produced.

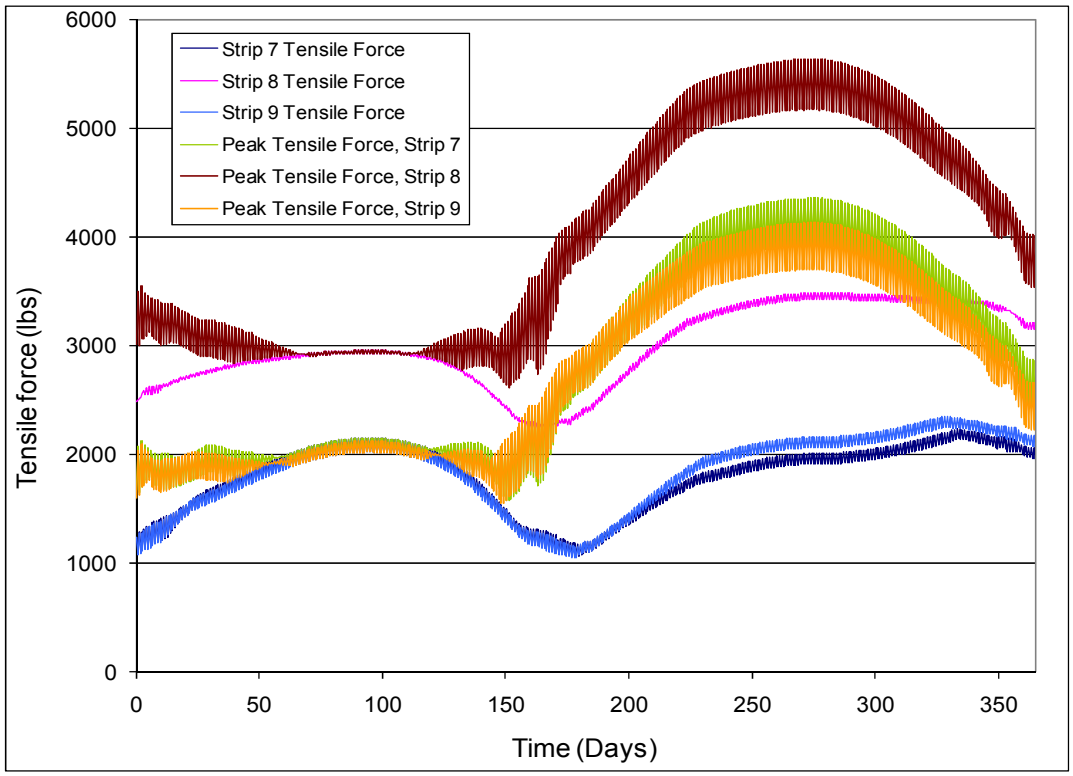

Figure B.23 – Strip tensile force at MSE wall connection and peak value.

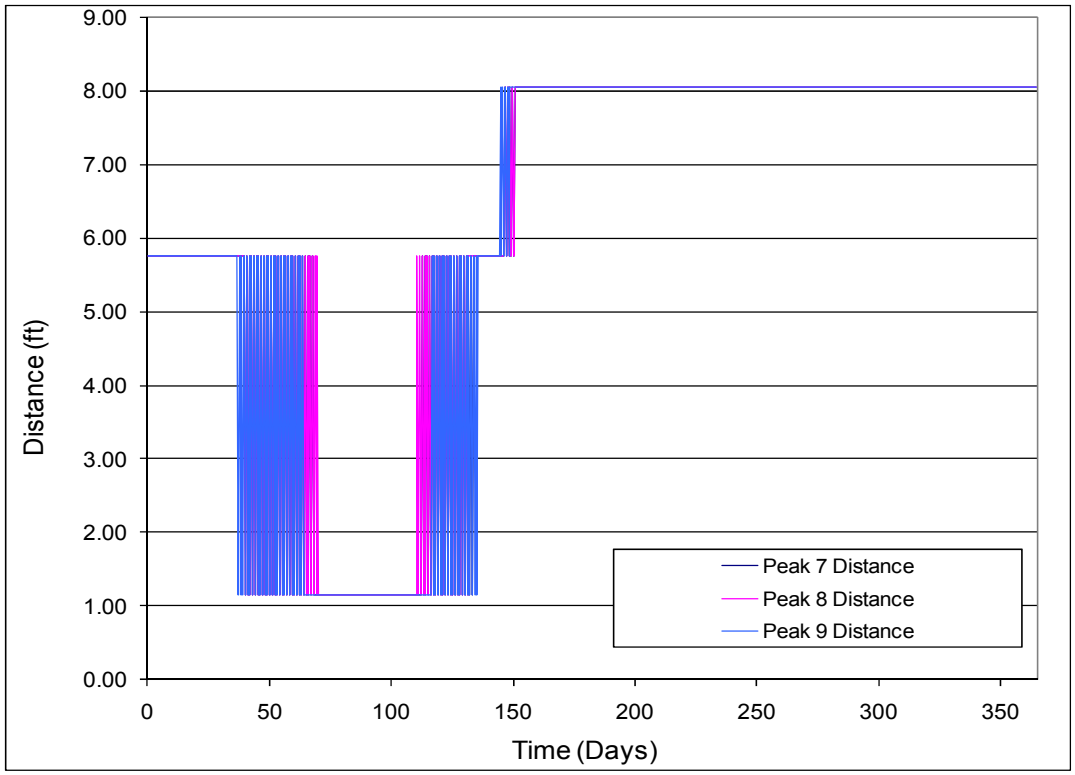

Figure B.24 – Distance measured from MSE wall at which peak values are produced.

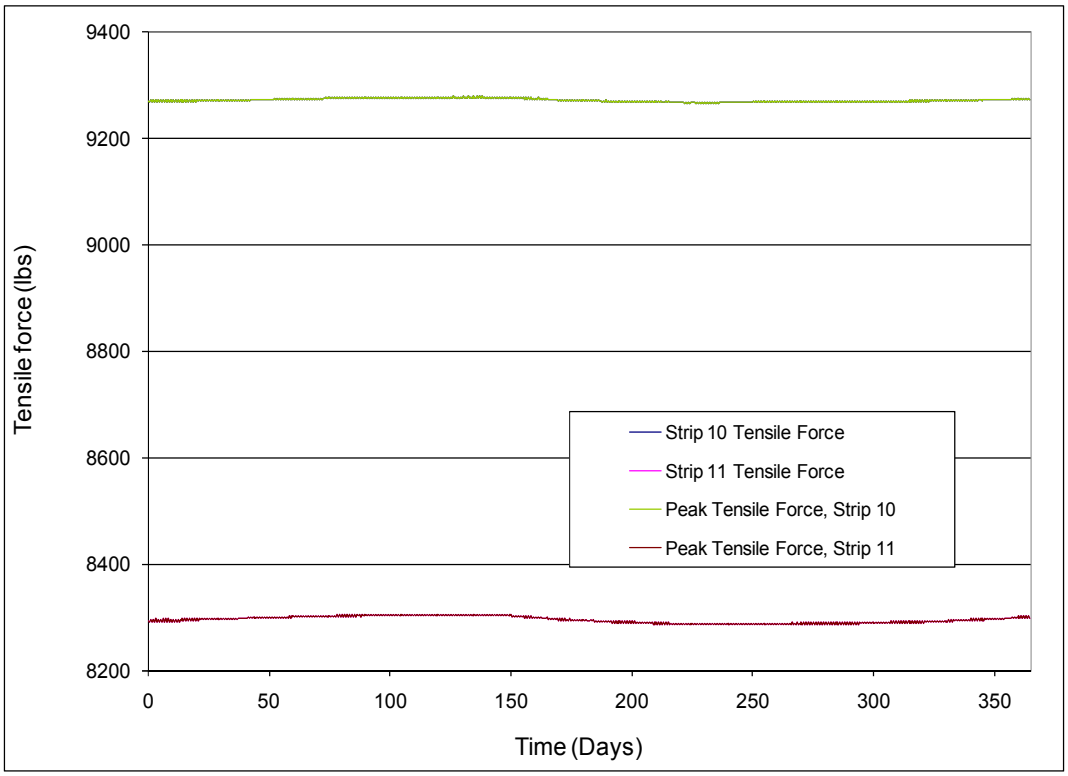

Figure B.25 – Strip tensile force at MSE wall connection and peak value.

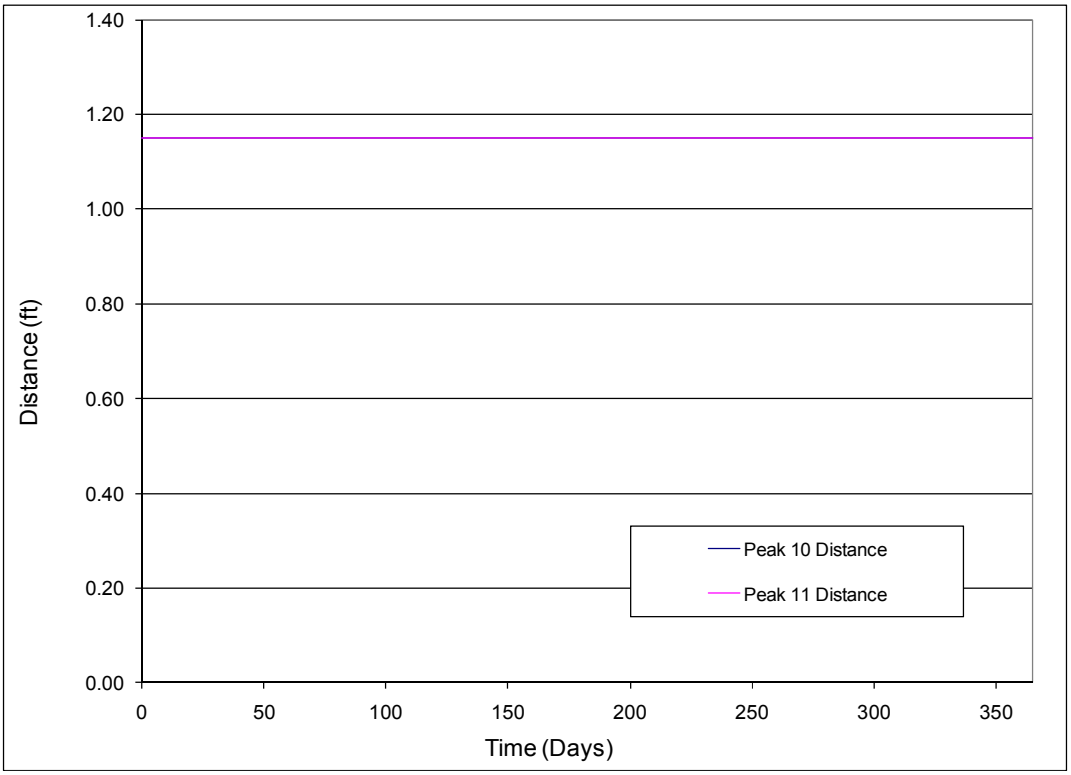

Figure B.26 – Distance measured from MSE wall at which peak values are produced.

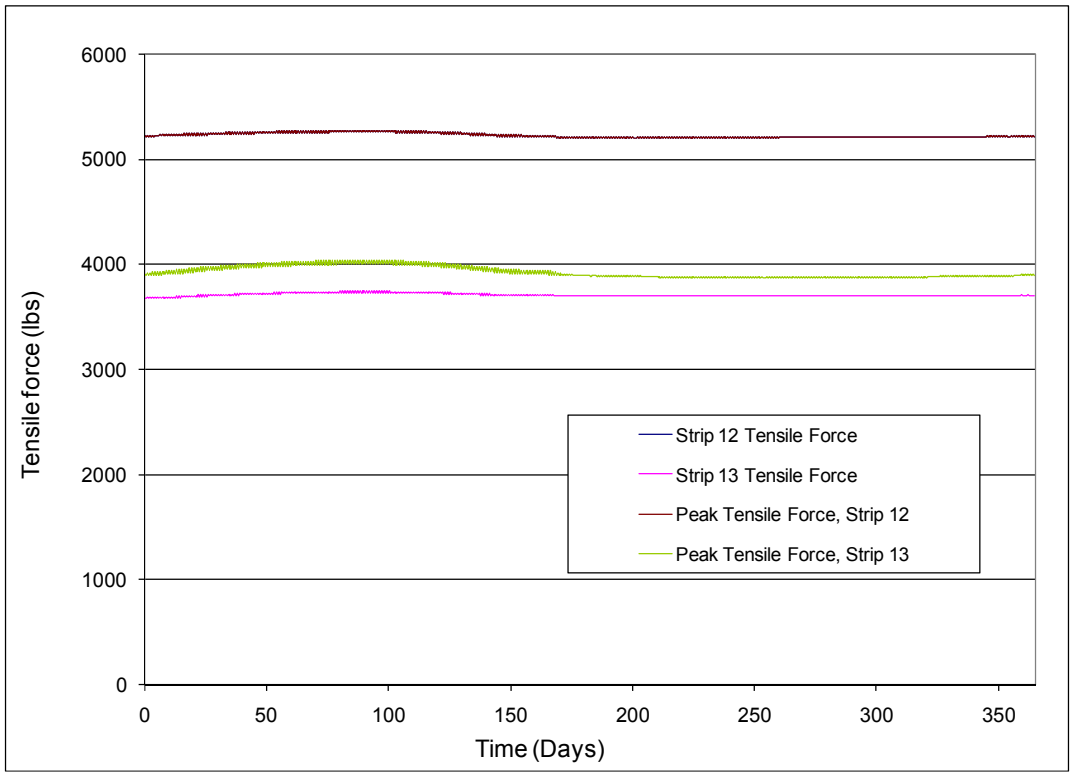

Figure B.27 – Strip tensile force at MSE wall connection and peak value.

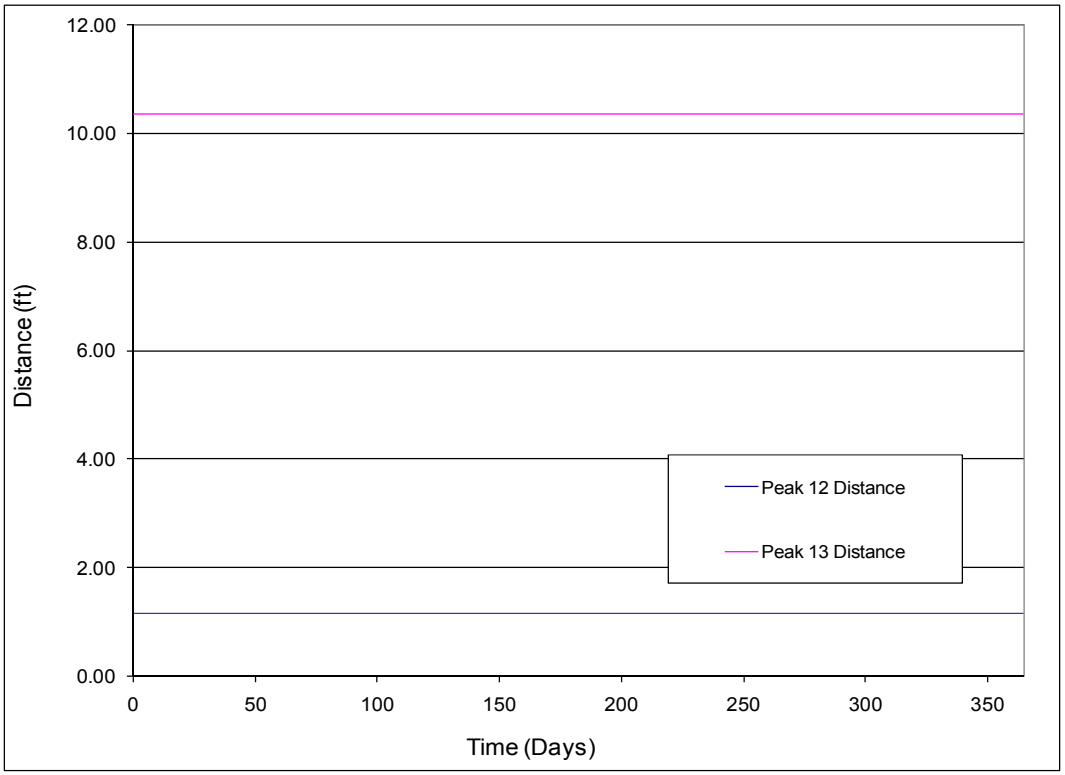

Figure B.28 – Distance measured from MSE wall at which peak values are produced.

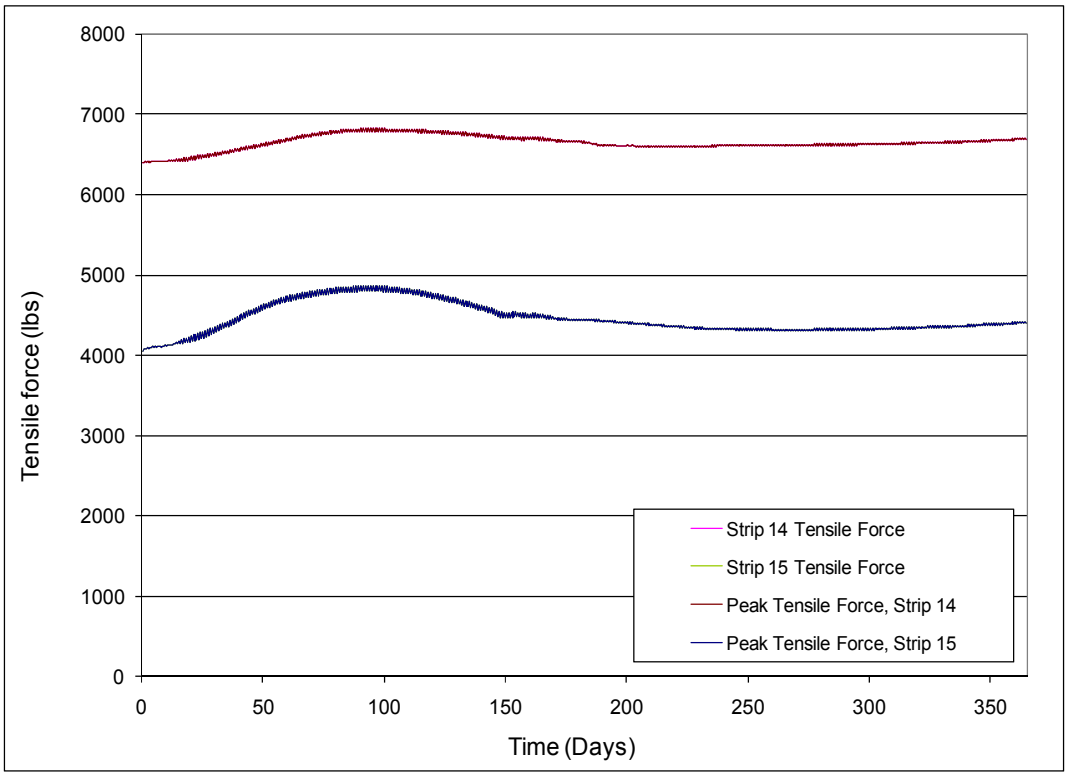

Figure B.29 – Strip tensile force at MSE wall connection and peak value.

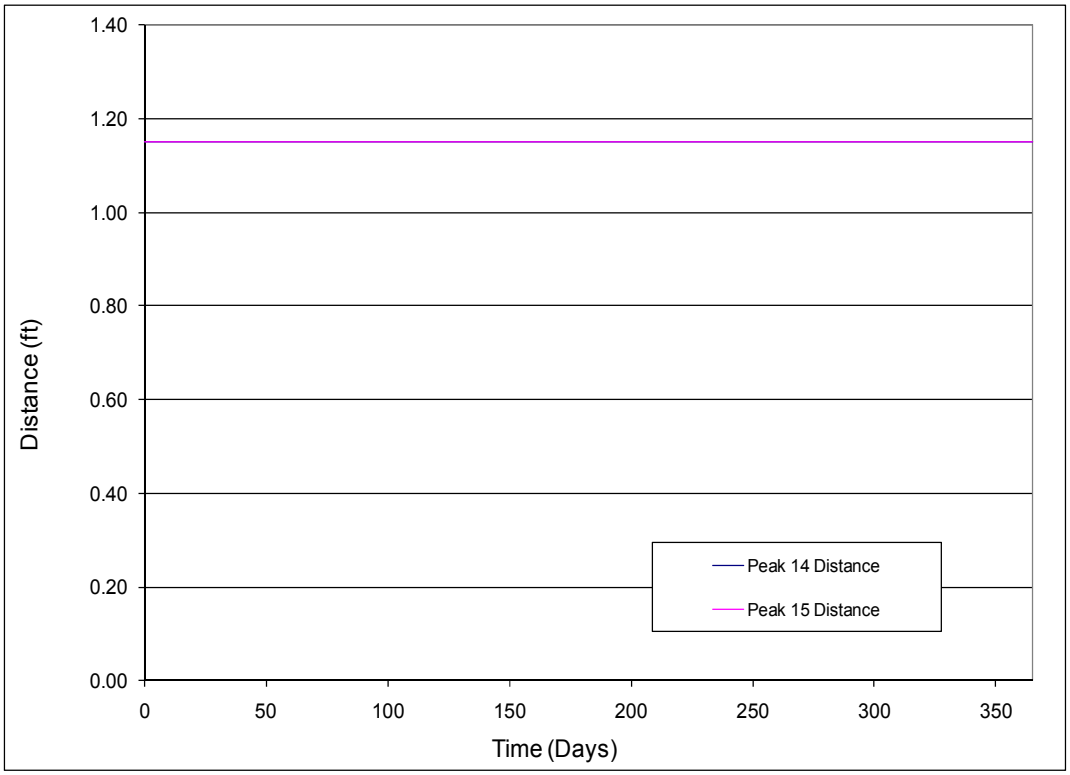

Figure B.30 – Distance measured from MSE wall at which peak values are produced.

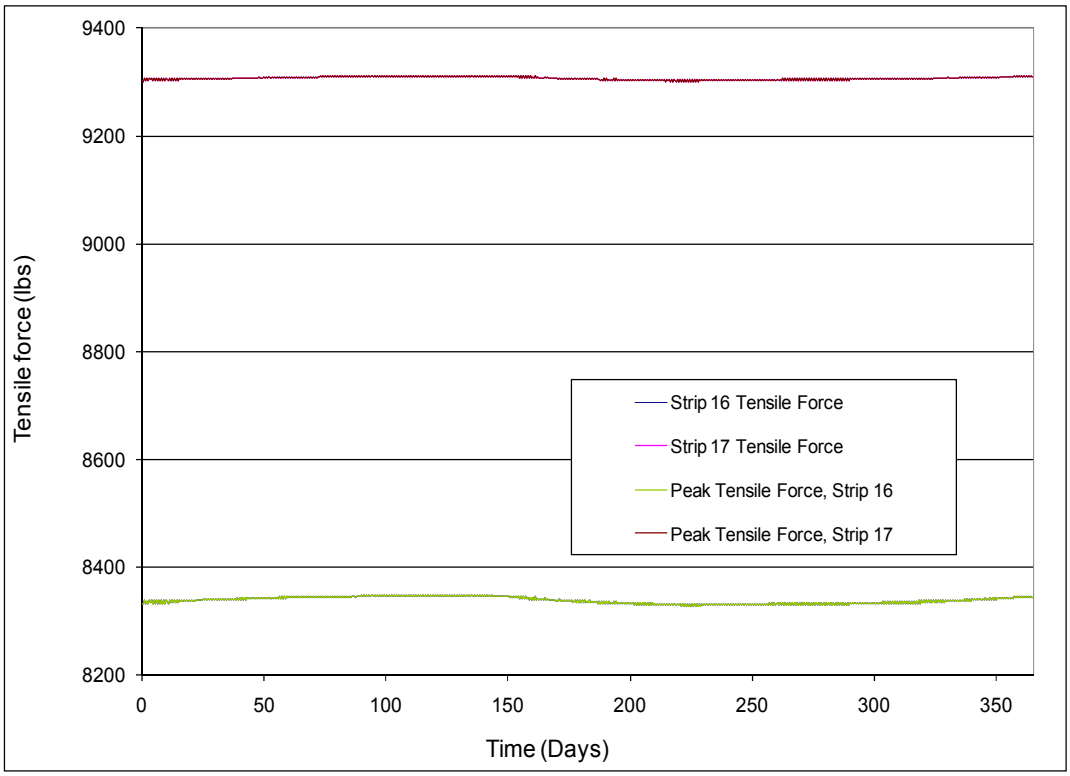

Figure B.31 – Strip tensile force at MSE wall connection and peak value.

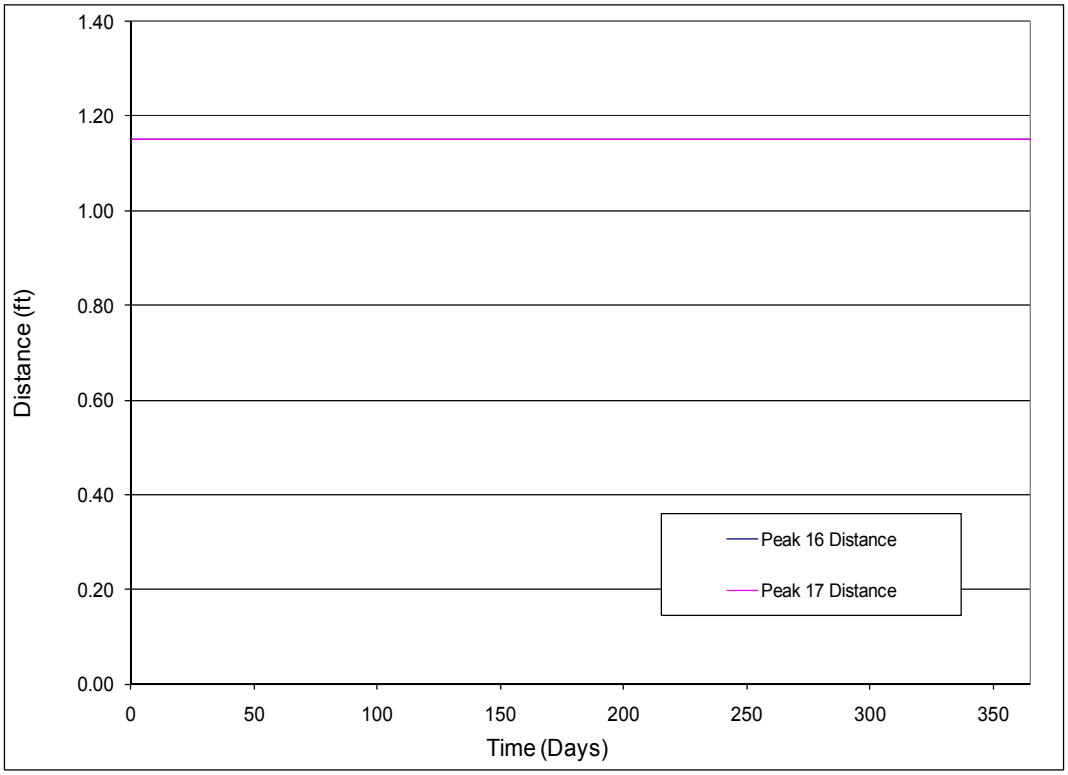

Figure B.32 – Distance measured from MSE wall at which peak values are produced.

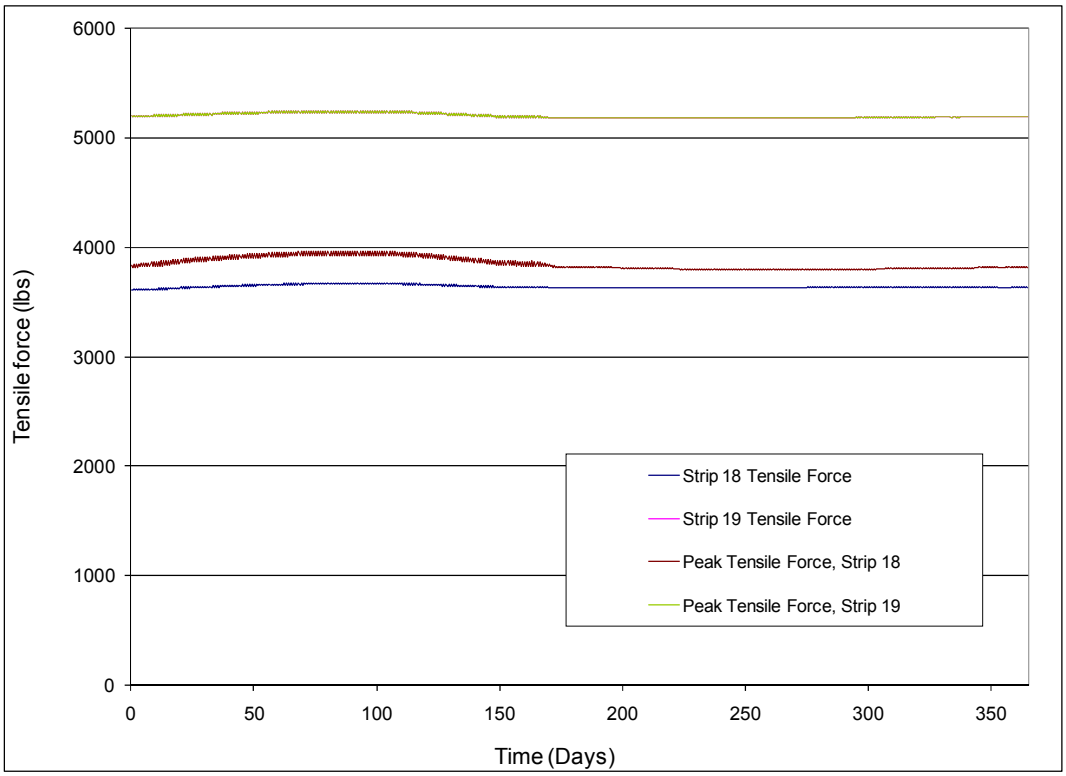

Figure B.33 – Strip tensile force at MSE wall connection and peak value.

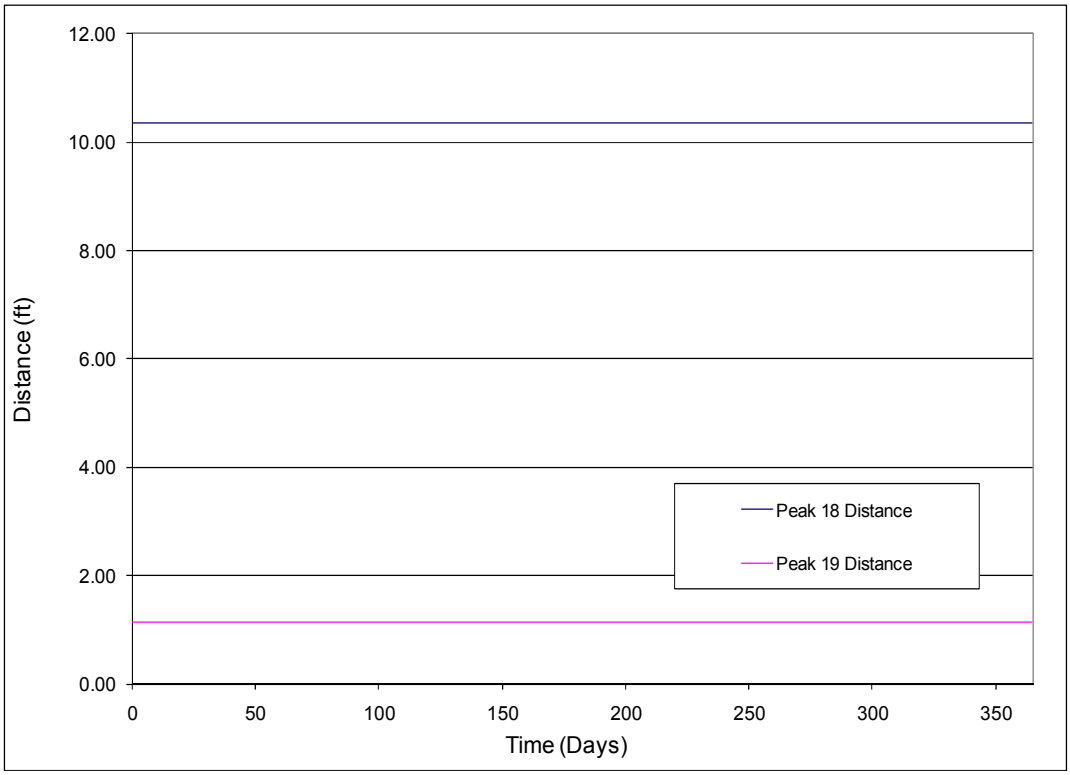

Figure B.34 – Distance measured from MSE wall at which peak values are produced.

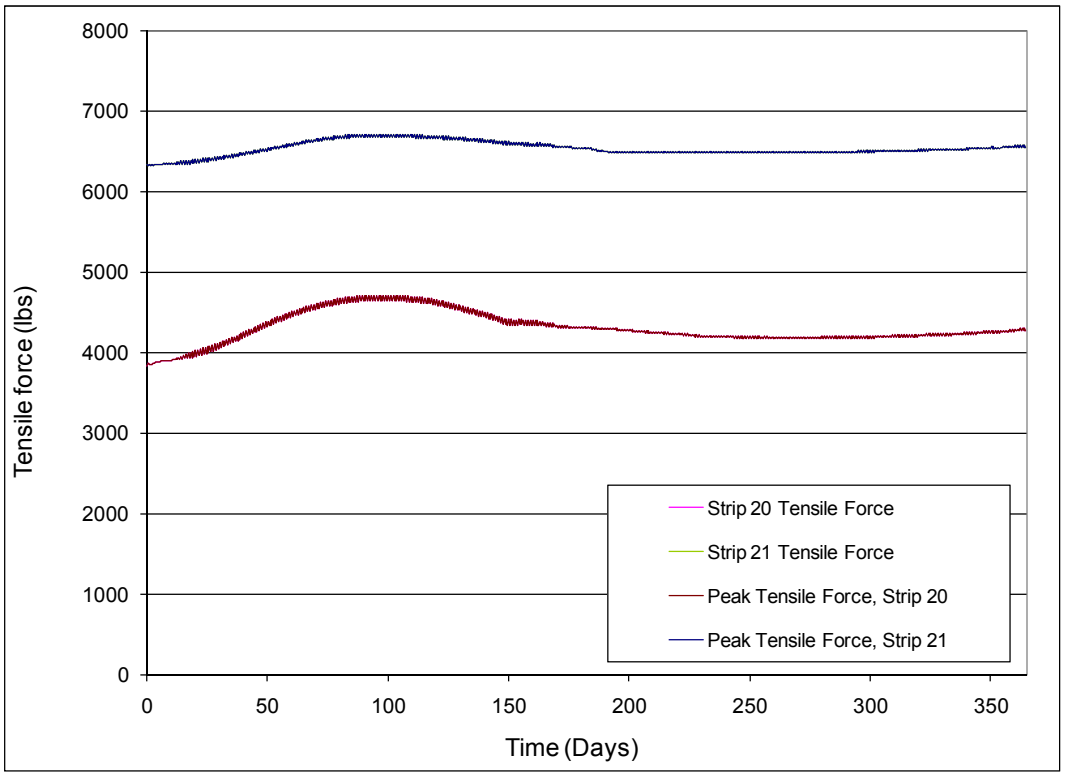

Figure B.35 – Strip tensile force at MSE wall connection and peak value.

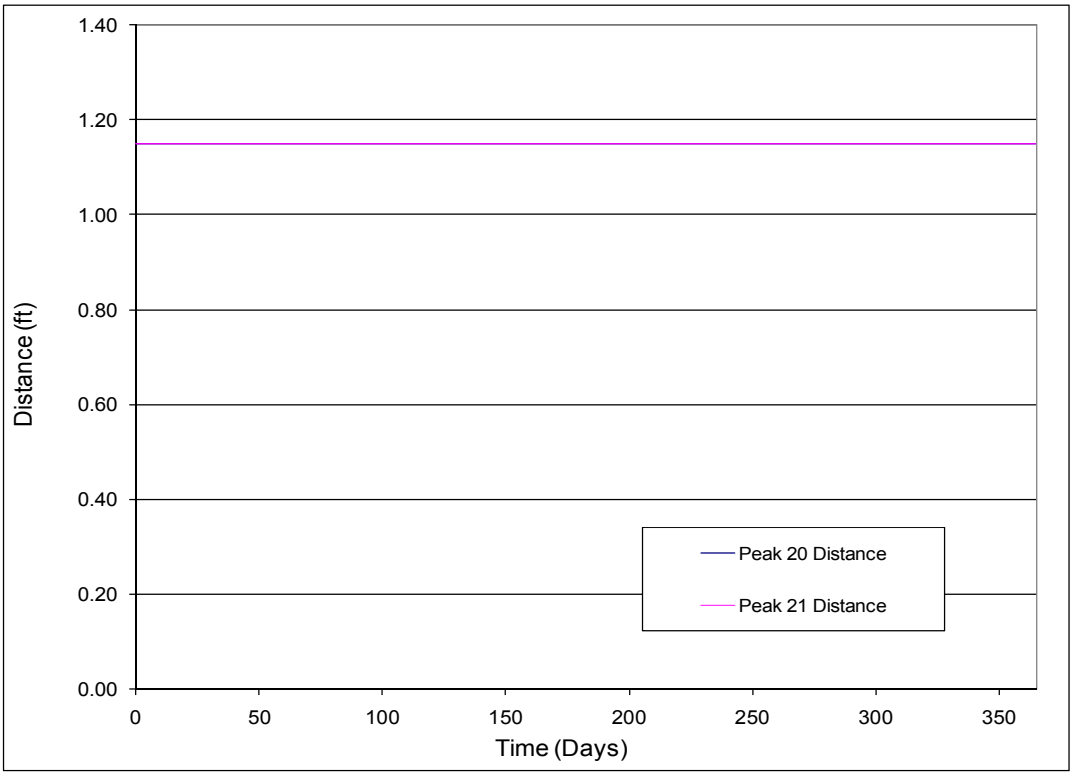

Figure B.36 – Distance measured from MSE wall at which peak values are produced.

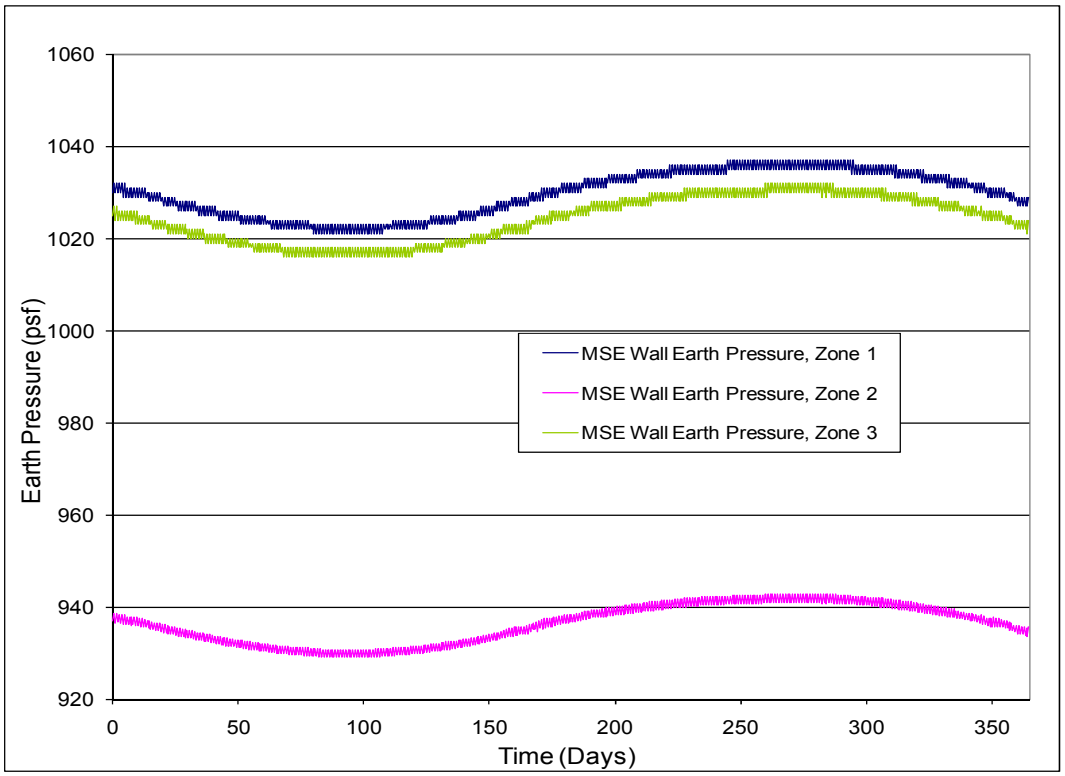

Figure B.37 – Earth pressure behind MSE wall.

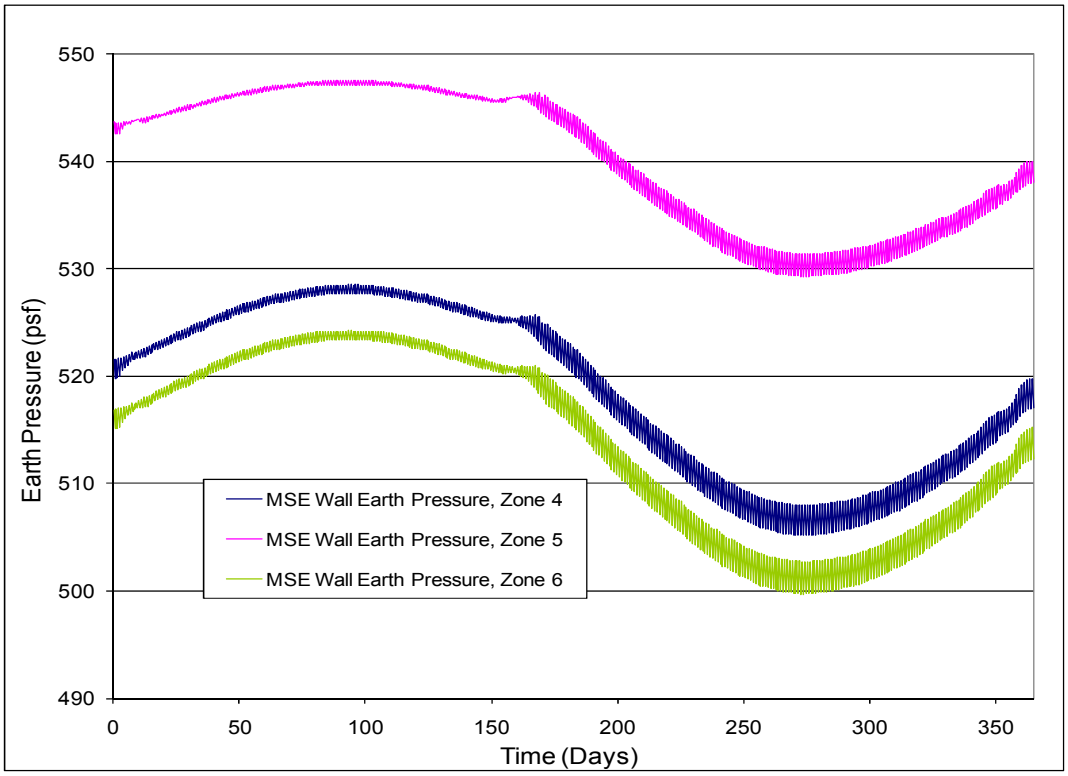

Figure B.38 – Earth pressure behind MSE wall.

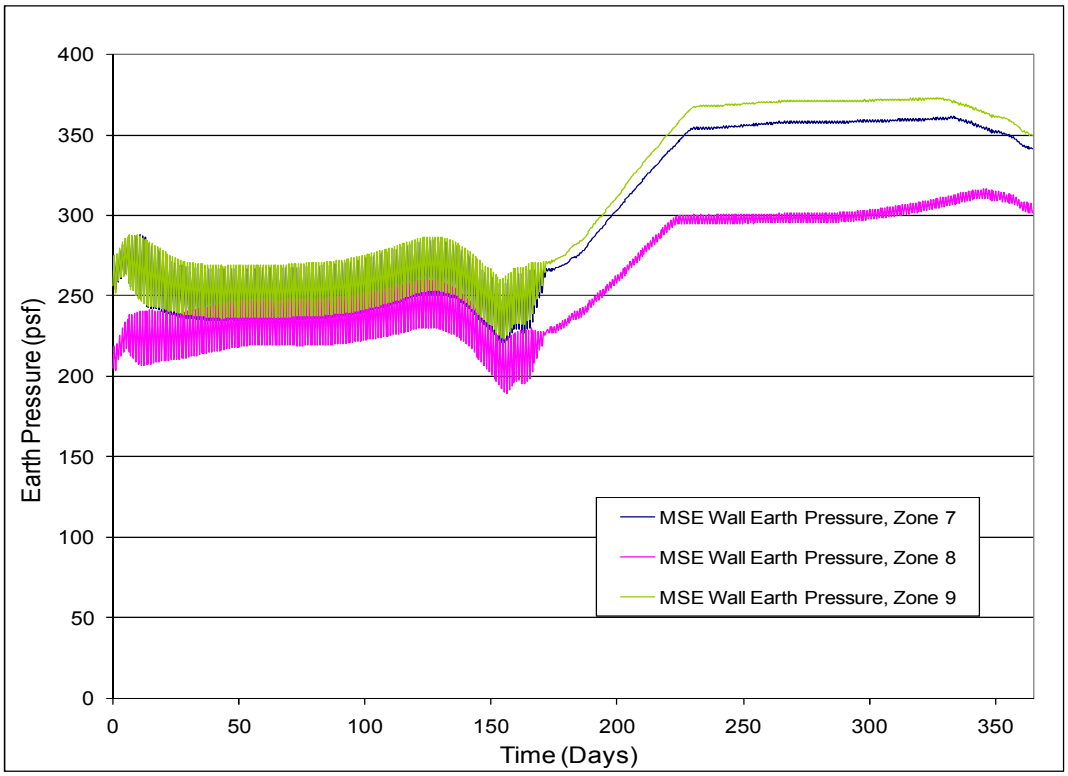

Figure B.39 – Earth pressure behind MSE wall.

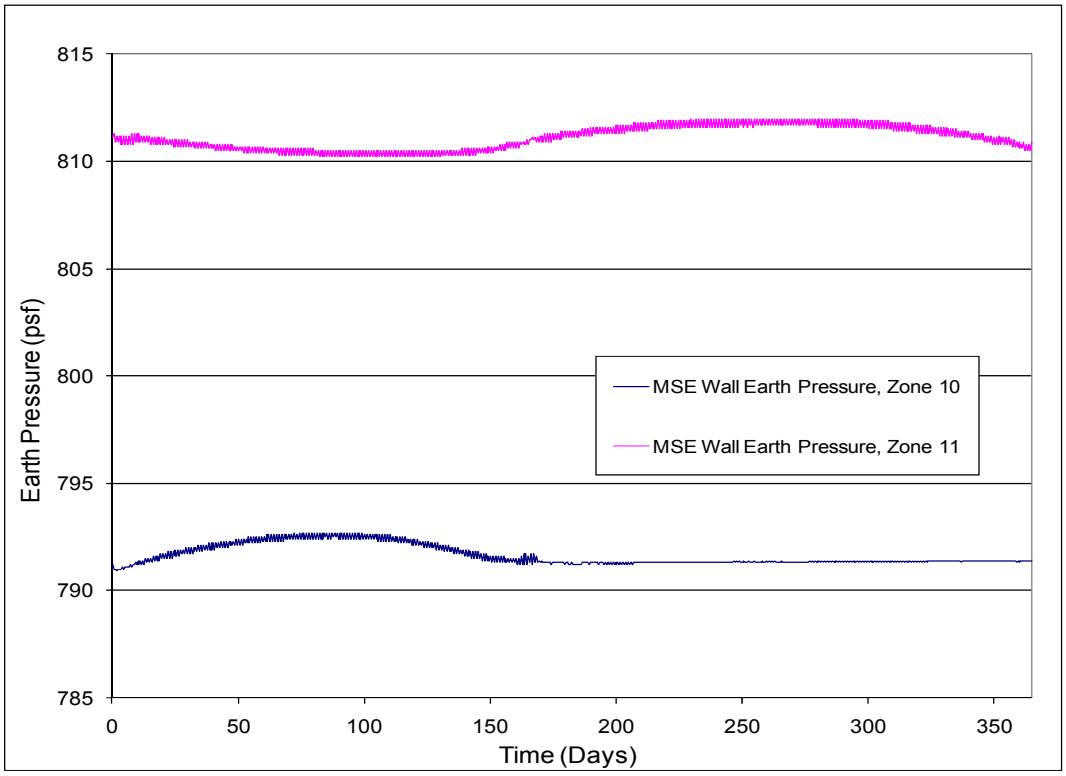

Figure B.40 – Earth pressure behind MSE wall.

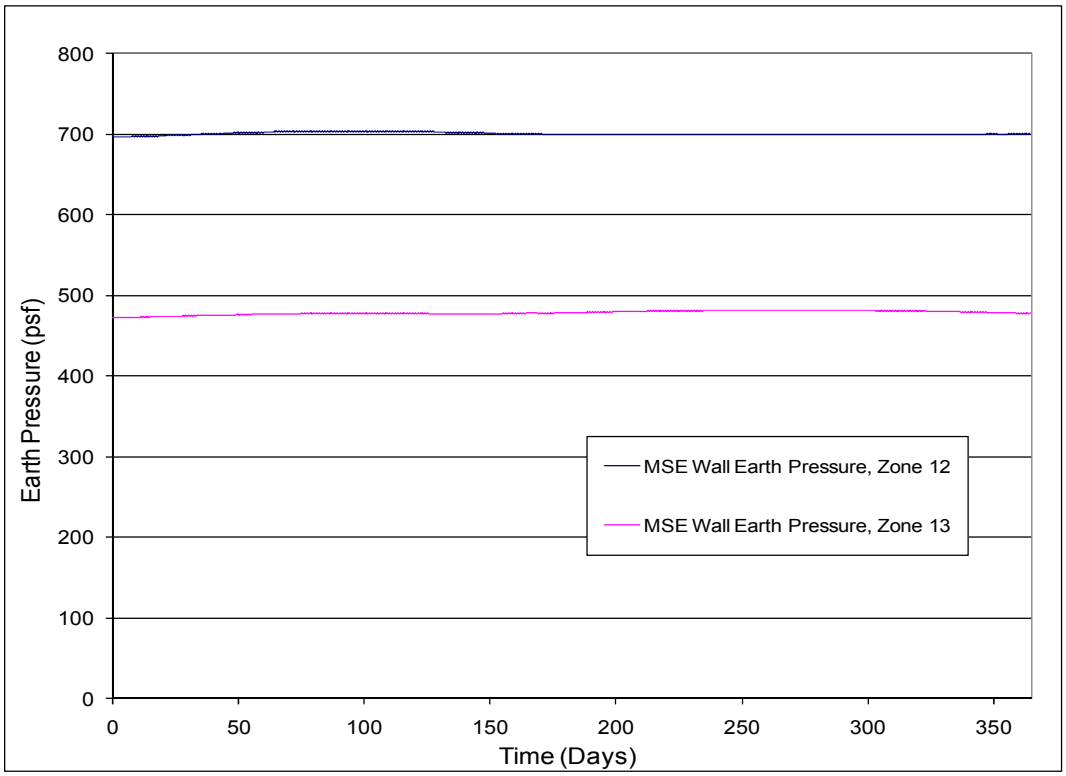

Figure B.41 – Earth pressure behind MSE wall.

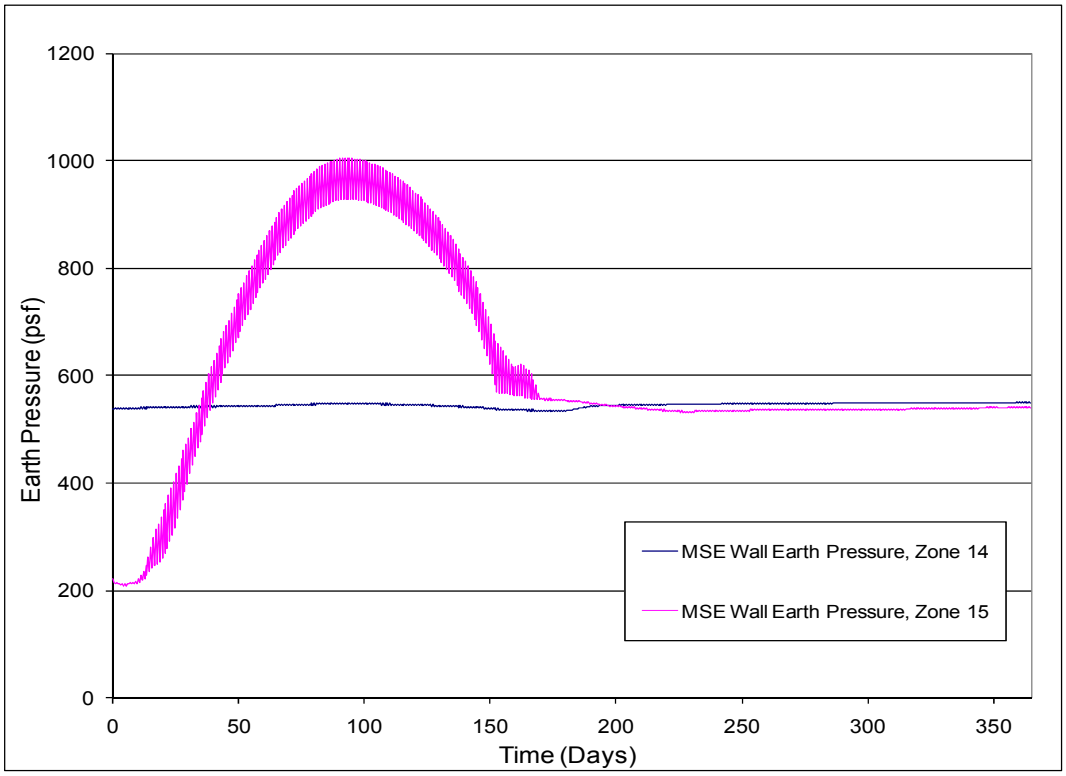

Figure B.42 – Earth pressure behind MSE wall.

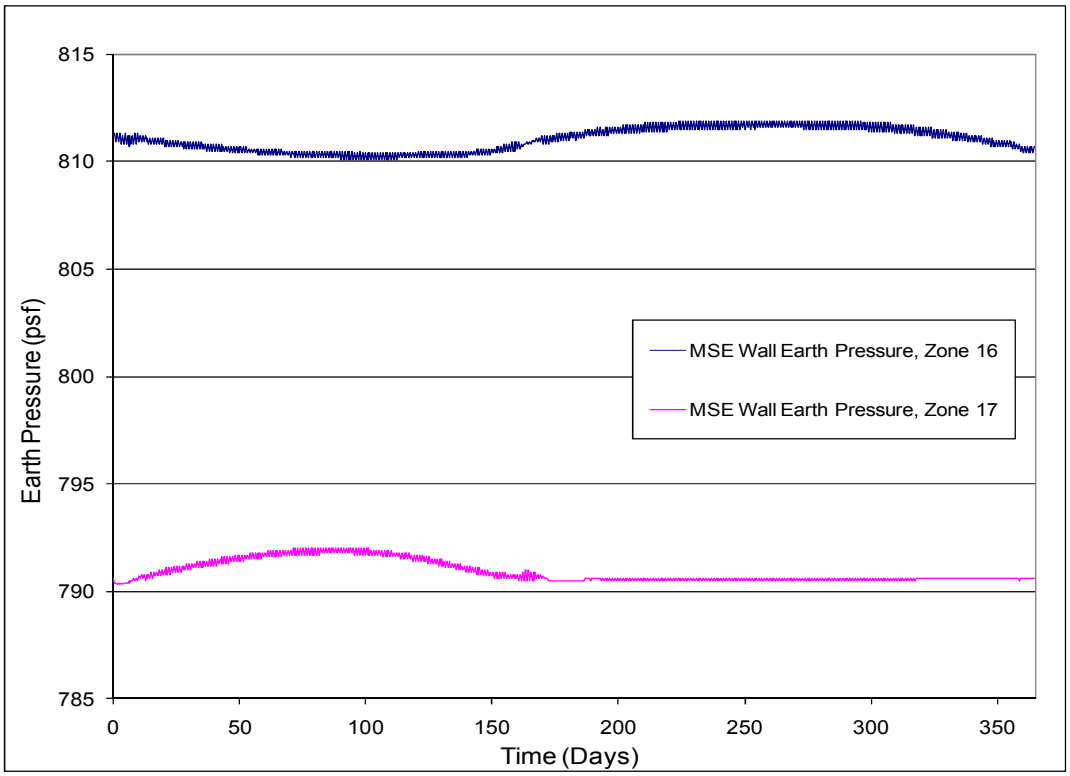

Figure B.43 – Earth pressure behind MSE wall.

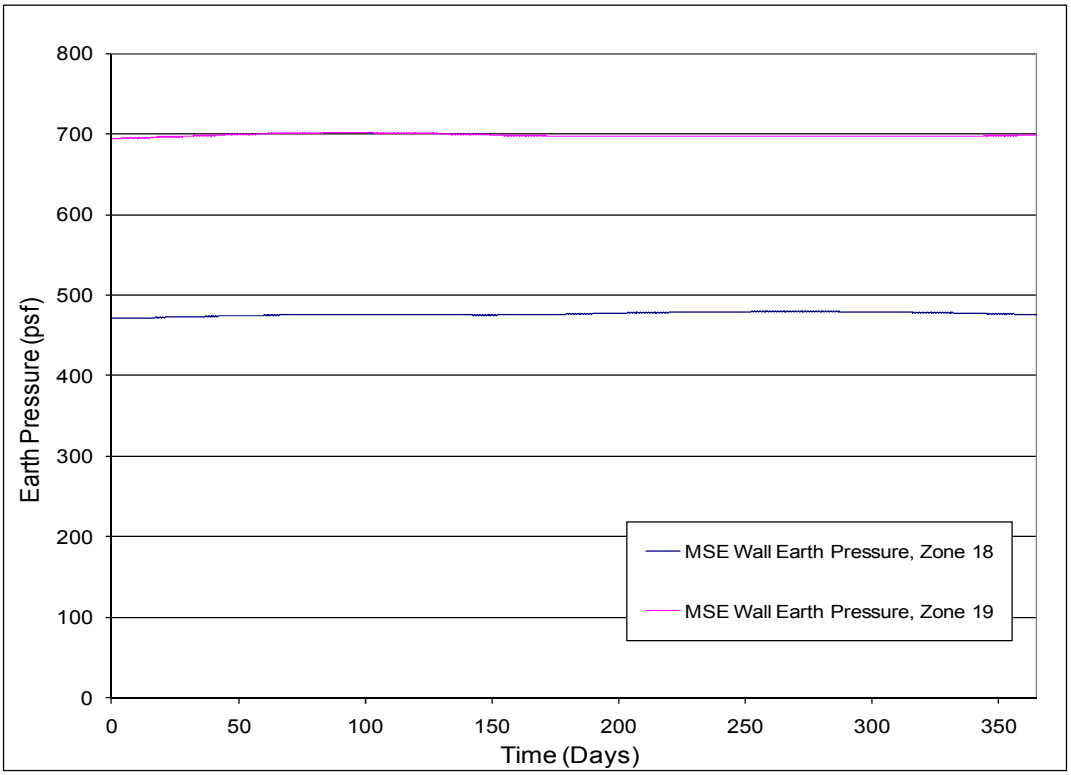

Figure B.44 – Earth pressure behind MSE wall.

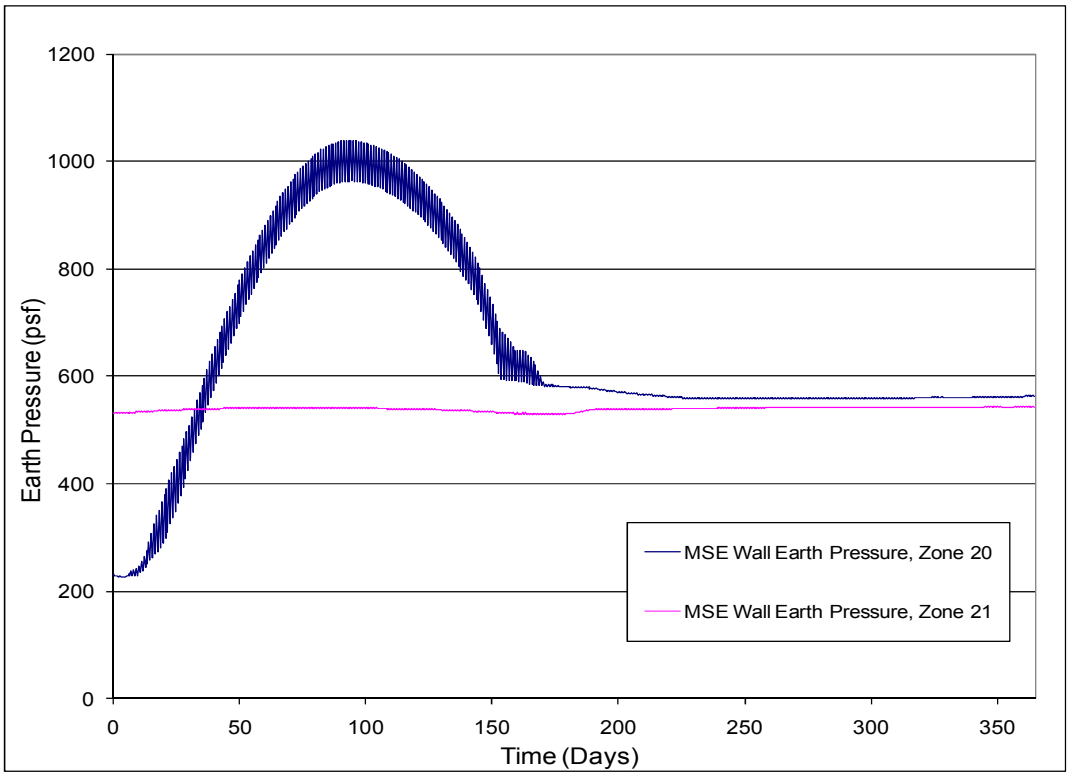

Figure B.45 – Earth pressure behind MSE wall.

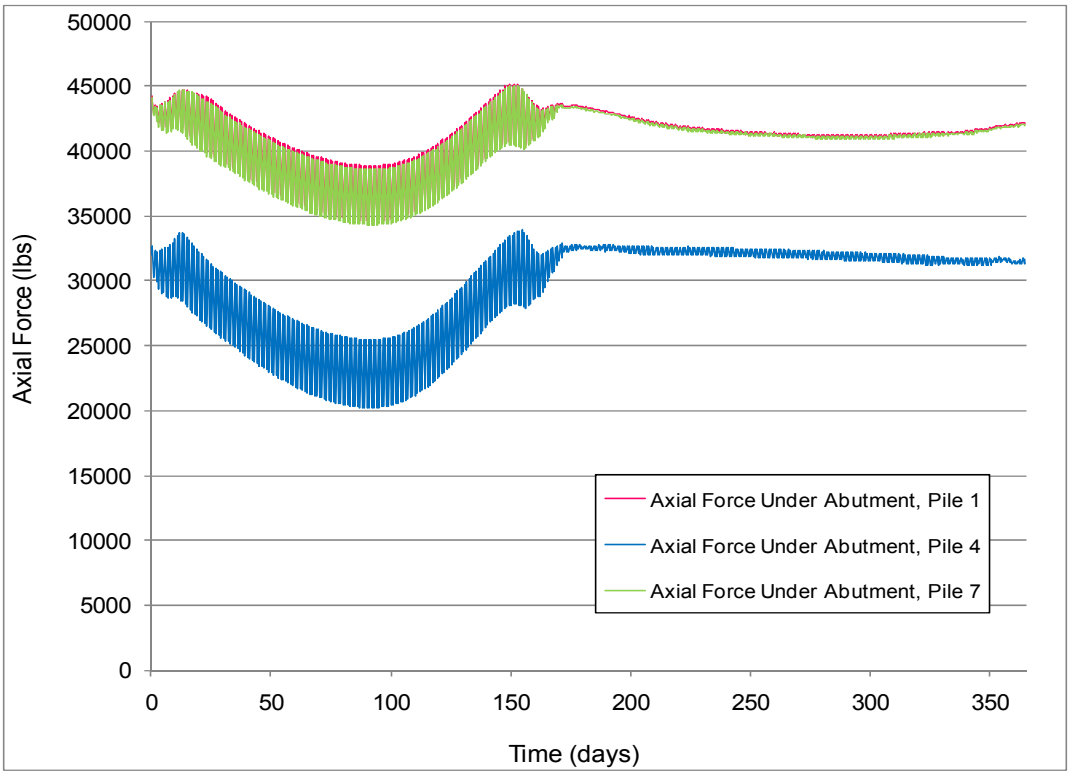

Figure B.46 – Axial force in piles under the abutment.

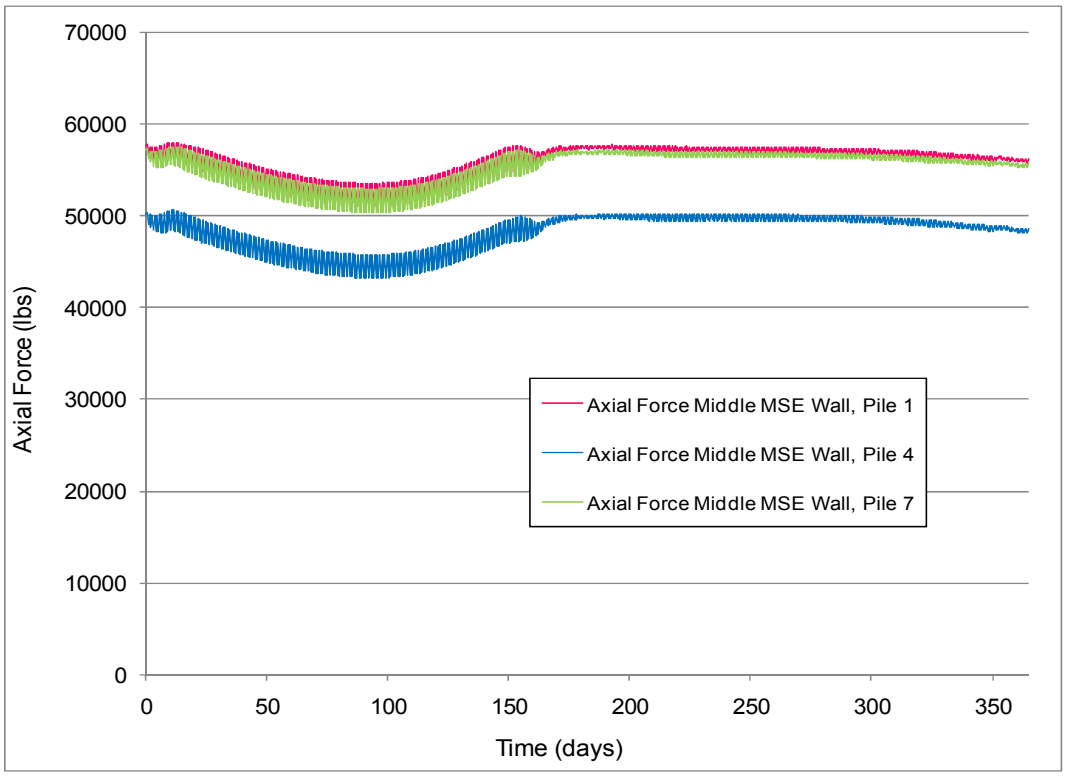

Figure B.47 – Axial force in piles at MSE middle height.

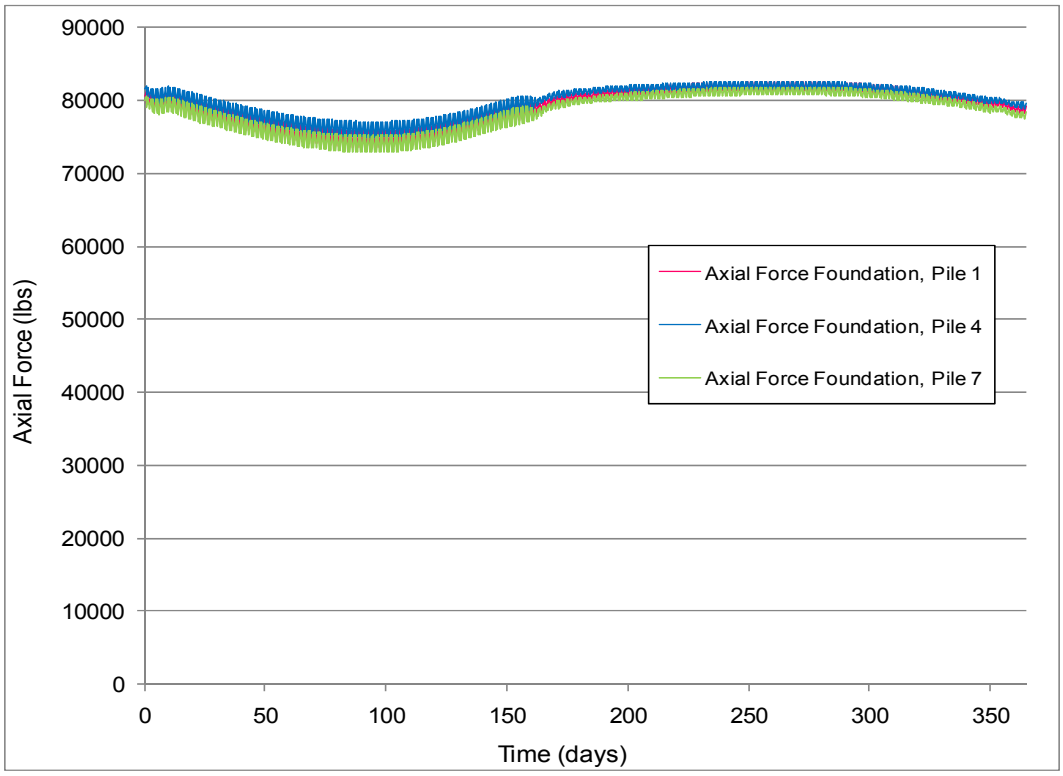

Figure B.48 – Axial force in piles at foundation elevation.

APPENDIX C

SINGLE MONITORING OUTPUT POINT LOCATIONS

C.1 Displacement

Displacements were recorded in longitudinal and transverse directions (x and y directions in Figure C.1), at three elevations and at three positions along the bridge.

The selected elevations for measuring displacements were Top, Cap, and Bottom, as shown in Figure C.1. Thus, rotation of the cap and upper section of the abutment were captured. Along the abutment direction, displacements were recorded at left, middle, and right positions. Thus, horizontal rotation of the bridge abutment and cap were captured.

Altogether, displacements were recorded at 18 positions in the bridge, 9 in the x direction and 9 in y direction.

C.2 Shear Forces in Piles and Dowels

Shear forces were recorded in the longitudinal and transverse directions, i.e., x direction and y direction, respectively (Figure C.2).

Shear forces were obtained from piles 1, 2, 4, 6, and 7, right under the abutment, and they were recorded in both directions. In addition, shear forces in both directions were obtained from dowels that best aligned with those piles, as shown in Figure C.2.

Therefore, shear forces were recorded at 20 positions, 10 in the longitudinal direction (5 dowels and 5 piles) and 10 in the transverse direction (5 dowels and 5 piles).

C.3 Moments in Piles

Moments in piles were recorded in the longitudinal and transverse directions, as shown in Figure C.3.

Moments were monitored in piles 1, 4, and 7 at four elevations: right under the abutment, next downward element, middle pile elevation (above ground level), and ground level.

Therefore, moments in piles were recorded at 24 positions, 12 in the longitudinal direction and 12 in the transverse direction.

C.4 Lateral Pressure at Abutment

Lateral earth pressures were recorded at 20 different positions, as shown in Figure C.4. Ten of them are between the EPS and the upper part of the abutment, and the rest of them are between the backfill and the EPS. Five of the lateral pressures between the abutment and the EPS are at the upper elevation of 2/3 of the abutment height, and the other five are at the lower elevation of 1/3 of the abutment height. The same is true for the monitoring points between the backfill and the EPS.

Therefore, there are four groups of five measurement positions, at two different elevations and in front and back of the EPS, for a total of 20 monitoring points.

C.5 Strap Tensile Forces

Sixty three parameter histories were obtained from the MSE wall straps. Figure C.5 shows 21 selected positions for extracting strap information, 9 at the front wall, 6 at the left wall, and 6 at the right wall. At each one of these positions, 3 parameters histories were extracted: strap tensile force at the connection with the MSE wall panel, strap peak tensile force, and distance from the wall where the peak occurs.

C.6 Earth Pressure at MSE Wall

Earth pressure was recorded at 21 positions on the back of the MSE wall. The positions are the same as those shown in Figure C.5.

C.7 Pile Axial Forces

Axial forces were recorded at pile 1, 4, and 7 at the following elevations: under the abutment, pile middle height, and ground level, as shown in Figure C.3.

Therefore, axial forces in piles were recorded at 9 positions.

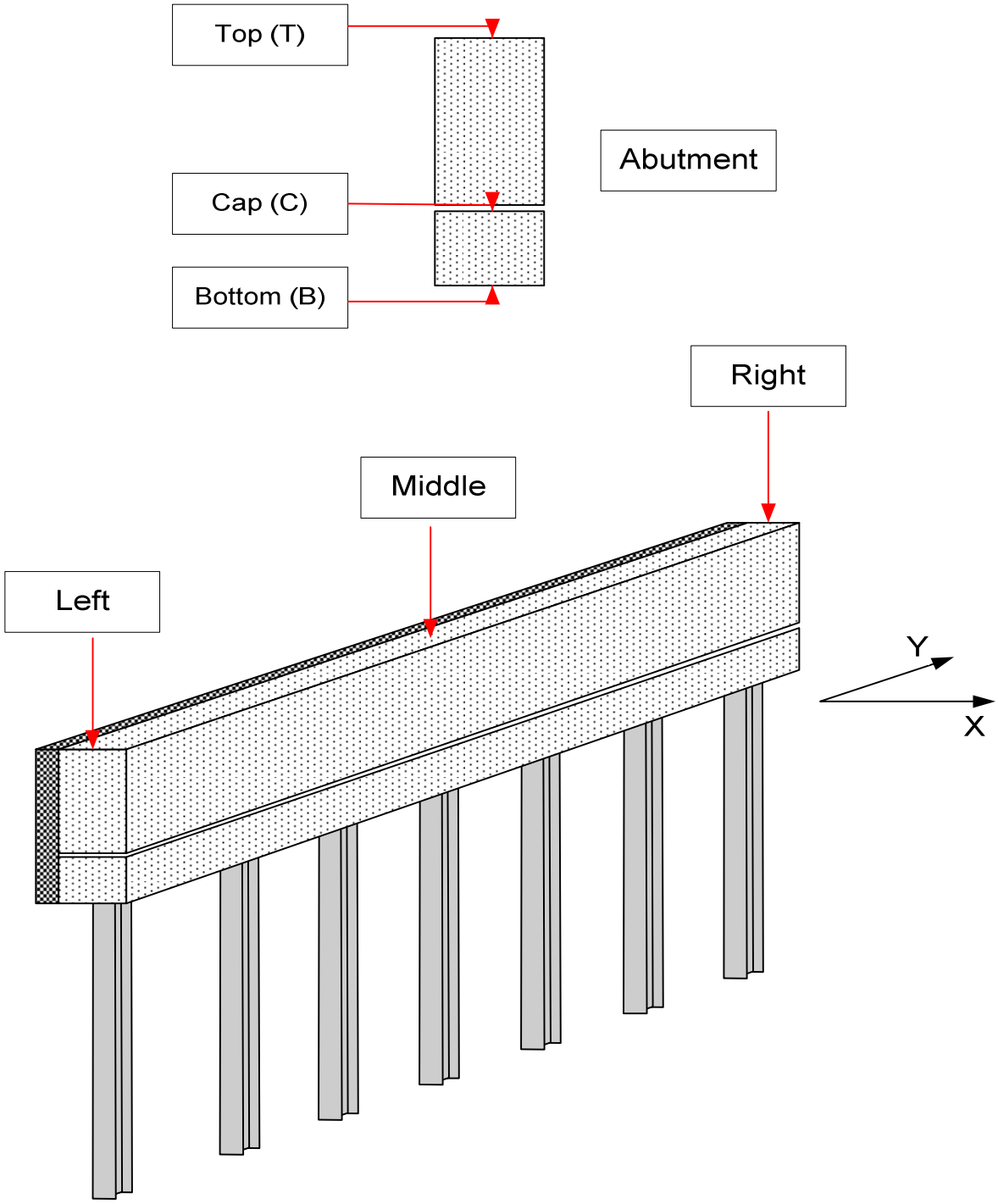

Figure C.1 – Displacement monitoring positions

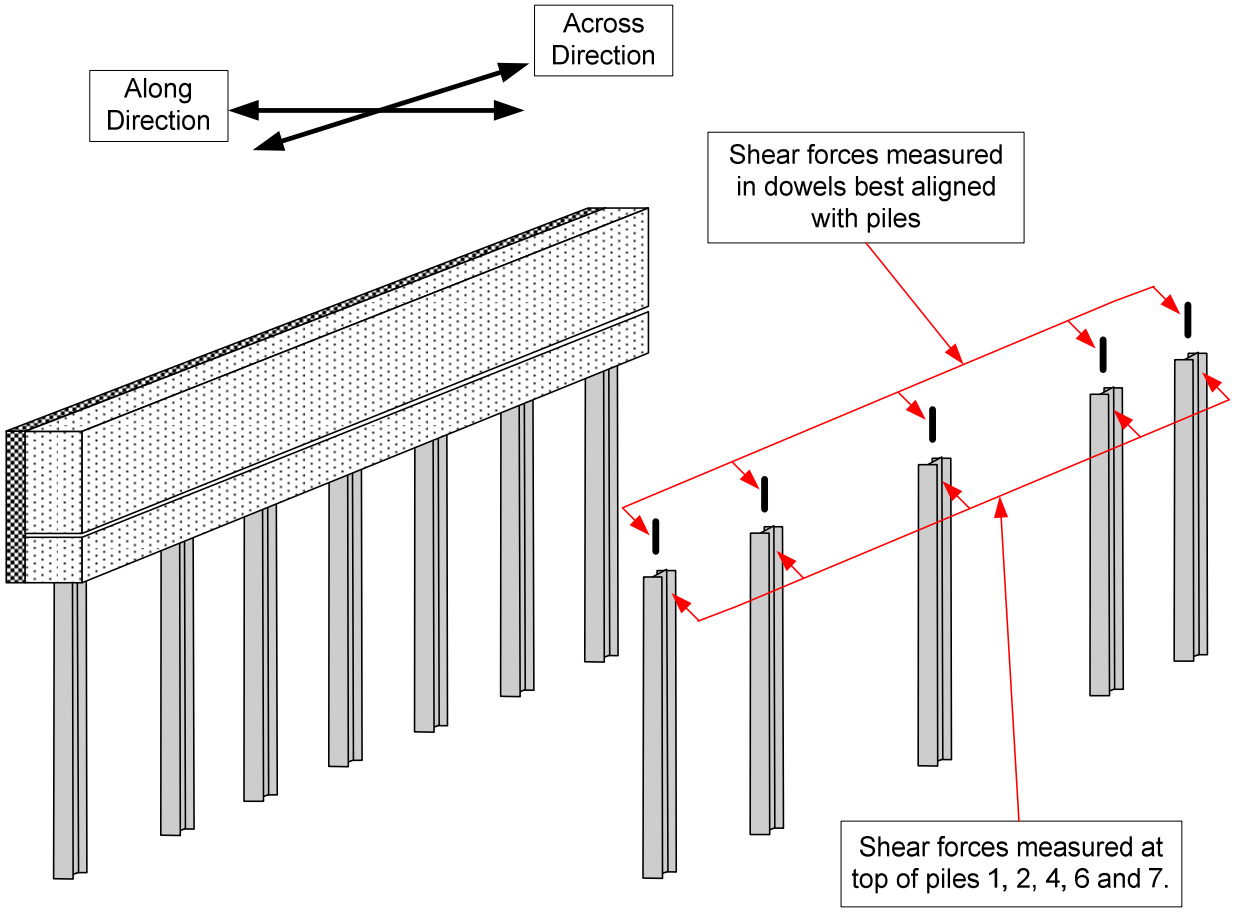

Figure C.2 – Shear force monitoring positions

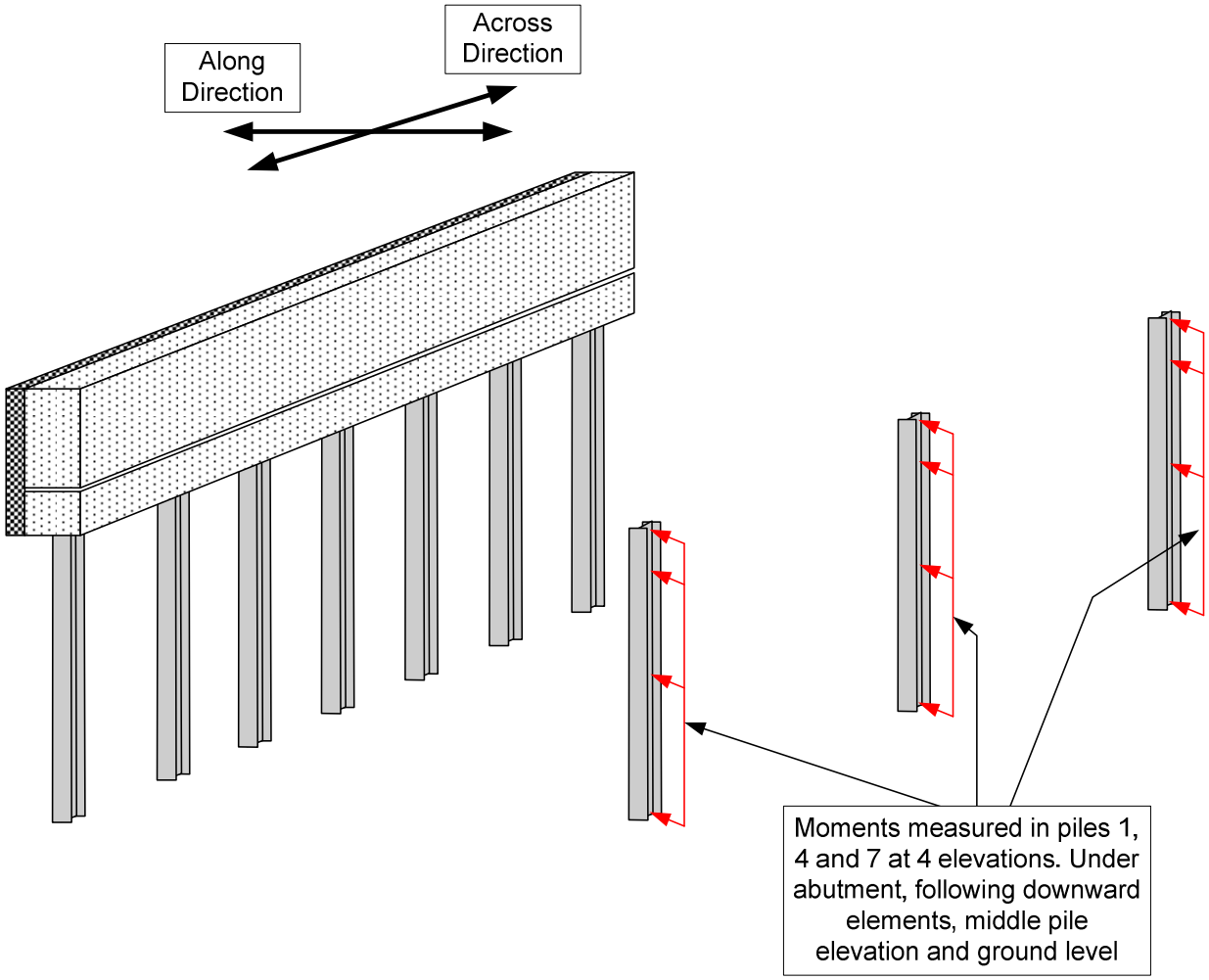

Figure C.3 – Moment monitoring positions

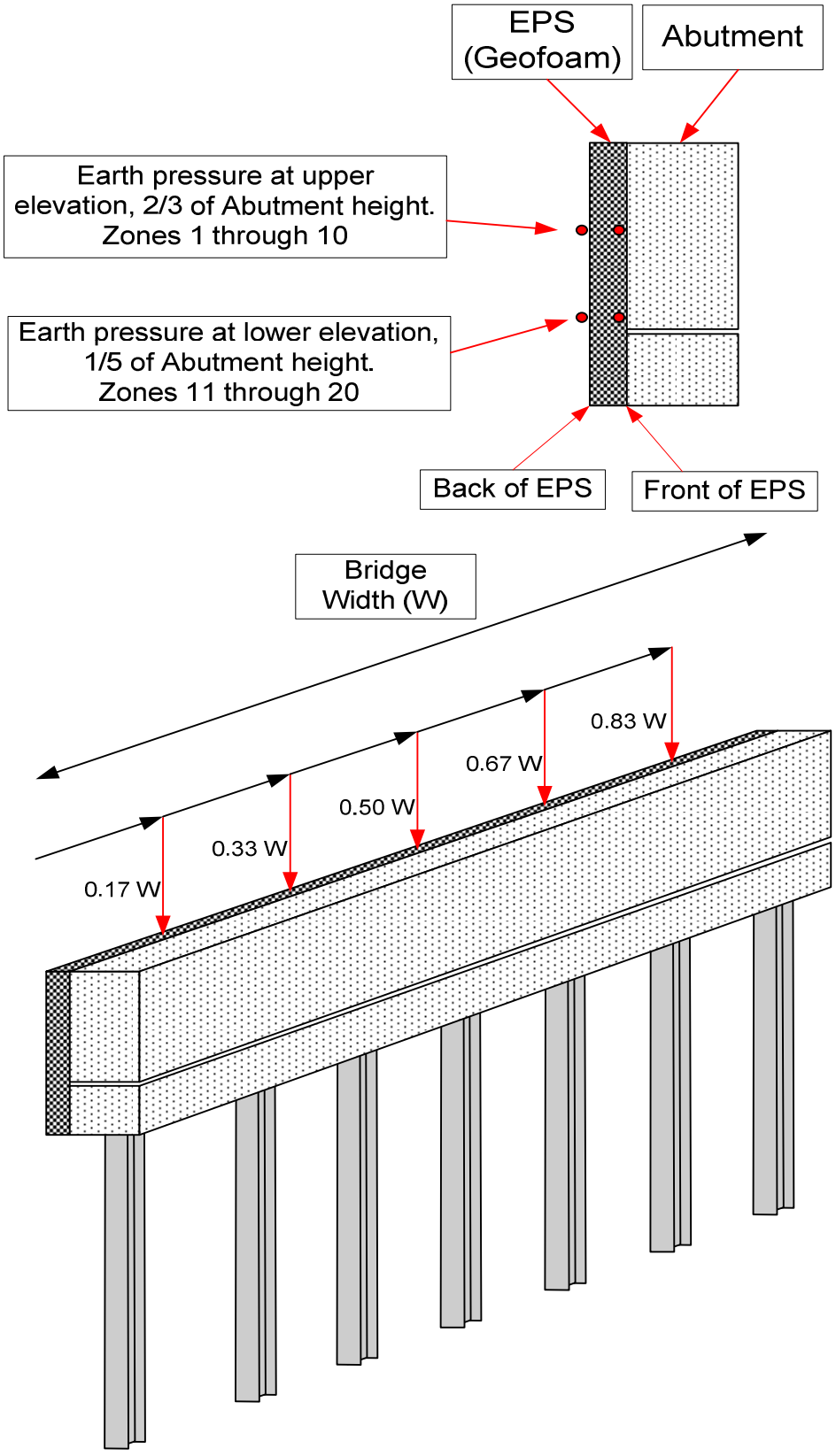

Figure C.4 – Lateral pressure monitoring positions

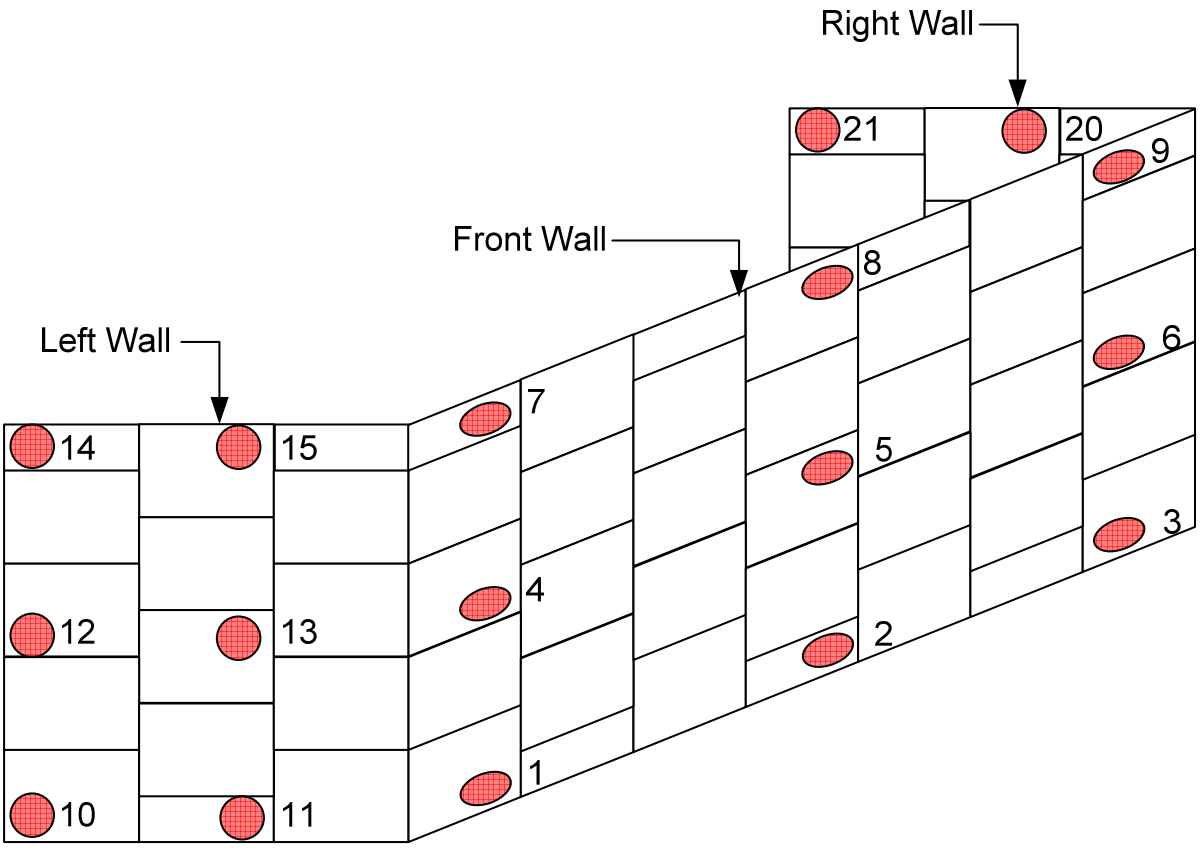

Figure C.5 – Strip tensile force and MSE wall earth pressure monitoring positions

APPENDIX D

GLOBAL MONITORING OUTPUT

Single Parameter Variation Cases		Global Monitoring Points																	
		Dowel					Pile												
		Longitudinal		Transverse		Axial	Longitudinal 1		Transverse 1		Longitudinal 2		Transverse 2		Axial	Interface 2		Interface 3	
		Moment	Shear	Moment	Shear		Moment	Shear	Moment	Shear	Moment	Shear	Moment	Shear		Normal	Shear	Normal	Shear
		lbs - ft	lbs	lbs - ft	lbs	lbs	lbs - ft	lbs	lbs - ft	lbs	lbs - ft	lbs	lbs - ft	lbs	lbs	lbs	lbs	lbs	lbs
Base Case		22,998	114,963	-104	209	10,975	-243,593	-46,503	619	-215	245,777	-38,751	172	-114	73,075	125,414	-78,245	72,325	-7,347
Abutment Desgin	Lam Pad						-57%	101%			-147%	-5%			-5%	2%	4%	-3%	-16%
	Solid						-393%	-712%			-50%	254%			-29%	-16%	-70%	-32%	-48%
Abutment - MSE Wall Distance	0.5'	0%	0%			32%	3%	7%			3%	3%			9%	11%	6%	-3%	39%
	1'	-3%	-3%			79%	1%	11%			6%	0%			10%	6%	7%	1%	104%
	3'	1%	1%			46%	3%	12%			9%	2%			12%	12%	10%	-2%	46%
	5'	7%	7%			28%	6%	6%			3%	6%			13%	17%	13%	-3%	29%
Thermal Displace.	0.75"	-70%	-70%			74%	-74%	-63%			-72%	-74%			-77%	-72%	-70%	-49%	-34%
	1.5"	-54%	-54%			68%	-46%	-32%			-47%	-46%			-53%	-38%	-34%	-25%	-12%
	4.5"	30%	30%			21%	38%	35%			39%	36%			3%	16%	14%	20%	28%
EPS MSE		-1%	-1%			-5%	-1%	-11%			-10%	-2%			-2%	-2%	-1%	4%	-5%
Foundation	Shale	4%	4%			-11%	4%	3%			2%	4%			-3%	3%	3%	4%	1%
Geometry	S gir	0%	0%			-11%	-1%	0%			0%	-1%			0%	-1%	0%	2%	0%
	B gir	1%	1%			13%	0%	0%			0%	0%			0%	0%	0%	1%	18%
	S MSE	1%	1%			19%	1%	-5%			-2%	1%			4%	6%	5%	0%	3%
	B MSE	2%	2%			24%	1%	6%			4%	1%			-2%	3%	2%	3%	0%
No EPS Abut		-16%	-16%			1933%	-169%	44%			11%	-29%			279%	-5%	-2%	1101%	3236%
Pile Strg Axis		23%	23%			13%	-230%	56%			-255%	-20%			2%	3%	5%	1%	-7%
Pile Types	12x53	13%	13%			21%	18%	37%			37%	1%			0%	2%	2%	1%	9%
	14x73	27%	27%			15%	38%	94%			92%	3%			-4%	-1%	2%	2%	-7%
Straps Abut		2%	2%			1%	2%	-2%			0%	2%			2%	3%	2%	2%	0%
Skew Angle	10	1%	1%	2558%	6546%	10%	-14%	4%	26638%	12313%	-3%	-15%	-64651%	20206%	-10%	-9%	-10%	1%	12%
	20	2%	2%	4034%	10235%	51%	-39%	17%	45696%	20645%	-20%	-42%	-110659%	34679%	-16%	-15%	-16%	7%	47%
	35	18%	18%	6581%	16602%	24%	-125%	50%	66124%	28910%	-45%	-45%	-159977%	50194%	-32%	-18%	-29%	23%	3%
	40	23%	23%	7055%	17787%	9%	-137%	71%	69702%	29975%	-50%	-50%	-168616%	52911%	-47%	-26%	-42%	30%	-2%
	45	24%	24%	7639%	19249%	27%	-147%	83%	72120%	31016%	-59%	-171%	-174453%	54747%	-63%	-39%	-57%	34%	6%
	50	27%	27%	8050%	20275%	33%	-169%	94%	72899%	31352%	-68%	-201%	-176333%	55339%	-75%	-47%	-70%	36%	16%

Table D.1 – Global monitoring points. Summary table of section 7.2

APPENDIX E

CALIBRATED POLYNOMIAL CONSTANTS

Constants / R^2	Dowels					Piles								
	Longitudinal		Transverse		Axial	Longitudinal Pos 1		Transverse Pos 1		Longitudinal Pos 2		Transverse Pos 2		Axial
	Moment	Shear	Moment	Shear		Moment	Shear	Moment	Shear	Moment	Shear	Moment	Shear	
a0	-1463	-7141	-1115	5582	10947	3622	-15405	-88954	-19544	-53321	4394	148141	1725	-18898
a1	5944	29697	-1475	7372	3338	-71607	-11388	13992	-8055	100243	-12829	27602	-6650	37687
a2	61	301	36	-181	-32	174	53	60	478	384	-248	-1568	180	88
a3	-42	-211	-68	338	-336	-9782	1115	9522	-1315	1545	4852	-7572	-1263	777
a4	-59	-294	221	-1107	-400	592	1286	-1573	744	-5101	1192	-6130	572	-3569
a5	-0.16	-0.81	-0.11	0.55	0.04	-0.03	-0.22	-1.23	-1.36	0.66	0.74	5.26	-0.48	-0.28
a6	1.17	5.89	0.72	-3.61	3.18	558.18	-21.90	-180.44	19.97	13.53	-212.35	143.90	20.60	-15.53
a7	10.51	52.61	0.24	-1.18	1.97	-222.12	-61.90	271.66	-7.87	157.88	-3.45	-217.58	-12.50	6.48
a8	53.09	265.44	-37.40	186.98	39.88	1263.14	-302.33	2569.38	-254.51	-1469.48	-933.17	-1994.29	-292.98	-295.28
a9	-0.04	-0.18	0.07	-0.35	0.22	-12.33	-0.76	13.08	-0.34	-18.47	-8.26	-10.26	-0.49	-0.02
a10						-7.36					2.40			
a11						21.21					28.74			
a12						0.19					0.20			
a13						7.56					-0.10			
R^2	**1.00**	**1.00**	**0.99**	**0.99**	**0.82**	**0.99**	**0.99**	**0.99**	**0.98**	**0.98**	**0.86**	**0.99**	**0.99**	**0.98**

Table E.1 – Calibrated constants group DW1.

Constants / R^2	Dowels					Piles								
	Longitudinal		Transverse		Axial	Longitudinal Pos 1		Transverse Pos 1		Longitudinal Pos 2		Transverse Pos 2		Axial
	Moment	Shear	Moment	Shear		Moment	Shear	Moment	Shear	Moment	Shear	Moment	Shear	
a0	4409	21800	-9637	-9636	2857	-989807	-16338	-9552	-9620	276486	283910	-9587	-9622	33454
a1	7409	37135	2154	2160	2482	425521	-12934	2539	2233	-189955	-105586	2378	2223	15236
a2	9	46	0	1	8	163	-96	55	11	-491	9	32	10	-23
a3	111	551	-218	1091	-52	-27326	-685	11608	1794	8764	5726	7871	1605	-1317
R^2	**1.00**	**1.00**	**1.00**	**1.00**	**0.97**	**1.00**	**1.00**	**1.00**	**1.00**	**0.99**	**1.00**	**1.00**	**1.00**	**1.00**

Table E.2 – Calibrated constants group DS2.

Constants / R^2	Earth Pressure at Abutment			
	Acute Corner		Obtuse Corner	
	Elev. 1/3	Elev. 2/3	Elev. 1/3	Elev. 2/3
a0	-12.487	89.574	-27.994	86.592
a1	114.257	58.455	132.935	59.614
a2	0.123	-0.491	-0.005	-0.338
a3	-10.079	-1.005	-13.524	-1.188
a4	-0.003	0.028	0.007	0.015
a5	-0.487	0.347	-0.355	0.064
R^2	**0.95**	**0.93**	**0.92**	**0.91**

Table E.3 – Calibrated constants group DEA3.

Constants / R^2	MSE Wall Earth Pressure	Strip Tensile Force-Connection	Strip Tensile Force-Peak
a0	14.629	48.767	-94.628
a1	-29.871	-44.905	-2.151
a2	74.156	21.114	167.127
a3	0.117	0.314	0.467
a4	4.958	10.030	1.807
a5	-7.010	16.127	-7.369
a6	0.000	0.000	0.000
a7	-3.433	-17.636	-11.398
a8	-0.007	-0.044	-0.028
a9	0.023	0.118	0.101
R^2	**0.97**	**0.97**	**0.99**

Table E.4 – Calibrated constants group DETM4.

Constants / R^2	Transverse Displacement
a0	0.003533
a1	0.000000
a2	0.015925
a3	-0.000055
a4	0.000000
a5	0.000116
a6	0.000000
a7	0.000000
a8	0.000000
a9	-0.000018
R^2	**0.98**

Table E.5 – Calibrated constants group DTD5.

Constants / R^2	Piles								
	Longitudinal Pos 1		Transverse Pos 1		Longitudinal Pos 2		Transverse Pos 2		Axial
	Moment	Shear	Moment	Shear	Moment	Shear	Moment	Shear	
a0	-59273.50	-6789.61	-94979.29	617.31	-1151.30	5187.57	-98535.76	4914.46	-1240.88
a1	-24723.62	-25762.48	-62558.71	264.12	-8336.58	-10373.42	-58664.31	3140.44	24012.14
a2	568.95	-110.43	1265.85	-13.46	-275.20	-91.58	1156.07	-38.50	34.35
a3	1997.34	263.43	7230.12	-488.19	15.51	212.05	6940.56	-753.88	127.49
a4	3785.42	657.16	13480.28	-661.60	-1926.65	-334.12	11416.24	-932.02	-819.88
a5	-1.01	0.29	-4.19	0.05	0.42	0.23	-3.85	0.14	-0.10
a6	-19.03	-4.46	-137.76	6.10	18.71	-23.77	-136.60	11.75	-4.01
a7	-173.20	-41.64	172.98	-2.67	-245.15	6.55	171.54	-10.56	-4.85
a8	-1033.01	-134.15	2266.77	-308.68	-895.49	-203.26	1583.15	-293.08	-308.27
a9	-11.09	-0.41	11.98	-0.19	-3.21	-2.15	11.36	-0.59	0.23
a10					-0.41	0.33			
a11					29.61	4.51			
a12					0.15	0.05			
a13					5.69	-0.70			
R^2	**0.99**	**1.00**	**0.99**	**1.00**	**0.98**	**0.99**	**0.99**	**1.00**	**0.99**

Table E.6 – Calibrated constants group LPW1.

Constants / R^2	Piles								
	Longitudinal Pos 1		Transverse Pos 1		Longitudinal Pos 2		Transverse Pos 2		Axial
	Moment	Shear	Moment	Shear	Moment	Shear	Moment	Shear	
a0	-970182	41771	-10255	-9714	453405	-67026	-9586	-9622	43720
a1	560569	-41152	87054	13360	-311760	23874	3366	2391	12748
a2	541	-141	-13280	-1651	-750	-3	1085	325	-32
a3	4851	883	8538	1427	77936	-1660	7831	1603	-1232
a4	-74731	166	-89	0	45772	-5834	7360	1250	-830
a5	0	0	18	2	0	0	-2	0	0
a6	-343	-20	1	0	-1616	25	-34	-5	8
R^2	**0.97**	**0.99**	**0.97**	**0.98**	**0.98**	**1.00**	**0.97**	**0.98**	**1.00**

Table E.7 – Calibrated constants group LPS2.

Constants / R^2	Earth Pressure at Abutment			
	Acute Corner		Obtuse Corner	
	Elev. 1/3	Elev. 2/3	Elev. 1/3	Elev. 2/3
a0	0.372	18.892	-8.844	6.808
a1	85.329	61.234	97.709	78.973
a2	-0.267	0.017	-0.330	-0.234
a3	-3.434	2.799	-6.024	-1.445
a4	0.004	0.003	0.009	0.008
a5	-0.520	0.491	-0.194	0.092
R^2	**0.98**	**0.97**	**0.87**	**0.97**

Table E.8 – Calibrated constants group LPEA3.

Constants / R^2	MSE Wall Earth Pressure	Strip Tensile Force-Connection	Strip Tensile Force-Peak
a0	24.739	66.977	-62.793
a1	-36.670	-51.577	-7.902
a2	91.351	41.595	198.525
a3	0.078	0.227	0.236
a4	5.844	11.740	2.629
a5	-9.143	17.325	-9.870
a6	0.000	0.000	0.000
a7	-3.762	-20.143	-12.668
a8	-0.004	-0.050	-0.025
a9	0.017	0.104	0.093
R^2	**0.99**	**0.98**	**1.00**

Table E.9 – Calibrated constants group LPETM4.

Constants / R^2	Transverse Displacement
a0	0.00000
a1	0.00000
a2	0.00005
a3	0.00075
a4	0.00000
a5	0.00031
a6	0.00000
a7	0.00000
a8	0.00000
a9	-0.00001
R^2	**0.96**

Table E.10 – Calibrated constants group LPTD5.

APPENDIX F

H PILE PROPERTIES

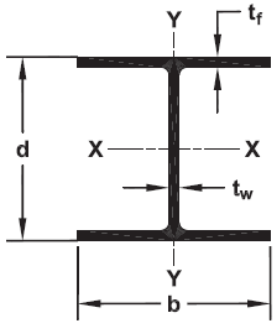

HP

SECTION	Weight lb/ft (kb/m)	Area in² (cm²)	Depth d in (mm)	Flange Width b in (mm)	THICKNESS Flange t_f in (mm)	THICKNESS Wall t_w in (mm)	Coating Area ft²/ft (m²/m)	ELASTIC PROPERTIES AXIS X-X I in⁴ (cm⁴)	AXIS X-X S in³ (cm³)	AXIS X-X r in (cm)	AXIS Y-Y I in⁴ (cm⁴)	AXIS Y-Y S in³ (cm³)	AXIS Y-Y r in (cm)
HP 8 HP 200	36 54	10.6 68.4	8.02 204	8.155 207	0.445 11.3	0.445 11.3	3.92 1.19	119 4950	29.8 487	3.4 8.53	40.3 1680	9.88 162	1.95 4.60
HP 10 HP 250	42 63	12.4 80.0	9.7 246	10.075 256	0.420 10.7	0.415 10.5	4.83 1.47	210 8740	43.4 711	4.13 10.5	71.7 2980	14.2 233	2.41 6.12
	57 85	16.8 108	9.99 254	10.225 260	0.565 14.4	0.565 14.4	4.91 1.50	294 12200	58.8 969	4.18 10.6	101 4200	19.7 323	2.45 6.22
HP 12 HP 310	53 79	15.5 100	11.78 299	12.045 306	0.435 11.0	0.435 11.0	5.82 1.77	393 16400	66.8 1080	5.03 1208	127 5290	21.1 346	2.86 7.26
	63 94	18.4 119	11.94 303	12.125 308	0.515 13.1	0.515 13.1	5.86 1.79	472 19600	79.1 1290	5.06 12.9	153 6370	25.3 415	2.88 7.32
	74 110	21.8 141	12.13 308	12.215 310	0.610 15.5	0.605 15.4	5.91 1.80	569 23700	93.8 1530	5.11 13.0	186 7740	30.4 498	2.92 7.42
	84 125	24.6 159	12.28 312	12.295 312	0.685 17.4	0.685 17.4	5.97 1.82	650 27100	106 1730	5.14 13.1	213 8870	34.6 567	2.94 7.47
HP 14 HP 360	73 109	21.4 138	13.61 346	14.585 370	0.505 12.8	0.505 12.8	6.96 2.12	729 30300	107 1770	5.84 14.8	261 10900	35.8 587	3.49 8.86
	89 132	26.1 168	13.83 351	14.695 373	0.615 15.6	0.615 15.6	7.02 2.14	904 37600	131 2150	5.88 14.9	326 13600	44.3 726	3.53 8.97
	102 152	30 194	14.01 356	14.785 376	0.705 17.9	0.705 17.9	7.06 2.15	1050 43700	150 2480	5.92 15.0	380 15800	51.4 842	3.56 9.04
	117 174	34.4 222	14.21 361	14.885 378	0.805 20.4	0.805 20.4	7.11 2.17	1220 50800	172 2830	5.96 15.1	443 18400	59.5 975	3.59 9.12

Table F.1 – H pile properties (Skyline Steel, Feb 2008)